ISHIK UNIVERSITY

ERBIL POLYTECHNIC UNIVERSITY

PROCEEDINGS OF THE 4TH IEC

INTERNATIONAL ENGINEERING CONFERENCE ON DEVELOPMENTS IN CIVIL & COMPUTER ENGINEERING APPLICATIONS

2018

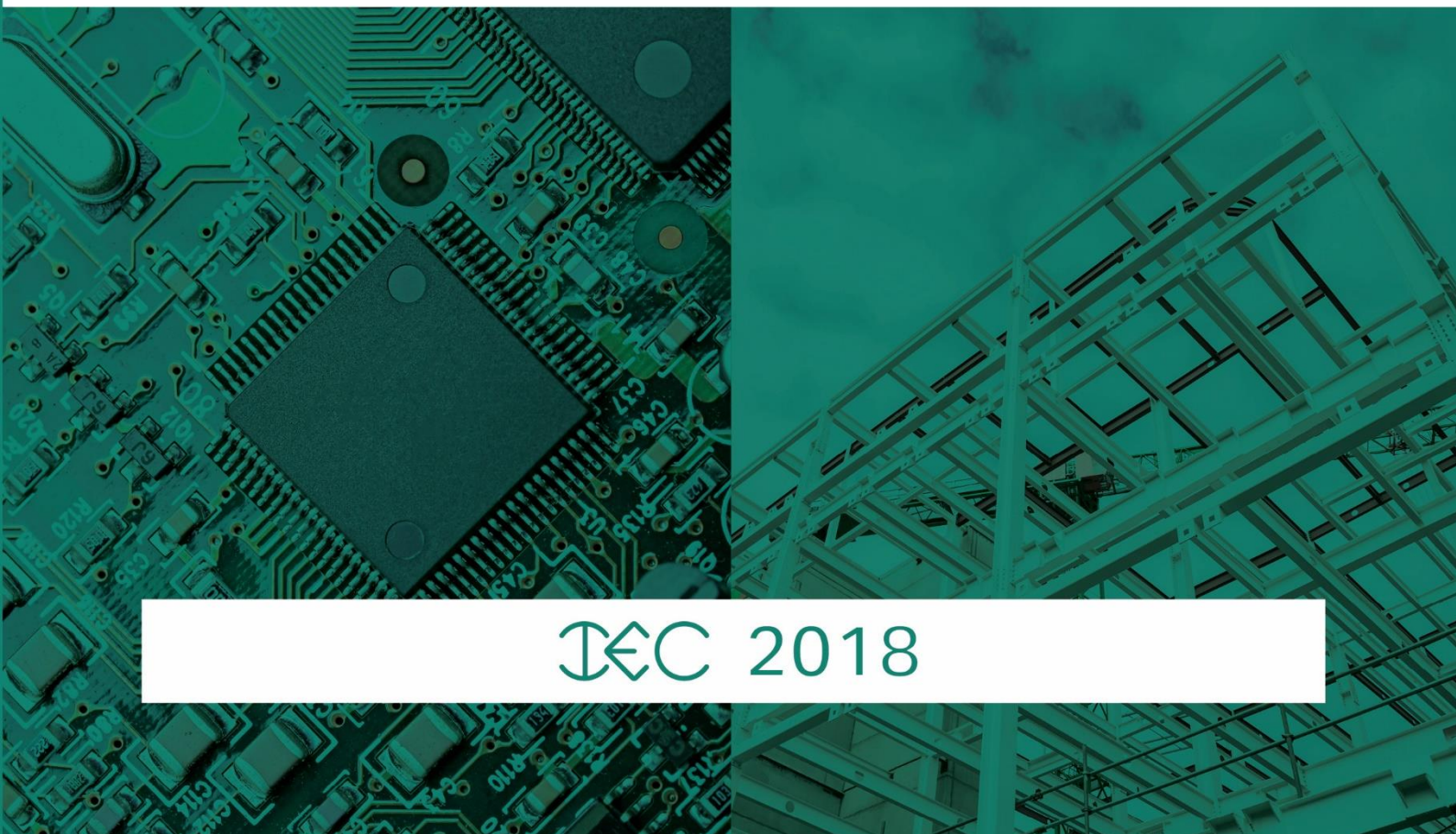

IEC 2018

4th International Engineering Conference on Developments in Civil & Computer Engineering Applications

Feb 26-27, 2018

ISSN 2409 - 6997

This Page Intentionally Left Blank

Preface

The 4th International Engineering Conference on Developments in Civil and Computer Engineering Applications (IEC 2018, Erbil) is held for the period from 26 to 27 February 2018. The conference is jointly organized by Ishik University and Erbil Polytechnic University.

The International Engineering Conference on Developments in Civil and Computer Engineering Applications (IEC2018) is the interdisciplinary forum for the presentation of new advances and research results in the fields of Civil and Computer Engineering applications. The conference tracks included the following research topics: Geo-Technical Engineering, Environmental Engineering, Fluid and Hydraulic Engineering, Green Buildings, Smart Buildings, Transportation Engineering, Restoration and Rehabilitation of Historical Buildings, Construction Management, Mechanical Energy, Sustainability of Concrete and Steel Structures, Petroleum and Mining Engineering, Artificial and Computational Intelligence, Control and Robotics, Communications, Networking and Protocols, Parallel and Distributed Processing, Signal and Multimedia Processing, Biomedical and Health Informatics, Mobile and Smartphone Applications, Software Engineering and Applications, Green Computing for Sustainable Energy, Cloud Computing, Computer Security, Smart Houses, Mechatronics and Surveying and Geomatics Engineering.

The program committee (the reviewers) is comprised of 56 members, all of which are Ph.D holders in certain fields of engineering, relevant to one or more conference tracks mentioned above. The same international conference standards that were adopted in the previous IEC2017, Erbil were adopted in IEC2018, as well. All paper submissions are blind peer-reviewed by at least three program committee members to ensure that submissions conform to certain quality measures. The quality measures included several criteria such as writing skill, quality of the content, fitness of the title, significance for theory or practice, originality and innovation level.

This year, the total number of submitted manuscripts stood at 45 from several countries including Iraq, Nigeria, Peru, Turkey, Australia, Portugal, Iran and Hungary. By category, 32 papers were related to Civil Engineering topics while 13 articles were written in the Computer Engineering related fields. The names of the institutions and the number of submissions received from those institutions are as follows: Cihan University (2), Duhok Polytechnic University (2), Eastern Mediterranean University (1), Erbil Polytechnic University (8), Halabja University (1), Ishik University (7), Koya Technical Institute, EPU (2), Soran University (1), Middle Technical University (1), Ministry of Electricity (1), Mosul University (1), University of Ninevah (2), Salahaddin University-Erbil (3), Universidad Nacional del Callao (1), University of Duhok (3), University of Sulaimani (4), Western Sydney University (1), University of Anbar (1), University of Miskolc (1), American University of Kurdistan (1), Koya University (1).

In IEC2018, a 69% article acceptance rate has been reached after a thorough reviewing process. The authors of manuscripts exceeding certain plagiarism percentage were notified to adjust their manuscripts or otherwise these submissions were rejected with a plagiarism note to the authors. Each submitted manuscript was double-checked for plagiarism and template format while reviewed by at least three members. Some reviewed submissions were marked as "revise" and authors of those submissions were given the chance to revise their manuscripts considering the reviewers' professional feedback. These revised manuscripts were resubmitted for one final review process either to get accepted or declined. Some other manuscripts were not accepted or withdrawn because they were not within the conference scope.

Regarding the conference, two panels were organized, one in the field of Computer Engineering and the other one in Civil Engineering. The first panel was titled as "*New Trends in IoT*" and chaired by Dr. Saman Mirza Abdullah (Faculty of Engineering, Software Engineering, Koya University). The other members for this panel were Assist. Prof. Dr. Tara Ibrahim Ali Yahiya (School of Science and Engineering, University of Kurdistan-Hewler) and Mr. Dler Mawlod (Director of CISCO ASC/ITC).
The topics of the second panel were "*Plate Tectonics and Earthquakes*" and "*Unmanned Aerial Vehicle (UAV) in Disaster Management*", respectively. The chair of this panel was Prof. Dr. Bayan Salim Al-Numan from the Civil Engineering Department of Ishik University. The other panelists were Assist. Prof. Dr. Qubad Zeki,Head of Surveying and Geomatics Engineering (Ishik University) and Assist. Prof. Dr. Srood Farooq Omar, Head of Petroleum and Mining Engineering (Ishik University).

Dr. Günter Şenyurt

Editor-in-Chief

IEC2018
Organizing Committee

Dr. Idris Hadi
Honarable Chair
President of Ishik University,
Erbil, Iraq

Assist. Prof. Dr. Kawa Sherwani
Honarable Chair
President of Erbil Polytechnic University, Erbil, Iraq

Dr. Selcuk Cankurt
Chair
Faculty of Engineering,
Computer Engineering Department,
Ishik University

Dr. Ranj Sirwan Abdullah
Co-Chair
Vice Dean of Engineering
Technical College,
Erbil Polytechnic University

Dr. Günter Şenyurt
Editor-in-Chief
Faculty of Engineering,
Computer Engineering
Department, Ishik University

IEC2018
Higher Committee

Assist. Prof. Basil Younis
Head of Civil Engineering Department, Erbil Polytechnic University

Dr. Ranj Sirwan Abdullah
Vice Dean of Engineering Technical College,
Erbil Polytechnic University

Dr. Mehmet Özdemir
Vice President for Scientific Affairs
Ishik University, Erbil, Iraq

Dr. Nageb Toma Bato
Vice President for Scientific Affairs
Erbil Polytechnic University, Erbil, Iraq

Dr. Halit Vural
Dean of Engineering Faculty,
Ishik University, Erbil, Iraq

Dr. Bzar Khidir Hussan
Head of Information System Engineering Department, Erbil Polytechnic University

IEC2018
Organizing Committee

IEC2018
Organizing Committee

IEC2018
Program Committee

Prof. Dr. Bayan Salim AL-Nu'man
Civil Engineering Department
Ishik University, Erbil, Iraq

Prof. Dr. Omar Qarani Aziz
College of Engineering, Civil Engineering Department, Salahaddin University, Erbil,Iraq

Prof. Dr. Moayad Y. Potrus
College of Engineering, Software Engineering Department, Salahaddin University-Erbil

Assoc. Prof. Dr. Thamir Mohammed Ahmed
Faculty of Engineering, Civil Engineering Department, Ishik University

Assist. Prof. Dr Basil Younus Mustafa
Head of Civil Engineering Department
Erbil Polytechnic University, Erbil, Iraq

Assist. Prof. Dr. Shuokr Qarani Aziz
College of Engineering, Civil Engineering Department, Salahaddin University-Erbil

Assoc. Prof. Dr.Shirzad B.Nazhat
Petroleum Engineering Department
Soran University, Soran, Erbil, Iraq

Assist. Prof. Dr. Husein Ali Husein
Architectural Engineering Department
Koya University, Koya, Iraq

Assist. Prof. Dr. Tara Ibrahim Ali Yahiya
School of Science and Engineering, Computer Science and Engineering Department, University of Kurdistan-Hewler

Assist. Prof. Dr. Jafar A. Ali
Petroleum Engineering Department
Koya University, Koya, Iraq

IEC2018
Program Committee

Assist. Prof. Dr. Younis Mahmood M.Saleem
College of Engineering, Architectural Engineering Department, University of Technology

Assist. Prof. Dr. Faris Ali Mustafa
College of Engineering, Architectural Engineering Department, Salahaddin University-Erbil

Assist. Prof. Dr. Noori Sadeq Ali
College of Engineering, Civil Engineering Department, Cihan University-Erbil

Assist. Prof. Dr. Wrya Muhammad Ali Monnet
School of Science and Engineering, Computer Science and Engineering Department, University of Kurdistan-Hewler

Assist. Prof. Dr. Hassan Majeed Hassoon
Faculty of Engineering, Interior Design Department, Ishik University

Assist. Prof. Dr. Mazin S Al-Hakeem
College of Engineering, Computer Techniques Engineering, Al-Mustafa University College

Assist. Prof. Dr. Ayad Zeki Saber Agha
Erbil Technical Engineering College, Civil Engineering Department, Erbil Polytechnic University

Assist. Prof. Dr. Lokman H. Hassan
College of Engineering, Electrical and Computer Engineering Department, University of Duhok

IEC2018
Program Committee

Assist. Prof. Dr. Bengin Awdel Herki
College of Engineering, Civil Engineering Department, Soran University

Assist. Prof. Dr. Srood Farooq
Head of Petroleum and Mining Engineering Department
Ishik University

Assist. Prof. Dr. Tarik A. Rashid
School of Science and Engineering, University of Kurdistan-Hewler

Assist. Prof. Dr. Nejdet Dogru
Information Technologies Department, International Burch University

Assist. Prof. Dr. Faiq M. Sarhan Alzawiny
Al-Nahrain University
Faculty of Engineering

Assist. Prof. Dr. Abdullah Salman
University of Technology
Faculty of Engineering

Assist. Prof. Dr. Abbas Hamza
University of Technology
Faculty of Engineering

Assist. Prof. Dr. Falah Al-Jabery
University of Technology
Faculty of Engineering

Assist. Prof. Qubad Zeki Henari
Head of Surveying and Geomatics Engineering Department, Ishik University

Dr. Saman Mirza Abdullah
Faculty of Engineering, Software Engineering Department, Koya University

IEC2018
Program Committee

IEC2018
Program Committee

IEC2018
Program Committee

IEC2018
Editorial Board

IEC2018
Organizing Committee

Technical Support Team

Mr. Abulkareem Habbab, Mechatronics Department, Ishik University
Mr. Arkan Yousif, Publication and Media Office, Ishik University
Mr. Ahmed Azmi, Publication and Media Office, Ishik University
Mr. Ahmed Nariman, Architecture Engineering Department, Ishik University
Ms. Avan Azad, Information Technology Department, Ishik University
Mr. Baban Jamal, Rectorate, Ishik University
Ms. Farah Maysan, Interior Design Department, Ishik University
Mr. Halmat Muslih, Civil Engineering Department, Ishik University
Mr. Hawraz Hamid, Rectorate, Ishik University
Ms. Hazheen Nasih, Interior Design Department, Ishik University
Mr. Hevar J. Abdulrahman, Civil Engineering Department, Ishik University
Mr. Hunar Mahdi Salih, Petroleum Engineering Department, Ishik University
Ms. Israa Nazhat, Computer Engineering Department, Ishik University
Mr. Karzan Abdulmajid, IT Service, Ishik University
Mr. Kewan Hama Amen,IT Service , Ishik University
Mr. Mohammed Kamal, Information Technology Department, Ishik University
Mr. Mohammed Qadir, Surveying Engineering Department, Ishik University
Mr. Mohammed Salam, Computer Engineering Department, Ishik University
Mr. Mohammed Sherwan, Publication and Media Office, Ishik University
Mr. Muhammed Abdulsattar, Accounting Office, Ishik University
Ms. Naz Noori, Civil Engineering Department, Ishik University
Ms. Naza Ghani, Engineering Faculty, Ishik University
Mr. Nurullah Darici, Rectorate, Ishik University
Mr. Rebin Mohammed, Information Technology Department, Ishik University
Ms. Samiha Habbal, Information Technology Department, Ishik University
Ms. Shaida Mustafa, Petroleum Engineering Department, Ishik University
Mr. Shallaw Hamza, Interior Design Department, Ishik University
Mr. Shamal Mohammed, Surveying Engineering Department, Ishik University
Mr. Shkar Latif, Civil Engineering Department, Ishik University
Mr. Usman Eschanov, IT Service, Ishik University
Mr. Yasar Yilmaz, IT Service, Ishik University
Mr. Wafaa Wasfi, Architecture Engineering Department, Ishik University
Ms. Zainab Akram, Engineering Faculty, Ishik University
Mr. Ranjdar Kamal, Erbil Polytechnic University
Mr. Safeen Majeed, Erbil Polytechnic University
Mr. Himdad Tahir, Erbil Polytechnic University
Mr. Farhad Thahir, Erbil Polytechnic University
Mr. Abdulsattar, Erbil Polytechnic University
Mr. Shahab Rafaat, Erbil Polytechnic University
Mr. Hawre Mahmood Abbas, Erbil Polytechnic University

This Page Intentionally Left Blank

IEC2018
Keynote Speaker

Prof. Dr. Riadh Al-Mahaidi

Professor of Structural Engineering,
Vice President (International Engagement)
Director, Smart Structures Laboratory

Dr Riadh Al-Mahaidi is a Professor of Structural Engineering and Director of the Smart Structures Laboratory at Swinburne University of Technology. He also holds the position Vice President (International Engagement) at Swinburne. Prior to joining Swinburne in January 2010, he was the Head of the Structures Group at Monash University. Over the past 20 years, he focused his research and practice on life time integrity of bridges, particularly in the area of structural strength assessment and retrofitting using advanced composite materials.He currently leads a number of research projects on strengthening of bridges using fibre reinforced polymers combined cement-based bonding agents, fatigue life improvement of metallic structures using advanced composite systems and shape memory alloys. He recently started some projects on hybrid testing of structures. He received a BSc (Hon 1) degree in civil engineering from the University of Baghdad and MSc and PhD degrees in structural engineering from Cornell University in the United States. To date, Riadh published over 185 journal and 235 conference papers and authored/edited 10 books and conference proceedings. He was awarded the 2012 Vice Chancellor's Internationalization Award, the RW Chapman Medals in 2005 and 2010 for best journal publication in Engineers Australia Structural Journal, best paper awards at ACUN-4 (2002) and ACUN-6 (2012) Composites conferences. Prof Al-Mahaidi and his research group won the 2016 Engineers Australia Excellence Award for Innovation, Research and Development (High Commendation) for the Multi-Axis Substructure Testing (MAST) System they built at Swinburne. He was recently awarded the 2017 WH Warren Medal by Board of the College of Civil Engineers of Engineers Australia.

This Page Intentionally Left Blank

IEC2018
Keynote Speaker

Prof. Dr. Sabah A. Jassim

Professor of Mathematics and Computation, Applied Computing Department University of Buckingham, Buckingham, UK

Prof. Dr. Sabah A. Jassim is a pure mathematician by training but have a strong interest in computing research that are intensively reliant on mathematical techniques and structures. My original interest was in Group theory and Riemann surfaces influenced to varying degrees my different computational research activities. My research profile covers a wide range of mathematics and computation areas of Computational Geometry; Graph and group algorithms; classification of Riemann surfaces and Riemannian manifolds; Biometrics authentications and crypto-systems; Security of multimedia objects; Dimension reduction and Compressive sensing; Dynamic cryptography; Bioinformatics; Visual speech and word recognition. My recent research investigations are focused on developing smart machine learning algorithms that exploit topological features (persistent homology). These algorithms are currently applied for biomedical image analysis and intelligent diagnostics, as well as for digital Forensics. I published over 120 papers, in refereed journals and conferences, on the work done above research areas. I also contributed 5 book chapters, and edited the proceedings of an annual international SPIE conference held in the USA since 2007. I have successfully supervised 21 PhD and 8 MSc theses in areas of Mathematics and Computation. Currently I am supervising 10 PhD students at different stages of their program.
I act as External examiner of PhD thesis at various UK and EU universities, and review publications for international journal and conferences. I participated in EU funded FP6 projects, e.g. the SecurePhone and the BROADWAN projects. I am contributing to supervision of Innovate-UK funded Knowledge Transfer Projects (KTP) with industry.

This Page Intentionally Left Blank

Table of Contents

Table of Contents

Table of Contents

A Review of Person Recognition Based on Face Model

Shakir F. Kak[1], Firas Mahmood Mustafa[2], Pedro Valente[3]

[1]Duhok Polytechnic University (DPU), Akre Technical Institute, [2]Duhok Polytechnic University
[3] Univ Portucalense (UPT), Research on Economics, Management and Information
[1]shakir_fattah@yahoo.com, [2]Firas.mah.m@gmail.com, [3]pvalente@upt.pt

doi:10.23918/iec2018.01

ABSTRACT

Face recognition has become an attractive field in computer based application development in the last few decades. That is because of the wide range of areas they used in. And because of the wide variations of faces, face recognition from the database images, real data, capture images and sensor images is challenging problem and limitation. Image processing, pattern recognition and computer vision are relevant subjects to face recognition field. The innovation of new approaches of face authentication technologies is continuous subject to build much strong face recognition algorithms. In this work, to identify a face, there are three major strategies for feature extractions are discussed. Appearance-based and Model-based methods and hybrid techniques as feature extractions are discussed. Also, review of major person recognition research the characteristics of good face authentication applications, Classification, Distance measurements and face databases are discussed while the final suggested methods are presented. This research has six sections organized as follow: Section one is the introduction. Section two is dedicated to applications related to face recognition. In Section three, face recognition techniques are presented by details. Then, classification types are illustrated in Section four. In section five, standard face databases are presented. Finally, in Section six, the conclusion is presented followed by the list of references.

Keywords*:* Appearance -based model. Model based, Hybrid based, Classification, Distance Measurements, Face Databases, Face Recognition.

1. INTRODUCTION

Over the most recent couple of decades, face recognizing is considered as standout among the most imperative applications compared to other biometric based systems. The face recognition issues can be stated as follows: Given a database consists of many face pictures of known people and a one input face picture, the process aims to verify or determine the identity of the person in the input image [1]. Biometric-based strategies have developed as the most capable alternative for perceiving people as of late since, rather than confirming individuals and conceding them access to physical and virtual spaces based on passwords, PINs, keen cards, plastic cards, tokens, keys etc., these strategies analyze a person's physiological as well as behavioral attributes with a specific end goal to decide and/or ascertain his/her identity. Passwords and PINs are difficult to recollect and can be stolen or speculated; cards, tokens, keys and so forth can be lost, overlooked, purloined or copied; attractive cards can wind up noticeably tainted and garbled. However, natural biological of people cannot be lost, overlooked, stolen or manufactured. For example, physiological characteristics of person, such as facial images, fingerprints, finger geometry, hand geometry, hand veins, palm, iris, retina, ear and voice and behavioral traits, such as gait, signature and keystroke dynamics, which are used in biometric strategies for person verification or identification especially for security systems. Security application witnessed a huge development during the last few decades which is a natural result of the technology revolution in all fields, especially in smart environment sectors. Face features in face recognition for individual identification are considered a major method of the biometric area. Nowadays, the person appears in the video or digital image can automatically be identifying that person by Facial Recognition System (FRS) which is a significant technique to enhance security problems [2]. Recently, many researchers focused on the face recognition techniques. The human face in a person recognition application is a unique and valuable trait. It seems to offer a few points of interest over other biometrics, many methods are illustrated here, almost all other innovations require some deliberate activity by the client, i.e., the client needs to put his/her hand on a hand-rest for fingerprinting or hand geometry location and needs to remain in a settled position before a camera for iris or retina recognizable proof. Be that as it may, it should be possible using face recognition inactively with no express activity or cooperation with respect to the member since face pictures can be gained

from a distance by a camera. In contrast, low resolution, light, person poses, and illumination variation are some of the drawbacks of faced person recognition. Sometimes person face might be invisible. Therefore, face recognition system provides the researchers the opportunity to invent a new method to solve these drawbacks, which will enhance security and help in discovering new optimization techniques for face recognition [1]-[3]. The idea behind the face recognition system is to determine the known and unknown faces, so a face recognition system is basically, use pattern recognition. Because of the person recognition challenges, such as; faces are highly dynamic and pose, scantiest in this area of pattern recognition, artificial intelligence and computer vision had suggested many solutions to enhance the accuracy and robustness of recognition [4].

1. APPLICATION OF FACE RECOGNITION

Nowadays, the biometric base security application has dramatically increased, especially on face recognition area. Thus, because face recognition application is a powerful way to accurate and robust personal security such as smart home, smart card, law enforcement, surveillance, entrainment [4]-[6]. Table 1. Illustrate the most methods that face recognition are covers.

TABLE 1.
Illustrate the most method that face recognition are covers [4]-[6]

Fields	Scenarios of applications (Examples)
Security	Terrorist alert, secure flight boarding systems, stadium audience scanning, computer security.
Face ID	Driver licenses, entitlement programs, immigration, national ID.
Face Indexing	Labeling faces in video.
Access Control	Border-crossing control, facility access, vehicle access, smart kiosk and ATM, computer access and computer program access.
Multimedia Environment	Face-based search, face-based video segmentation summarization and event detection.
Smart Cards Application	Stored value security and user authentication.
Human Computer Interaction (HCI)	Interactive gaming and proactive computing.
Face Databases	Face indexing and retrieval, automatic face labeling and face classification.
Surveillance	Advanced video surveillance, nuclear plant surveillance, park surveillance and neighborhood watch, power grid surveillance as well as CCTV Control and portal control.

2.1 SMART HOME

Recently, the design of smart homes or cities has become one of the things that many researchers have focused. For example, design a smart house for people with special needs, patients or the general public to help them meet their needs in the easiest and fastest way. With the development of the devices and the possibility of connecting with the outside world and the use of home appliances remotely using modern technology, for example, facial recognition techniques or speech or gate behavior without the needs to physical connection from the person, such as fingerprint reaction depends on the recognized person prompted researchers to design the smart home depending on the person needs. Hence the importance of using facial recognition techniques to design smart homes.

2. PRINCIPLES OF FACE RECOGNITION SYSTEM

Face recognition is an action that humans perform routinely and effortlessly in our daily lives. The person identification for the face appears in the input data is the face recognition process. The face recognition process shown in Figure 1.

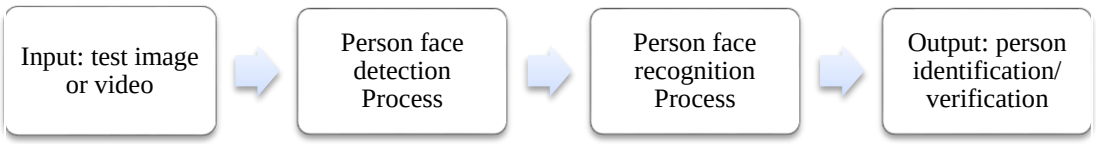

FIGURE 1. Face recognition process

There are several methods used for person face feature extraction which illustrated in Figure 2 [5]-[6].

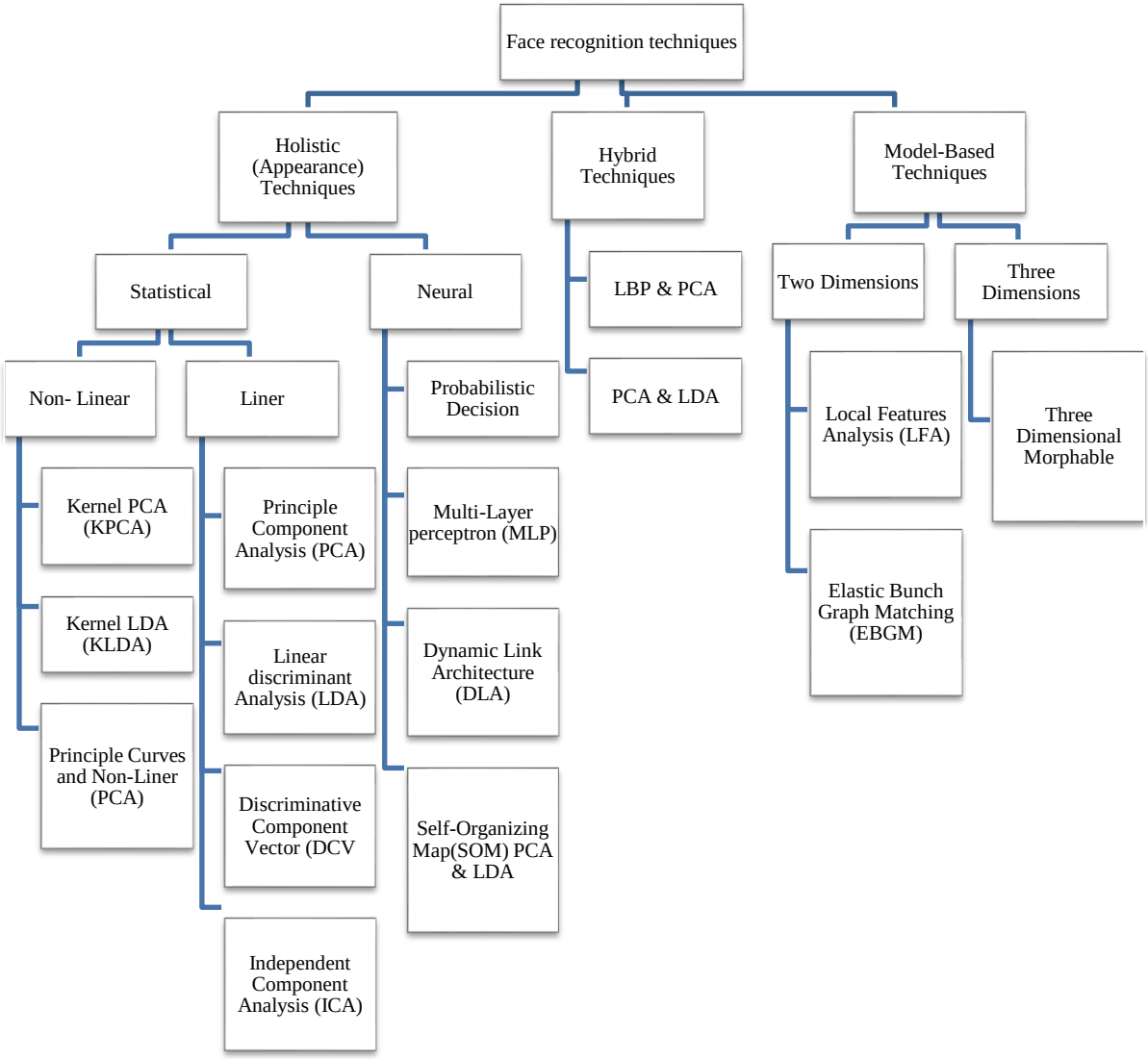
Face recognition techniques
Holistic (Appearance) Techniques
Hybrid Techniques
Model-Based Techniques
Statistical
Neural
LBP & PCA
Two Dimensions
Three Dimensions
Non- Linear
Liner
Probabilistic Decision
PCA & LDA
Local Features Analysis (LFA)
Three Dimensional Morphable
Kernel PCA (KPCA)
Principle Component Analysis (PCA)
Multi-Layer perceptron (MLP)
Elastic Bunch Graph Matching (EBGM)
Kernel LDA (KLDA)
Linear discriminant Analysis (LDA)
Dynamic Link Architecture (DLA)
Principle Curves and Non-Liner (PCA)
Discriminative Component Vector (DCV
Self-Organizing Map(SOM) PCA & LDA
Independent Component Analysis (ICA)

3.1 MODEL BASED TECHNIQUES

Face recognition techniques uses model-based strategies to develop a model of the person facial that extract facial features [7]. These strategies can be made invariant to lighting, a size and alignment. In addition, other advantages of these techniques such as rapid matching and compactness of the representation of face images [8]. In contrast, the main disadvantage of this model is the complexity of face detection [9].

3.1.1 3D MORPHABLE MODEL

The 3D strategies for face recognition use the 3D sensor to capture data from face. This model can be classified into two major types: 3D poses estimation and the 3D face reconstruction [10]. In the research [11] (Hu et al., 2014) presented "A novel Albedo Based 3D Morphable Model (AB3DMM)" is presented. They used in the proposed method the illumination normalization in a pre-processing stage to remove the illumination component from the images. The results of this research reached 86.76% of recognition on Multi- PIE database which used to evaluate SSR+LPQ. Also, in [12] (Changxing Ding et al. 2016) mentioned that 3D facial landmarks are projected in a grid shape in the 2D image, and then by aligning five facial landmarks semantically of the corresponding face images with a generic 3D face model.

3.1.2 ELASTIC BUNCH GRAPH MATCHING (EBGM):

This algorithm identifies a human in a new appearance picture by comparing his/her new face image with other faces in the database. The process of this algorithm started by extracting feature component vectors using Gabor Jets from a highlighted point on the face. Next, the extracted features are matched to corresponding features from the other faces in the database [13]-[14].

3.2 HOLISTIC (APPEARANCE) BASED METHODS

These methods are based on global representations of faces instead of local representation on the entire image for identifying faces. This model takes into consideration global features from the given set of faces in face recognition process. This model can be categorized into three main subspaces: Statistical (Linear (e.g. PCA, LDA, and ICA) and Non- Linear (e.g. KPCA)), Neural (e.g. DLA, MLP) and Hybrid (e.g. PCA with DLP) [9], [14]-[15].

3.2.1 PRINCIPLE COMPONENT ANALYSIS:

This method is used for dimension reduction and feature extractions. Turk and Pentland were first used PCA for human face recognition [16], and the person faces reconstruction was done by Kirby and Sirovich [17]. This strategy helped to reduce
the dimensionality of the original data by extracting the main components of multidimensional data [18]-[19]. The face recognition process is based on the new obtained data. The illumination normalization is very much necessary for Eigenfaces. Instead of Eigenfaces, Eigenfeatures like eye, nose, mouth, cheeks, and so forth is used. Calculating the subspace of the low dimensional representation is used for data compression [16], [20]-[23]. The work [24] done by (Abdullah et al., 2012) presented three experiments to enhance PCA efficiency by reducing the computational time while keeping the performance same. The results showed that the accuracy is same with the second experiment with less computational time. According to this approach, the computation time reduced by 35% compared with the original PCA method especially with a large database. While, (Mohit P. Gawande et al., 2014) [25] has proposed a new face recognition system for personal identification and verification using different distance classifiers with PCA. This technique is applied on ORL database. The experiment results show that PCA provided improved results using Euclidian distance classifier and the squared Euclidian distance classifier than the City Block distance classifier, which gives better results than the squared Chebyshev distance classifier. While, using the Euclidian and the Squared Euclidian distance classifier, the recognition rate is the same. In addition, (Poon et al., 2016) [26] presented several techniques for illumination invariant were examined and determine powerful one for face recognition that works better with PCA. The selected technique is named Gradient faces and at the pre-processing stage the experimental results showed that improves the recognition rate. Whereas, (Barnouti, N.H., 2016) [27] Illustrate a system using PCA-BPNN with DCT. In this method, PCA is combined with BPNN, and from face recognition view, the technique

will distinguish human faces easily. Also, the face databases are compressed using DCT. The recognition rate of this method is more than 90% that carried out on Face94 and Grimace face databases. In contrast, (Fares Jalled 2017) [28] Proposed "Normalized Principal Component Analysis (NPCA) for face recognition". The experiment result of face recognition performance rate is carried out on the ORL and Indian Face Database.

3.2.2 INDEPENDENT COMPONENT ANALYSIS (ICA)

This algorithm is a linear combination of statistically independent data points. The main goal of this technique in contrast of PCA which supply an independent image representation instated of uncorrelated one of PCA [29]. ICA minimizes the input of both second-order and higher-order dependencies. It follows the Blind Source Separation (BSS) problem; it aims to decompose an observed signal into a linear combination of unknown independent signals [30]-[31]. The research [32] (Sharma and Dubey, 2014) provided face recognition system using PCA–ICA, and training using neural networks as a Hybrid feature extraction. This technique extracts the invariant facial features by implementing PCA/ICA-based facial recognition system to build a refined and reliable face recognition system. Also, in [33] (Kailash J. et al., 2016) it has been illustrated that the cost function is reduced to maximizing the independence of extracted features as well as the sum of the mutual information between extracted features and a target variable. The global feature extraction based on edge information, and the local features based on modular ICA which is used in this research. As a summary, the new technique of feature extraction work will give future direction for the research in biometrics field.

3.2.3 HIDDEN MARKOV MODEL (HMM)

This approach is used within speech application. Using this method in face recognition will automatically split the faces into different areas, such as the eyes, nose, and mouth, which can be related with the situations of an HMM [30]-[34]. (P. Phaneemdra et al.,2015) [35] presented that, the insignificants pixels of the face have been taken as blocks and apply the Discrete Cosine Transform (DCT) on face image's blocks. Also, reducing the dimensionality for the result of applying the DCT using PCA method directly which makes the technique very fast. The experiments show the recognition rate obtained using this method is 95.211% when using half of the images for training from ORL database.

3.2.4 KERNEL PRINCIPAL COMPONENT ANALYSIS (KPCA)

The main idea of KPCA is to first map the input space into a feature space using nonlinear mapping and then to calculate the principal components in that feature space. Also, KPCA requires the solution of an eigenvalue problem, which does not requires additional optimization. Furthermore, the number of principal components need not be specified previously to modeling [8].

(Wang and Zhang, 2010) [36] Proposed a new method for extracting suitable features and handling face expressions. In this study, the polynomial kernel is successfully employed. Also, for classification, they used the Euclidean distance and k-nearest neighbor. The experiment results are similar of these obtained by traditional PCA-based methods. While, (Vinay et al., 2015) [37] presented a study, a comparison between Gabor-PCA and Gabor-KPCA variants has performed to show the dissimilarity in performance between them. The comparison used the ORL database to test the system performance. The results illustrated that the GABOR-PCA was more successful than Gabor-KPCA by 6.67%, 0.83%, 12.00% and 4.17% using Euclidean, Cosine, City Block and MAHCOS distances respectively.

3.2.5 LINEAR DISCRIMINANT ANALYSIS (LDA)

This algorithm also is called Fisherface which uses a supervising learning method by it using more than one training image for individual class. Also, this method searches linear mixtures of features while conserving class separately. In addition, it is tries to model the differences among different classes (unlike PCA algorithm) and it distinguishes between the differences inside a person and the others persons. Whereas, PCA emphases on discovering the all-out variation within a pool of pictures. LDA is less sensitive to light, pose, and expressions [38],[46]. (Changhui Hu et al. 2015)[39] presented decomposition of an image sample and its transpose is performed by the reverse thinking method which is applied by using experimental analysis, using the Lower-Upper (LU) decomposition algorithm. After that, a projection space evaluation is done using the Fisher Linear Discriminant Analysis (FLDA). Finally, the Euclidean distance is adapted as classifier. This technique is applied on face FERET, AR, ORL and Yale B databases and the results gives a better efficiency. While, Arabia SOULA et al, 2016[40] offered a method of classification using the distinctiveness of Gabor features and the robustness of ordinal measures based on Kernel Fisher Discriminant Analysis. The face image blocks are concatenated and the PCA is used

in dimension reduction of a feature vector. Each feature vector is considered as a feature input for the proposed Multi-Class KFD classifier based on RBF Kernel is represented by the feature vector. The results obtained on ORL and Yale face showed that the performance improved as (88.8%) over the LDA (33.3%).

3.2.6 KERNEL LINEAR DISCRIMINANT ANALYSIS (KLDA)

Kernel algorithm exploits the higher order statistics. This technique can calculate the dot products of two feature vectors. The kernel strategy constructs of nonlinear forms for any method that can be communicated exclusively in term of dot products results. And increase in dimensionality is given, the mapping is done by using kernel functions that satisfy Mercer's theorem which is more economical and efficient [9],[41]. In [42] (Naveen Kumar H N et al.) , Histogram of Oriented Gradient (HOG) elements, and Support Vector Machine (SVM) is utilized for characterization. The proposed work is applied on Cohn-kanade data index for six essential expressions. The result showed that, it has a superior rate when shape and appearance elements are utilized as opposed to surface or geometric elements. But, in (Farag G. Zbeda et al. 2016) [43] they used HOG and PCA techniques, the proposed technique firstly, extracted features at different scales using HOG method, next, PCA used on these feature vectors. The experiment results show gives an equivalent recognition rate at very small size with a low resolution where the face details are hard to be distinguished.

4. DISTANCE MEASUREMENTS AND CLASSIFICATION

There are several distance measurements methods for face recognition are used as illustrated below:

4.1 EUCLIDEAN DISTANCE

It is a common method and it is defined as the straight-line distance between two points, which examines the root of square differences between the coordinates of a pair of images. Euclidean distance computed using the Equation (1)

$$D(x.y) = \sqrt{\sum_{i=0}^{n}(x_i - y_i)^2} \qquad (1)$$

Suppose *x* is a test image and *y* is a training image, where n is the number of images. A minimum Euclidean Distance classifier is used as a condition to find the best- matched test image in the training samples [45].

4.2 SQUARE EUCLIDEAN DISTANCE (SED)

This method is obtained without the square roots. The equation becomes as shown in Equation (2): [25],[46]:

$$\text{Squerd ED}(x.y) = \sum_{i=1}^{No.\ of\ images}(x_i + y_i)^2 \qquad (2)$$

4.3 CHEBYSHEV DISTANCE

Chebyshev distance also is known maximum metric. The maximum metric (distance) between two vectors x and y, with standard coordinates x_i and y_i, respectively, is obtained by the Equation (3): [25],[9]

$$\lim_{n\to\infty}(\sum_{i=1}^{n}|x_{i-}\ y_i|n)^{\frac{1}{n}} \qquad (3)$$

4.4 CITY BLOCK DISTANCE:

This method also is known Manhattan Distance Classifier. The sum of absolute differences between two vectors is called the L1 distance, or city-block distance. This classifier used the Equation (4): [25],[46]:

$$City\ Block(x.y) = |x - y| = \sum_{i=0}^{No.of\ Images}|x_i - y_i| \qquad (4)$$

4.5 K-NEAREST NEIGHBOR

The K-NN classifier is a popular classifier for face recognition in terms of time consuming. Also, this classifier is the simplest one among other classifier algorithms. While other methods for example SVM is better in term of accuracy. The K-NN is based on the closest training samples on the feature space. The input image test recognized due to the nearest point with the training images data set [47].

4.7 SUPPORT VECTOR MACHINE (SVM) AND MULTI-CLASS SVM (MCSVM)

Support Vector Machine (SVM) is one of the most popular techniques in classification problems. A classification algorithm that has successfully been used in this framework is the all-known (SVM). In contrast, this method cannot be applied only when the feature vectors defining samples have missing entries. The SVM classifier has the advantage over the traditional neural network which it can achieve better generalization performance and Multi-Class SVM has better performance and accuracy with other classification types [48]-[49].

4.8 ARTIFICIAL NEURAL NETWORK (ANN)

It is a well-known and robust classification technique which is used for face recognition systems. In the face recognition process, several structures of ANN are utilized for classification, such as Retinal Connected Neural Network, Polynomial Neural Network, Convolutional Neural Network, Evolutionary Optimization of Neural Networks and Back Propagation Neural Networks. The importance of this classifier because of its reacts as human brain [50].

5. STANDARD FACE DATABASES IN BIOMETRIC

Biometric systems for recognition based human faces are based on several databases. The database shows “usual” variability in facial expression, resolution, pose, gender, age, lighting, focus, background make-up, photographic, quality, accessories, occlusions, and race. [27],[51]. Below some of these databases:

5.1 FACE94 DATABASE

The Face 94 database holds 153 images, each with a resolution of 180x200 pixels, and the directories include images of female and male persons in separate directories. Some of the images are taken with glasses, and a mixture of tungsten and fluorescent overheads and the lighting is artificial [51]-[52].

5.2 FERET DATABASE

The images included in this database are parted into two sets: gallery and probe images. The images in Gallery parts are with known labels, while the images in probe part are matched with gallery images for identification [53].

5.3 AT&T (ORL) DATABASE

The ORL database contains 40 different persons (subjects) with 10 images for the individual person, with the total of 400 images. The resolution of each image is 92x112 pixels, for a total of 10,304 pixels, and the file's extension is stored in PGM format [44],[54].

5.5 YALE FACE DATABASE B

The database images consist of 10 persons and recorded in 9 poses (5 poses at 12°, 3 poses at 24°, and 1 frontal view from the camera axis) under 64 different lighting conditions [44],[54].

5.7 INDIAN DATABASE

The Indian contains person face images in JPEG, 24-bit RGB format, and the resolution of these images is 180x200 pixel portrait formats with the plain background. There are 20 persons each having 20 images. All the images have a bright homogeneous background, with variant positions [41],[51].

6. CONCLUSIONS

This paper has attempted to review a significant number of papers to cover the recent development in the field of face recognition. This paper has attempted to illustrate the importance of face recognition and its various applications field, techniques, classification, distance measurements, face databases are deliberated. Also, review a significant number of papers to cover the recent development in the field of face recognition. Face recognition is done by several types of algorithms – appearance-based and model-based or combination of this tow types named hybrid approaches. Present research reveals that for enhanced face recognition new algorithm must evolve using hybrid methods. Face expression, occlusion, pose variation and illumination problems are still challenging. Distance Measurement methods such as Euclidean Distance, City Block ... etc. are necessary for recognition process are discussed. In addition, some of the standard face recognition databases and its properties such as ORL, and Indian etc., are discussed which are used to test any new proposed system performance. Finally, for more detailed understanding of reviewed approaches, the list of references is enlisted.

REFERENCES

[1] Rabia Jafrial, "A Survey of Face Recognition Techniques", Journal of Information Processing Systems, Vol.5, No.2, June 2009.

[2] Ghazi Mohammed Zafaruddin et al., "Face Recognition: A Holistic Approach Review", IEEE, 2014.

[3] Ardinintya Diva Setyadi et al., "Human Character Recognition Application Based on Facial Feature Using Face Detection", IEEE, International Electronics Symposium (IES), 2015.

[4] Stan Z. Li and Anil K. Jain, "Handbook of Face Recognition", Springer, ISBN 978-0-85729-931-4, e-ISBN 978-0-85729-932-1, Second Edition, 2011.

[5] Divyarajsinh N. Parmar et al., "Face Recognition Methods & Applications ", IJCTA, Int.J.Computer Technology & Applications, Vol. 4 (1), 84-86, ISSN: 2229-6093, 2013.

[6] Pallabi Parveenet al.," Face Recognition using Multiple Classifiers", Proceedings of the 18th IEEE International Conference on Tools with Artificial Intelligence (ICTAI'06) 2006.

[7] Laurenz Wiskott et al., " Face Recognition by Elastic Bunch Graph Matching", In Intelligent Biometric Techniques in Fingerprint and Face Recognition, eds. L.C. Jain, publ. CRC Press, ISBN 0-8493-2055-0, Chapter 11, pp. 355-396, (1999).

[8] Uma Shankar Kurmi et al. "Study of Different Face Recognition Algorithms and Challenges", International Journal of Engineering Research (ISSN:2319-6890)(online),2347-5013(print),Volume No.3, Issue No.2, pp:112-115 01 Feb. 2014.

[9]Nawaf Hazim Barnouti et. al., "Face Recognition: A Literature Review", International Journal of Applied Information Systems (IJAIS) – ISSN: 2249-0868 Foundation of Computer Science FCS, New York, USA Volume 11 – No. 4, September 2016 – www.ijais.org, 2016.

[10] Ankur Patel et al., "3D Morphable Face Models Revisited", 978-1-4244-3991-1/09, IEEE, 2009.

[11] Guosheng Hu et al., "Robust face recognition by an albedo based 3D morphable", 2014.

[12] Changxing Ding et al. "Pose-invariant face recognition with homography-basednormalization",Elsevier,http://dx.doi.org/10.1016/j.patcog.2016.11.024; Accepted 28 November 2016.

[13] Deepali H. Shah et al.," The Exploration of Face Recognition Techniques ", International Journal of Application or Innovation in Engineering & Management (IJAIEM) Volume 3, Issue 2, February 2014 ISSN 2319 – 4847, 2014.

[14] Michelle Strout et al, "FacePerf: Benchmarks for Face Recognition Algorithms",Conference Paper October 2007 DOI: 10.1109/IISWC.2007.4362187 · Source: IEEE Xplore, 2007.

[15] Ghazi Mohammed Zafaruddin et al., "Face Recognition: A Holistic Approach Review", IEEE, 2014.

[16] Sujata G. Bheleet al., "A Review Paper on Face Recognition Techniques", International Journal of Advanced Research in Computer Engineering & Technology (IJARCET), Volume 1, Issue 8, October 2012.

[17] Yong Xu et al., "Using Discriminant Eigenfeatures for Image Retrieval", IEEE, Transaction on pattern analysis and machine intelligence, VOL. 18, NO. 8, AUGUST 1996 .

[18] Marijeta Slavković et al., "Face Recognition Using Eigenface Approach", Serbian journal of electrical engineering,Vol. 9, No. 1, February 2012, 121-130.

[19] Nawaf Hazim Barnouti et al.,"Improve Face Recognition Rate Using Different Image Pre-Processing Techniques", International Journal of Computer Applications (0975 – 8887) Volume 142 – No.6, May 2016.

[20] Nilind Sharma et al.," Face Recognition Analysis Using PCA, ICA and Neural Network", International Journal of Digital Application & Contemporary research Website: www.ijdacr.com (Volume 2, Issue 9, April 2014).

[21] Krishna Dharavath et al., "Improving Face Recognition Rate with Image Preprocessing", Indian Journal of Science and Technology, Vol 7(8), 1170–1175, August 2014.

[22] Parvinder S. Sandhu et al., "Face Recognition Using Eigen face oefficients and Principal Component Analysis", International Journal of Computer, Electrical, Automation, Control and Information Engineering Vol: 3, No: 4, 2009.

[23] Ratnawati Ibrahim et al., "Study of Automated Face Recognition System for Office Door Access Control Application", IEEE, 2011.

[24] Manal Abdullah et al., "OPTIMIZING FACE RECOGNITION USING PCA", International Journal of Artificial Intelligence & Applications (IJAIA), Vol.3, No.2, March 2012.

[25] Mohit P. Gawande et al., "Face recognition using PCA and different distance classifiers" IOSR Journal of Electronics and Communication Engineering (IOSR-JECE) e-ISSN: 2278-2834, Volume 9, Issue 1, Ver. VI (Feb. 2014), PP 01-05.

[26] Bruce Poon et. al., "PCA Based Human Face Recognition with Improved Methods for Distorted Images due to Illumination and Color Background", IAENG International Journal of Computer Science, 43:3, IJCS_43_3_02, 2016.

[27] Nawaf Hazim Barnouti, "Face Recognition using PCA-BPNN with DCT Implemented on Face94 and Grimace Databases International Journal of Computer Applications (0975 – 8887) Volume 142 – No.6, May 2016.

[28] Fares Jalled, "Face Recognition Machine Vision System Using Eigenfaces", arXiv: 1705.02782v1 [cs.CV] 8 May 2017.

[29] Aapo Hyv¨arinen et al., "Independent Component Analysis", A WileyInter science Publication, JOHN WILEY & SONS, INC,2001.

[30] Deepali H. Shah et al., "The Exploration of Face Recognition Techniques", International Journal of Application or Innovation in Engineering & Management (IJAIEM), Volume 3, Issue 2, February 2014.

[31] Önsen et al., "FACE RECOGNITION USING PCA, LDA AND ICA APPROACHES ON COLORED IMAGES", ISTANBUL UNIVERSITY – JOURNAL OF ELECTRICAL & ELECTRONICS ENGINEERING, 2003.

[32] Nilind Sharma et al., "Face Recognition Analysis Using PCA, ICA And Neural Network International Journal of Digital Application & Contemporary research Website: www.ijdacr.com (Volume 2, Issue 9, April 2014).

[33] Kailash J. Karande et al., "Facial Feature Extraction using Independent Component Analysis", Annual Int'l Conference on Intelligent Computing, Computer Science & Information Systems (ICCSIS-16) April 28-29, 2016 Pattaya (Thailand).

[34] Yi Sun, Xiaochen Chen et al., "Tracking Vertex Flow and Model Adaptation for Three-Dimensional Spatiotemporal Face Analysis", IEEE: System and humans, VOL. 40, NO. 3, MAY 2010.

[35] P. PHANEEMDRA et al., "Human Face Detection and Recognition using PCA and DCT in HMM", International journal of scientific engineering and technology research, ISSN 2319-8885 Vol.04, Issue.35, pp.: 7080-7085, 2015.

[36] Yanmei Wang et al., "Facial Recognition Based on Kernel PCA", Third International Conference on Intelligent Networks and Intelligent Systems, 2010.

[37] Vinay.A et al., "Face Recognition using Gabor Wavelet Features with PCA and KPCA - A Comparative Study", 3rd International Conference on Recent Trends in Computing (ICRTC-2015).

[38] Marryam Murtaza et al., "Face Recognition Using Adaptive Margin Fisher's Criterion and Linear Discriminant Analysis (AMFC-LDA)" , The International Arab Journal of Information Technology, Vol. 11, No. 2, March 2014.

[39] Changhui Hu et al., "A new face recognition method based on image decomposition for single sample per person problem", Neurocomputing, http://dx.doi.org/10.1016/j.neucom. 2015.

[40] Arbia SOULA et al., "A Novel Kemelized Face Recognition System" , Proceedings of 2016 4th International Conference on Control Engineering & Information Technology, Tunisia, Hammamet- December, 16-18, 2016.

[41] Umesh Ashok Kamerikar et al., "Experimental Assessment of LDA and KLDA for Face Recognition", International Journal of Advance Research in Computer Science and Management Studies, ISSN: 2321-7782 (Online), Volume 2, Issue 2, February 2014.

[42] Naveen Kumar H N et al., "Human Facial Expression Recognition from Static Images using Shape and Appearance Feature", IEEE, 2016.

[43] Farag G. Zbeda et al., "PCA-HOG Descriptors for Face Recognition in very Small Images", International Journal of Advanced Research in Computer Science and Software Engineering, Volume 6, Issue 9, September 2016.

[44] Nawaf Hazim Barnouti et al., "Improve Face Recognition Rate Using Different Image Pre-Processing Techniques", American Journal of Engineering Research (AJER) e-ISSN: 2320-0847 p-ISSN: 2320-0936 Volume-5, Issue-4, pp-46-53, 2016.

[45] Jiali Yu et al., "Face Recognition Based on Euclidean Distance and Texture Features", IEEE, International Conference on Computational and Information Sciences, 2013.

[46] Kuldeep Singh Sodhi et al., "FACE RECOGNITION USING PCA, LDA AND VARIOUS DISTANCE CLASSIFIERS", Journal of Global Research in Computer Science, Volume 4, No. 3, March 2013.

[47] Dhriti et al., " K-Nearest Neighbor Classification Approach for Face and Fingerprint at Feature Level Fusion International Journal of Computer Applications (0975 – 8887) Volume 60– No.14, December 2012.

[48] Navpreet Kaur, "Review of Face Recognition System Using MATLAB", International Journal of Computer Science Trends and Technology (IJCST) – Volume 4 Issue 3, May - Jun 2016.

[49] Supriya D. Kakade, "A Review Paper on Face Recognition Techniques", International Journal for Research in Engineering Application & Management (IJREAM), ISSN: 2494-9150 Vol-02, Issue 02, MAY 2016.

[50] Omaima N. A. AL-Allaf, " REVIEW OF FACE DETECTION SYSTEMS BASED ARTIFICIAL NEURAL NETWORKS ALGORITHMS", The International Journal of Multimedia & Its Applications (IJMA) Vol.6, No.1, February 2014.

[51] Nawaf Hazim Barnouti et al., "Face Detection and Recognition Using Viola-Jones with PCA-LDA and Square Euclidean Distance", International Journal of Advanced Computer Science and Applications, Vol. 7, No. 5, 2016.

[52] Kiran D. Kadamet al., "Face Recognition using Principal Component Analysis with DCT" , International Journal of Engineering Research and General Science Volume 2, Issue 4, ISSN 2091-2730, June-July, 2014.

[53] A. Gumedeal. , "Hybrid Component-based Face Recognition", IEEE, 2017.

[54] Kuldeep Singh Sodhi, "Comparative Analysis of PCA-based Face Recognition System using different Distance Classifiers", International Journal of Application or Innovation in Engineering & Management (IJAIEM), ISSN 2319 - 4847 ,Volume 2, Issue 7, July 2013.

CLASSICAL CRYPTOGRAPHY FOR KURDISH LANGUAGE

Najdavan A. Kako

Duhok Polytechnic University
najdavan.kako@dpu.edu.krd

doi:10.23918/iec2018.02

ABSTRACT

The most important concern in different data communication and transmission is to secure this data for every county individually. To transmit data through unsecure channel we need to use cryptographic algorithms, Kurdish language spoken by more than five million people. Unfortunately, there is no use of this language alphabet in data encryption and decryption. The purpose of this paper is to introduce the Kurdish alphabet usage in cryptography with a new symmetric algorithm which consist of 34 letters with using its ASCII Unicode and distributing the keys over the secure channel to decipher the text. This is the first attempt to apply an algorithm on the Kurdish characters.

Keywords: Symmetric, Asymmetric, Kurdish language, Modular.

1. INTRODUCTION

Data security known is a set of techniques to write a message in an encrypted form and sent it between the sender and the recipient, the first use of cryptography goes back to 1900 BC when the Egyptians used hieroglyphs to serve the Pharaohs [1]. According to some experts' statements, the cryptography appeared spontaneously after the invention of the writing arts with applications between diplomatic letters to the battle plans in the war [2, 3]. After the widespread of computers and developing it in communications and networking fields the new format of cryptography is appeared. When transferring and communicating data, the encryption is very important, especially in non-trusted environment, which includes networks in general and the internet in special. The clear text or plaintext is the data that can be easily read and understood without any particular alteration. The way to hide and disguise this data is called encryption. The ciphertext or the mysterious text is a non-readable and not understandable text, which was conducted by the cryptographic operations. Restoring the ciphertext to the original text is called decryption. The goals that must be achieved to achieve data security are:

- Authentication: The emphasis that the communicating object is the one that it affirms to be.
- Access Control: The averting of unauthorized employ of a recourse
- Data Confidentiality: The averting of data from unauthorized detection.
- Data Integrity: to ensure that data receipted are exactly as sent by an authorized object.
- Nonrepudiation: Provides security against negation by one of the entities included in a connection of having shared in all or part of the connection.
- Availability Service: Proof that the message was sent from a specific destination [4, 5].

The secret key is also embedded to the encryption algorithm, donor and recipient must have gained copies of the secret key in a secure pattern and must keep the key secure. The secret key is classified in cryptography in general either is stream cipher or a block cipher. Stream cipher works on one bit at time with implementation some form of feedback, so the key is constantly changing. Therefore, the cryptography

does not only protect data from theft or changing, but, can be used to authenticate users. In general, there are three schemes of cryptographic that typically used to realize these goals: symmetric cryptography (or secret key), asymmetric cryptography (or public-key) and hash functions. Anyways, preliminary unencrypted data have referred to as plaintext. It is enciphered into cipher text, which will in turn usually be deciphered into usable plaintext [6, 7].

2. LITERATURE REVIEW

Symmetric key algorithm using ASCII characters proposed by Ayushi (2010). Anyone can be understood the message in clear text knowing the language if there is no codified method applied to the message in any way. Thus, we have to hide information from anyone for whom it is purposed, even they are on observation for encrypted data to ensure that we must use coding scheme [8].

An encryption algorithm based on ASCII value of data proposed by Satyajeet R. Shinge, Rahul Patil proposed (2014). They used a symmetric cryptographic algorithm based on the ASCII values of characters in the plaintext to encrypt and decrypt data. The timely execution of suggested algorithm was better and less. To encrypt the message the technique generates key spontaneously and it is transformed to another string for both encryption and decryption [9].

The effective symmetric key algorithm on Arabic characters introduce by Prakash Kuppuswamy, Yahya Alqahtani (2014). They proposed an integer value numerate from 0-9 called synthetic value assigning to a modular 37 and Arabic letters. Select an integer value and calculate its inverse with modular 37. To decrypt messaging the symmetric key allocation should be executed over the secured channel [10].

A. Vijayan, T. Gobinath and M. Saravanakarthikeyan (2016) in this research, they introduce an algorithm called AVB algorithm "ASCII value based encryption system" which is used to improve the data safety. The algorithm use ASCII value of data. ASCII value of the character is coded using normal mathematical calculation for number of time on a specific character and transformed to numerical value. Then, the cipher text is decoded to obtain the plain text [11].

In 2016 Pramod Gorakh Patil, Vijay Kumar Verma proposed "a reliable secret key algorithm for encryption and decryption of text data". An effective, reliable

symmetric key based algorithm was proposed by them to encrypt and decrypt the data text. They use ASCII (8 bit) value of characters and implement some simple logical NOT and binary division to calculate and produce. The implementing of the proposed technique is very simple to understand [12].

3. PROPOSED WORK

Since it is a first attempt to use Kurdish letters in cryptography to ensure data transmission their environment. Kurdish language is read and write in two ways either as a Latin alphabet or Arabic (Persian) alphabet, which is the official language in the country and starting from right to left, but we have proposed in our experiences the text that begins from left to right as it is in the English alphabet. One of the defying parts of modern computer science is to encipher and decipher the data in an effective way. In this research, we propose an algorithm that uses the ASCII values of the plaintext to encrypt it. This method randomly generates a key to uses it with encryption and decryption. Because of using the same key in the encryption and decryption procedure, it can be said that this is symmetric cryptographic algorithm. Whoever, the user Identification involve of Kurdish alphabets consist 34 letters. We are making a synthetic table using Kurd letters and their ASCII given in the Table 1.

TABLE 1.

ASCII for Kurdish Letters

ڕ	ر	د	خ	ح	چ	ج	ت	پ	ب	ا	ئ
12	11	10	9	8	7	6	5	4	3	2	1
1685	1585	1583	1582	1581	1670	1580	1578	1662	1576	1575	1574
ل	گ	ک	ق	ڤ	ف	غ	ع	ش	س	ژ	ز
24	23	22	21	20	19	18	17	16	15	14	12
1604	1711	1705	1602	1700	1601	1594	1593	1588	1587	1688	1586
		ێ	ی	ه	ھ	وو	ۆ	و	ن	م	ڵ
		34	33	32	31	30	29	28	27	26	25
		1742	1740	1749	1607	1735	1734	1608	1606	1605	1717

New Symmetric Key Algorithm

Key generation

Step 1: Choose randomly any number to be a key1

Step 2: Choose again any number making key2 then repeat step 2.

Step 3: Using modulo 1720 to find the inverse of key2.

Encryption algorithm

Step 1: Generate the decimal value of the character using text-to-decimal converter

Step 2: Add character value with random selected key1.

Step 3: Multiply the step 2 output with random selected key2

Step 4: Calculate with modulo 1720.

Step 5: Convert Decimal to Text

Decryption algorithm

Step 1: Convert text to decimal

Step 2: Multiply received letter with inverted key2

Step 3: Subtract the result of step 2 with key1

Step 4: Calculate with modulo 1720.

Step 5: Convert decimal to text.

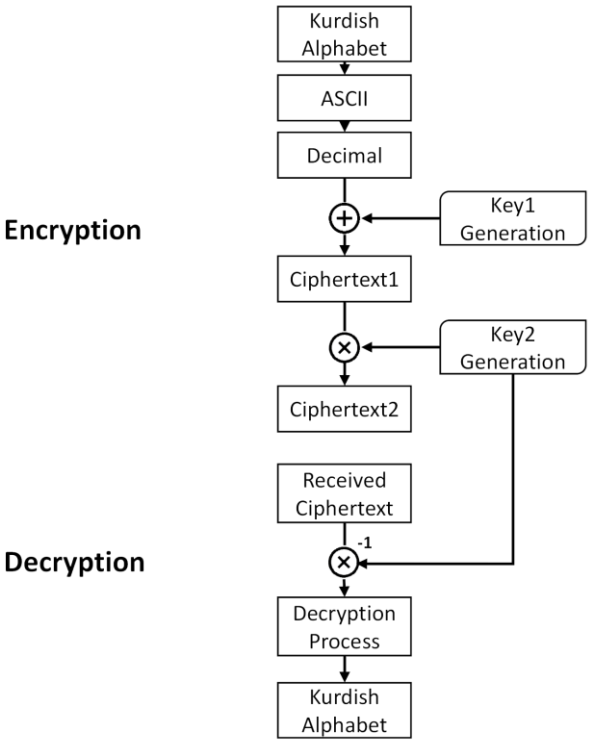

FIGURE 1. Encryption/Decryption Algorithm

4. IMPLEMENTATION

The effect of security is to encrypt text professionally that can abate the value of protest and capability of edition and falsehood. The confidentiality of data needs the encryption clearly to address. Furthermore, it can be used to achieve the privacy of data that can be read only for authorized one and difficult to modify in significant behavior. It is a keystone of network protocols security to be provided to accomplish network tasks. The results are described through an agreed-on sequence of protocol action. A good example when some users required the availability of resources for some operating system at different tasks. Hence, encryption is support availability. So, the heart of computer security is encryption.

ئەگەر هوین نەبن یەک

TABLE 2.
Kurdish Decimal Values.

ی	و	ھ	ر	ە	گ	ە	ئ
1740	1608	1607	1585	1749	1711	1749	1574
ک	ە	ی	ن	ب	ە	ن	ن
1705	1749	1740	1606	1576	1749	1606	1606

Processing of key

1) Choosing a two random integer number to be key1 =17 and key2= 41.

2) Finding modular multiplicative inverse for key2 = 881 to use in decrypting.

Encrypti

TABLE 3.
Encryption Method.

PT	Text to Decimal	add key1 = 17	Multiply by key2 =41	mod 1720	Decimal to Text
ئ	1574	1591	65231	1591	ط
ه	1749	1766	72406	166	¦
گ	1711	1728	70848	328	ň
ه	1749	1766	72406	166	¦
ر	1585	1602	65682	322	ł
ھ	1607	1624	66584	1224	ђ
و	1608	1625	66625	1265	ÿ
ی	1740	1757	72037	1517	□
ن	1606	1623	66543	1183	ƙ
ن	1606	1623	66543	1183	ƙ
ه	1749	1766	72406	166	¦
ب	1576	1593	65313	1673	ۄ
ن	1606	1623	66543	1183	ƙ
ی	1740	1757	72037	1517	□
ه	1749	1766	72406	166	¦
ک	1705	1722	70602	82	R

Decryption

TABLE 4.
Decryption Method.

CT	Text to Decimal	Multiply by inv. key2 = 881	Subtract with key1 =17	mod 1720	Decimal to Text
ط	1591	1401671	1401654	1574	ئ
¦	166	146246	146229	29+1720	ه
ň	328	288968	288951	1711	گ
¦	166	146246	146229	29+1720	ه
ł	322	283682	283665	1585	ر
ђ	1224	1078344	1078327	1607	ھ
ÿ	1265	1114465	1114448	1608	و
□	1517	1336477	1336460	20+1720	ی
ƙ	1183	1042223	1042206	1606	ن
ƙ	1183	1042223	1042206	1606	ن
¦	166	146246	146229	29+1720	ه
ۄ	1673	1473913	1473896	1576	ب
ƙ	1183	1042223	1042206	1606	ن
□	1517	1336477	1336460	20+1720	ی
¦	166	146246	146229	29+1720	ه
R	82	72242	72225	1705	ک

5. CONCLUSION

In this work we attempted an algorithm to encipher and decipher Kurdish letters employing decimal value of its letters to secure Kurdish communications. A two keys are used for encryption/decryption. The algorithm was tested for different sizes of messages and the method of trying Kurdish letters it has been used on other cryptography algorithm. The results exhibits that the proposed method is progressed the performance interaction, however the good quality of security services are provided for Kurds communication in different fields.

6. FUTURE WORKS

Each letter of international languages have a certain frequency depending on its repetition in writing and this method is used as an aid to breaking algorithms. In future we will conduct the frequency analysis of Kurdish letters in both dialects (Kurmanji and Surani) over many sources to get stable distribution of letter frequency analysis.

REFERENCES

[1] A. D'Agapeyeff, "Codes and Ciphers," A History of Cryptography, Blackfriars Press, 1949.

[2] W. F. Friedman, "History of the Use of Codes," Aegean Park Press, Laguna Hills, CA, 1977.

[3] R. Nichols, Lanaki's. "Classical Cryptography Course," Lecture 6, Part II: "Arabian Contributions to Cryptology", American Cryptogram Association, Jan. 1996. Accessed from the web February 9, 2013.

[4] S. William, "Cryptography and Network Security" Principles and Practice, 7th edition, Pearson, Inc., 2017 pp 21-45.

[5] S. Singh, “The Code Book,” The Science of Secrecy from Ancient Egypt to Quantum Cryptography, Anchor Books (a division of Random House), New York, 1999.

[6] M. Cozzens and S. J. Miller, "The Mathematics of Encryption," An Elementary Introduction, Vol. 09, Mathematical World, Providence, Rhode Island: The American Mathematical Society, 2013, pp. 133-180.

[7] S. Singh, “Arab Code Breakers,” SimonSingh.net, 2012, accessed February 14, 2013.

[8] Ayushi, “A Symmetric Key Cryptographic Algorithm”, International Journal of Computer Applications, Vol. 1, No. 3, pp. 1-4, Feb 2010, ISSN: 0975 - 8887.

[9] S. R. Shinge, R. Patil, “An Encryption Algorithm Based on ASCII Value of Data”, International Journal of Computer Science and Information Technologies, Vol. 5, Issue 6, pp. 7232-7234, November 2014, ISSN 0975-9646.

[10] P. Kuppuswamy, S. Al-Khalidi, “New Innovation of Arabic Language Encryption Technique Using New Symmetric Key Algorithm”, International Journal of Advances in Engineering & Technology, Vol. 7, Issue 1, pp. 30-37, March 2014, ISSN: 2231-1963.

[11] A. Vijayan, T. Gobinath and M.Saravanakarthikeyan, “ASCII Value Based Encryption System (AVB)”, International Journal of Engineering Research and Applications, Vol. 6, Issue 6, pp. 08-11, April 2016, ISSN: 2248-9622.

[12] P. G. Patil1, V. K. Verma, “A Reliable Secret Key Algorithm for Encryption and Decryption of Text Data”, International Journal of Recent Trends in Engineering & Research, Vol. 2, Issue 2, pp. 114-118, February 2016, ISSN: 2455-1457.

A COMPARATIVE STUDY OF THE SEISMIC PROVISIONS BETWEEN IRAQI SEISMIC CODES 2014 AND 1997 FOR KURDISTAN REGION/IRAQ

Bahman Omar Taha[1],Sarkawt Asaad Hasan[2]

[1&2] Erbil Polytechnic University
[1]bahman.omar@epu.edu.krd,[2]sarkawt.ashad@epu.edu.krd

doi:10.23918/iec2018.03

ABSTRACT

This paper addresses the effect of the seismic design response spectral acceleration parameters recommended by the Iraq Seismic code 2014 (ISC 2014) compared to that recommended by the previous Iraq Seismic code 1997 (ISC 1997) for the cities of Kurdistan Region of Iraq (Erbil, Duhok, Sulaymaniyah and Halabja). The seismic design response spectral recommended by the ISC 2014 for these cities have been prepared for hard rock, rock, very stiff soil, stiff soil, and soft soil. Then, based on the equivalent lateral force procedure, the base shear calculated using both codes have been compared for two case studies of reinforced concrete building consists of 5 and 15 floors. the results showed that ISC 2014 provisions results in a dramatic increase in the base shear forces especially for the cities of Halabja and Sulaymaniyah, followed by Erbil city, while the effect on Duhok city was relatively low. As a supplementary work, modal response spectrum analysis has been performed using ISC 2014 on a 5 and 15 story regular reinforced concrete framed building constructed on soil type D-stiff soil and located in Erbil to evaluate the results of the equivalent lateral force procedure.based on ISC 2014 provisions, all the buildings in KRI should be assigned to the seismic risk class D, meaning that the building construction system should be either special reinforced concrete frame, special reinforced shear wall, special reinforced masonry wall, special steel frame, or ordinary/intermediate steel frame for specific frame configurations.

Keywords: Iraqi Seismic Code, Response Spectrum, Equivalent Lateral Force, Modal Analysis

1. INTRODUCTION

In spite of the fact that the Kurdistan Region of Iraq (KRI) exhibits low seismicity; it is adjacent to regions that have seen moderate to high seismic activity in the past. The source of the earthquakes affecting KRI exists beyond the north and eastern borders of Iraq (Turkey and Iran), where the Arabian, and Eurasian plates collide generating Intense earthquake activity [1]. In general, small to moderate sized earthquakes frequently occur in Kurdistan, however, in the recent years, the number and the intensity of earthquake hit KRI increased, and the largest one happened recently in Halabja on 12 November 2017; the epicenter of the earthquake was reported to be located at 34.905°N latitude 45.956°E longitude, 93 km SE of As Sulaymaniyah , 30 kilometers south of Halabja with a focal depth of 19 km according to the US Geological Survey [2]. The epicenter was located outside the Iraqi border, but it had a destructive effect on the Iraqi city of Darbandikhan, where many buildings collapsed and many buildings experienced severe damage. The location of the earthquake is consistent with the plate boundary related structures in this region, where the Arabian plate is moving towards the north with respect to Eurasian plate at a rate of about 26 mm/year [3].

The first Iraq seismic code was published on 1997 (ISC 1997) [4], which based mainly on the UBC 1985 [5]. In the ISC 1997, Iraq was divided into four zones, Duhok city was specified as the most active seismic zone (zone III with Z=0.09), while Halabja, Sulaymaniyah and Erbil cities were located in the 2nd zone (zone II with Z=0.07), see Figure 1. In 2013, the draft version of the new Iraqi seismic code ISC 2013 [6] has been published, and the official version of the code appeared as first edition of ISC 2014 [7]. The code is based mainly on the IBC 2012 [8] and ASCE/SEI07-10 [9] with local mapped acceleration parameters S_1 (1.0 Sec period) and S_S (0.2 Sec period) given for soil type B rock. These parameters are taken from the GSHP-USGS-Geologic Hazards Science Center, as stated in the code.

As could be seen in Figure 2, in the ISC 2014, the most vulnerable zone for earthquake is located within the strip from Darbandikhan city to Rania city passing through Sulaymaniyah city. On the other side, Duhok city turned from the city that was more vulnerable to earthquake in ISC 1997 within the Kurdistan region to be the city that is the less vulnerable to earthquake in ISC 2013-Draft and ISC 2014. In

the next sections, ISC 2013-Draft will not be mentioned, as it similar to ISC 2014 for the parameters reported in the current study.

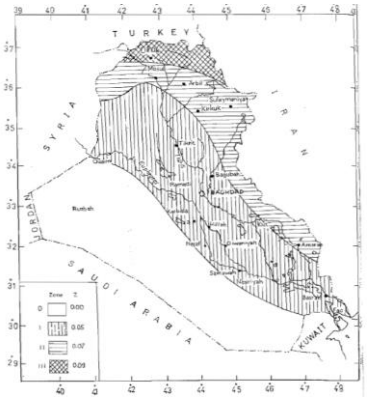

FIGURE 1. Seismic zonic map for Iraq **(**ISC 1997)

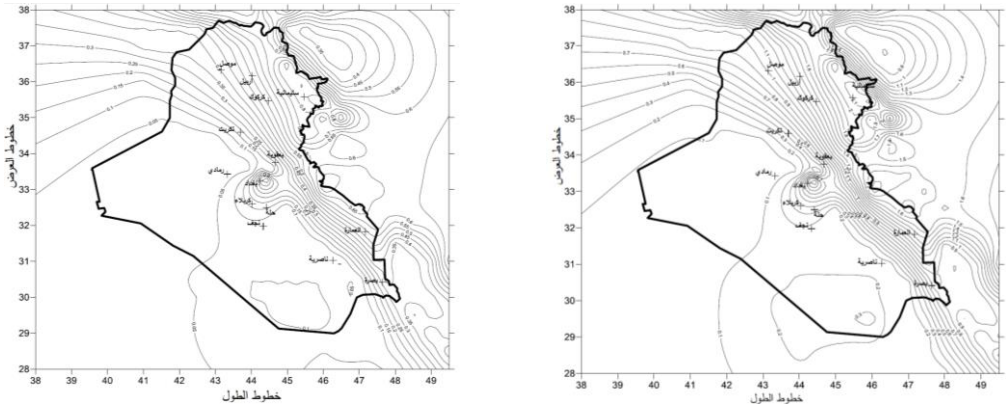

a) 0.2 Sec b) 1.0 Sec

FIGURE 2. Spectral response acceleration (5% of critical damping), site class B rock (ISC 2013-draft and ISC 2014)

In this paper, the ISC 2014 provisions is evaluated through the effects on the base shear force in comparison with that found using ISC 1997 provisions, calculated using equivalent lateral force analysis. For this purpose, two case studies of reinforced concrete framed buildings (5 story and 15 Story) located in the main cities of the KRI (Erbil, Duhok, Sulaymaniyah and Halabja) were taken. The base shear force is the key indicator on the level that the building needs to be proportionated, designed and detailed to resist earthquake forces.

2. ISC 2014 RESPONSE SPECTRUM

The response spectrum components defined in the ISC 2014 is similar to that defined in the IBC 2012 [8] and ASCE/SEI7-10 [9], except for having no long-period transition at large period range, where for all buildings with periods greater than T_s, the spectral response acceleration (S_a) is found by S_{D1}/T, see Figure 3.
Based on ISC 2014 [7], the response spectrum has been prepared for all four main cities in KRI for all soil types as classified by ISC 2014 (A: hard rock, B: rock, C: very stiff soil, D: stiff soil, E: soft soil), see Figure 4. As could be seen, the most vulnerable cities to the effect of the earthquake are Halabja and Sulaymaniyah, while Duhok city is the least vulnerable city within the KRI.

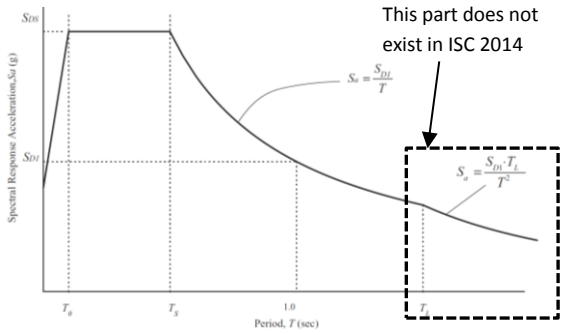

S_s=0.2-second spectral response acceleration, from maps.
S_1=1-second spectral response acceleration, from maps.

S_{MS} = Fa S_S
S_{M1} = Fv S_1
Fa, Fv = Site coefficient, taken from tables based on the soil type and the spectral response acceleration

S_{DS}= 2/3 S_{MS}
S_{D1}= 2/3 S_{M1}
T = the fundamental period of the structure, sec
T_0 = 0.2 (S_{D1} / S_{DS})
Ts = (S_{D1} / S_{DS})

From ISC 2014
S_S= 1.08, S_1= 0.43 (Duhok)
S_S= 1.38, S_1= 0.55 (Erbil)
S_S= 2.10, S_1= 0.84 (Sul.)
S_S= 2.16, S_1= 0.86 (Halabja)

FIGURE 3. Seismic design response spectrum, as defined in ASCE/SEI7-10 [9] and IBC 2012 [8]

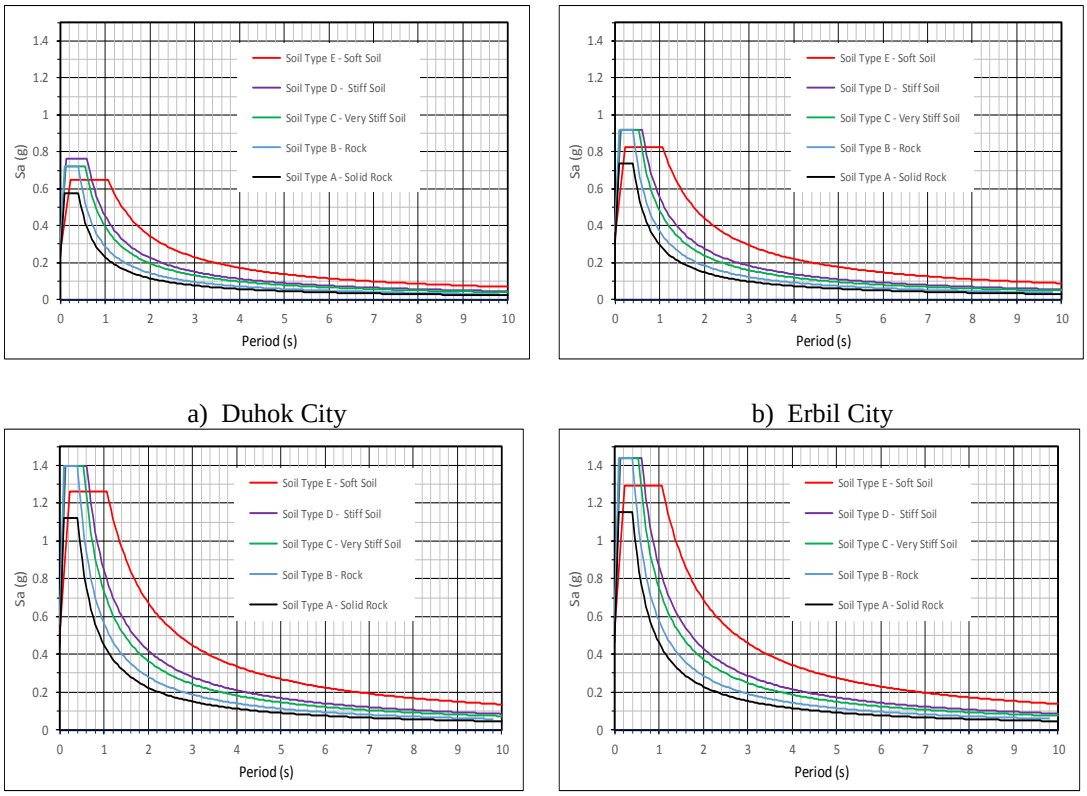

a) Duhok City

b) Erbil City

c) Sulaymaniyah City

d) Halabja City

FIGURE 4. Seismic design response spectrum for the Kurdistan region of Iraq, based on the ISC 2014 [7]

Abdulhameed A. Y et. al. [10] suggested three response spectrums for building design in KRI, see Figure 5, dividing the region into two zones: zone A (the strip at the border with Iran and Turkey) and B (the remaining parts of KRI). These spectra were based on using PGA (Peak Ground Acceleration) equal to 0.5g for zone A, and 0.4g for zone B. In Figure 6, the response spectra for Halabja, Erbil and Duhok cities for the soil types B (rock) and D (stiff soil) as suggested by the ISC 2014 are presented to be compared with Figure 5.

The comparison shows good agreement for Halabja (rock), Erbil (rock) and Erbil (Soil). However, for Duhok city, it is not clear from Figure 5 whether it is included within zone A or B, and no information was found in the paper in the respect. The spectra for Sulaymaniyah is not reported in Figure 6, as they are very close to those reported for Halabja city, see Figure 4.

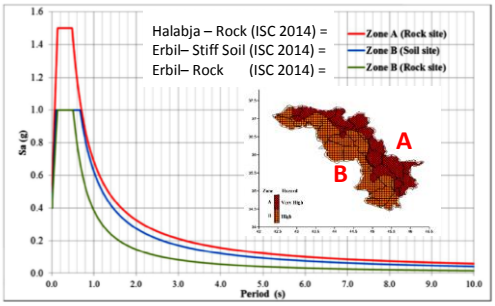

FIGURE 5. Response spectrums for KRI as recommended by Yaseen A. A. et. Al. [10]

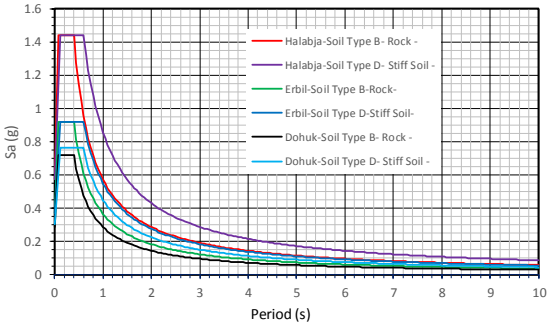

FIGURE 6. Response spectrums for KRS as recommended by ISC 2014 [7]

1. SEISMIC RESPONSE COEFFICIENT (ISC 2014 - ISC 1997)

The reported response spectrums given in Figure 4 could be used in any of the two seismic analysis methods specified by the ISC 2014 [7]: i) Equivalent Lateral Force Analysis (ELFA); ii) Modal Response Spectrum Analysis (MRSA). On the other side, ISC 1997 [4] does not include MRSA as an analysis tool; instead, it specifies the Dynamic Time History Analysis (DTHA) as the 2nd analysis tool. Therefore, for a rational comparison between these two codes, only the ELFA results will be compared in the current paper. for both ISC 1997 and ISC 2014, the seismic response coefficient (Cs), required for the ELFA method, has been constructed for a study case (special reinforced concrete frame building) with high occupancy rate (more than 300 persons) with no special or high importance to the public for all four cities. This case has been chosen because it has the same live load ratio included within the effective seismic weight (W = total dead load + 25 % of the floor live load) in both codes; further, it represents the large percentage of the frame buildings constructed in the KRI region. the Seismic Response Coefficient (C_S) represents the amount of the base shear at the bottom floor taken as a ratio of the total gravity vertical seismic load (W). The procedure for the calculation of the Cs in both codes are summarized in Table 1. The calculated C_S coefficient is shown in Figure 7 for soil of types A, B, C, D and E as classified in the ISC 2014 [7]; by comparing this coefficient between the ISC 2014 and ISC 1997, the change in the base shear will be clear; for comparison purposes, soils of Types I, II and III as specified in the ISC 1997 [4] are equivalent to soil types A-B, C-D, E-F in the ISC 2014 [7], respectively.

TABLE 1.

Details of the equivalent lateral force analysis procedure

ISC 1997 [4]		ISC 2014 [7]	
I	I = 1.0 Class III	I	I = 1.25 Class III
T	0.1 N ; N: Number of floors	T	T = 0.1 N (for 5 story); N: Number of floors $T = 0.044\ h^{0.9}$ (for 15 story); h: floor height
K	K = 0.85 (High ductility moment resisting frame)	R	R = 6.5 (Special RC frame)
Z	Z= 0.09 Duhok Z= 0.07 (Halabja, Sulaymaniyah , Erbil)	(S_S) (S_1)	S_S= 1.08, S_1= 0.43 (Duhok) S_S= 1.38, S_1= 0.55 (Erbil) S_S= 2.10, S_1= 0.84 (Sulaymaniyah) S_S= 2.16, S_1= 0.86 (Halabja)
S	S=0.5/T (rock) S=0.75/T (stiff, medium Stiff Soil) S= 1.0/T (soft Soil); S≤ 1.0 (all soils)	S_{MS} S_{M1}	$S_{MS} = Fa\ S_S$ $S_{M1} = Fv\ S_1$ Fa, Fv = Site coefficient
		S_{DS} S_{D1}	S_{DS}= 2/3 S_{MS} S_{D1}= 2/3 S_{M1}
Cs	Cs=Z K I S	Cs	$Cs = S_{DS} / (R / I)$ $Cs \leq S_{D1} / (R . T / I)$ $Cs \geq 0.044\ S_{D1} I$; $Cs \geq 0.01$
Vs	Vs = Cs W	Vs	Vs = Cs W

I, Importance Factor

T, Building Fundamental period

K, Structural System Coefficient

Z, Seismic Hazard Coefficient

S, Dynamic Coefficient

Cs, Seismic Response Coefficient

Vs, Base Shear

I, Importance Factor

T, Building Fundamental period

R, Response modification coefficient

S_S, Mapped spectral accelerations for short period

S_1, Mapped spectral accelerations for 1-Sec period

S_{MS} S_{M1}, Maximum Considered Earthquake (MCE) spectral response acceleration

S_{DS} S_{D1}, 5% damped Design spectral response acceleration

Cs, Seismic Response Coefficient

Vs, Base Shear

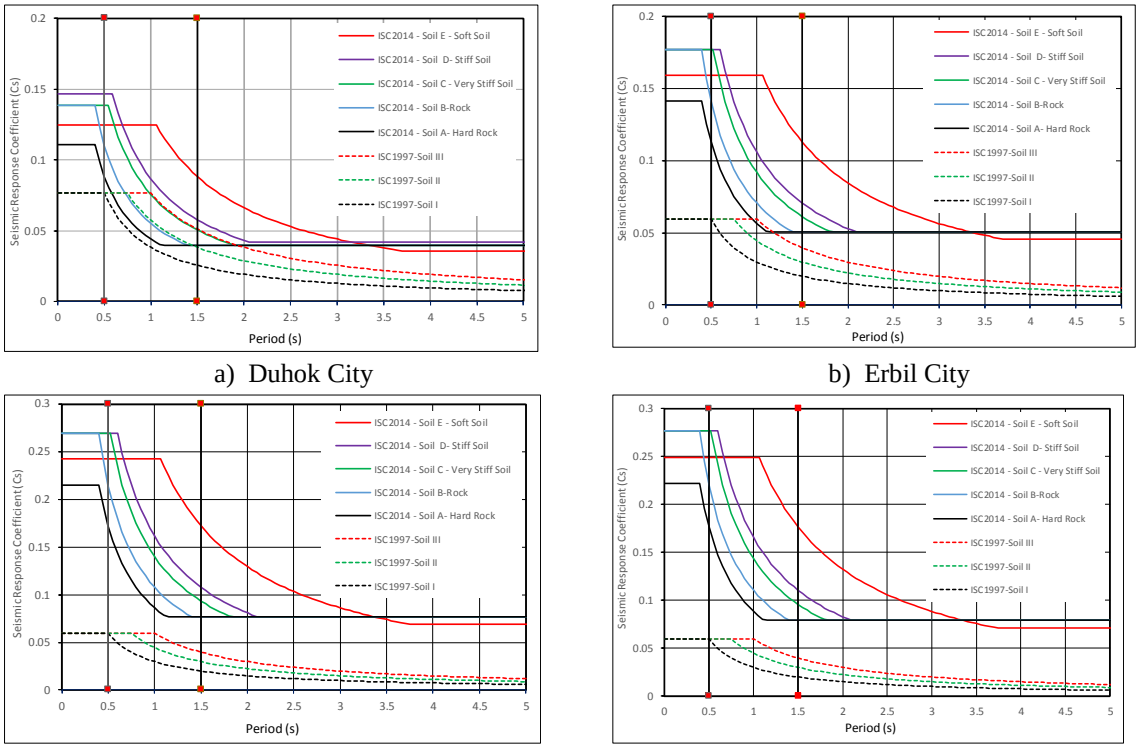

a) Duhok City

b) Erbil City

c) Sulaymaniyah City

d) Halabja City

FIGURE 7. Seismic response coefficient (C_s) using ISC 1997 [4] and ISC 2014 [7]

As two case studies, two values of building periods are taken, T=0.5 Sec (low-rise concrete frame building of 5 stories), T=1.5 Sec (intermediate-rise concrete frame building of 15 stories). For these two-time periods, C_S have been extracted from Figure 7 for both ISC 2014 and ISC 1997 codes; further, the ratios between C_S coefficients, which are equal to the base shear ratio, are reported in Table 2 and shown graphically in Figure 8 for different soil types and for all four main cities.

As could be seen, there is a significant increase in the base shear forces for the two building cases in Halabja and Sulaymaniyah, followed by Erbil then Duhok. This shows the massive impact that the introduction of the ISC 2014 has on the value of design seismic forces, and consequently the design implications.

TABLE 2.

Base shear ratio (ISC 2014/ISC 1997)

	Base shear ratio (ISC 2014/ISC 1997), %											
	5 story building, T=0.5 Sec						15 story building, T=1.5 Sec					
	Soil type					average	Soil type					average
	hard rock	rock	very stiff	stiff	soft		hard rock	rock	very stiff	stiff	soft	
	A	B	C	D	E		A	B	C	D	E	
Duhok	115	144	181	192	163	159	124	155	132	151	173	147
Erbil	190	237	297	297	268	258	204	255	205	237	284	237
Sulaymaniyah	290	362	452	452	407	393	311	388	314	362	434	362
Halabja	296	371	465	465	419	403	319	399	321	371	434	369

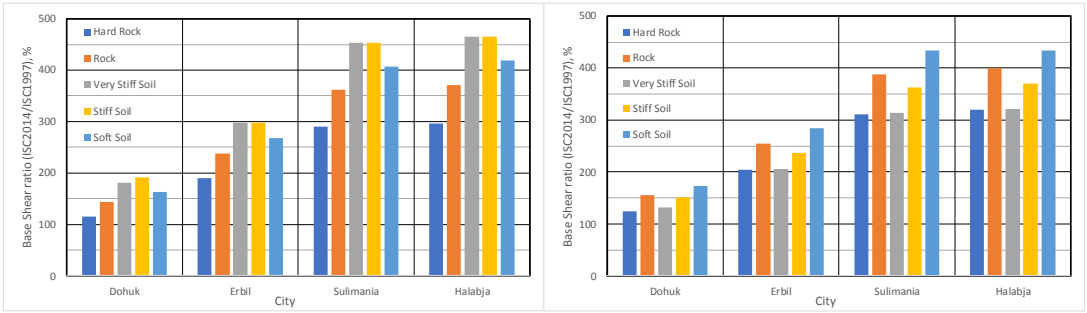

a) 5-Storey Building b) 15-Storey Building

FIGURE 8. Base shear ratio (ISC 2014/ISC 1997)

2. MODAL RESPONSE SPECTRUM ANALYSIS

Apart from the ELFA, there is no common seismic analysis procedure between ISC 2014 and ISC 1997; this was the reason for choosing ELFA for comparison. To confirm that the ELFA is the driving seismic analysis tool for regular low-rise to intermediate-rise building, modal response spectrum analysis has been conducted according to ISC 2014 for 5-storey and 15-storey special reinforced concrete frame building (Importance Class III) located in Erbil city, constructed on a site class D stiff soil using ETABS 16.2.0, see Figure 9.

The seismic base shear determined by both methods (equivalent lateral force (V_s) and maximum response spectrum analysis (Vd)) are reported in Table 3. According the ISC 2014, as Vd is less than 0.85Vs, then the Vd must be raised to be equal to 85% of Vs. Based on that, the ELFA is superior to MRSA for regular RC buildings

in the range of number of floors tested; this justify the use of the ELFA as the base for comparison between the ISC 2014 and ISC 1997 in the current paper

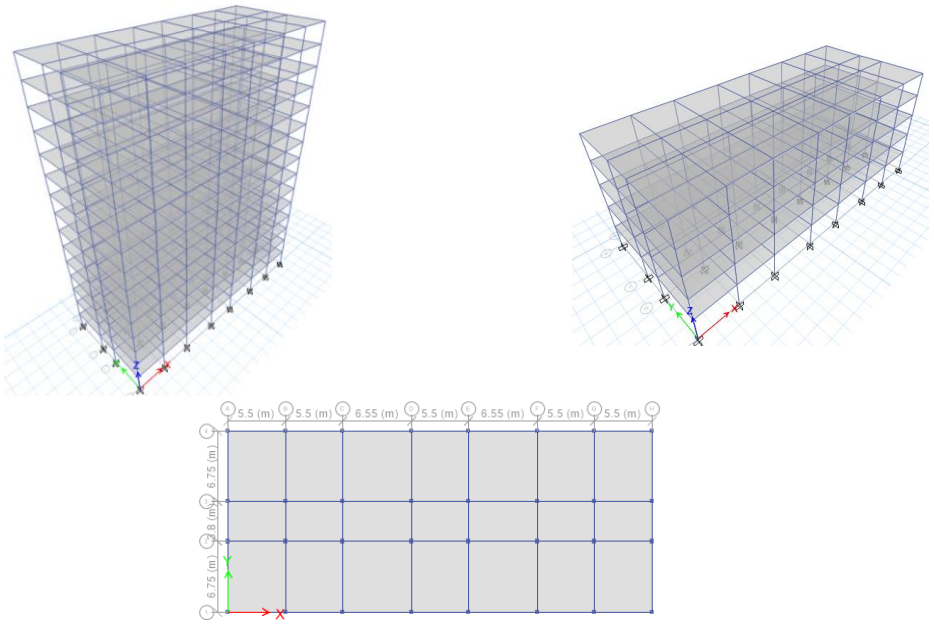

FIGURE 9. ETABS model geometry of the buildings.

TABLE 3.

Static and dynamic calculated base shear

Building	Direction	Vs (Static) kN	Vd (Dynamic) kN	0.85Vs/Vd
5 Story	X	7304.76	2591.62	2.396
	Y	7304.76	2524.03	2.460
15 Story	X	8979.99	3393.49	2.249
	Y	8979.99	3255.56	2.345

3. STRUCTURAL DESIGN CONSIDERATION FOR KRI

Based on the ISC 2014, there are four classes (A, B, C, D) for seismic design classification. This does not match ASCE/SEI7-10 [9], where six seismic design classes are defined (A, B, C, D, E, F). In the ISC 2014, the class for each site depends on the values of S_{DS} and S_{D1}; if $S_{DS} \geq 0.5$ g or $S_{D1} \geq 0.2$ g, the category of the site is assigned to be class D. Referring to Figures 3 and 4, both conditions are valid, therefore, all buildings constructed in the KRI region is considered to be of class D for all soil types no matter what it is the function or the construction system of the building. Based on ISC 2014 [7] and ASCE/SEI7-10 [9], for class D, all concrete frame building should be special type, as no ordinary or intermediate concrete frame is allowed to be built. ISC 2014 refers to ACI318 code [11] as the

designing and construction tool of reinforced concrete buildings for ordinary and seismic loading; therefore, these special concrete frame buildings built in KRI should confirms to ACI requirements, which requires special member size and strength limitations and reinforcement details for the columns, beams and foundation that are not applied currently in the construction in KRI region. The effects of the building systems in KRI to be in seismic design class D will be increasing the requirements for detailing and proportioning, with expectations of increased deformation capacity, meaning that further design criteria need to be applied as listed in Tables 4 and 5.Regarding the Seismic Analysis Procedure Selection, Table 6 lists the selection criteria used in ISC 1997 [4] and ISC 2014 [7]. As seen, ISC 1997 considers only the importance class of the building, while ISC 2014 bases the selection on the building height (T value) and the irregularity in the building, which is more rational, as the dynamic behavior of the building is related to these two factors.

TABLE 4.

Seismic design criterial needs for masonry and steel construction constructed in KRI (seismic class D), based on ISC 2014 [7]

Building system	Structural system allowed	Limits (ISC 2014, Table 3-2-1)
Masonry wall system *	Special* masonry reinforced shear wall is allowed.	Height ≤ 50 m
Moment resisting steel frame#	Special	No limit
	Intermediate & ordinary	Specific limitations listed

*: Building Code Requirements for Masonry Structures (ACI 530-02/ASCE 5-02/TMS 402-02) [12] is the code permitted by the ISC 2014 for designing Masonry Wall system.

#: Seismic Provisions for Structural Steel Buildings (ANSI/AISC 341-16) [13] is the code permitted by the ISC 2014 for designing Masonry Steel frame.

TABLE 5.
Design criterial needs for reinforced concrete frame Buildings constructed in KRI (seismic class D), based on ISC 2014 [7] and ACI 318-14 [11]

Building system	Structural system allowed	Limits (ISC 2014, Table 3-2-1)	Ordinary ACI chapters to satisfy	Additional ACI sections to satisfy
Cast-in-place RC concrete shear wall	Special*	Height ≤ 50 m	CH 1 to 17 CH 19 to 26	Sections 18.2.2 - 18.2.8 Sections 18.10
Reinforced concrete shear walls in dual systems with **special** reinforced concrete frame	Special*	No Limit	Same	Sections 18.2.2 - 18.2.8 Sections 18.10
Reinforced concrete shear walls in dual systems with **intermediate** reinforced concrete frame	Special*	Height ≤ 50 m	Same	Sections 18.2.2 - 18.2.8 Sections 18.10
Cast-in-place moment resisting RC concrete frame	Special*	No limit	Same	Sections 18.2.2 - 18.2.8 Sections 18.6 - 18.8
Foundation			Same	Sections 18.13

* the term "special" (Compared with "ordinary", "intermediate", and) refer to increasing requirements for detailing and proportioning, with expectations of increased deformation capacity, as defined in ACI 318.

TABLE 6.

Seismic analysis selection procedure

Analysis Procedure	ISC 1997 [4]	ISC 2014 [7]
Equivalent lateral force analysis	All cases apart from buildings of I=1.5	Regular buildings with T < 3.5 Ts
		Irregular buildings with T < 3.5 Ts, but with specific type of irregularity
Modal response spectrum analysis	Not included in the code	All other cases
Dynamic time history analysis	Buildings of Importance class I=1.5	Not included in the code

4. PEAK GROUND CANCELATION (PGA)

The comparison presented in this study showed that there is a significant increase in the base shear for buildings constructed in KRI according to ISC 2014 compared to ISC 1997. This increase is mainly due to S_1 and S_S parameters assigned to this region by ISC 2014, which are affecting the values of the parameters S_{D1} and S_{DS}. To assess these values, they need to be returned back to their original status, which is Peak Ground Acceleration (PGA), the maximum amplitude of recorded acceleration, termed also as zero period acceleration [14, pp. 1-11].Therefore, at T=0:

$$PGA = S_a \qquad (1)$$

From Figure 1, the first inclined part in the response spectrum is defined as:

$$S_a = S_{DS} (0 .4 + 0.6 (T/T_0)) \qquad (2)$$

Then, at T=0:

$$S_a = 0.4\, S_{DS} \qquad (3)$$

The S_{DS} value is related to an earthquake with a 10% probability of occurrence in 50 years (Corresponding to 475-year recurrence interval) [15, p. 385]. On the other hand, the PGA map for Iraq (given in Figure 10) is for the same probability of occurrence, therefore by substituting Equation (1) in Equation (3)

$$PGA = 0.4\, S_{DS} \qquad (4)$$

$$PGA = 0.4 \times (2/3) \times F_a \times S_S \qquad (5)$$

As $F_a = 1$ for Site Class B rock in ISC 2014 [7] , then

$$PGA = S_S \,/\, 3.75 \qquad (6)$$

Based on Equation (6) and Figure 3, the PGA values for Site Class B rock taken by ISC 2014 seems to be as follows: 0.282g for Duhok, 0.368g for Erbil, 0.56g for Sulaymaniyah and 0.576g for Halabja. On the other hand, the 475-year return period PGA map in Figure 10, provided by the Global Seismic Hazard Assessment Program [2], shows the PGA values to be around 0.21g for Duhok, 0.24g for Erbil, 0.42g for Sulaymaniyah and 0.42g for Halabja. The comparison suggests that the values of S_S and S_1 recommended by ISC 2014 are overestimated,

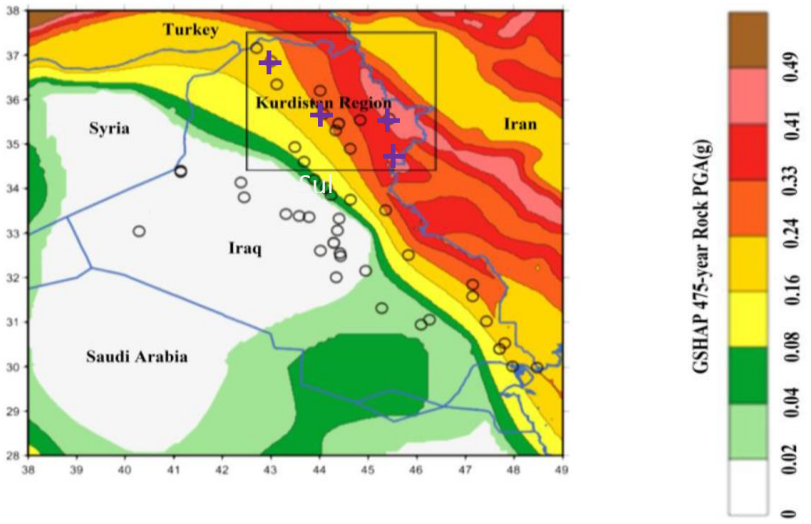

FIGURE 10. Peak ground acceleration (PGA) map for rock with a 10% probability of exceedance in 50 years (475-year return period) as reported by Global Seismic Hazard Assessment Program [16]

5. CONCLUSIONS

The conclusions drawn from the current study could be summarized as below:

1- The equivalent lateral force analysis for the two case studies of Reinforced Concrete Frame buildings (5 and 15 Stories) showed an increase in the Base shear using ISC 2014 compared with that obtained using ISC 1997 in the percentages shown below
   -115 % to 192 % for Duhok city; 190 % to 297 % for Erbil city.
   -290 % to 452 % for Sulaymaniyah city; 296 % to 465 % for Halabja city.

2- The applications of the current ISC 2014 imply considerable change in the building systems built in KRI, including the requirement of having:
   -Special system (according to ACI318-14) for reinforced concrete frames, reinforced shear wall systems.
   -Special system for steel frames in general (according to ANSI/AISC 341-16), with some exception to use ordinary or intermediate systems for some specific cases of low rise buildings.
   -Special system for Masonry Bearing Wall system (according to ACI 530-02/ASCE 5-02/TMS 402-02).
   These require a dramatic change in the structural analysis and the design procedures applied currently on the buildings constructed in KRI region.

3- The Equivalent lateral force analysis is proved to be superior to the modal response spectrum analysis as a seismic analysis tool for regular reinforced concrete buildings up to 15 floors in the ISC 2014.

4-The recommended S_S and S_1 values in the ISC 2014 seems to be overestimated compared with the local values for the peak ground acceleration given by GSHAP.

REFERENCES

[1] Ghassan I. Aleqabi and Hafidh A. A. Ghalib , "Seismic Hazard Assessment of Northern Iraq," Journal of Zankoy Sulaimani-Part-A- (Pure and Applied Sciences), no. Special Issue, GeoKurdistan II, pp. 319-330, 2016.

[2] " National Earthquake Information Center website," United States Geological Survey, Earthquake Hazards Program, [Online]. Available: https://earthquake.usgs.gov/. [Accessed 02 December, 2017].

[3] "Swiss Seismological Service (SED)," , [Online]. Available: http://www.seismo.ethz.ch. [Accessed 02 December 2017].

[4] Ministry of Industrial and Mineral-Centeral Organaziation for Standarazation and Quality Control, "Iraqi Seismic Code Requirements for Buildings," Building Research Centre, Baghdad, 1997.

[5] UBC 1985, "Uniform Building Code," International Conference of Building Officials, California, USA, 1985.

[6] Ministry of Construction and Housing-Centeral Organaziation for Standarazation and Quality Control, "Seismic Code 2013 - Draft Version," Baghdad, 2013.

[7] Ministry of Construction and Housing-Centeral Organaziation for Standarazation and Quality Control, "Seismic Code - Iraqi Building Code 303," Ministry of Construction and Housing-Federal Government, Baghdad, 2014.

[8] IBC 2012, "International Building Code," International Code Council, USA, 2011.

[9] ASCE/SEI 7-10, "Minimum Design Loads for Buildings and Other Structures," American Society of Civil Engineers, Virginia, 2010.

[10] Abdulhameed A. Y., David B., Nikos N., "Time History Analysis of Existing Buildings in the Kurdistan Region of Iraq," in First International Engineering

Conference (IEC2014), Erbil, Iraq, 2014.

[11] ACI 318-14, "Building Code Requirments for Reinforced Concrete (ACI 318-14) and Comentray," American Concrete Institute, Farmington Hills, Detroit, 2014.

[12] ACI 530-02/ASCE 5-02/TMS 402-02, "Building Code Requirements for Masonry Structures," Masonry Standards Joint Committee (MSJC), USA, 2002.

[13] ANSI/AISC 341-16, "Seismic Provisions for Structural Steel Buildings," AISC, Chicago,, 2016.

[14] Chen W.F., Lui E.M., Earthquake Engineering for Structural Design, NW, USA: CRC Press, 2006.

[15] B. S. Taranath, Reinforced Concrete Design of Tall Buildings, NW: CRC Press, 2010.

[16] " Global Seismic Hazard Assesment Program," [Online]. Available: http://www.seismo.ethz.ch/static/GSHAP/. [Accessed 07 12 2017].

INVESTIGATION OF SEISMIC PERFORMANCE AND RELIABILITY ANALYSIS OF PRESTRESSED REINFORCED CONCRETE BRIDGES

M. Hosseinpour[1], M.Celikag[2], H. AkbarzadehBengar[3]

[1&2]*EMU, Gazimagusa*
[3]*University of Mazandaran,*
[1]*mehdi.hosseinpour@cc.emu.edu.tr* ,[2]*murude.celikag@emu.edu.tr*,[3]*h.akbarzadeh@umz.ac.ir*

doi:10.23918/iec2018.04

ABSTRACT

Given the vital importance of bridges in life arteries, safety of these structures against destructive agents such as earthquake is of utmost importance. Using pre-stressed columns in bridges will improve their seismic response, because these columns have high displacement capacity during earthquake and a small permanent displacement after earthquake. Therefore, the need for further study on these structures is felt more than ever. In this paper, firstly, pre-stressed columns were analyzed under reciprocating static load using OpenSees software and results show that pre-stressing bridge columns will improve the quasi-static response of columns and column section bearing. Below, we examine the reliability analysis of pre-stressed bridge samples against force of the earthquake and the effect of different random variables on reliability of bridge. The results show that structural damping and earthquake magnitude have a significant effect on reliability of bridges. Changes in characteristic strength of concrete at ultimate limit and mean resistance of section, effect significantly on reliability of bridge structure.

Keywords: Concrete Bridge, Pre-stressed concrete structures, seismic performance, finite element analysis, Structural reliability.

1. INTRODUCTION

One of the important steps in development of each country is to construct roads and highways. The bridges as key components of arterial network of a country roads have unique and important role in economic, social, political and military fields. Damages caused by recent earthquakes, express necessary measures for earthquake resistant design and further study and research in order to better understand the seismic behavior of bridges. Earthquakes in the last two decades in United States, Japan and Turkey showed that many of bridges have had bad behavior due to poor design of components even using the latest research achievements in this area and compiled regulations [1]. Examining the concrete bridges built in the world shows that, these types of bridge are replaced with existing steel bridges, and using pre-stressed methods since its development has been growing rapidly and a lot of researches have been reported on pre- stressed concrete structures [2]. Pre- stressed concrete structures are attractive alternatives for long-span bridges and have been used throughout the world since 1950. Widespread application of pre-stressed concrete in buildings, military structures and civil infrastructure has been increased generally, being aware of principles, practices and developments in design and manufacturing [3]. Billington and Yoon [4] in 2004 demonstrated that using pre-stressing systems can reduce significantly permanent displacements and cracks. Mahin et al [5] provided a new approach in order to reduce permanent displacements generated in conventional concrete columns. They do this through placement of pre-stressed non-attached cable in the center of light concrete columns. Wang et al [6] studied on regular, attached pre-stressed, non- attached columns and hybrid system in two modes of prefabricated and concrete. Kim et al. [7] provided analytical model for normal and pre-stressed prefabricated hollow columns with an equivalent section that has the same moment of inertia with hollow circular or hollow rectangular sections. They concluded that pre-stressing increases bearing and reduces permanent displacements. The probabilistic design presented herein is towards a numerical approach to the safety analysis of a simply supported post-tensioned concrete bridge beam, within an acceptable probability that the given structure will not fail during its intended life [8]. Haukaas [9] performed research work on the finite element reliability and sensitivity methods for performance-based engineering". He developed a modern and comprehensive computational framework for a nonlinear finite element reliability analysis. Moreover, much advanced research work on this subject has been reported in the literature [10]. Frangopol and Imai [11] studied the reliability of suspension bridges located in Japan, when under wind and

earthquake loads. They applied spectral analysis and evaluated the reliability of the structure. The mechanical and geometrical properties of the sections were taken as the random variables. In this paper, the behavior of pre-stressed and attached columns under seismic loading as well as seismic reliability of arch concrete bridge using the finite element method are studied.

2. THEORY OF THE PROBLEM

The equation of system motion affected by earthquake forces can be expressed as follows:

$$[M]\{\ddot{u}\} + [C]\{\dot{u}\} + [K]\{u\} = \{P_{eff}(t)\} \quad (1)$$

In this equation [M] is concentrated mass matrix, [C] is damping matrix, [K] is stiffness matrix, $\{P_{eff}(t)\}$ is earthquake effective force vector, $\{u\}$ is displacement vector, $\{\dot{u}\}$ is velocity vector and $\{\ddot{u}\}$ is acceleration vector. Calculating the response of bridge structure of equation (1) is resolved using standard modal conversion technique.

$$q_n(t) + 2\xi_n\omega_n q_n(t) + \omega_n^2 q_n(t) = -\Gamma_n \ddot{u}_g(t) \quad (2)$$

In this equation, $q_n(t)$ is normal coordinates, ξn is structural damping percent of nth mode, $\omega_n$is natural frequency of nth mode, Γ_n is modal distribution coefficient and $\ddot{u}_g(t)$ is the vertical acceleration caused by earthquake. Equation (2) can be expressed as follows:

$$\frac{q_n(t)}{\Gamma_n} + 2\xi_n\omega_n \frac{q_n(t)}{\Gamma_n} + \omega_n^2 \frac{q_n(t)}{\Gamma_n} = -\ddot{u}_g(t) \quad (3)$$

Assuming$\frac{q_n(t)}{\Gamma_n} = D_n(t)$, the equation (2) is expressed as follows:

$$D_n(t) + 2\xi_n\omega_n D_n(t) + \omega_n^2 D_n(t) = -\ddot{u}_g(t) \quad (4)$$

Equation (3), is system motion equation with a single degree of freedom and it can be easily solved using numerical methods. Solving equation (3) we can obtain structural displacements in different modes. Since the response of total structure and applied would be calculated as follows.

$$\{u(t)\} = \sum_{n=1}^{N} \{u_n(t)\} = \sum_{n=1}^{N} \Gamma_n \{\phi_n\} D_n(t) \quad (4) \quad \text{and} \quad \{f_s(t)\} = [K]\{u(t)\} \quad (5)$$

Failure due to bending compared to other modes of failure is the most common type of failure mode in reinforced concrete structures. Thus, in the present study, reliability of structure is calculated for flexural failure. Bridge structure is modeled using finite element software as

continuous beam with Beam two-dimensional element. Dead load is distributed evenly as linear load along elements. Vertical seismic accelerations are considered as earthquake load on structures. Bridge structural reliability analysis was conducted using FOSM Method. For calculating the reliability of bridge structure, a certain percentage of ultimate bending strength is considered as a resistance force and bending moment caused by earthquake is considered as force due to loading. Bridge structure is analyzed for a number of earthquakes as 50 accelerogram and finally, mean and standard deviation values of bridge structure reactions are calculated according to results of analysis. In general, if equations related to probability distribution functions of random variables are available, the reliability of structures will be calculated using integral equations listed in Equations 6 and 7.

$$P_f = 1 - R_0 = 1 - \int_{-\infty}^{+\infty} f_s(s)[1 - F_R(s)]ds = \int_{-\infty}^{+\infty} f_s(s)F_R(s)ds \quad (6)$$

$$P_f = 1 - \int_{-\infty}^{+\infty} f_R(r)F_s(r)dr \quad (7)$$

Where P_f is structural failure probability, R_0 is reliability of structures, $f_x(x)$ is probability density function and $F_x(x)$ is cumulative distribution function. The failure probability function can be expressed as the following equation:

$$P_f = \emptyset\left(\frac{\mu_S - \mu_R}{\sqrt{\sigma_R^2 + \sigma_S^2}}\right) \quad (8)$$

In equation 8, $\emptyset$ is standard normal distribution function, μ_S is mean force applied on structure, μ_R is mean structure strength, σ_R is structure standard deviation and σ_S is standard deviation value of loading. If structural reliability index is $\beta = \frac{\mu_g}{\sigma_g}$, therefore, structural failure probability can be expressed as: $P_f = \emptyset(-\beta)$ (9)

Finally, the reliability index of structures is expressed by Equation 10. $\beta = -\emptyset^{-1}(P_f)$ (10)

Ultimate strength limit state and allowable stresses limit state are considered as limit conditions. For these two cases, the limit conditions are defined as follows: $\varepsilon_{cu} \leq 0.0035$

In this equation ε_{cu} is compression stress of concrete tension area. For limit requirement, security margin equation is considered as: $g_u = \alpha M_u - M_s$ (11)

Where, M_u is sectional ultimate resistance moment, M_s is loading moment and α is a coefficient smaller than 1 that each stage represents the percentage of ultimate moments dedicated to

counter loading moment due. For allowable limit stress, the below equation is established:

$f_{ct} \leq f_{ct}^{'}$ (12)

Where, f_{ct} is tension stress of concrete tension area and $f_{ct}^{'}$ is allowable tension stress of concrete. Security margin equation for this state is considered as: $g_e = \alpha M_e - M_s$ (13)

3. STUDYING PRE-STRESSED COLUMNS UNDER RECIPROCAL QUASI-STATIC LOAD

Loading is done according to Figure 1. Loading pattern by controlling displacement for applying load of reciprocating wheels. Loading continues until the load of reaches to maximum value of 0.85.

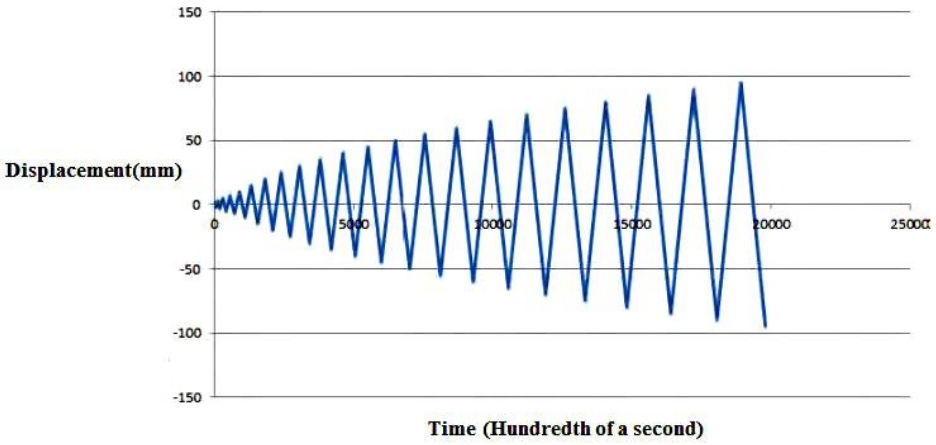

FIGURE 1. The procedure of loading pattern and experiment

Cross-section of columns is 50 × 36 cm for typical and pre-stressed columns. 26 armatures of 12 mm diameter were used in conventional concrete columns round cross-section and six wires of 5 mm diameter were used around a wire with the same diameter for pre- stressed section. Lateral load applied point is 1550 mm above the column fixed base and studying is based on flexural failure. Concrete design strength is 32.5 MPa and conventional bars yield strength is 335 MPa and ultimate stress of pre-stressed tendons is 1860 MPa. Constant compressive force of 576 KN is applied to simulate the gravity loads applied at the time of service at the top of column. Modeling is carried out using OpenSees software where the structural analysis is done using finite element method. Nodes are defined in OpenSees software for pre-stressed system and a graphical form of nodes were drawn using OPS software in order to ensure the accuracy. All parts of fiber section move fully coherent, total cross section

is defined using fiber section that is able to define simultaneously bars, tendons and concrete with different stress-strain diagram in different locations of a cross-section. According to the fact that in pre-stressed systems tendons are involved with concrete, therefore, it shows the necessity of using a single fiber. However, the materials used in fiber cross section must be defined previously. Material Initial Stress is used in order to apply pre-stressed force.

Also, effects of growth and Pinching of Hysteresis curve and considering Boushinger principle and the ability to change are features of this type of material. Figures 2 and 3, show the results of conventional and pre-stressed concrete column analysis. These figures are related to proposed model using the materials. As can be seen in Figure 2, it is found that permanent displacement is reduced greatly and bearing capacity is increased. Also, according to Figure 3, which corresponds to pre-stressed post- tension concrete column, permanent displacement is reduced and bearing capacity is more than post- tension state.

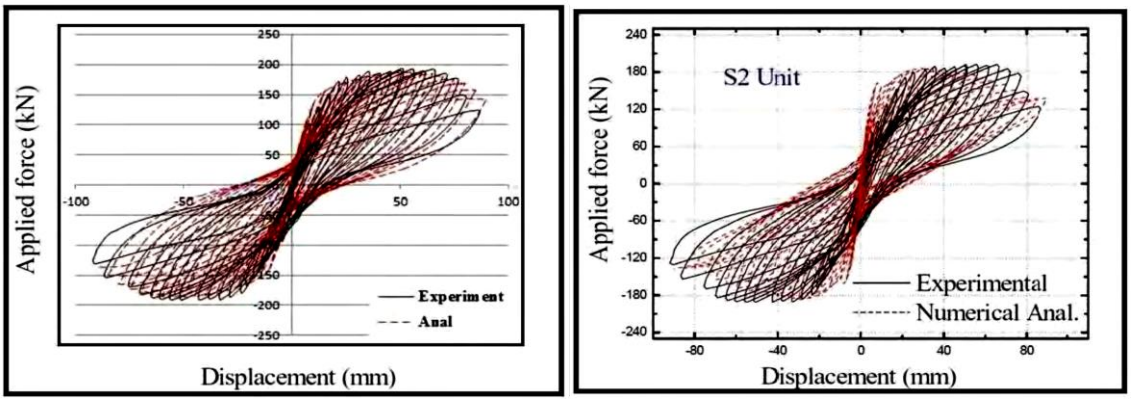

FIGURE 2. Non- attached pre-stressed hysteresis curve diagram

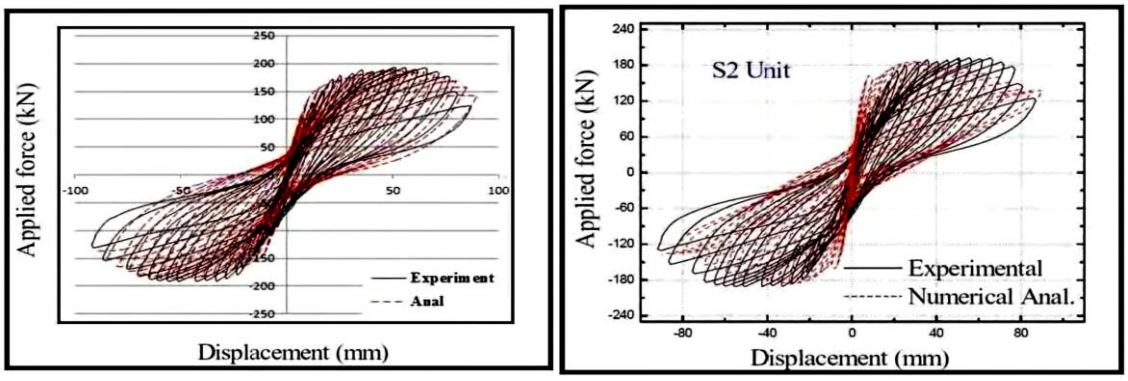

FIGURE 3. Attached pre-stressed hysteresis curve diagram

4. THE RELIABILITY OF BRIDGES AGAINST EARTHQUAKE-INDUCED FORCES

According to partial surveys conducted on reliability analysis of bridge structures against earthquake forces, in this section, the reliability of an arch pre-stressed concrete bridge against earthquake forces are examined. In this section, the mechanical properties of materials, geometric characteristics of sections, structural damping rate, magnitude and maximum acceleration of earthquake are considered as random variables. The bridge is modeled as a continuous beam and linear system behavior is assumed. Vertical accelerations of earthquake are considered as loads applied on bridges for time history analysis of bridge structure during an earthquake and probability density distribution function of random variables are extracted from existing sources and normal probability distribution function is assumed for those variables that had no sources. The examined pre-stressed arched bridge sample includes a three-span bridge with central span of 125 m length and first and second lateral span with length of 55.35 and 45 meters, respectively.

Figure 4 shows the changes of reliability index of bridge structure based on standard deviation of concrete characteristic strength for final resistance limit state. Each curve corresponds to a certain percentage of section ultimate strength. As can be seen, a bridge reliability index change is not considerable per high percentage of cross-resistance but structural changes reliability index is increased as cross-resistance decreased. The reason is that effects of fluctuations arising from changes of concrete characteristic strength on reliability index against section ultimate resistance are trivial. Increasing the percentage of concrete ultimate strength that is used to deal with the external load, the characteristic resistance of concrete changes effects on reliability index is decreased. Figure 5 shows the changes of bridge structure reliability for allowable stress limit state. In limit state, due to the low level of resistance, total resistance of section is considered to cope with the effects of external loading. As can be seen from diagram, changes in specific strength of concrete does not effect on bridge structure reliability index. The interesting point is percentage of structural damping effect because 3 percent increase of structural damping results in double increase of structural reliability index.

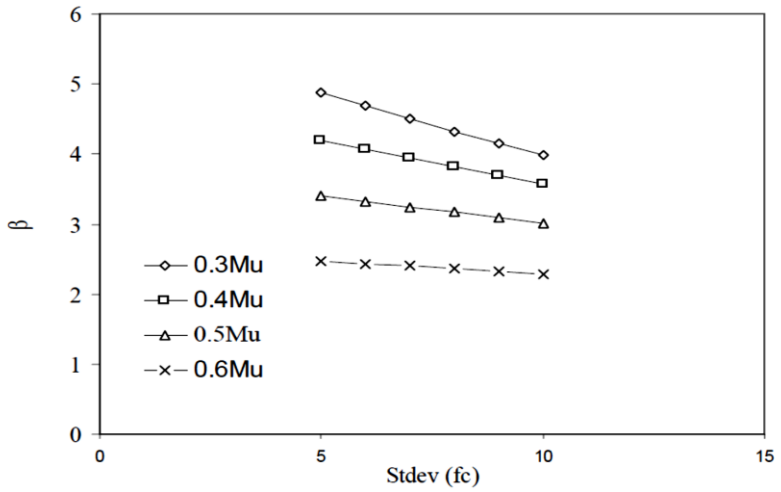

FIGURE 4. The effect of characteristic resistance changes on reliability index for damping percentage (5% ultimate strength limit state)

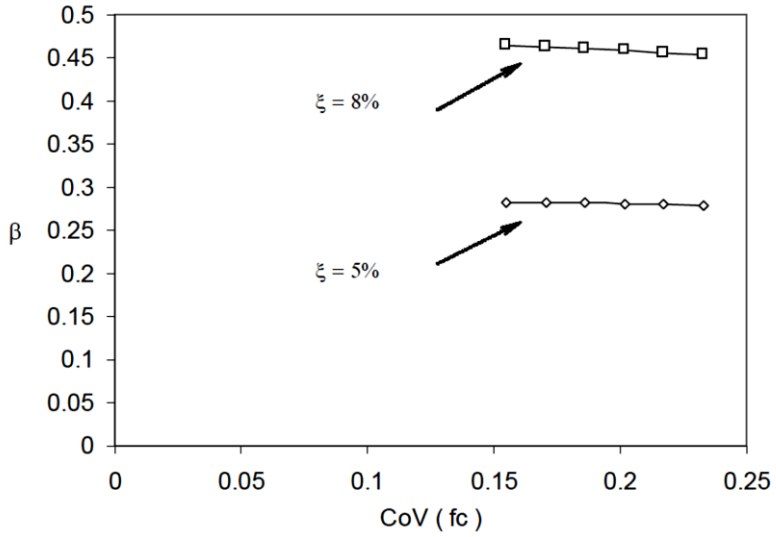

FIGURE 5. The effect of characteristic resistance changes on reliability index (allowable stress limit state)

Figure 6 shows the effect of structural damping changes on reliability index of bridge structure for ultimate strength limit state per different percentages of section resistance. As can be seen from the figure, changes of structural damping effect are evident on reliability changes of bridge structure. The changes of lower amounts of section resistance are more than high levels of section resistance, so that increasing resistance results in curve section tendency to flat and horizontal state.

Figure 7 shows the percentage of structural damping effect changes on reliability index of bridge structure in allowable stress limit state. As can be seen, the effect of random variable changes on reliability index changes in limit state is somewhat obvious. In a general conclusion

we can say that the important random variable of this issue is bridge structural damping percentage.

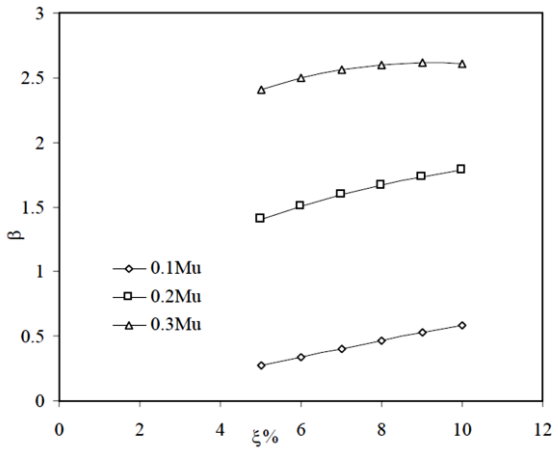

FIGURE 6. Changes of bridge structure reliability index per changes of structural damping percentage, ultimate strength limit state

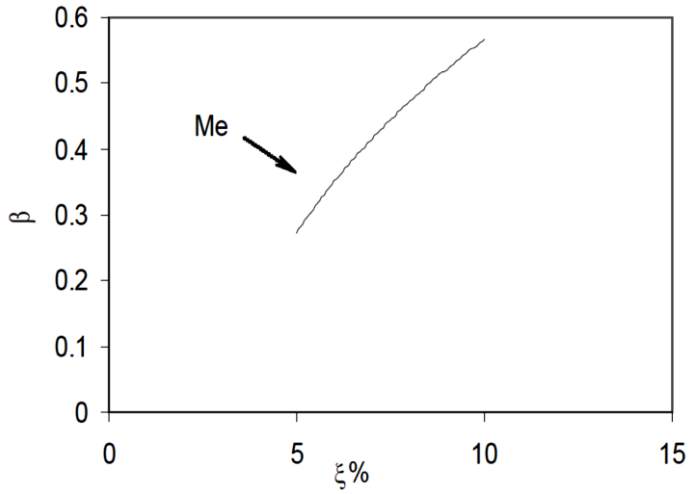

FIGURE 7. Changes of bridge structure reliability index per changes of structural damping percentage, ultimate allowable tension limit state

5. CONCLUSION

The study examines behavior of attached and non- attached pre-stressed column under reciprocating quasi-static load by controlling the displacement using the finite element model and effects of concrete characteristic strength parameters and the percentage of structural damping on bridge structure reliability. the results show that using new materials and direct apply of pre-stressing force will increase the accuracy of analytical models. It was found that pre-stressing improves the quasi-static response of concrete columns and meets concrete weakness largely in tension. In the case of non- attached pre-stressing, it can also be expressed that pre- stressing increases section bearing significantly and on the other hand, it reduces permanent displacement. the structural damping percentage is one of the key parameters in seismic design of bridge structures and results show that controlling this parameter is necessary for safe design. In most cases, except in the case of structural damping percentage for other random variables, fluctuations of bridge structure reliability index per changes in random variables for low percentages of section resistance and high percentages of section resistance is trivial and nearly tends to be uniform. changes of concrete characteristic strength in allowable tension limit state does not effect on reliability of bridge. But in ultimate limit state and mean resistance level, it effects significantly on structural reliability and fluctuations of bridge reliability caused by changes of concrete specific strength are less compared to fluctuations arising from changes of structural damping.

REFERENCES

[1] R. M Pablo, "Risk Assessment of Highway Bridges", A Reliability-based Approach, Paper 158, ENT 209 Indiana University-Purdue University Fort Wayne, 2008.

[2] H. Weiher, and K. Zilch, "Condition of Post-tensioned Concrete Bridges - Assessment of the German Stock by a Spot Survey of Damages". In: Proc. of First International Conference on Advances in Bridge Engineering, Brunel University, London, 2006.

[3] P.J Barr, J.F Stanton, and M.O Eberhard, "Effects of Temperature Variations on Precast, Prestressed Concrete Bridge Girders". Journal of Bridge Engineering, ASCE, March / April 2005.

[4] Billington, S.L. and J. Yoon, "Cyclic response of unbonded posttensioned precast columns with ductile fiber-reinforced concrete". Journal of Bridge Engineering, 2004. 9(4): p. 353-363.

[5] Mahin, S., J. Sakai, and H. Jeong. "Use of partially prestressed reinforced concrete columns to reduce post-earthquake residual displacements of bridges". In Fifth National Seismic Conference on Bridges & Highways, San Francisco, California. 2006.

[6] Wang, Z., et al., "Numerical Analytical Model for Seismic Behavior of Prestressing Concrete Bridge Column Systems". Procedia Engineering, 2011. 14: p. 2333-2340.

[7] Kim, T.H., D.J. Seong, and H.M. Shin, "Seismic Performance Assessment of Hollow Reinforced Concrete and Prestressed Concrete Bridge Columns". International Journal of Concrete Structures and Materials, 2012: p. 1-12.

[8] Biondini, F., Frangopol, D.M., Bontempi, F., Malerba, P.G., "Reliability of material and geometrically non-linear reinforced and prestressed concrete structures", Journal of Computers and Structures, 2004.

[9] Haukaas, T. "Finite element reliability and sensitivity methods for performance-based engineering", Ph.D. Thesis, Dept. of Civil and environmental Engineering, University of California, Berkeley, 2003.

[10] Kiureghian, A.D., Haukaas, T. and Fujimura, K. "Structural reliability software at the University of California, Berkeley", Structural Safety, 28, pp. 44-67, 2006.

[11] Frangopol, D.M. and Imai, K. "Reliability of long span bridges based on design experience with the Honshu-Shikoku bridges", Journal of Constructional Steel Research, 60(3), pp. 373-392, 2004.

INVESTIGATING FLEXURAL STRENGTH OF BEAMS MADE WITH ENGINEERED CEMENTITIOUS COMPOSITE (ECC) UNDER STATIC AND REPEATED LOADING

Kawa O. Ameen[1], Bayar J.Al-Sulayvani[2], Diyar N. Al-Talabani[3]

[1&2] Mosul University
[3]Cihan University-Erbil
[1]Kawa.civil@yahoo.com, [2]Diyarnasih90@gmail.com, [3]Diyar.nasih@cihanuniversity.edu.iq

doi:10.23918/iec2018.05

ABSTRACT

The main purpose of this research is to investigate the flexural strength of reinforced ECC beams under static and repeated loading. Eighteen reinforced ECC beams with deferent fiber content and deferent steel ratio were constructed and tested by applying static and repeated loading. The experimental variables considered in this study include fiber content, steel ratio, and loading type (static or repeated). All beams were geometrically similar with the dimension of (120mm in width, 200mm in depth, and 1000mm in length) and the applied loads were subjected to the beams with two point loads and simply supported span. The experimental outputs divided into four parts: the first part concerned with the effect of fiber content on the load-deflection curves. The second part focused on the effect of steel ratio on the load-deflection curves. Furthermore, the third part studied the comparison between static and repeated loading. Eventually, the last part investigated the effect of fiber content and steel ratio on flexural toughness. In reinforced ECC, with increasing fiber content (for the same flexural reinforcement) the sample will increase its flexural strength. In general, to increase the ultimate flexural strength, the addition of steel ratio has much higher effect than increasing fiber content. Finally, for identical reinforced ECC beams, the flexural strength will be lower when applying repeated load other than static one.

Keywords: Engineered Cementitious Composite (ECC); Repeated Load; Flexural Strength; Flexural Toughness.

1. INTRODUCTION

In the past several decades, concrete with increasingly high compressive strength have been used for many structural applications. However, most of these materials remained brittle. In some cases, the brittleness as measured by brittleness number actually increases as the compressive strength goes up [1]. This poses potential danger and limitation of high strength concrete in structural fields. in the last several years, the University of Michigan has been investigating a composite material named Engineered Cementitious Composites (ECC). In many respects, this material has properties similar to medium to high strength concrete. Furthermore, the tensile strain capacity generally exceeds 1%. a number of investigations have been achieved on the applications of ECC in structural applications at the University of Michigan in the US, Kajima Corporation, University of Tokyo, and Building Research Institute, Tsukuba City in Japan. These studies involve the usage of ECC in shear elements subjected to cyclic loading, in beam-column connections, in shear wall retrofitting of reinforced concrete (R/C) buildings, in R/C beams as durable cover for re-bar corrosion control, and in general concrete structural repair [2].

The principal aims of this study are summarized as follows:

1. Investigating experimentally the effect of fiber volume fraction on the mechanical properties of the flexural beams.
2. Investigating practically the effect the steel ratio on the response of beam deflection.
3. Investigating experimentally the effectiveness of loading types on the flexural strength of reinforced ECC beams.

2. EXPERIMENTAL PROGRAM

The eighteen reinforced ECC beams were casted in the steel molds with 1000mm length, 120mm width, and 200mm height. Although ECC has excellent shear strength, extra shear reinforcement was added to make sure that the beams will fail by flexural first. All of the specimens were reinforced with compression reinforcement 2Ø8mm and the tensile reinforcements were 2Ø8mm, 3Ø8mm, and 4Ø8mm. The shear regions were reinforced with stirrups Ø6mm at 110mm, but the middle third part was unreinforced with stirrups. Figure (1) explained the internal details for one of the specimens. The reinforced beams were tested under two point load test.

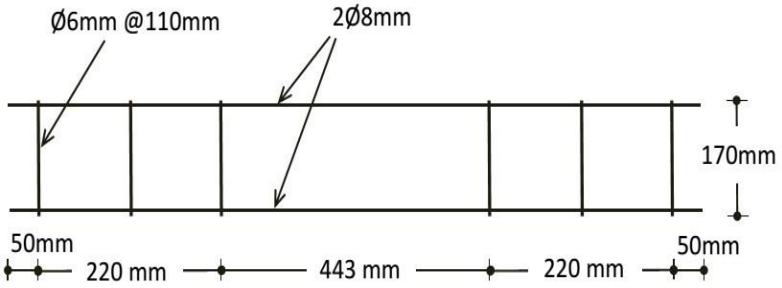

FIGURE 1. Reinforcement details of LS beams

The experimental works were divided into three parts: the first part studied the effect of flexural steel ratio, the second part studied the effect of fiber content, and, the last part studied the effect of load types.

Part I: the effect of flexural steel ratio

For this part, three flexural reinforcement ratio, ρ (ρ=As/bd), were used; namely, LS, MS, and HS. Each of specimen has ρ as 0.004911, 0.007367, and 0.009822, respectively. To represent this effect, eighteen samples were tested, each six sample with the same steel ratio.

Part II: the effect of fiber volume fraction

For this part, three fiber volume fraction were used; namely LF, MF, and HF, each of them were 0.75%, 1.5%, and 3% respectively. To study the effect of fiber volume fraction on the response of ECC beams, eighteen beams were tested each six had the same fiber content (first six samples had 6.76 kg/m3 of fiber, second six samples had 13.52 kg/m3 of fiber, and third six samples had 27.04 kg/m3 of fiber).

Part III: the effect of load type

The overall tested specimens were divided into two groups, the first nine samples were tested by applying static load until the failure, and another remained nine specimen tested using repeated loads.

3. CONSTITUENT MATERIAL PROPERTIES

3.1 . CEMENT

Ordinary Portland cement (Type I) of Kirkuk mark was used in casting all the beams and cylinders. Before using cement, it was kept in a dried place to avoid it from the atmospheric severe. The physical properties of the used cement is given in Table (1). The results are conformed to the Iraqi Standard Specification (IS-No.5, 1984) [3].

TABLE 1.

Physical properties of cement

Property		Result	Iraqi Specification Limits I.O.S 5/1984
Fineness (residual on sieve		4	Not more than 10
Fineness (Blain), cm2/gr		3277	
Initial setting time, min.		12 7	Not less than 45
Final setting time, min		18 8	Not more than 600
Compressive strength (MPa)	3-day	3.39	Not less than 16
	7-day age	2.36	Not less than 24

3.2 .SILICA FUME

In the present study, MasterRoc MS 610 was used which was the trade name of the high quality silica fume powder for high performance concrete. The use of this type of silica fume was changed the porous structure of the concrete making it denser and more resistant to any type of external influence. The technical data was explained in Table (2).

TABLE 2.

Technical data of MasterRoc MS 610

Density	0.55-0.7 kg/l
Recommended	5-15% of the cement
Chloride Contend	<0.1
Colour	Gre
Form	Powd

3.3. FIBER

To obtain multiple and nearly spaced crack, the use of fiber was essential which was made the brittle property of the matrix to the ductile one. Polypropylene fibers of C080 FiberCem mark was used in preparing all samples. The physical and the mechanical properties were showed in Table (3).

TABLE 3.

Physical and mechanical properties of C080 FberCem

Length	12 mm
Density	3
Yield Point	35.52 MPa
Elongation at Yield	11%
Tensile Break	35.52 MPa
Elongation at Yield	400 %
Tensile Modulus	1.312 GPa
Physical state at 20oC	solid
Melting point	160-165 oC
colour	white opaque

3.4. SUPERPLASTICIZERS

The Flocrete SP90S was used as plasticizers which complies with ASTM C494 [4], Type B, D, and G, depending on the dose. The Flocrete SP90S can be used with all types of Portland cement and cement replacement materials and should be added to the concrete with the mixing water to attain optimum performance. Table (4) shows the technical data of Flocrete SP90S.

TABLE 4.

Technical properties of Florcrete SP90S at 25 ºC

Density	1.17∓ 0.01 kg/l
Recommended Dosage	0.80-2.10 liters/100 kg of cementitious materials
Chloride Contend	Nil
Freezing point	≈ -2ºC
Color	Brown liquid

3.5. WATER

Ordinary clean tap water was used for casting and curing all beams and cylinders. The constituent materials (cement, silica fume, fibers, plasticizers, and water) used in this study was shown in Figure (2).

FIGURE 2. Constituent materials

3.6. STEEL REINFORCEMENT

Two types of steel reinforcement were used to reinforce the beam specimen one of them as flexural reinforcement and another as shear reinforcement. The flexural and shear reinforcement were deformed steel bars of size (8 mm in diameter) and (5.59 mm in diameter), respectively. Three specimens of each type were tested under tension according to ASTM A370-05 [5]. The yield stress and the ultimate strength and other experimental results will summarize in Table (5).

TABLE 5.

Reinforcement properties

Sample	Flexural			Shear		
Diameter (mm)	8			5.59		
Area (mm2)	50.26			24.54		
Ultimate load	803	767	739	689	575	559
Yield Stress (MPa)	712	671	639	675	557	527
	674 (average)			586 (average)		
Elongation (%)	10.11	10.17	9.07	4.10	4.36	4.10

4. SAMPLE PREPARATION

4.1. MIX PROPORTIONS

The mixture details for one cubic meter and mix proportion were shown in Table (6). This mixture had showed the unique properties of ECC [6].

TABLE 6.

Mix proportions

Parameters	Amount (kg/m3)	Fraction (%)
Cement	1339.75	1.00 by weight
Silica Fume	133.97	0.10 by weight
Plasticizers	26.79	0.02 by weight
Water	468.56	0.35 by weight
LF	6.76	0.75 by volume
MF	13.52	1.50 by volume
HF	27.04	3.00 by volume

4.2 .MIXING PROCESS

FIGURE 3. Mixing procedures

The eighteen reinforced ECC beams were prepared using the following steps:

1. All quantities were weighed and packed in a dry container.
2. After measuring the weight of all mix constituents, silica fume was slowly added to the cement and mixed together.
3. Plasticizers were added to water and then they added to the mixture of cement and silica fume.
4. Mix became uniform by used rotated drill with three steel blade head.
5. After the mixed materials became uniform, the dispersed fibers were slowly added by hand to the matrix.

The mixing steps were clarified in Figure (3). The total mixing time ranged between 15 and 30 min, depending on the batch size and the amount of fiber used (fiber volume fraction). Note that the workability of the 3% fiber composites was not as good as that for the lower fiber volume fraction composites.

4.3. CASTING AND CURING

FIGURE 4. Casting and curing steps

When the mix was ready, the casting and curing stages were begun by following the steps below:

1. Steel mold were treated with oil prior to putting the reinforcement cage to prevent adhesion with concrete after hardening of ECC. (Figure (4a)).

2. Placing the required steel reinforcement in the steel mold (Figure (4b)). The clear concrete cover of 20mm was maintained by using crushed tile to prevent the effective depth, d, from changing its quantity.

3. Concrete was poured in the steel molds, and it was compacted using electrical handle vibrator. The cylindrical and beams were filled with ECC into three equal layers. Each layer was vibrated for 30 seconds (Figure (4c) and (4d)).

4. The upper surface of concrete was smoothly treated after casting was completed using hand trowel.

5. After casting, all reinforced ECC beam specimens and cylinders were covered with nylon for one day prior to demolding.

6. After 24 hours, the samples were demolded, symbolized, and placed in a water curing tank for 4 weeks (Figure (4e) and (4f)).

7. When curing time was completed, they were removed from water and prepared for testing. The specimens were painted by white emulsion before testing to better monitor the development of cracks.

5. DESCRIPTION OF TESTING MACHINE

During the experimental work many devices were used some of them used for applying loads another used for measuring purpose. A brief description for their capacities were mentioned below:

1. Three point testing machine: it has the capacity of

   3000 kN and used for testing ECC beams. By attaching sensor to the middle of reinforced ECC beams, deflections could be computed electrically.

2. Data collector: it has four channels each one connected to sensor with capacity of computing deflections and/or strains. With the manufacturer software, the load deflection curves data were obtained.

3. Hydraulic universal testing machine (UTM 4000): with capacity of 600 kN, it was used for reinforcement testing.

FIGURE 5. Testing machines

6. DESCRIPTION OF REPEATED LOADS

Concrete behavior subjected to repeated loads is different from the one subjected to static loads. Repeated loads caused crushing in some part of concrete because of loading and unloading process and also it were applied at low number of cycles and high intensity loading. the mechanism of applied repeated load is differ from static one. The ultimate static load (Pult) must be recorded first by testing one of the specimen. The first cycle should begin with 0.4Pult and increased 0.1Pult for every cycle until the failure of specimen. The use of 40 as the first applied load depend on the principle that the loads bellow that limit will not effect on the elastic behavior of the sample. Figure (6) shows the history of applied repeated loads.

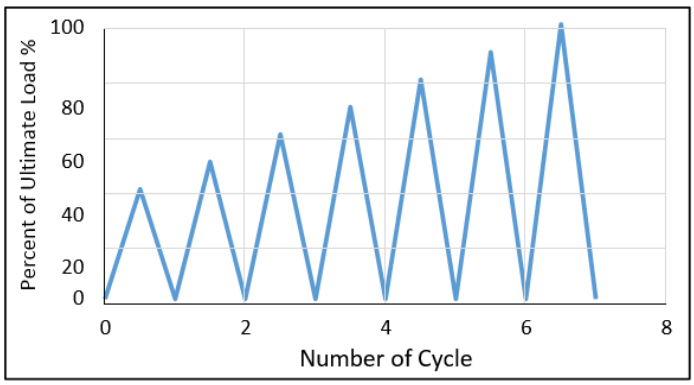

FIGURE 6. Mechanism of applying repeated load

7. LOAD-DEFLECTION CURVES (P- Δ)

Generally, the load-deflection curve defines behavior of tested sample during its loading stages. Many important parameters are depending on the shape of load-deflection curve such as toughness, stiffness, ductility, first cracking load and deflection, and so on. in this study, two types of load-deflection curves were plotted for applied static and repeated loading. Figure (7) to (9) or (13) to (15) showed the load-deflection curves for nine samples tested by applying static load .And, Figure (10) to (12) or (16) to (18) explained the applied load versus central deflection for remained nine samples which were tested by applying repeated load.

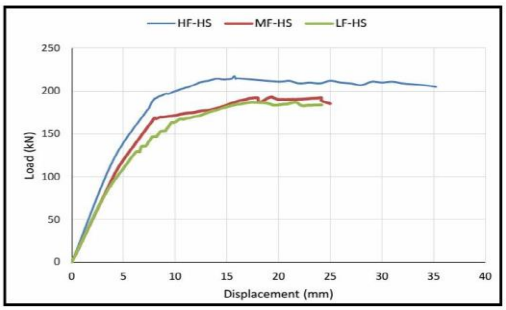

FIGURE 7. Load-deflection curves for HF-HS, MF-HS, and LF-HS with static load

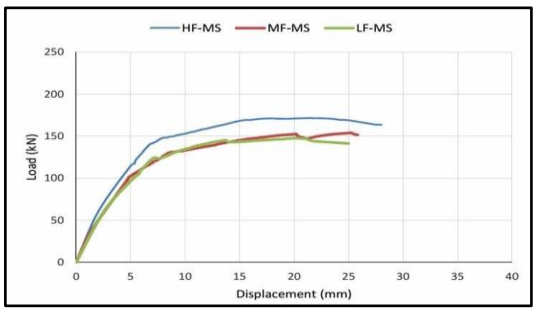

FIGURE 8. Load-deflection curves for HF-MS, MF-MS, and LF-MS with static load

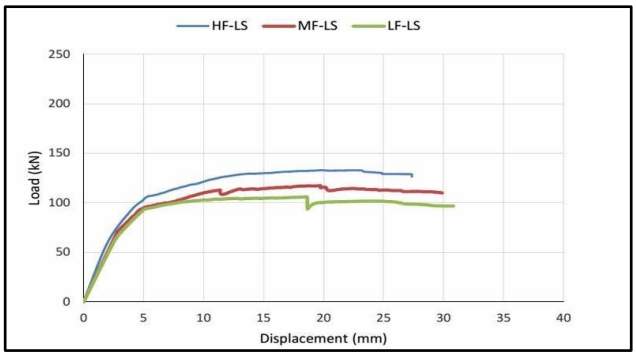

FIGURE 9. Load-deflection curves for HF-LS, MF-LS, and LF-LS with static load

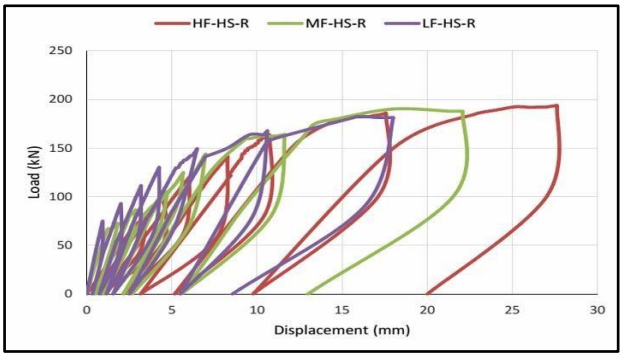

FIGURE 10. Load-deflection curves for HF-HS, MF-HS, and LF-HS with repeated load

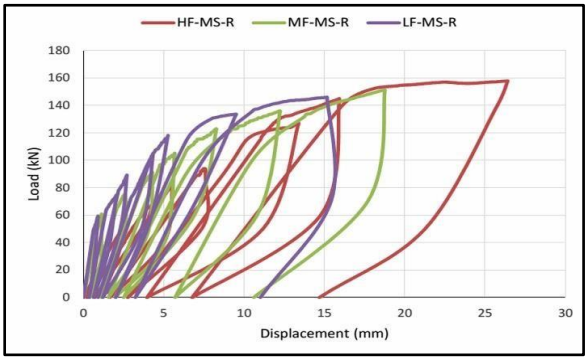

FIGURE 11. Load-deflection curves for HF-MS, MF-MS, and LF-MS with repeated load

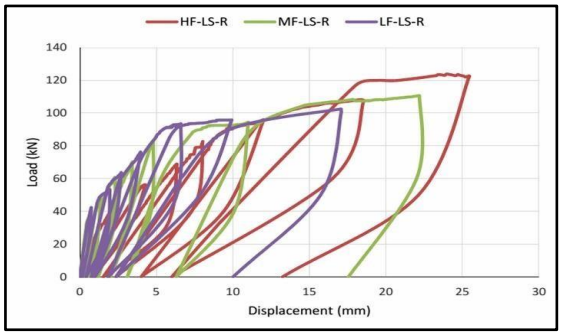

FIGURE 12. Load-deflection curves for HF-LS, MF-LS, and LF-LS with repeated load

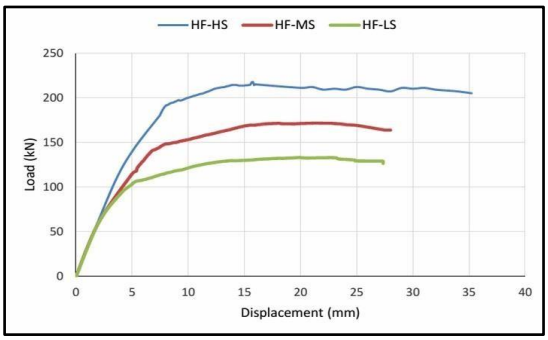

FIGURE 13. Load-deflection curves for HF-HS, HF-MS, and HF-LS with static load

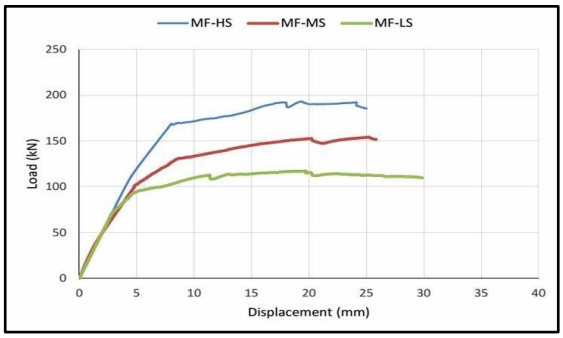

FIGURE 14. Load-deflection curves for MF-HS, MF-MS, and MF-LS with static load

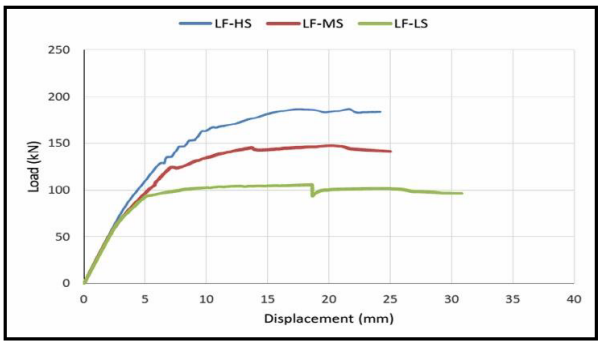

FIGURE 15. Load-deflection curves for LF-HS, LF-MS, and LF-LS with static load

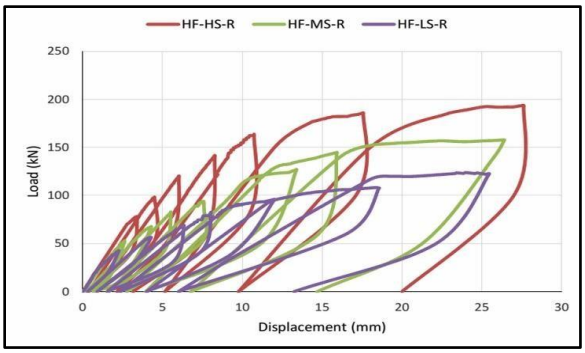

FIGURE 16. Load-deflection curves for HF-HS, HF-MS, and HF-LS with repeated load

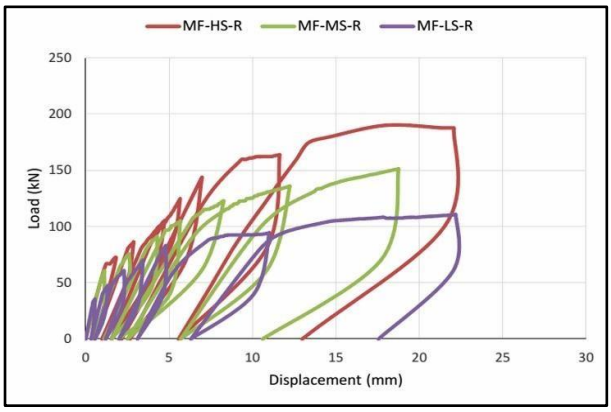

FIGURE 17. Load-deflection curves for MF-HS, MF-MS, and MF-LS with repeated load

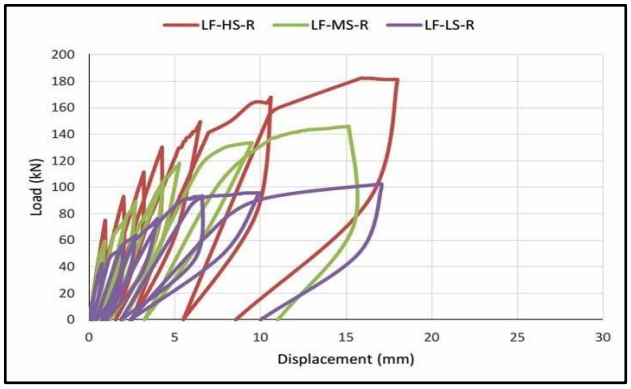

FIGURE 18. Load-deflection curves for LF-HS, LF-MS, and LF-LS with repeated load

7.1. EFFECT OF FIBER VOLUME FRACTION ON P-Δ

Figure (7) to (9) showed the effect of fiber content on load-deflection curve for each steel ratio by applying static load and Figure (10) to (12) explained the same effect but with applying repeated loading. Figure (7) showed the effect of fiber content for HS beams. It was showed that with increasing fiber content from 0.75% to 1.5% and 3%, the ultimate strength was increased by 3.16% and 14.05%, respectively.
Also, Figure (8) explained the effect of fiber content for MS beams. It was stated that with increasing fiber content from 0.75% to 1.5% and 3%, the ultimate strength was increased by 4.09% and 13.87%, respectively. Finally, Figure (9) clarify the effect of fiber content for LS beams. It was explained that with increasing fiber content from 0.75% to 1.5% and 3%, the ultimate strength was increased by 9.68% and 20.34%, respectively.

7.2. EFFECT OF STEEL RATIO ON P-Δ

The effect of steel ratio on load-deflection curves was indicated in Figure (13), (14), and (15) for applied static loading and Figure (16), (17), and (18) for applied repeated load. Figure (13) was used to show the effect of steel ratio on load-deflection curves for HF beams. It was clear that with increasing steel ratio from 0.004911 to 0.007367 and 0.009823, the ultimate strength was increased to 22.51% and 38.89%, respectively. and, Figure (14) was used to explain the effect of steel ratio on load-

deflection curves for HF beams. It was showed that with increasing steel ratio from 0.004911 to 0.007367 and 0.009823, the ultimate strength was increased by 23.89% and 39.27%, respectively. also, Figure (15) was used to state the effect of steel ratio on load-deflection curves for HF beams.it was clear that with increasing steel ratio from 0.004911 to 0.007367 and 0.009823, the ultimate strength was increased to 28.33% and 43.36%, respectively.

7.3. COMPARISON BETWEEN STATIC AND REPEATED LOADING

Usually the load types affect the final results of tested sample. For identical beams, the strength will be lower when applying repeated load other than static one due to the effect of fatigue during loading and unloading processes.

Figure (19) showed the load deflection curves for two beams having the same properties, LF-LS, one of them tested under static load and the other with repeated load.

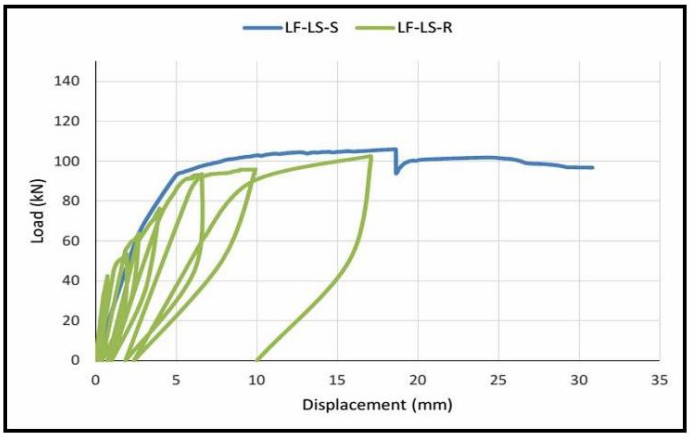

FIGURE 19. Effect of load type on load-deflection curve for LF-LS beam

Table (8) illustrated the results of all eighteen samples from which it can be concluded that the percent of decreasing strength had significant effect with steel ratio compared to fiber effect. The results showed that HF-HS beams had maximum percent of difference between ultimate static load and ultimate repeated load (12.4%), however, LF-MS showed the minimum value (1.1%).

TABLE 8.

Maximum static and repeated loads

Sample	Ultimate Static Load (kN)	Ultimate Repeated Load (kN)	Percent Difference (%)
HF-HS	217.67	193.73	12.4
HF-MS	171.65	157.93	8.7
HF-LS	133.02	123.98	7.3
MF-HS	193.18	190.30	1.5
MF-MS	154.14	151.43	1.8
MF-LS	117.32	110.68	6.0
LF-HS	187.08	182.58	2.5
LF-MS	147.84	146.18	1.1
LF-LS	105.96	102.64	3.2

8. CONCLUSIONS

Depending on the experimental results, the study comes up with the following conclusions:

1. For HS beams, it was showed that with increasing fiber content from 0.75% to 1.5% and 3%, the ultimate strength was increased by 3.16% and 14.05%, respectively.

2. For MS beams, it was concluded that with increasing fiber content from 0.75% to 1.5% and 3%, the ultimate strength was increased by 4.09% and 13.87%, respectively.

3. For LS beams, it was explained that with increasing fiber content from 0.75% to 1.5% and 3%, the ultimate strength was increased by 9.68% and 20.34%, respectively.

4. To increase the ultimate strength, the addition of steel ratio has much higher effect than increasing fiber content.

5. For identical beams, the strength will be lower when applying repeated load other than static one due to the effect of fatigue in the times of loading and unloading processes. The results showed that HF-HS beams had maximum percent of variation between ultimate static load and ultimate repeated load (12.4%), however, LF-MS showed the minimum value (1.1%).

6. With specific fiber content the specimens with high steel ratio had the highest toughness, the specimens with medium steel ratio showed intermediate toughness, and the specimens with the minimum steel ratio showed the lowest toughness.

ACKNOWLEDGEMENTS

Many thanks to Bakhtiar A. Muheiddin for his supporting in my study and research and I ask Allah to put his pure soul in paradise.

REFERENCES

[1] Hillerborg, A., "Analysis of one single crack in fracture mechanics of concrete", edited by F.H. Wittmann, Elsevier Science Publishers B.V., Amsterdam, 1983, pp. 223-249.

[2] Victor C. Li, "Engineered cementitious composite for structural applications", ASCE J, Materials in Civil Engineering, Vol. 10, No. 2, 1998, pp. 66-69.

[3] Iraqi Specification No.05, "Portland cement", Baghdad, Iraq, 1984, (In Arabic).

[4] ASTM C494/C 494M-99a, "Standard Specification for Chemical Admixtures for Concrete", Annual Book of ASTM Standards, pp. 9.

[5] ASTM A 370-03a, "Standard test methods and definitions for mechanical testing of steel products", Annual Book of ASTM Standards, pp. 49.

[6] Salahuddin Qudah, Mohamed Maalej, "Application of engineered cementitious composites (ECC) in interior beam–column connections for enhanced seismic resistance", Engineering Structures, Vol. 69, 2014, pp. 234-245.

[7] ASTM C1018-97, "Standard test method for flexural toughness and first-crack strength of fiber-reinforced concrete (using beam with third-point loading)", Annual Book of ASTM Standards, pp. 8.

[8] JSCE-SF4, "Method of tests for flexural strength and flexural toughness of steel-fiber-reinforced concrete", Concr Libr JSCE, Japan Soc of Civ Eng, Tokyo, Vol. 3, 1984, pp. 58-61.

AN EVOLUTIONARY MODEL FOR OPTIMIZING RAIL TRANSIT STATION LOCATIONS

Chro H. Ahmed[1], Hardy K. Karim[2],Hirsh M. Majid[3]

[1,2&3]University of Sulaimani, Iraq.
[1]chro.ahmed@univsul.edu.iq,[2] hardy.karim@univsul.edu.iq ,[3]hirsh.majid@univsul.edu.iq

doi:10.23918/iec2018.06

ABSTRACT

Optimizing rail transit station locations is a very complex engineering problem. The requirements and constraints that should be considered in locating rail transit stations are complex and interrelated. Although several optimization models have been developed to solve the rail transit station location problem, most of them focus on a single objective and only yield a suboptimal solution to the problem. Multiple-objective models for optimizing rail transit station locations are rare in the literature and their capabilities are very limited. This paper, addresses the limitations in the existing models by developing an evolutionary model, taking into account various local conditions and the multiple planning requirements that arise from passenger, operator and the community to optimize station locations. The model uses an evolutionary solution algorithm (a search algorithm that imitates the natural evolution process) based on genetic algorithm (GA) integrated with geographic information system (GIS) tools to perform the optimal search. The model was applied to an artificial case study and the results demonstrate that the model can optimally locate stations that satisfied the identified planning requirements and constraints.

Keywords: Rail Transit Station, Optimization, Genetic algorithm, GIS.

1. INTRODUCTION

Continuous growth of urban areas and associated needs for mobility have given rise to the need for building new rail transit systems or expanding existing ones. A rail transit system can play a crucial role in reliving transport problems, such as congestion, increased travel time and air pollution. At the same time, it can also provide safe, reliable and convenient service for population within major corridors and to important activity areas. However, the establishment of a rail transit system requires massive investments and exerts permanent impacts on the travel pattern, land use development and even environmental characteristics across potential service areas. Therefore, its actual implementation requires rigorous planning and evaluation processes. The planning of a rail transit system involves determination of station locations and network of lines linking the stations. It is, however, a truism that rail transit stations represent a point at which people can have access to a rail transit system and that it is an important factor for a rail transit system to be selected as an alternative transport mode. Therefore, rail transit stations represent a crucial part of the planning process. The determination of station locations requires consideration of various local factors including travel demand patterns, land use patterns, existing transport network, and topography while satisfying a number of complex and interrelated requirements of the various rail transit system stakeholders (passenger, operator and the community). This necessitates the application of optimization models to achieve an optimal (reliable and cost effective) solution. Subsequently, this paper formulates the rail transit planning process as an optimization problem to seek the optimal locations of stations. It is, however, difficult to model the rail transit station requirements with simple mathematical functions due to their complexities which involve non differentiable, nonlinear, discontinuous structure. Therefore, an evolutionary optimization algorithm based on a GA is designed to efficiently solve the problem. A GA is an evolutionary optimization technique widely utilized for solving various complex problems. Following the concept of biological evolution, a GA evolves a population of different alternative solutions towards the optimal solution. The evolution begins with a population of random alternative solutions and progresses over a number of generation/iterations. In each generation/iteration, the fitness of the population is evaluated with respect to the desired objectives of the problem. Thereafter, a number of individuals are selected stochastically from the

current population based on their fitness values and modified with genetic operators (crossover and mutation) to produce a new population for the next generation/iteration. This process is continued until a specified number of generations, which is fixed a priori, either have elapsed or other predetermined convergence criteria are met [1, 2].

1. LITERATURE REVIEW

Many researchers and planners have made many attempts to develop various optimization models for solving rail transit station location problem. Vuchic and Newell [3] developed an analytical model to determine spacing between stations along a predetermined rail line. With respect to the objective of minimum passenger travel time, the model calculated interstation spacing by solving a set of partial differential equations specifying the optimality condition. Vuchic [4], Kikuchi and Vuchic [5], and Wirasinghe [6], considered various improvements to the Vuchic and Newell's approach for determining the optimal station spacing. However, these models have only limited practical applications due to oversimplification of the problem by assuming uniform distribution of population along rail transit lines and that the population of an area served by the rail line commutes to one central points. Recent studies therefore, attempted to further improve these models through removing unrealistic assumptions and incorporating various planning and real world constraint requirements. Laporte et al., [7] developed a model for locating a prefixed number of stations on a predetermined rail transit alignment with the objective to maximize population coverage while satisfying interstation spacing constraint. The study estimated the demand for each potential station by triangulation of census tracts, assuming that the percentage of the captured travellers decreases with their access distance from the station. Schöbel et al. [8] presented a model to locate additional stations along existing rail line networks, considering the trade-off between positive and negative effects of additional stations. The objective of the model was to minimize the number (cost) of additional stations while ensuring coverage of all demand centers. The demand center, which may represent a settlement area, shopping center, school, etc., was assumed to be covered if the next station was within a specified radius from it. In an extended effort, Hamacher et al. [8] built up on Schöbel et al. [9]

study by seeking to satisfy two different objective functions of demand covering and accessibility to stations. Following the same approach, Carrizosa et al. [10] proposed a model seeking a set of additional stations covering all demand centers but, instead of minimizing the number of additional stations, the additional passenger travel time due to the additional stations were minimized. In another study, Jha and Oluokun [11] addressed the determination of the optimal station locations along a predetermined rail transit alignment using artificial intelligence based optimization techniques and GIS. Similarly, using GIS tools Samanta and Jha [12] used GA to seek the best set of station locations along a rail transit line to minimize total system cost while ensuring that the interstation distances remain constraints. The model defined the total system as a function of passenger total travel time, system operation and construction costs. Despite the capabilities of the aforementioned optimization models in addressing many aspects of rail transit station locations, most of them have a number of limitations that necessitate further improvements in order to achieve optimal (reliable and cost effective) solution to the problem. These limitations include: (a) primarily, many of these models neglect initial feasibility study to identify potential station locations, assuming that rail transit stations can be located anywhere in the study area or along the rail transit line without considering the various environmental, topological and budget constraints; (b) most of these models disregard the effects of various local factors of the study area , such as land use pattern, land values, existing roadway network and topography on the overall system performance and cost and; (c) many of these models address partial aspects of the problem by focusing mainly on the coverage of traffic demand or population with other critical passenger, operator and community related aspects being ignored. This paper addresses these limitations by developing a new evolutionary based model integrated with GIS tools to determine the optimal set of station locations for a rail transit line. The proposed model takes into account initial feasibility of station sites, various local factors and multiple planning requirements that arise from passenger, operator and the community.

3. THE MODEL FRAMEWORK

The model framework comprises two stages, as shown in Figure 1. In the first stage, the model measures the feasibility of station sites to identify a pool of feasible station locations using a GIS-based algorithm. In the second stage, the model selects the best set of stations from the feasible station pool identified in the first stage using an optimization procedure based on a GA while interacting with GIS supporting system. Once the optimal station locations are determined, they are connected to obtain the rail line alignment. However, since the focus of this paper is to find optimal station locations along a rail transit line, it is assumed that the final alignment of the rail line is obtained through the linear connections of the stations. The mathematical formulations of these two stages are discussed and detailed in the next section.

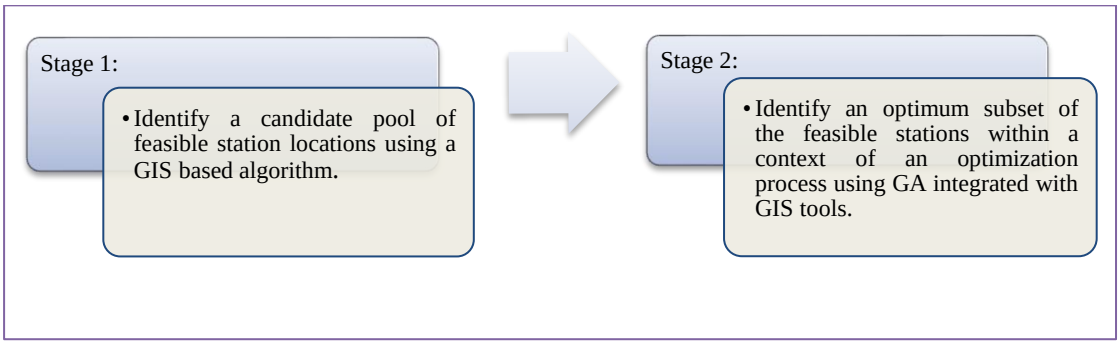

FIGURE 1. The Model Framework

4. MATHEMATICAL FORMULATION

As mentioned in section 3, prior to the optimization process the model evaluates the feasibility of station locations to identify a candidate pool of stations using a GIS-based algorithm. Performing such a feasibility analysis can effectively speed up the planning process and improve decision-making in selecting reliable and cost effective solutions. This is by: (1) excluding environmental protected areas that may result in significant unnecessary increases in the station construction cost from the optimization search space. In addition, the exclusion of these areas results in significant decreases of computation time in exploring unnecessary areas of the search space (2) identifying areas that have high intensity of residential and commercial land use areas . The coordination of rail transit stations with these land use areas can significantly increase the number of potential passengers utilizing the system, which

in turn results in reduced overall vehicle travel, and thereby reduced traffic congestion and improved mobility. The proposed GIS-algorithm applies the following three main steps to screen the potential served area and perform evaluation analysis for generating a pool of feasible station locations.

Step 1: dividing the study area into grids (G_i) and creating a GIS layer for stations (Ω_{st}). It is assumed that each of the generated grids represents a potential location for a rail station. The size of each grid, therefore, should represent the typical size of a rail station.

Step 2: finding all station grids that intersect with environmentally protected areas and excluding them from the search space of feasible station locations. This is done by laying the generated station grid layer (Ω_{st}) over the environmentally sensitive areas layers (Ω_{env}) to generate the feasible grid layer for station(Ω_{fs}). The environmentally protected areas include historic buildings, green parks, woodlands, rivers and sites of scientific interest.

$$\Omega_{fs} = \Omega_{st} \cap \overline{\Omega_{env}} \quad (1)$$

Step 3: identifying all the grids within the feasible station layer (Ω_{fs}) with the average commercial land use areas within the defined walking distance of stations greater than the pre-specified threshold value of commercial land use areas and assigning them with an integer value. In this paper, the commercial land uses areas include recreational centers, shopping malls, office complexes, industrial complexes and university campuses.

$$\forall G_i \in \Omega_{\mathrm{fs}} \rightarrow= 1 \; if \; (\sum \overline{CA} \,|\mathrm{D_w}) \geq \mathrm{V_{CA}} \quad (2)$$

Where: $\overline{CA}$ is the average commercial land use areas within walking distance of station; $\mathrm{D_w}$ is the defined walking distance to stations and; $\mathrm{V_{CA}}$ is the pre-specified threshold value of average commercial land use areas within $\mathrm{D_w}$.

Step 4: identifying all the grids within the feasible station layer (Ω_{fs}) with the average population density within the defined walking distance of stations greater than the pre-specified threshold value of population density and assigning them with an integer value.

$$\forall G_i \in \Omega_{fs} \rightarrow = 1 \; if \; (\sum \overline{PD} \,|D_w) \geq V_{PD} \tag{3}$$

Where: $\overline{PD}$ is the average population density within D_w and; V_{PD} is the pre-specified threshold value of average population density within D_w.

Once the pool of feasible station locations is generated, the model selects the best set of stations from the generated pool within the context of an optimization procedure using an evolutionary search algorithm based on a GA supported by a background GIS database. The optimization framework is designed to accommodate various local factors, incorporate multiple objectives and constraints that arise from passenger, operator and community requirements and compute the optimal solution. The objective of the optimization process is to minimize passenger, operator and community costs. The following are key steps of the developed GA based optimization algorithm:

Step 1: generating the alternative solutions (i.e., population) by randomly selecting a set of stations (S_i) from the station pool generated in the first stage and connecting them linearly while ensuring that: (a) the number of the selected stations falls within predefined minimum (Ns_{min}) and maximum (Ns_{max}) limits set by rail transit system planners and; (b) the distance between selected stations fall within predefined minimum (Δs_{min}) and maximum (Δs_{max}) station spacing. It is assumed that, depending on the major traffic flow patterns of the area to be served, rail transit system planners are able to locate the terminal stations prior to the optimization process. That is, the model seeks the best locations of intermediate stations.

Step 2: evaluating the fitness value of each alternative solution which is a function of three main components; passenger, operator and community costs.

$$T_C = P_C + O_C + C_C \tag{4}$$

Where: T_C is the total system cost (\$), P_C ,O_C, C_C are the passenger, operator and community costs (\$) respectively.

$$P_C = T_a \times A_0 + T_w \times W_0 + T_t \times T_0 \tag{5}$$

Where: T_a is the passenger's access time to/from station (min); A_0 is the costs of access time (\$/min); T_w is waiting time at station (min); W_0 is the cost of waiting time (\$/min); T_t is on train travel time (min) and; T_0 is the unit cost of on train travel time (\$/min). The passenger access time to/from rail stations is a function of the passenger walking distance and speed to/from stations. It is computed through artificial links that created between traffic analysis zones (TAZs) and feasible station locations. These links measure the distance between the centroids of the each TAZ and feasible station location (D_a), thus the access time is calculated by dividing this distance (D_a) to passenger walking speed (V_a). The waiting time is assumed to be equal to half of the train headway (H_w) which is a function of train frequency. The on-train travel time is calculated by dividing the distance between boarding and alighting station (D_s) by the train speed (V_t).

$$O_c = L_t \times M_0 \tag{6}$$

Where: L_t is the total train km travelled distance and ; $M_0$is the unit operation and maintenance cost for train (\$/km).

$$C_C = L_S + B_s \tag{7}$$

Where: L_S is the land acquisition cost for stations (\$); B_s is the cost of building stations (\$). The land acquisition costs are fed into the evaluation process via interaction with GIS while the cost of building stations is assumed to be fixed.

Step 3: evolving the initial solutions generated in step 1 over a series of generations/iterations based on their fitness values calculated in step 2 to converge towards the optimal solution. This is by applying three genetic operators, selection, crossover and mutation, adopting the approach developed by [13].

Step 4: terminating the evolution process when searching through the predefined number of generations is reached or improvement in the objective function value is negligible (less than 1%).

5. CASE STUDY

The effectiveness of the proposed model was examined by applying it to an artificial case study. The size of the case study was 36 km^2 (8.0 km x 4.5 km). Each of the land use pattern, population density and land value datasets were created artificially for the study area and digitized for the analysis purpose. The land use pattern dataset contained commercial land use areas and environmentally protected areas. As discussed in section 4, the commercial land use areas include recreational centers, shopping malls, office complexes, industrial complexes and university campuses while the environmentally protected areas include historic buildings, green parks, woodlands, rivers and sites of scientific interest. After the preparation of the required datasets and defining the model input parameters, the model was implemented. Figure 2 presents the candidate pool of feasible station locations generated in stage 1 of the model evaluation process. It is very interesting to note that the candidate feasible stations mainly cover the most densely populated and commercial areas of the study area. This is in addition to excluding the environmentally protected areas from the search space. These results indicate that screening the study area for feasible station locations prior to the optimization process plays an important role in directing the search towards the promising region of the search space.

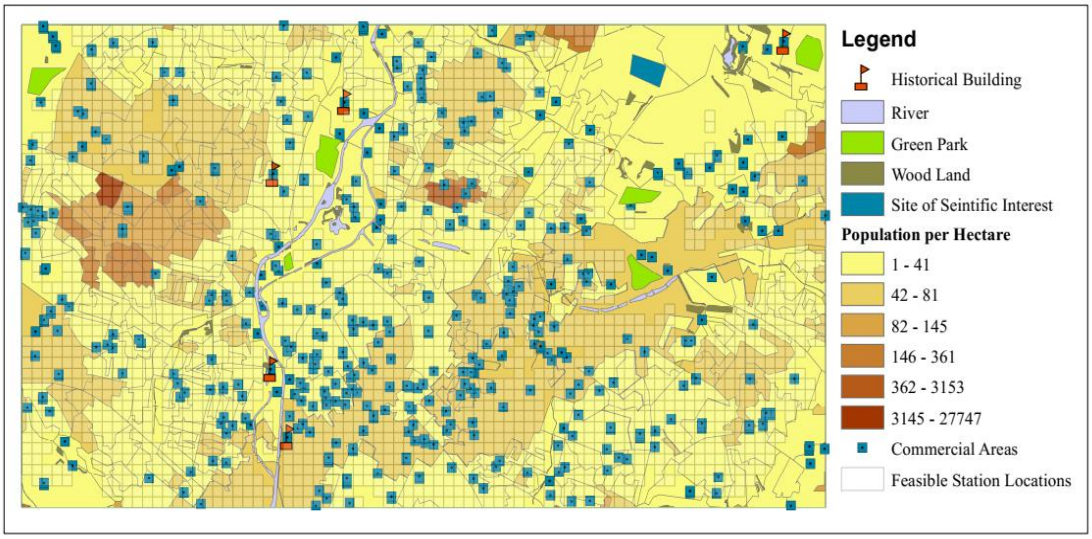

FIGURE 2. Generated Feasible Station Locations

Figure 3 shows the best locations of stations, obtained in stage 2 of the model evaluation process, which were selected from the generated feasible station pool. The optimal solution consists of 7 stations, covering more than 138,700 people within 800 meters walking distance of stations, which comprises almost 27 percent of the case study's total population. Furthermore, the obtained solution covers more than 45 percent of the case study's commercial areas, which include recreational areas, shopping malls, office complexes and industrial complexes within 800 meters walking distance of the stations. These results, therefore, indicate that the model can effectively find a robust and reliable solution.

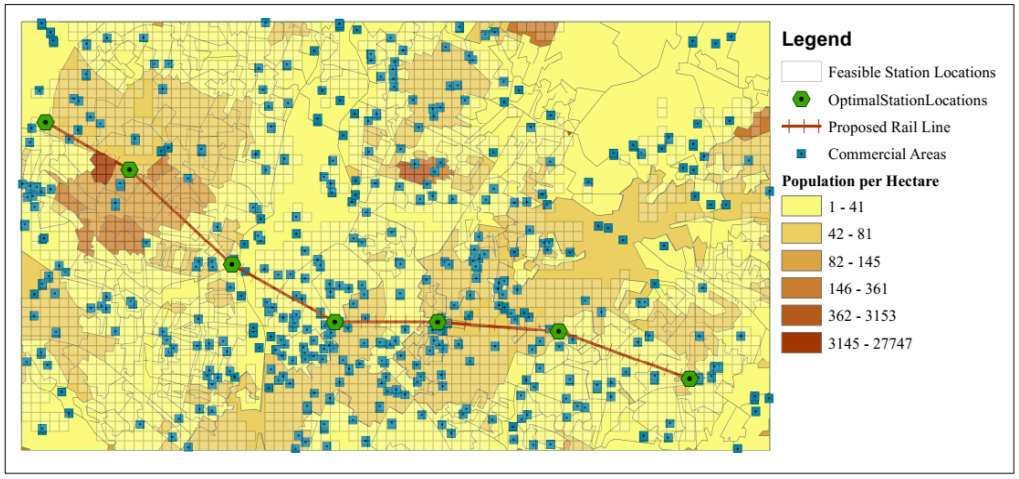

FIGURE 3. Optimized Station Locations

6. CONCLUSION

This paper presented an evolutionary optimization model for locating rail transit stations. The model first evaluated the feasibility of the potential served area to generate a pool of feasible stations considering various local and environmental factors. The best set of these feasible stations were then selected within the context of an optimization process using GA while interacting with GIS supporting system. The optimization framework accommodated complex correlation and interaction of the multiple requirements and constraints arising from different rail transit system stakeholders; passenger, operator and the community, and made trade-off between them in order to achieve a reliable and cost effective solution. To demonstrate its

effectiveness in finding good solutions, the model was applied to an artificial case study. The results revealed that the model can effectively resolve the essential trade-off between minimum passenger travel time and operation and maintenance cost on the one hand, and the minimum construction cost of the stations on the other hand, while also satisfying various constraints. Furthermore, the results revealed that performing a feasibility analysis for potential station locations prior to the optimization process can effectively improve the performance of the model to realize an optimal (reliable and cost effective) solution, by directing the search to explore the most promising regions in the search space.

REFERENCES

[1] Goldberg, D. E., *Genetic Algorithms in Search, Optimization, and Machine Learning*, Massachusetts: AddisonWesley, 1989.

[2] Goldberg , D. E. and Deb, K. , "A comparison analysis of selection schemes used in genetic algorithms", in *Foundations of Genetic Algorithms,* G.J. E. Rawlins, Ed. California: Morgan Kaufmann, 1991.

[3] Vuchic, V. R. and Newell, G. F., "Rapid transit interstation spacings for minimum travel time," *Transportation Science*, Vol.2, (4) pp. 303-309,1968.

[4] Vuchic, V. R., "Rapid transit interstation spacings for maximum number of passengers,"
Transportation Science, Vol.3, (3) pp. 214-232, 1969.

[5] Kikuchi, S. and Vuchic, V. R., "Transit vehicle stopping regimes and spacings," *Transportation Science*, Vol.16, (3) pp. 311-331, 1982.

[6] Wirasinghe, S. C. and Vandebona., U., "Some aspects of the location of subway stations and routes, " in *Fourth International Symposium on Locational Decisions (ISOLDE),* Belgium, *1987.*

[7] Laporte, G., Mesa, J. A. and Ortega, F. A., "Locating stations on rapid transit lines," *Computers& Operations Research*, Vol.29, (6) pp. 741-759, 2002.

[8] Schöbel, A., Hamacher, H., Liebers, A. and Wagner, D., "The continuous stop location problem in public transportation networks," Technical Report 81, Wirtschaftsmathematik, University of Kaiserslautern, Germany, 2002.

[9] Hamacher, H. W., Horn, S. and Schöbel, A., "Stop location design in public transportation

networks: Covering and accessibility objectives," *TOP*, Vol.17, (2) pp. 335-346, 2009.

[10] Carrizosa, E., Harbering, J. and Schöbel, A., "Minimizing the passengers' traveling time in the stop location problem," *Journal of the Operational Research Society,* Vol 67,(10) pp. 1325-1337, 2016.

[11] Jha, M. K. and Oluokun, C., "Optimizing station locations along transit rail lines with geographic information systems and artificial intelligence", in Computers in Railways IX, Allan, J., Brebbia, C.A., Hill, R.J., Sciutto, G., Sone, S. , Eds. Southampton: WIT Press, 2004.

[12] Samanta, S. and Jha, M., "Identifying feasible locations for rail transit stations: Two-stage analytical model," *Transportation Research Record*, (2063) pp. 81-88, 2008.

[13] Chro, A. , "GIS and genetic algorithm based integrated optimization for rail transit system planning, " Ph.D. dissertation, Imperial College London, London, UK, 2016.

THERMAL AND FINANCIAL EVALUATIONS OF MUNICIPAL SOLID WASTE FROM ERBIL CITY-IRAQ

Shuokr Qarani Aziz[1],Jwan Sabah Mustafa[2]

[1]*Salahaddin University-Erbil, Iraq*
[2]*General Directorate of Dams and Reservoirs, Erbil*
[1]*shoker71@yahoo.com, shuokr.aziz@su.edu.krd,*[2]*juan.sabah@yahoo.com,* [2]*jwan.mustafa1@su.edu.krd*

doi:10.23918/iec2018.07

ABSTRACT

This work was aimed to study municipal solid waste (MSW) disposal problems and energy income from it. Open dumpsite and only buried of MSW causes risks to the people and the environment. Burring mixed MSW (without separation, leachate and gas collection) at Erbil Landfill Site (ELS) leads to leftover income and energy. Recyclable materials such as plastic, metals, glass, paper and cartons at ELS are income sources. Results revealed that average amount of daily disposed plastic, food waste, corrugated paper, other organics, wood, diapers, other inorganics, ferrous, and glass at ELS were 34%, 27%, 14%, 7%, 6%, 5%, 2%, 2%, 2%, and 1%, respectively. Additionally, thermal solution is required to convert the MSW and natural emitted gas from ELS to be a great source for the energy. Currently, produced methane gas and electricity from ELS are estimated to be 3,839,669.265 m^3 and 18,000.762 Kw for 1,223,834 populations, respectively. Expected annual income from recyclable materials is 97.528 $*10^6$ $. Finally, proper solution for disposed of MSW in Erbil City results in decreasing risks and environmental pollution, attainment of income by recyclable materials and release energy from gas and electricity.

Keywords: Solid waste, Methane gas, Energy, Income, Erbil City, Landfill.

1. INTRODUCTION

Communal systems for disposal and treatment of municipal solid waste (MSW) are open dumping, sanitary landfill, thermal treatment (anaerobic, pyrolysis, incineration, gasification, and plasma arc gasification) and composting. Technical landfills has been discovered to be the utmost economic MSW disposal method when equated with other systems of disposal, such as thermal and composting [1-3]. But the produced landfill leachate and gas emissions are common shortcomings of the MSW [4-5]. Without scientific solution, disposed landfill leachate and emitted gas from Erbil Landfill Site (ELS) cause pollution of the environment.

ELS regards as anaerobic landfill with daily cover-Level II [6]. In type II landfills, proper gas and leachate managements are not available [7]. Organization of emitted gas leads to decreasing environmental pollution and achieving income from the produced energy.

Increments of population numbers, growth of investment and economy, tourist, and industrialization are between the key parameters that promote the generation rate of MSW. Disposal of around 2000 tons/day of mixed MSW at ELS requires sufficient landfilling area, proper design, and management [8]. Issues on the engineering designs of landfill sites can often be detected in the developing countries, such as Iraq. Presently, more than 40 open dumpsites and landfills are available in Erbil City- Iraq. Most of the landfills consist only of dumping sites of mixed MSW without any managements to protect environment [6]. In addition, mixed disposed MSW leads to rapid finishing of landfill areas and lost huge income from daily covering the recyclable materials by soil. A study on domestic solid waste components published by [2]. The percentage of the recyclable materials plastic, metals, glass, and papers were 6.28%, 3.6%, 3.42%, 5.9%, respectively. The average amount of recyclable materials is more than 30 % in southern Asia Nations [7]. Based on the study conducted by Erbil Municipality in 2016, the percentage amount for plastic, food waste, paper, other organics, wood, diapers, other in-organics, ferrous, glass, and aluminum are 34%, 27%, 14%, 7%, 6%, 5%, 2%, 2%, 2%, and 1%, respectively [8].The disposed MSW at ELS is a massive amount which results environmental pollution and losing of affordable amount of money.

The objectives of the present work were: 1) to study the achievable income from recyclable MSW materials and 2) feasible produced energy (methane gas and electricity) from disposed MSW in Erbil City.

2. MATERIALS AND METHODS

The current work presented the ELS problems, especially mixed MSW without separation and emitted gas, and attainment of income and energy from MSW at ELS. The data were obtained from literature and Presidency of Erbil Municipality [2-6, 8-9]. To see the risks directly and to get extra information, site visit were carried out to ELS in June and November 2017. The quantity of produced methane gas and energy was based on equations and information from references [9-12]. Information and data given in the present research were obtained from published works, presidency of Erbil Municipality and administration staff for ELS and it became a scientific document for the upcoming works. The details for ELS, recyclable materials, and energy production are shown below.

2.1 ELS (ERBIL LANDFILL SITE)

ELS is located on the left side of Erbil-Mosul main road near Kani-Qrzhala Sub-district in Erbil City, Iraq. The geographical coordinates are 36°10'23" N and 43°35'32" E. It is opened in 2001 and it is approximately 15 km from Erbil City center. The total site area of ELS is 37 ha. Most part of the area has been used. In 2017, the site receives about 2000 tons of mixed MSW daily (Based on Administration Staff of ELS, 5 November 2017), Figure 1:

FIGURE 1. Satellite image of Erbil Landfill (Kani-Qrzhala) site.

The buried MSW is mixed without proper separation of the components. A small portion of recyclable materials, such as plastic, glass, and metals, are being separated by scavengers persons. Due to lack of scientific sanitary landfill design in this site, the formed gas is emitted to the atmosphere without any gas collection system which can be used as renewable source of energy, Figures 2 and 3.

FIGURE 2. Gas emission at ELS (13 June 2017)

FIGURE 3. Separation and collection of recyclable MSW at ELS (13 June 2017)

2.2 RECYCLABLE MATERIALS

In this research, recyclable materials for MSW at ELS represent plastic, metals, glass, and papers [9].

2.3 ENERGY PRODUCTION

2.3.1 METHANE GAS PRODUCTION

Usually, proper landfill management required to enhance both yield and quality of gas. In order to estimate gas production, four parameters should be known which are: (a) gas yield per unit weight of waste, (b) the lag time prior to gas production, (c) the shape of the lifetime gas production curve, (d) and the duration of gas production [10].

An equation is used to determine gas production, which published by Environmental Protection Agency (EPA) and the model called Landfill Gas Emission Model (Land GEM), and the equation ranging from single value to linear increase/ linear decline, to exponential decline as follow [10]:

$$\boldsymbol{Q_T = \sum_{i=1}^{n} 2kL_{\circ} M_{ie} e^{-kti}} \qquad (\mathbf{1})$$

Where:
Q_T = total gas emission rate from a landfill, volume/time.
n = total time periods of waste placement.
k = landfill gas emission constant, time $^{-1}$.
L_o= methane generation potential, volume/mass of waste.
t_i = age of the i^{th} section of waste, time.
M_i = mass of wet waste, placed at time i.

Erbil landfill opened in 2001 year, and it receiving 2000 tons/day, which means 730,000 tons/year. Assume landfill emission gas constant is (0.0307 year^{-1}), and the methane generation potential is (140 m^3/tons), to estimate peak gas production:

For the first year of opening in (2001):

Q_T= 2(0.0307)*(140)*(730,000)*(e $^{-0.0307(1)}$)
Q_T=6,085,362.114 m^3

For age at ti =15 (in 2016)
Q_T= 2(0.0307)*(140)*(730,000)*(e $^{-0.0307(15)}$)
Q_T=3,959,375.196m^3
For age ti =16 (in 2017)
Q_T= 2(0.0307)*(140)*(730,000)*(e $^{-0.0307(16)}$)
Q_T=3,839,669.265 m^3

2.3.2 POWER GENERATION

The generation rate (GR) of disposed garbage, plastic, paper and fabric = 608.02 g/cap/d (excluding glass and metals) [2, 9].

608.02 g/cap/d = 1.34 Ib/cap/d

Energy available in each 10^5 population [9, 11-12].

= 1.34 * 10^5*4500/24

= 2.51 * 10^7 BTU/h

Where BTU is British thermal unit

But, the efficiency is 20% and the theoretical value of the mechanical equivalent of heat is 3413 BTU/h. Therefore the heat rate is:

3413 / 0.2 = 17065 BTU / KWh

$$\text{Energy generated (KW)} = \frac{\text{Heat available in fuel}}{\text{heat rate}}$$

= 2.51 * 10^7 / 17065
= 1470.85 KW for each 10^5 population
For population of 1,223, 834 [8]:
Energy generated (KW) = 18000. 762 for 1,223, 834 populations

For MSW at ELS, GR= 1270 g /cap/d =2.803 Ib/cap/d [8].
Energy available in each 10^5 population
= 2.803 * 10^5*4500/24
= 5.256 * 10^7 BTU/h
Disposed MSW at ELS produces from 1,223, 834 [8]:
Energy available for 1,223, 834 populations = 6.432 * 10^8 BTU/h

3. RESULTS AND DISCUSSIONS

3.1 CURRENT SITUATION OF ELS

ELS considered as Level 2, which is sanitary landfill with daily cover, and anaerobic landfill, it also in the methane formation phase [6]. Based on the landfill structures shown in literature, upgrading the site from Level 2 to Level 3 Level 4 is essential [2]. Disposal of mixed MSW at ELS leads to terminate the provided areas for Landfilling. A part of recyclable materials is separated by scavengers only, Figures 3-4. Providing suitable system for separation of recyclable materials is recommended. In addition, a mixed-waste materials recovery facility (MRF) technology is recommended [9]. On the other hand, formed landfill leachate still discharges to the natural environment without treatment [3-4, 13].

FIGURE 4. Collected recyclable materials by scavengers at ELS (5 November 2017)

3.2 INCOME FROM RECYCLABLE MATERIALS

Recycling is an important subject in life, especially when it used final disposal products and again reused [14]. The recycling targets of the global waste management system, therefore focusing on the complete waste collection in future, and the achievement of waste management in study area. Therefore the necessary recycling facility required, but the waste still not separately collected. The aim of MSW recycling programs should not be to increase MSW recycling [15]. The objective should be to upgrade environmental quality and the sustainability of the economy, and from construction and demolition materials.

Recycling of MSW materials lead to achieving income, decreasing amount of MSW in landfills, minimizing environmental pollution, decreasing number of MSW collector

truck and crew size, decreasing scavengers problems in the landfill site, injury, increasing area for landfilling, and upgrading control/management of the landfill site.
Table 1 illustrates the details for calculation of income from the recyclable materials in Erbil City. The recyclable materials were plastic, ferrous, aluminum, glass and paper. The recoverable of recyclable materials are different [16]. Due to lack of scientific documents for the recoverable materials, Average recoverability of 80 % was proposed for the present work. Annual expected income for the recyclable materials in Erbil City is 97.528 * 10^6 $/year.

TABLE 1.
Details of income from recyclable materials

Recyclable Material	Ratio (%)	Amount * (tons/day)	Assumed average Price ($/tons)**	Average recoverable materials (tons/day)**	Income ($/day)	Income (10^6 $/year)
Plastic	34	680	400	544	217600	79.424
Ferrous	2	40	200	32	6400	2.336
Aluminum	1	20	1500	16	24000	8.76
Glass	2	40	75	32	2400	0.876
Paper	7	140	150	112	16800	6.132
Total	46	920		736	267200	97.528

*Total daily MSW disposal = 2000 tons/day
**Source: [16]

3.3 METHANE GAS AND ENERGY PRODUCTION

Depending on the equation, it is clear that for the second year, the waste produces les gas, but the next new layer produces more gases, and the two are added to yield the total gas production for the second year. The emitted methane gas from landfill site can be used to produce electricity, heat, and fuels by decomposing garbage, Figures 2 and 5.
The emitted gas can be directly used in boiler, furnaces, or kilns in the treatment system. Since ELS gas emissions are a global problem, so that, it must direct attention to improve these problems. If this can be provided, so it can be a major source of energy for the study area.
On the other hand, the study presented the assessment of environmental impact of ELS, and proposed applying processed waste to provide income and power generation especially in a manufacturing process where heat is required.

By using refused derived fuel (RDF) for the purpose of achieving high calorific fractions from processed (MSW) and industrial wastes or any other wastes are alternative to convert (waste to energy) plants.

RDF production appear most common way to achieve relatively high levels of recycling and composting ELS as high rates of source separation leave non-recyclable residues, which are suitable for RDF production.

Even in cities where the source of separation is not so well-developed, and where the source of separation with or without residual waste processed, it might be sufficient to get the landfill directive target, especially in waste management system will be very important.

In the present work, the expected total gas emission rate (Q_T) form ELS in 2017 is 3,839,669.265 m^3 which is huge amount and need proper management. Estimated electric energy generation is 18,000.762 KW for 1,223, 834 populations. Authority has problem for supplying 24 hours electricity for Erbil population due to loses and bad using of electricity, increasing population number etc. Finding another source for supplying electric with 18,000.762 KW from disposed MSW to Erbil City is very important and leads to environmental pollution. Furthermore, predictable energy available for 1,223, 834 populations in Erbil City is $6.432 * 10^8$ BTU/h. Nowadays, achieving this quantity of energy to Erbil City from discarded MSW is so valuable and results in decreasing pollution in the city.

FIGURE 5. Gas emission from ELS (5 November 2017)

4. CONCLUSIONS

In this study, it was observed that there is a lack from MSW management as ELS. Gas emission, leachate production, burring and inadequate of recyclable materials, and non-acceptable view are main characteristics of ELS. A number of buildings and facilities such as offices for administration, laboratory, guard house, weighing station, storerooms, fence, gas collection, leachate collection and treatment unit, and wells for groundwater monitoring are essential for ELS. Upgrading ELS from Level 2 to level 4 by proper management for emitted gas and produced landfill leachate is recommended. Providing suitable system for separation of recyclable materials is suggested as well. Expected annual income from recyclable materials is 97.528 $*10^6$ $. Foreseeable quantity of methane gas at ELS in 2017 is 3,839,669.265 m^3. Predictable amount of energy and electric from MSW at ELS are 6.432 * 10^8 BTU/ h and 18,000.762 KW, respectively.

Form ELS the measured methane gas from obtained data have the wide variability over space, in some cases, the land fill has been shown to act as net sinks for atmospheric methane, it should be incorporate to measure the influence of the produced gas and controlling it by the presence of gas recovery wells. At different locations at ELS huge amount of gas emitted to the environment, Figure 2. In July and August 2017, 18 gas collection pipes were penetrated to the landfill site ground. Distances between pipes are around 80 m and surrounded by filter materials.

For the entire ELS, a dis-acceptable view is seen. Administration building, laboratory, drivers and labors building, guard house, garage, fence, green area, sanitary system, weighing station etc. are essential for ELS.
The classification of solid waste form ELS revealed that most of the wastes are consists of plastic, food waste, corrugated paper, by percentages of 34%, 27%, 14%, respectively.

The ratios refer to that if the waste managed properly, it can provide a very large income and energy as well. The amount of recyclable materials from domestic wastes is 20.66%. Due to life style and economic factors in Erbil most parts of the domestic waste is food and organic wastes which was 79.34%.

REFERENCES

[1] Davis, M.L., Cornwell, D.A., Introduction to Environmental Engineering .4th edition. (International Edition). McGraw Hill, New York, 2008.

[2] Aziz, S.Q., Aziz, H.A., Bashir M.J.K., and Yusoff, M.S. "Appraisal of domestic solid waste generation, components, and the feasibility of recycling in Erbil, Iraq". Waste Management & Research, Vol. 29, No. 8, pp. 880-887, 2011

[3] Aziz, S.Q. and Maulood, Y.I. "Contamination Valuation of Soil and Groundwater Source at Anaerobic Municipal Solid Waste Landfill Site", Environmental Monitoring and Assessment. Vol. 187, No. 12, DOI: 10.1007/s10661-015-4971-y., 2015.

[4] Aziz, S.Q., Aziz, H.A., Bashir, M.J.K., and Abu Amr, S. "Expected environmental risks of the produced leachate from Erbil landfill site on the surrounded water sources". 4th International Engineering Conference (IEC4), Gaza, Palestine. , 2012.

[5] Aziz, S.Q. "Produced Leachate from Erbil Landfill Site, Iraq: Characteristics, Anticipated Environmental Threats and Treatment". In 16th International Conference on Petroleum, Mineral Resources and Development, Cairo, Egypt, 2013, Feb.10-12.

[6] Maulood, Y.I. and Aziz, S.Q. (2016) Soil and Municipal Solid Waste Leachate Characterization at Erbil Anaerobic Landfill Site, The Official Scientific Journal of Salahaddin University-Erbil, ZJPAS Vol. 28, No.3, 104-113.

[7] Aziz, S.Q. "Landfill Leachate Treatment Using Powdered Activated Carbon Augmented Sequencing Batch Reactor (SBR) Process", Ph.D. dissertation, Un Published, School of Civil Engineering, Universiti Sains Malaysia (USM), Malaysia, 2011.

[8] Presidency of Erbil Municipality (2017) A study on Erbil municipal solid waste components, June 2016.

[9] Aziz, S.Q. "A Quantitative Study on Domestic Solid Waste Components in Arbil City". Zanco-Journal of Pure and Applied Sciences, Salahaddin University-Erbil, Vol.21, No.4, (59–71), 2009.

[10] Worrell, W.A. and Vesilind, P.A. Solid Waste Engineering. Second edition, Publisher, Global Engineering: Christopher M. Shortt, 2012

[11] Tchobanoglous, G., Theisen, H., ans Eliassen, R., Solid Waste- Engineering principles and management issues. Second edition. McGraw-Hill International ,1993.

[12] Sabir, S. "Domestic solid waste management in Erbil City & their effects on surface and sub-surface water". Journal of Zanco, Vol. 14, No. 2., 2002.

[13] Aziz, S.Q., Aziz, H.A., Yusoff, M.S., Bashir M.J.K., and Umar, M. "Leachate characterization in semi-aerobic and anaerobic sanitary landfills: A comparative study". Journal of Environmental Management, Vol. 91,2010, pp 2608-2614.

[14] Environmental Protection Agency (EPA) "Municipal Solid Waste Generation, Recycling, and Disposal in the United States: Facts and Figures for 2012", United States, 2012.

[15] Lave, B. L., Hendrickson, C.T., Conway-Schempf, N.M., and McMichael, F. C. "Municipal Solid Waste Recycling Issues". Journal Of Environmental Engineering, October 1999.

[16] COVEC, Expert Analysis plus Practical Advice "Recycling: Cost Benefit Analysis". Final report prepared for Ministry for the Environment, COVEC Limited Level 11 Gen-i tower 66 Wyndham Street, PO Box 3224 Shortland Street Auckland New Zealand, April 2007.

HEAVY METAL POLLUTANT LOAD FROM A MAJOR HIGHWAY RUNOFF - SULAIMANI CITY

Yaseen Ahmed Hamaamin

University of Sulaimani, KRG, Iraq
yassen.ahmed@univsul.edu.iq

doi:10.23918/iec2018.08

ABSTRACT

First flush is the first rainfall after a dry season, which washes out several months of contaminant buildup. Surface runoff from highways can be considered as a critical nonpoint source of water resources heavy metals pollution. In this study, samples of rainfall runoff were collected after the first and second rainfall from a major highway in Sulaimani City and tested for expected Zinc(Zn), Copper (Cu) and Lead (Pb) heavy metals pollutants. Results revealed levels of heavy metals pollution in the highway runoff from the first and second rainfalls which can be considered as heavy metal pollution source for receiving water bodies. After first flush, average test results of heavy metals pollutants were 0.062 part per million (ppm), 0.075 ppm and 0.051 ppm for Zn, Cu and Pb respectively. Low Impact Development (LID) practices found to be a new sustainable stormwater management. Though, the removal of heavy metals from water is costly, consequently, a set of LID techniques are recommended for stormwater treatment as cost effective stormwater treatment for streets and highway runoff treatment. Furthermore, as Sulaimani city uses combined (sanitary and stormwater) sewer system, LID systems can reduce flooding, which makes the treatment of combined wastewater more feasible, improving the quality of receiving water bodies.

Keywords: Sulaimani, Runoff, LID Systems, Heavy Metals, Bioretention Basins.

1. INTRODUCTION

Roadways and streets as the non-point source of pollution are considered as one of the largest sources of environmental heavy metals pollution. Zinc (Zn), Copper (Cu), and Lead (Pb) are most common heavy metals released from on road automobiles parts wearing and tearing [1]. However, Lead concentrations have been reduced due to prohibiting leaded gasoline worldwide, but it is still might be used as an octane booster additive to gasoline in some developing countries [2].

While rainfall runoff moves on ground, it carries away natural and manmade pollutants, in conclusion depositing them into downstream water bodies such as lakes, rivers and ground water [3]. Cu, Pb and Zn were found in almost all urban street and highway stormwater runoff in concentrations that would violate the U.S. Environmental Protection Agency (EPA) for water quality criteria, seldom cadmium and mercury were also present above those standards [4]. Car brake pads release Cu, while tire wear releases Zn, also motor oil and fuel burn or leakage can become another pollution sources to the environment [1,5]. Chronic exposure to heavy metals can result in many human disorders and increases cancer risks [6, 7, 8].

Since the 1970s, the non-point sources of pollutions are controlled using Best Management Practices (BMPs) that are designed to limit the quantity of pollutants released into a waterbody. BMPs, are structures, tools, or processes for removing or reducing stormwater runoff pollutants from reaching downstream receiving water bodies [5]. From the 1990s, EPA agencies have started to assess and adopt the local stormwater management plans through the adoption of local BMPs replicating the natural filtering and pollutants removals from storm runoffs which are known as Low Impact Development (LID) [5,9]. LID is an on-site interrupting and delaying of the runoff flow on pervious areas, LID utilizes the possible biological, chemical and physical processes that are found in the natural environment to maintain or restore the watershed's hydrologic and ecological functions [2,10].

The first half inch rainfall after the dry season (first flush) is considered the more hazardous and contaminated runoff, which washes away about 80% of the total mass of

pollutants built-up on roads and streets [11]. Sediment particles are more critical for pollutants adsorption and transporting with storm runoff [2,12]. Furthermore, sediments deposited in lakes and rivers impair the water quality and degrade the ecosystem of the water bodies, stormwater runoff contributes about 70 % of the pollution in rivers and lakes [10].

Urbanization and elevated number of automobiles in the Kurdistan Region of Iraq are contributed to the deterioration of the environment and water resources quality [13]. The objective of this study is to measure and estimate the heavy metal pollution involvement of streets to water resources in Sulaimani City which impair the quality of water in the area. Finally, from literature, the author suggested some effective methods to reduce and eliminate the impacts of highways and roads pollutants on water resources downstream of Sulaimani City by selecting sustainable LID practices for the stormwater runoff management.

2. LOW IMPACT DEVELOPMENT (LID)

LID is the on-site interrupting and delaying the runoff flow on pervious areas such as grassed or graveled swales and bioretention basins. LID gives the water a chance to infiltrate and also the removal of pollutants (settled, filtered and up-taken by plants), consequently reduce amount of runoff at the outlet and improve water quality as well [3,9]. LID is the stormwater management at the site or at the pollution source, using treatment and volume control practices for storm events at lower costs of construction [14]. The LID practices execution recharges groundwater, and decreases soil erosion which consequently reduces pollutant transport due to their attachments to the sediment particles. There are different types of LID systems such as bioretention (rain garden), lawn swales (vegetated channel), vegetated rooftops, rain harvesting (rain barrels), cisterns, vegetated filter strips and permeable pavements. Perhaps, the most practical and popular types are the following:

2.1. SWALES

Swales or Bioswales are small trenches usually constructed in the road medians or beside streets which convey and infiltrate the collected rainwater from roads and sidewalks (Figure 1). There are two types of swales rock surface infiltration swales and grass surface swales, which the bed and sides of bioswales channel covered with native grasses. Swales have underneath perforated pipe to convey the filtered water to the stormwater sewer pipe network. Also they usually have inlet risers to drain the excess stormwater overflow beyond the infiltration capacity of the swales. Continuous street curbstone should be interrupted, to let flowing runoff entrance from street to the swale management structure. Continuity of swales interrupted by building entrances and road branches can be achieved by underground pipes connecting between discontinuous swales [9,14].

2.2. BIORETENTION BASINS

Bioretention basins are depressed area designed to capture and retain the stormwater for a specific time before entering the stormwater management facilities (Figure 2). This depressed small pond usually contains plants such as native grasses and trees which help retard the flow rate and up-taking of the pollutants. Bioretention can be used to improve the treatment as secondary treatment units for streets runoff overflow from bioswales. Bioretention basins fundamental element is the filter media which consist of 60- 120 cm material composed from 65% sand, 20% sandy loam and 15% vegetation based feedstock. A shallow depth of water (about 30 cm) is hold inside the bioretention basin. Overflow inlets are provided to safeguard surface flooding from retention area to the surrounding lands during storm events [9,14].

2.3. PERMEABLE PAVEMENT

Local roads, parking lots and sidewalk surface can be constructed from permeable and perforated materials such as permeable pavements and porous tiles to allow water to infiltrate down to the ground. Also, parking lots and impervious pavements

can be interrupted by pervious soil strips as much as possible in areas which are not obstacle the movement of cars and parking activity. The technique of reducing impervious area and increasing pervious areas is known as green parking method. Implementing green parking practice reduces pollutants washout volume from parking areas, decreases the urban heat island effect, recharges groundwater and improves aesthetics of the site [15].

3. METHODOLOGY

3.1 STUDY AREA

For this study, Tasluja major highway was selected as the research area. The highway connects Sulaimani City with Kirkuk City and considered as one of the city's roadways with high volume of traffic load, Figure 3. The City of Sulaimani as one of largest cities of Kurdistan Regional Government in Iraq, is located at north east of Iraq on the Iran border with geographic coordinates of Latitude = 35°33′40″ N and Longitude =45°26′14″. The weather of the city is dry and warm in summer with average temperature of 31.5°C, while the city is cold and wet during winter season with average.

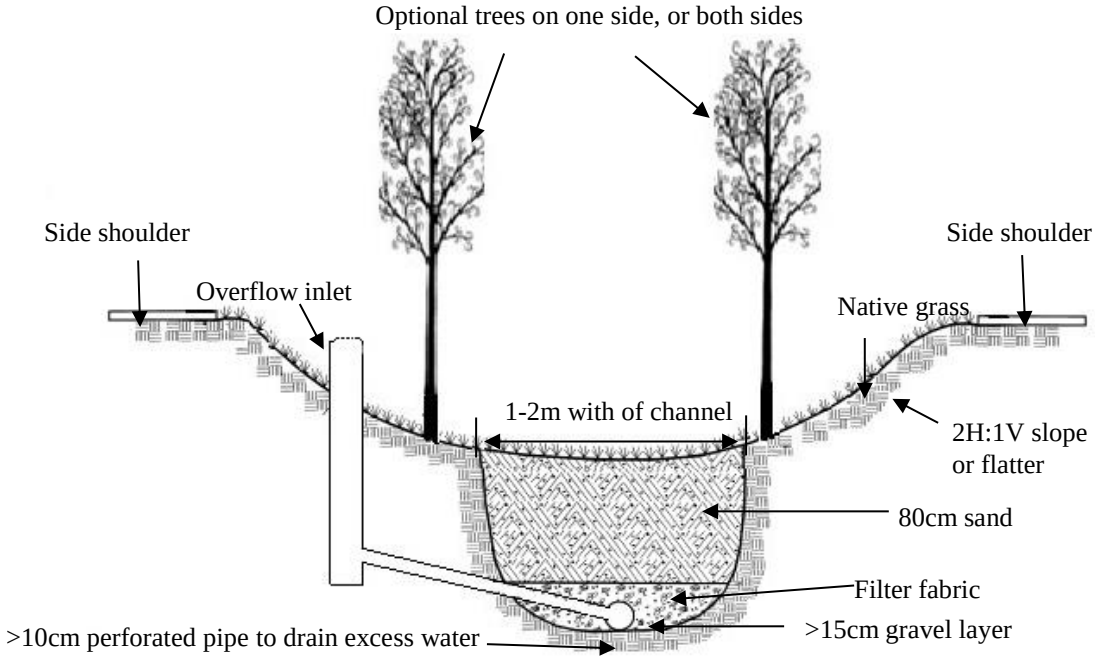

FIGURE 1. Bioswales for streets, [14]

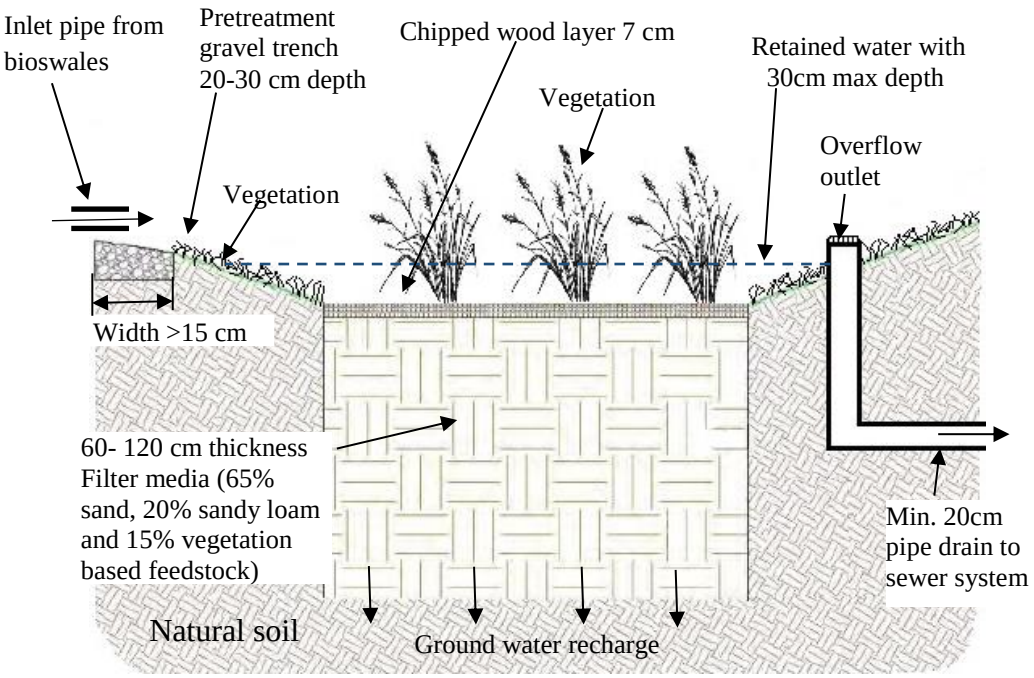

FIGURE 2. Typical bioretention basin, [14]

Temperature of 7.6ºC. The evaporation during summer and winter are 329.5 (mm) and 53 (mm) respectively. Precipitation starts with light rainfall in October and strengthens during November and mostly continues to May. The average annual precipitation varies between 328mm for dry years and 848mm for wet years [13,16]. Sulaimani as a developing city is observing a rapid growth and development, current population more than 735000 with massive traffic volume with high number of cars. Sulaimani city has a combined sewer system which collects the stormwater and sanitary sewage together in a single pipe system that drains the sewage downstream of the city without any treatment plants [17].

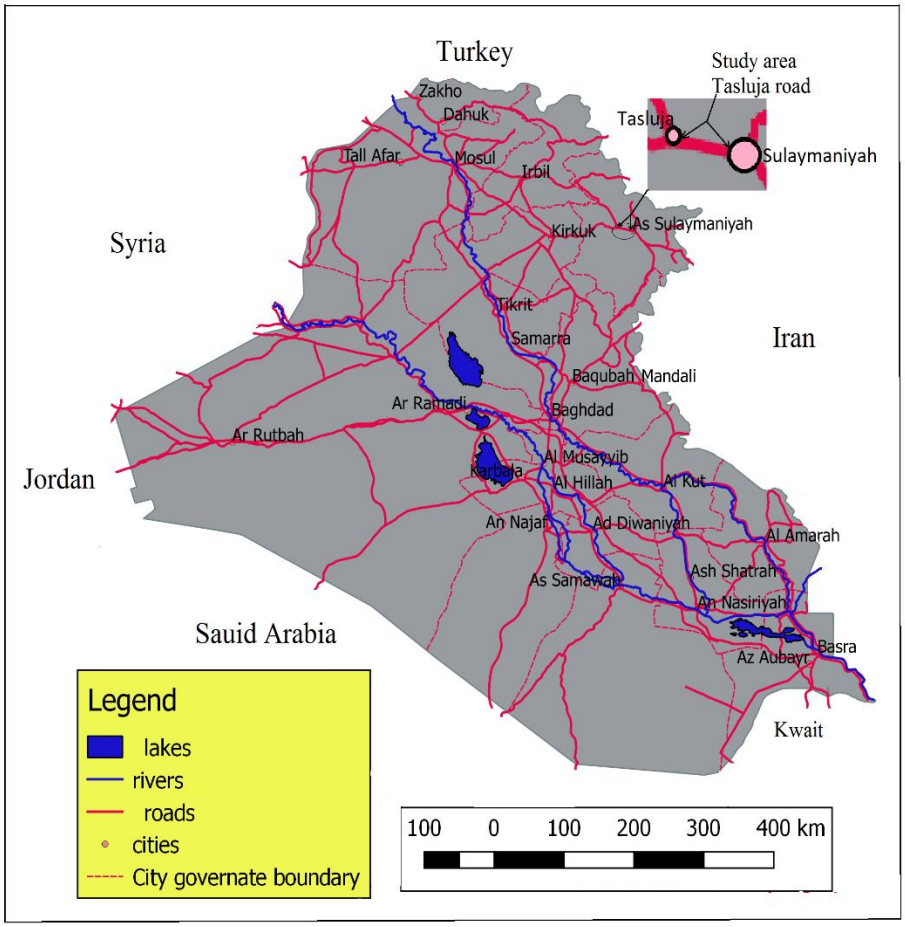

FIGURE 3. Study area: Tasluja Highway

3.2 RUNOFF SAMPLING

Rainfall runoff were collected from Tasluja highway. Four sampling points were assigned on the highway, two points at each side, to collect samples of runoff depending on the highest amount of drainage area from the highway surface. Two sets of samples were collected after the first and the second rainfall events. The first rainfall (first flush) occurred on November 2, 2016, and the second rainfall was happened on November 29, 2016. Four samples of runoff from the street were collected after each rainfall at the same specified sites along Tasluja highway. Water samples were collected, transferred in sealed plastic bottles and tested during the next 24 hours for heavy metals contents (Zn, Cu and Pb) using Perkin Elmer ICP-OES Optema 2100 Optical Emission Spectrometer.

4. RESULTS AND DISCUSSIONS

Tearing and wearing of operative vehicle parts on roads is the major source of heavy metal pollution in runoff from highways and roads. Results of the heavy metal tests for both first and second flush runoff samples are shown in Tables 1 and 2 respectively. Test results show that the samples of runoff from roads of the city are polluted with heavy Zn, Cu and Pb heavy metals which can deteriorate the quality of water in the downstream area. As the first flush washes out long dry season collected pollutants, for this reason, in general higher heavy metal concentration can be observed from the first flush sample results compared to the second rainfall results. However, Pb heavy metal could not be detected for all sample points for the second rainfall sample results. According to USEPA [18], maximum allowable concentration of Zn, Cu and Pb heavy metals in water are 5 mg/L (ppm), 1.3 mg/L and 0.015 mg/L. Tables 1 and 2 show that the average Zn concentration for first and second rainfalls of 0.062 mg/L and 0.022 mg/L respectively are below the maximum allowable limit in surface water. Also Cu average concentration of 0.075 mg/L for both rainfalls are below the maximum allowable limit of USEPA. Comparing to the standards, Pb contents of 0.051 mg/L is higher than the allowable limit of 0.015 mg/L. However, Lead was not detected in the second rainfall, this may be because of inexistence of the pollutant spill during the period between the two rainfalls. Nevertheless, the shown accumulated amount of pollution is out of only two rainfall events, therefore continuous receiving of heavy metals at the downstream water bodies results in the buildup of heavy metal which exceeds the maximum allowable limits resulting in pollution in the downstream environment.

TABLE 1.

First rainfall runoff water samples result of heavy metals tests

Sample Number	Zn (mg/L)	Cu (mg/L)	Pb (mg/L)
1	0.118	0.085	0.01
2	0.030	0.084	0.099
3	0.024	0.064	0.009
4	0.076	0.067	0.085
Average	0.062	0.075	0.051

TABLE 2.

Second rainfall runoff water samples result of heavy metals tests

Sample Number	Zn (mg/L)	Cu (mg/L)	Pb (mg/L)
1	0.01	0.078	Not detected
2	0.001	0.077	Not detected
3	0.002	0.076	Not detected
4	0.076	0.067	Not detected
Average	0.022	0.075	Not detected

Figure 4 shows Zn, Cu and Pb heavy metals concentration for first and second rainfalls at each of the sample locations of 1,2,3 and 4. Zn concentrations are reduced in the second rainfall compared to the first rainfall, this may due to spilling less amounts of Zn during the one-month period between the two rainfalls. Cu concentration stayed almost same for the two rainfalls, means existence of same amount of Cu during the period between the two rainfalls. As a final point, concentration of Pb was not detected in the second rainfall, which may be due to not existence of reasonable amount of Pb spill in the period between the two rainfall events. While LID practices can reduce the environmental impacts of roads and highways on receiving water, the city can use a set of LID systems to enhance quality of water.

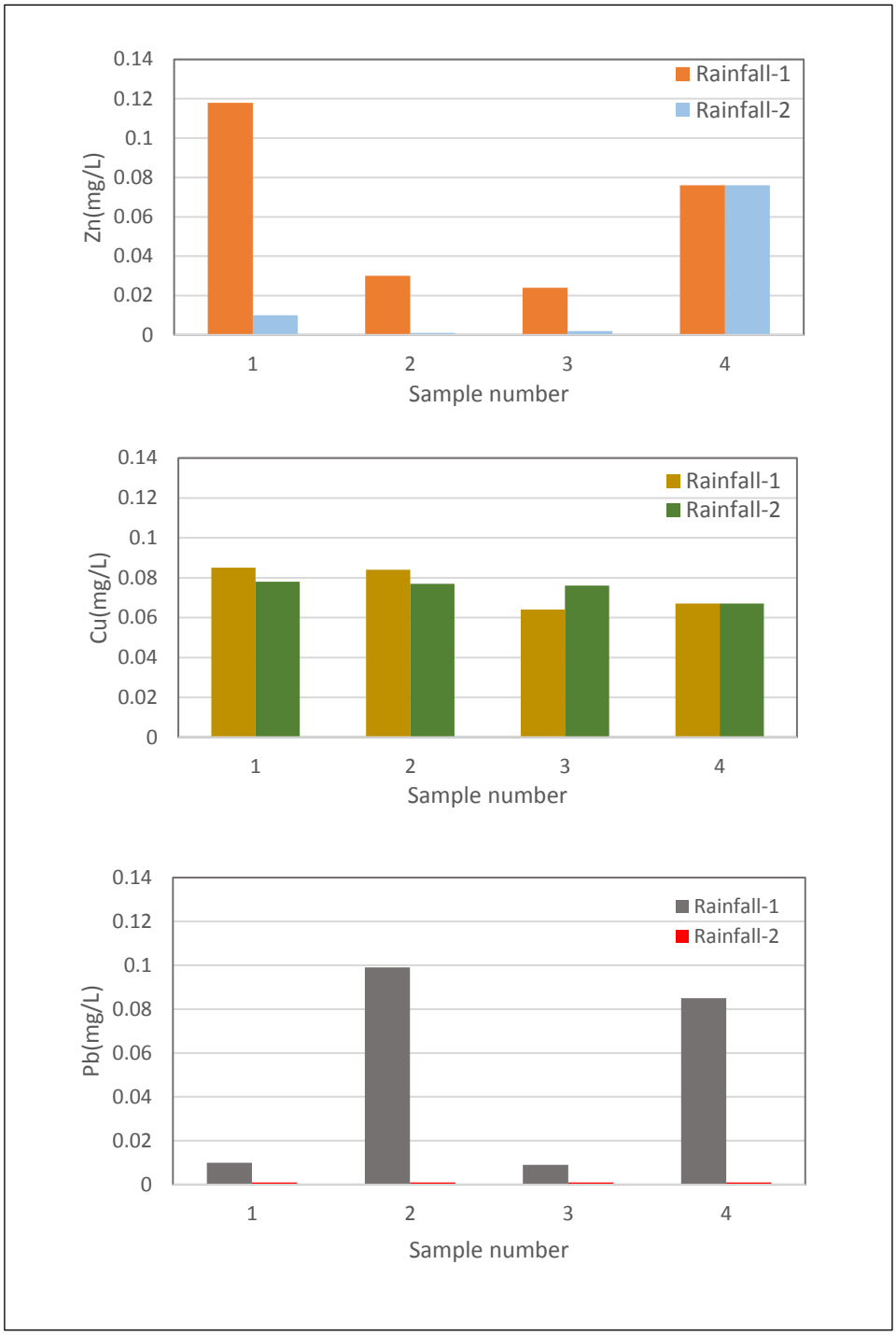

FIGURE 4. Comparison of Zn, Cu and Pb concentrations for 1st and 2nd rainfalls

5. CONCLUSIONS

Pollutants from tearing and wearing of cars parts and tires considered as a hazardous nonpoint source of heavy metal contaminations. Heavy metals namely Zn, Cu and Lead were detected in samples of stormwater from Sulaimani City main roads. First flush (1^{st} rainfall) runoff has more contamination load compared to 2^{nd} rainfall. After first flush, average test results of heavy metals pollutants were 0.062 ppm, 0.075 ppm and 0.051 ppm for Zn, Cu and Pb respectively. After second rainfall average test results were 0.022 ppm, 0.075 ppm for Zn, Cu respectively, while Pb heavy metal was not detected. Results of this study showed that the Pb concentration in highway runoffs are higher than the allowable Pb concentration in surface water, while the Zn and Cu concentrations are lower than the maximum allowable concentration. However, the concentration of heavy metals pollutants is relatively low, but continues receiving even small doses will be buildup and collected in water bodies to cause severe heavy metal pollution hereafter. Using LID systems to treat runoff from highways and impervious areas can reduce heavy metal pollutant and protect Sulaimani City environment.

6. RECOMMENDATION

This study suggests the following LID systems to manage the stormwater for streets and roads of Sulaimani City:

- Grass swales (with vegetation) and rock swales (without vegetation) in the medians and shoulder of the streets to treat rainfall flow from both sides of the street.
- Bioretention basins are recommended in the appropriate areas to improve the treatment as secondary treatment units for streets runoff overflow from bioswales.
- Parking lots and impervious pavements can be interrupted by pervious soil strips as much as possible (green parking), or using pervious pavements may be used.

- Implementing green parking practice reduces pollutants washout volume from parking areas, decreases the urban heat island effect, recharges groundwater and improves aesthetics of the site.
- Whereas the city has combined sewer network which collect sanitary wastewater and stormwater in one sewer pipe network, application of LID systems can reduce the amount of accumulated water during storms which make treatment of the combined sewer systems for the city feasible during storm events.

ACKNOWLEDGEMENTS

The author would like to express his deep gratitude to Kurdistan Region Strategic Research Center for their contribution to conduct this study.

REFERENCES

[1] National Cooperative Highway Research Program, (NVSWCD), 2006. Evaluation of Best Management Practices for Highway Runoff Control. No. 565. Transportation Research Board. http://www.fairfaxcounty.gov/nvswcd/newsletter/heavymetal.htm Accessed 10 July 2015.

[2] Zhang, J.J. and Day, D., 2015. Urban Air Pollution and Health in Developing Countries. In Air Pollution and Health Effects (pp. 355-380). Springer London.

[3] U.S.E.P.A., 2007. Reducing Stormwater Costs through Low Impact Development (LID) Strategies and Practices. EPA Publication No. EPA 841-F-07-006. Washington. D.C. www.epa.gov/nps/lid.

[4] Fred Lee, G. and Jones-Lee, A. 2005. Urban Stormwater Runoff Water Quality Issues. Water Encyclopedia. 3:432–437.

[5] Field, R., Struck, S.D., Tafuri, A.N., Ports, M.A., Clar, M., Clark, S. and Rushton, B., 2006. BMP Technology in Urban Watersheds. Current and future directions. Virginia: American Society of Civil Engineers (ASCE) ISBN: 0-7844-0872-6.

[6] World Health Organization (WHO), 1996. Health criteria and other supporting information.

[7] Councell, T.B., Duckenfield, K.U., Landa, E.R. and Callender, E., 2004. Tire-wear particles as a source of zinc to the environment. Environmental Science and Technology, Washington-DC, 38, pp.4206-4214.

[8] Geiger, A. and Cooper, J., 2010. Overview of Airborne Metals Regulations, Exposure Limits, Health Effects, and Contemporary Research. US Environmental Protection Agency. Accessed Accessed on August, 25, p.2015.

[9] Theis, T.; Tomkin, J., 2012. Sustainability: A Comprehensive Foundation; University of Illinois: Urbana-Champagne, Il, USA.

[10] Flint, K.R., 2004. Water quality characterization of highway stormwater runoff from an ultra-urban area (Doctoral dissertation, University of Maryland, College Park).

[11] Jones, D.E., 2012. Development and evaluation of best management practices (BMPs) for highway runoff pollution control.

[12] Gunawardana, C., Goonetilleke, A., Egodawatta, P., Dawes, L. and Kokot, S., 2011. Role of solids in heavy metals buildup on urban road surfaces. Journal of Environmental Engineering, 138(4), pp.490-498.

[13] Zakaria, S., Mustafa, Y.T., Mohammed, D.A., Ali, S.S., Al-Ansari, N. and Knutsson, S., 2013. Estimation of annual harvested runoff at Sulaymaniyah Governorate, Kurdistan region of Iraq. Natural Science, 2013.

[14] County of San Diego, 2014. Low Impact Development Handbook, Stormwater Management Strategies. Department of Public Works, 5510, San Diego, California 92123.

[15] Cahill, T.H., 2012. Low impact development and sustainable stormwater management. John Wiley & Sons.

[16] Al-Ansari, N., Abdellatif, M., Zakaria, S., Mustafa, Y.T. and Knutsson, S., 2014. Future Prospects for Macro Rainwater Harvesting (RWH) Technique in North East Iraq. Journal of Water Resource and Protection, 2014.

[17] Barzinji, Dana A. Mohammed, and Dilshad GA Ganjo. 2014." Water Pollution, Limnological Investigations in Kurdistan Region and Other Part of Iraq."

[18] U.S. E.P.A., 1994a. "Summary of EPA finalized National primary drinking water regulations: U.S. E.P.A. Region VIII, 7 p.

A CASE STUDY: EFFECT OF SOIL-FLEXIBILITY ON THE SEISMIC RESPONSE OF REINFORCED CONCRETE INTERMEDIATE-RISE REGULAR BUILDINGS IN HALABJA CITY

Rabar Hama Ameen Faraj

Halabja University, Kurdistan Region, Iraq
rabar.faraj@halabjauni.org

doi:10.23918/iec2018.09

ABSTRACT

On November 2017 an earthquake hit the city of Halabja which is located at Iraq-Iran border with the magnitude of 7.3 according to Richter scale. However, the damages still can be considered not that huge comparing to the intensity of the earthquake shake. Therefore, this paper has been carried out to investigate the effects of different soil profiles on the amount of damages and the behavior of buildings during earthquakes. In this paper the flexibility of soil or soil structure interaction (SSI) has not been considered and the conventional method (equivalent static lateral force procedure) which assumed that the structure is fixed at the base has been used for analysis. Three dimensional (3D) Model of eight storey residential building with plan dimensions of 20mX12m, each storey having a height of 3.2 m have been developed to analyze and compare the effect of seismic forces on multistory building by commercially available computer program, ETABS 2016. Various seismic parameters have been taken from ASCE7-10 and Iraqi Seismic code 2013 for Halabja city and five soil profile types (SA, SB, SC, SD and SE) have been considered during analysis according to both codes. The base shears, storey moments, max story displacements, and inelastic storey drift responses with respect to change in storey level and soil conditions of the structure have been calculated. Based on the current paper, It has been observed that the soil profile type have significant influences on the behavior of the building during earthquakes. Additionally, the seismic forces are significantly reduced for harder soil profiles which could be one of the most important factors behind having small damages during Halabja earthquake.

Keywords: Soil profile types, RC buildings, Standard Codes, Seismic behaviour, Halabja city.

1. INTRODUCTION

The Earthquake causes different shaking intensities at different site locations. Nowadays, it is significant to avoid damaging the structure while having earthquake at high level of intensity. This is because earthquake might destruct the buildings due to causing different shaking intensities. On November 2017 an earthquake hit the city of Halabja which is located at Iraq-Iran border with the magnitude of 7.3 by Richter scale according to the United States Geological Survey (USGS) [1]. However, the damages still can be considered not that huge comparing to the intensity of the earthquake shake. There are many aspects that have a clear impact on the intensity of shaking of the building, such as the strong shaking and its duration, the profile of the soil type in the area, frequency content of the motion, and distance from fault or epicenter [2]. The research and investigations conducted in the last decades, demonstrate a dynamic relation between the firmness of the structure and the type of soil on which it is built on. This dynamic soil-structure interaction (SSI) can sometimes have a remarkable role in determining the amount of displacements and forces faced to the built structure. The process of analyzing high rise RC of buildings is facilitated in the way that a fixed base is assumed and the influence of SSI is neglected. However, various types of soil can influence the dynamic and static characteristics of the building structures and consequently control the structures' dynamic and static behavior. In order to analyze the building structures with regard to their dynamic and static loadings, certain parameters such as storey bending moments, the basic natural periods, storey displacements or drifts, and base shear forces should be taken into consideration and assessed appropriately [3].

Anand N, et la 2010 [4] carried out an investigation in which they analyzed one to fifteen storey three dimension frames, once with shear wall and once without, along with three various kinds of soil and then analyzed them according to the codal provision and compared the results in different regards. It was shown that the base shear values in the three kinds of soil for frames up to three storeys were similar. However, the base shear values for frames above three storeys grew with change of soil type from hard to medium and medium to soft. The base shear reduction percentage for all the frames investigated varied from 0 to 18.5% when the soil changed from soft to medium whereas the amount reduced to 0 to 26.5% when the soil changed from medium to hard. Similarly, the lateral displacement increased with

reduction in the hardness of the soil on which the building frames were erected upon. The lateral displacement percentage for all the building frames witnessed a decrease of 0-26.5% when the soil changed from medium to hard and 0-18.7% when the type of soil changed from soft to medium. The Moment in the columns and the Axial force increases when the type of soil changes from hard to medium and medium to soft.

A. Massumi and H.R. Tabatabaiefar [5] considered SSI influences in seismic design of ductile RC- Moment Resisting Frame Systems (MRFS) according to Iranian code. Dynamic SSI is necessary for assessing structural safety during earthquakes. For this reason four types of buildings consisting 3, 5, 7 &10 stories resting on three different types of soils according to Iranian codes were analyzed. Soil was modeled by Finite Element method. The results led to a conclusion that SSI is necessary for buildings higher than three stories on soil type whose Vs<175 m/s and for buildings greater than seven stories on soil type 175< Vs<375m/s. However, due to reducing the computational effort, and the lack of information about local soil data to determine the soil profile types for Halabja city, this paper followed the foundation modeling of ASCE7-10 [6] and UBC 1997 [7] which permitted to consider the structure to be fixed at the base for the purposes of determining seismic forces.

2. ANALYSIS APPROACH

The Case study involves assessing the seismic performance of eight story residential regular building while varying site conditions. Nevertheless, the local soil profile data for Halabja city was not available due to not having previous site soil investigations in this regard in the city. Therefore, the building site soil classes were assumed in this analysis are: soil class A corresponding to ‘Hard rock’, soil class B corresponding to ‘Rock’, soil class C corresponding to ‘Very dense soil and soft rock’, soil class D corresponding to ‘Stiff soil’ and soil class E corresponding to ‘Soft clay soil’, in regard with ASCE 7-10 [6]. The flexibility of soil or SSI has not been considered and the building was assumed to be fixed at the base. Commercially available computer program, ETABS 2016 (CSI 2007) [8] has been used to compare the seismic forces, displacements and drifts in a (3D) model of multistory building.

2.1. THE BUILDING MODEL

The structure analyzed in this study is residential reinforced frame building, which consists of 5 grids in X-direction and 4 grids in Y-direction. To withstand lateral forces, a system consisting of special moment resisting frames (SMRF) was used assuming fixed base joints at the ground surface. A floor height of 3.2 m was assumed for all stories except ground level with 4 m. The details of the building are shown in Figure 1 and Figure 2.

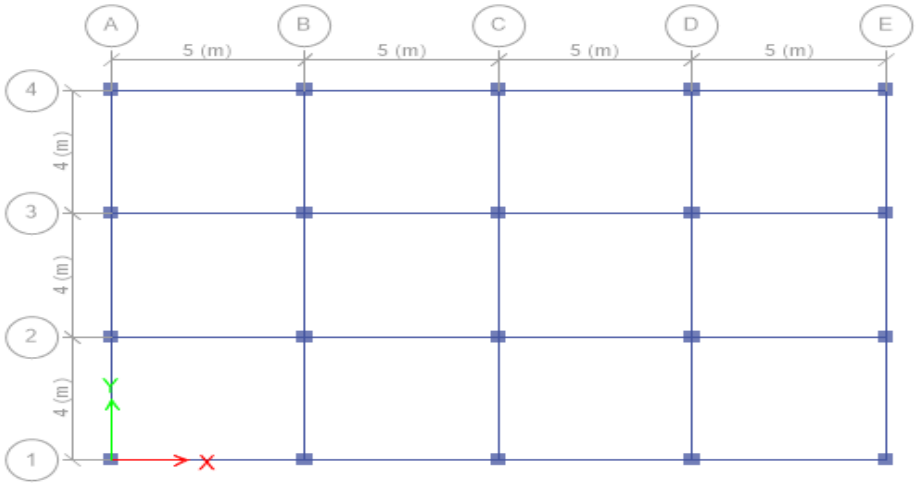

FIGURE 1. Typical Building Floor Plan

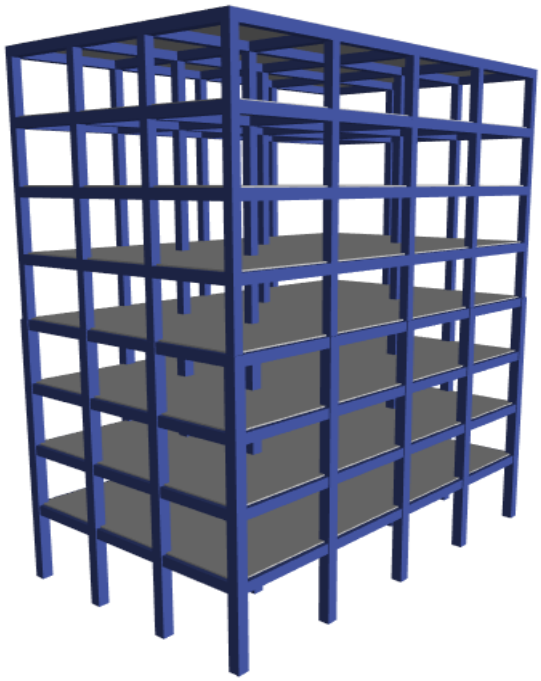

FIGURE 2. Typical 3D model

The materials were selected for the building based on their availability in the Kurdistan region market. It was assumed that the ultimate compressive strength of concrete f'c = 25MPa; the reinforcement yield strength fy = 420MPa, and a modulus of elasticity of 200GPa.

The gravity dead loads assigned to the building are the self-weights of the structural elements including the reinforced concrete columns, slabs and beams. The weights of the nonstructural elements (e.g. tiling, partitions, finishing, etc.) were modeled as a superimposed uniform dead load equal to 4kN/m^2. A uniform live load of 2kN/m^2 was used for all residential areas based on the ASCE 7-10 [6] load requirement criteria.

The Column dimensions are 0.5x0.5 m up to storey four and 0.4x0.4 m for upper stories. The beams were 0.5m in depth and 0.4m in width with the floor slab depth of 0.15m.

2.2. SEISMIC ANALYSIS

As an internationally acceptable method for this type of regular buildings (Equivalent Lateral Force Analysis) has been used to calculate all seismic forces and displacements according to ASCE7-10 Code [6] and the Iraqi seismic code 2013 [9] which is mainly adopted from ASCE7-10 [6]. The seismic coefficients and parameters have been taken from both previous codes as shown in table 1.

TABLE 1.
Seismic Load Parameters

Parameter	value
S_s: mapped MCE, 5 percent damped, spectral response acceleration parameter at short periods. (for halabja city)	2.16 (g)
S_1: mapped MCE, 5 percent damped, spectral response acceleration parameter at a period of 1 s. (for halabja city)	0.86 (g)
R = response modification coefficient (SMRF)	8
W = effective seismic weight of the building	Dead Loads+ %25 live load
Cd = deflection amplification factor	5.5
Ie = the importance factor (residential Building)	1
Ta = approximate fundamental period of the Building	0.886 sec.
Risk Category	II

3. RESULTS AND DISCUSSIONS

3.1 STOREY DISPLACEMENTS

Figure 3 and Figure 4 shows the maximum story displacements in both directions of the building. The results showed that, the max. Storey displacements for both directions significantly reduced through changing the soil profiles. For instance, the max. Story displacement at storey 8 in X direction is only 34.11 mm for soil profile type SA. However, this value dramatically increased to 92 mm for soil profile type SE. On the other hand, the Y direction follows the same trend with 36 mm and 99 mm max. storey displacements at storey 8 for soil profile types SA and SE respectively. However, Y direction displacements are relatively larger than the other direction due to smaller width compared to the length of the building. Similar results were found in other studies [4].

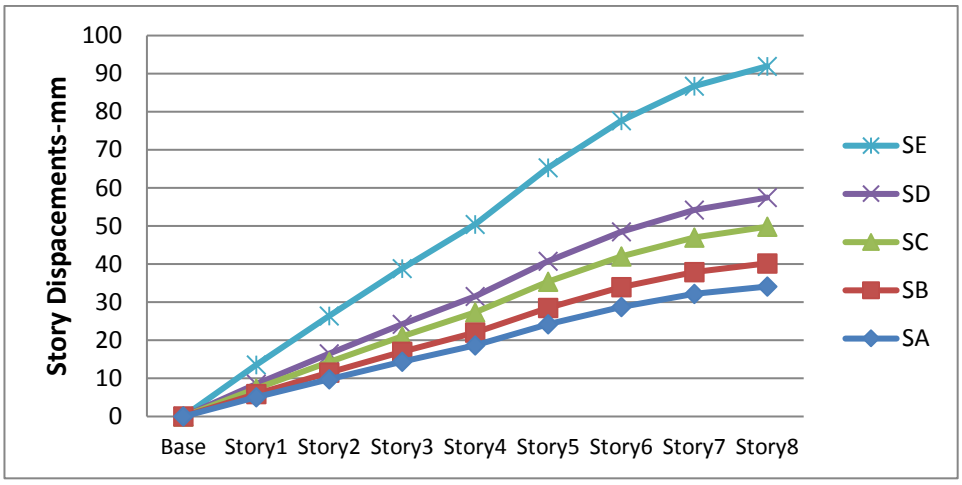

FIGURE 3. Max Storey Displacements in X direction

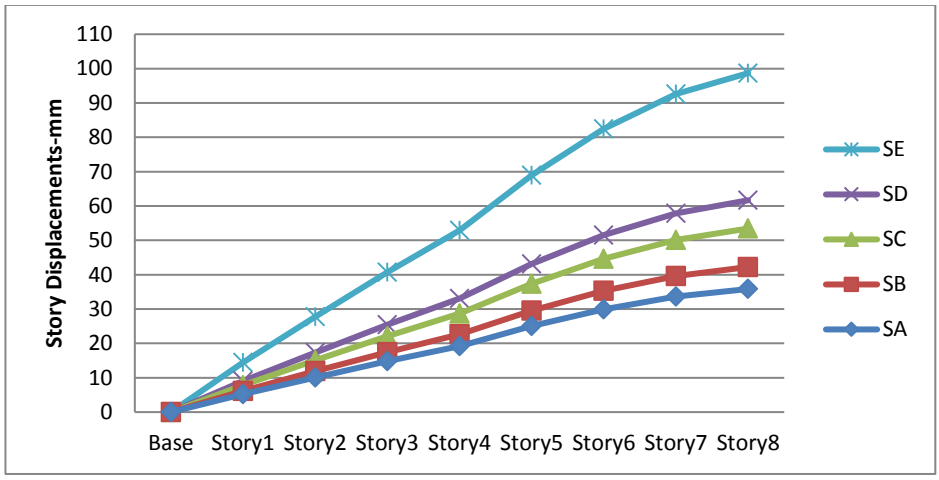

FIGURE 4. Max Storey Displacements in Y direction

3.2 INELASTIC STOREY DRIFTS

The inelastic storey drift results are presented in Figure 5 and Figure 6 for both X and Y directions. The figures illustrate that the inelastic storey drift will not necessarily occur at the top level and for the analyzed building it occurs at level 5. The highest inelastic storey drift values occurred in Y direction with approximately 88 mm for soil profile type SE at level 5. However, the lowest values were calculated for soil profile type SA in X direction with approximately 10.6 mm at level 8. Therefore, it can be said that with increasing the soil flexibility the inelastic storey drifts significantly increased especially for soil profile type SE.

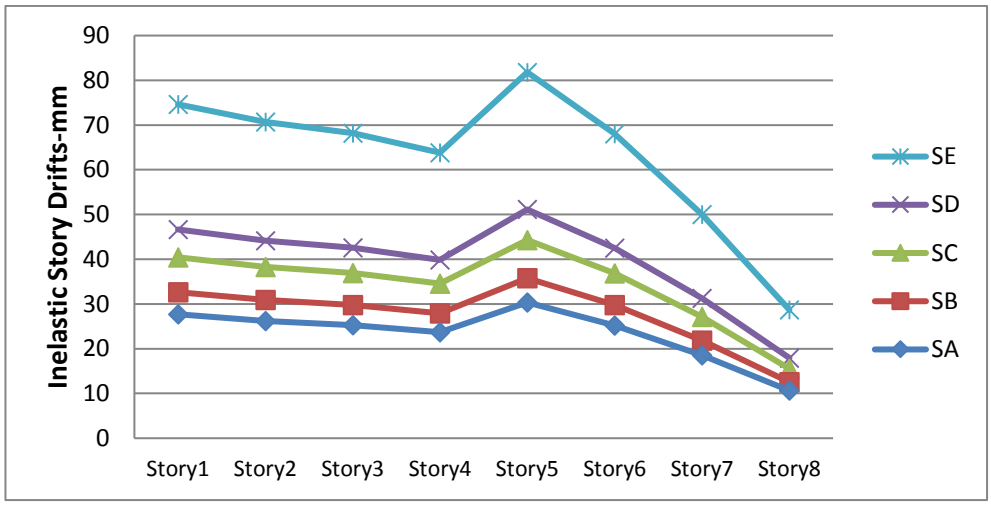

FIGURE 5. Inelastic Storey Drifts in X direction

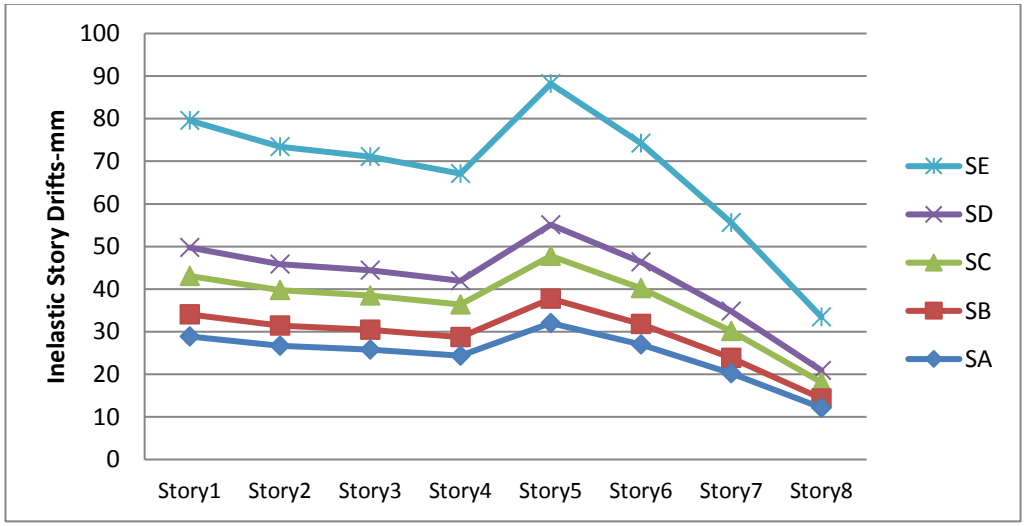

FIGURE 6. Inelastic Storey Drifts in Y direction

3.3 STOREY SHEARS

The results shown in Figures 7 demonstrate that the soil profile type has a significant contribution in increasing the storey shear of the building. This influence is more marked in buildings built on softer soils. The maximum storey shear was found at the base of the structure for soil profile type SE with 3384KN. There was about %270 increase in storey shear at the base of the building when the soil profile type changed from SA to SE. Similar results were observed in previous studies [10]

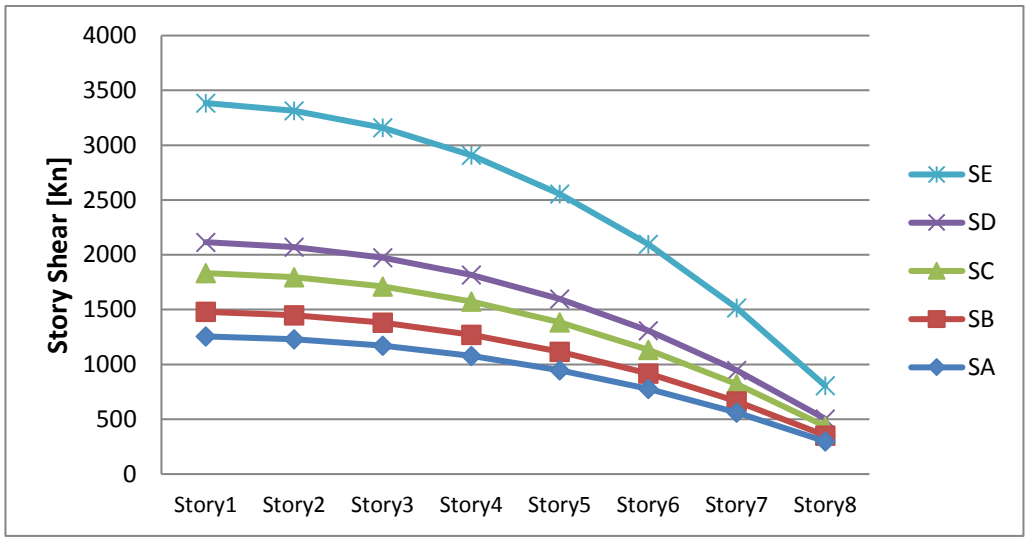

FIGURE 7. Story Shear

3.4 STORY MOMENTS

Figure 8 demonstrates the storey moments for different soil profile types and varying storey levels. The results show that there was a systematical increase in story moments through changing the soil profile type from SA to SE. There is also about %275 increase in storey moment at the base of the building when the soil profile type changed from SA to SE. However, the results indicated that the soil profile types SA and SB have approximately the same effect on the storey moments.

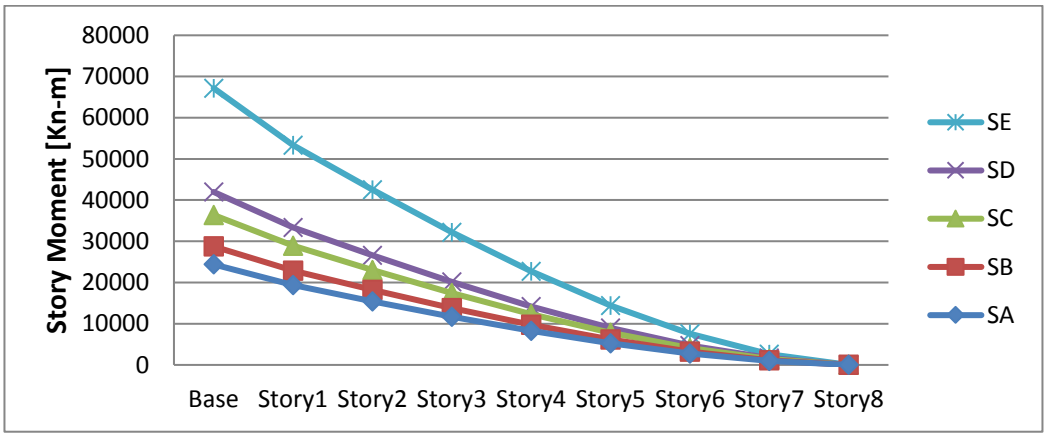

FIGURE 8. Story Moment

4. CONCLUSION

In the present study, a reinforced concrete 8 storey regular residential building was analyzed under different soil profile types to determine the effect of soil flexibility on the seismic forces and behavior of the building. Based on the previous results, it was found that seismic forces and response of structures is influenced greatly by soil profile types. Ignoring the soil site investigation to determine the soil profile type for a specific site can significantly affect the performance of the structures during earthquake and lead to devastating effects. Additionally, the seismic forces and displacements are significantly reduced for harder soil profiles which could be one of the most important factors behind having small damages during Halabja earthquake.

5. RECOMMENDATIONS

There is no local soil data available for halabja city to specify the soil profile types. Therefore, it seems that it is crucial to hold soil site investigations in the city to determine shear wave velocity and other related factors which are important to specify the soil types of the city. Then, a profound case study for buildings in the city could be conducted by considering soil structure interaction during analysis.

REFERENCES

[1] https://earthquake.usgs.gov/earthquakes/map/

[2] Hassoun MN, Al-Manaseer A. Structural concrete: theory and design. John wiley & sons; 2012 Jun 14.

[3] Khobragade, N. D., and A. Nikhade. "Effects of Seismic Forces on Multi-Storey Building for Different Zones & Soil Condition." International Journal for Technological Research in Engineering 3 (2016): 2368-2371.

[4] Anand N, Mightraj C, Prince Arulraj G. Seismic behaviour of RCC shear wall under different soil conditions. In Indian geotechnical conference 2010 Dec 16 (pp. 119-120).

[5] Tabatabaiefar, Hamid Reza, and Ali Massumi. "A simplified method to determine seismic responses of reinforced concrete moment resisting building frames under influence of soil–structure interaction." Soil Dynamics and Earthquake Engineering 30, no. 11 (2010): 1259-1267.

[6] American Society of Civil Engineers. Minimum design loads for buildings and other structures. Vol. 7. Amer Society of Civil Engineers, 2011.

[7] Code UB. Uniform building code. InInternational Conference of Building Officials, Whittier, CA 1997

[8] Computers and Structures Inc. Analysis Reference Manual for SAP2000, ETABS, and SAFE, (2007).

[9] Iraqi seismic code (303 .م.ب.ع) وزارة الاعمارو الاسكان والبلديات والاشغال العامة, 2013.

[10] Jayalekshmi BR, Chinmayi HK. Effect of Soil Flexibility on Seismic Force Evaluation of RC Framed Buildings with Shear Wall: A Comparative Study of IS 1893 and EUROCODE8. Journal of Structures. 2014 Mar 30;2014.

APPLICATION OF NANO MATERIALS TO ENHANCE MECHANICAL PERFORMANCE AND MICROSTRUCTURE OF RECYCLED AGGREGATE CONCRETE

Khaleel H. Younis[1], Shelan Muhammed Mustafa[2]

[1&2]Erbil Technology Institute, Erbil Polytechnic University (EPU), Erbil, Kurdistan-Iraq
[1]Ishik University
[1]Knowledge University, Erbil
[1]khaleelyounis@epu.edu.krd, [2]Shelan@epu.edu.krd

doi:10.23918/iec2018.10

ABSTRACT

The use of recycled aggregate in the production of concrete could enhance sustainability of concrete. This study aims at investigating the influence of using nanoparticles of SiO_2 to improve the behavior of recycled aggregate concrete (RAC) containing recycled aggregate (RA) derived from processing construction and demolition waste of concrete buildings. The examined properties included compressive strength and the microstructure of RA and RAC with and without nanoparticles of SiO_2. Nine mixes: one control mix with natural aggregate without nanoparticles, two mixes with RA at 50% and 100% contents (without nanoparticles) and three mixes for each content of RA with nanoparticles content of 0.4, 0.8 and 1.2% (by mass of cement) were investigated. The results showed that nanoparticles of silica can improve the compressive strength and modify the microstructure of RAC.

Keywords: Nanoparticles SiO_2, Compressive strength, Recycled aggregate, SEM.

1. INTRODUCTION

The world is currently facing a global sustainability and environmental issue due to the increasing generation of massive quantities of waste by construction and demolition activities. More than 500 million of tons of construction and demolition waste (CDW) are generated worldwide annually [1]. Such huge quantity of CDW requires substantial areas of landfill to dispose, causing serious environmental issues. Also, depletion of natural resources of natural aggregates used in the production of concrete contributes to other environmental and sustainability concerns. These environmental issues and concerns have led the researchers worldwide to examine methods to mitigate the impact of these issues on the environment. One way is recycling the CDW and reusing them as aggregate and as an alternative to the natural aggregate in concrete. The utilization of recycled aggregate (RA) in concrete can save the environment through conserving the scarce landfill areas and reduce the consumption rate of the natural resources of aggregates [1,2] . the use of the RA generated from processing CDW of concrete elements in new concrete has been investigated for decades. Nonetheless, the properties of the recycled aggregate concrete (RAC), as reported by the researchers, are inferior to that of the natural aggregate concrete (NAC). RAC exhibits low compressive, tensile and flexural strength as well as high water absorption, porosity and shrinkage [1,3]. Many researchers have attributed this performance of RAC to the heterogeneous nature of the RA caused by the attached mortar. The attached mortar is characterized by high porosity, microcracks and flaws which make the RA particle weak and having loose microstructure. Weak interfacial transition zone (ITZ) between the recycled concrete aggregate (RCA) and the cement matrix has also been identified [1,3,4]. Therefore, researchers have tried various approaches to improve the properties of RAC [4] . Some have examined the utilization of reactive, fine and ultrafine cementitious materials such as fly ash, ground granulated blast furnace slag and silica fume [4,5]. It is reported that these materials help to improve the performance of RAC due to the pozzolanic reaction and the filling ability resulting in a dense microstructure and strong ITZ [3]. However, the use of these materials in RAC does not always leads to a performance comparable to that of NAC. Hence, the need for investigating other materials is vital. nanomaterial, especially Nano SiO2 (Nano silica) is a promising material in this regard. Owing to its very small size (in

the range of nanometers) and the pozzolanic reaction, Nano silica particles are very effective in enhancing the performance of concrete [6]. Nanomaterial, particularly nano SiO_2, has the ability to improve the strength and the durability of concrete through accelerating the hydration reaction and filling the micropores in the cement paste structure. Studies [6-8] have shown that the addition of nano-silica results in increased compressive , tensile and flexural strength of normal concrete. Studies on the use of nano-silica to upgrade the performance of RAC are rare. Thus, this study aims at investigating the effect of using nano SiO_2 to improve the mechanical properties and modify the microstructure of RAC.

2. MATERIALS AND EXPERIMENTAL PROGRAMME

2.1 MATERIALS

Cement

Portland Cement (CEM I type) was used in this study meeting the requirements of Iraqi specifications [9]. The cement is manufactured by Mas company located in Sulymania –Iraq.

Aggregates

Two types of coarse aggregates were used, natural and recycled. The natural gravel was rounded river aggregate with a maximum size of 20 mm, water absorption of 0.8% and specific gravity of 2.6. The coarse RA was recycled concrete aggregate produced by crushing old concrete portions generated by demolishing old concrete buildings. The water absorption and the specific gravity of the RA were 3.3% and 2.45, respectively. The fine aggregate used in this study was sand with a maximum size of 5 mm.

Nano Materials

The materials phase used in this study was nano-silica supplied by HWNANO company in China. The nano SiO_2 was in the form of powder with purity of 99% SiO_2 (see Figure.1). The average particle size of the nan-silica was between 20- 30 nm with surface area of 125 m^2/g. The X-ray diffraction (XRD) analysis of a powder sample of the SiO_2 nanoparticles is shown in Figure 1.

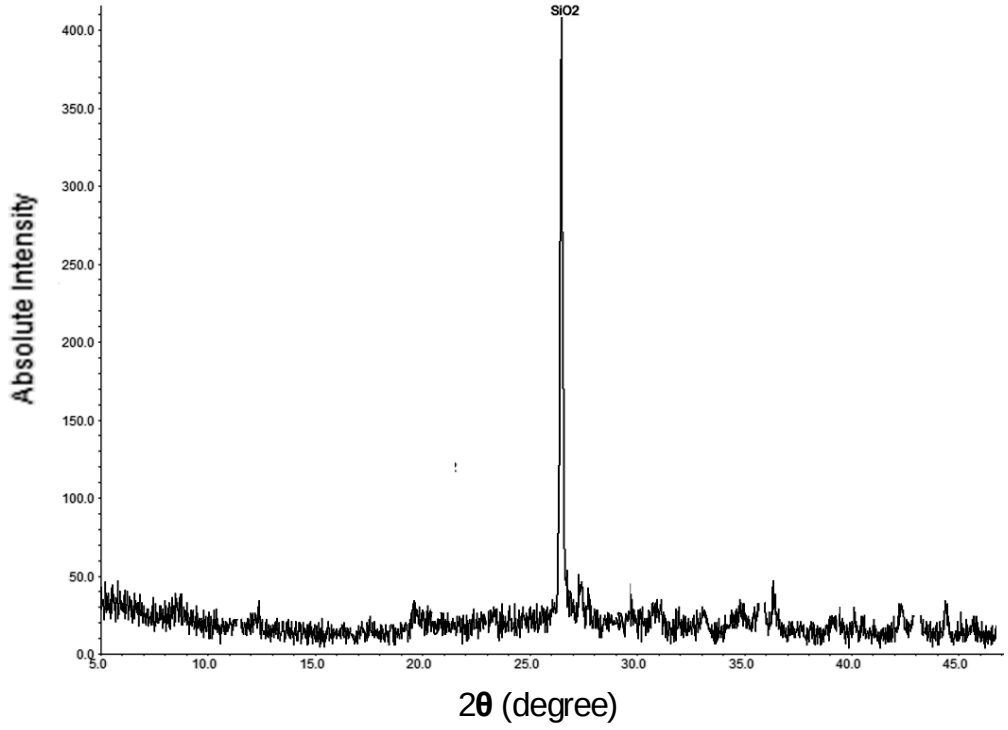

FIGURE 1. XRD analysis of SiO2 Nanoparticles used in the study.

Superplastisizers

Superplasticizers were used to ensure a uniform dispersion of the Nanoparticles as explained in section 2.3. The Superplasticizer was an aqueous solution containing polycarboxylate ether (PCE) polymers.

2.2 VARIABLES AND MIX PROPORTIONS

In total, nine different concrete mixes were prepared. The code of mixes and the variables of the study are shown in Table 1. The mixes are divided into three groups according to the type of coarse aggregate, content of coarse recycled aggregate and content of nano materials (Nano SiO_2). The study includes: one control mix made with natural coarse aggregate NCA (R0), two mixes made with recycled coarse aggregate RCA in which the NA is replaced by RA at contents of 50% and 100% and six mixes (three for each RA content) made with three contents (0.4%, 0.8%and 1.2% by cement mass) of Nano SiO2. All mixes had the same quantity of cement (400 kg/m^3), water (192 kg/m^3) and fine aggregate (719 kg/m^3), whilst the quantity of coarse aggregate used was 1125 kg/m^3. All mixes made with the same water/cement (w/c) ratio (0.48)

TABLE 1.

Code of mixes and variables of study

Mix no.	Mix code	Type of coarse aggregate	Nano SiO_2 content %[a]	Coarse recycled aggregate content (%)
1	R0	Natural	0	0
2	R50	Natural+Recycled	0	50
3	R100	Recycled	0	100
4	R50N0.4	Natural+Recycled	0.4	50
5	R50N0.8	Natural+Recycled	0.8	50
6	R50N1.2	Natural+Recycled	1.2	50
7	R100N0.4	Recycled	0.4	100
8	R100N0.8	Recycled	0.8	100
9	R100N1.2	Recycled	1.2	100

[a] By cement mass.

2.3 MIXING, SPECIMENS PREPARATION AND CURING

A pan mixer with capacity of 0.1 m^3 was used to mix the ingredients and prepare all concrete mixtures. For the mixes containing Nano SiO_2, the nano silica powder was added to a one liter of water and an amount of super plasticizer (0.5% by mass of cement) to form an aqueous solution. The solution was mixed using a high speed blender to ensure a uniform distribution of the Nano particles and avoiding the agglomeration of these particles. the procedure of mixing the ingredients of the concrete was as follows: Firstly, the coarse aggregate was added and mixed with the aqueous solution of Nano SiO_2 and part of the mixing water for 1 minute. Then, the ingredients were left in the mixer pan for 10 minutes to allow the recycled coarse aggregate to absorb the Nano particles and form a coat layer on their surfaces. Secondly, the fine aggregate, cement and the rest of the mixing water were added and mixed for 3 minutes. after the completion of mixing the ingredients, for each mix: three (100 mm) cubes were cast. The concrete was mixed using a pan mixer and compacted using a vibrating table. After casting, the specimens were then covered by plastic sheets and allowed to cure for 24 hours before being demoulded. Then, the specimens were kept in water tanks for 27 days for further curing.

2.4 TESTS

Compressive Strength Test.

The compressive strength was obtained at age of 28 days using the 100 mm cubes according to BS EN 12390-3 [10].

Microstructure Observations

Individual particles of recycled coarse aggregate were investigated using a digital microscope. Scanning electron microscopy (SEM) was also used to assess the microstructure of the RA particles and concrete samples with and without Nanoparticles of SiO_2.

3. RESULTS AND DISCUSSION

3.1 COMPRESSIVE STRENGTH

The results of the compressive strength at the age of 28 days for all mixes are presented in Table 2. The result of each mix is the average of three specimens. The table also shows the normalized strength (to that of the plain concrete, mix R0).

TABLE 2.

Results of compressive strength test

Mix	Compressive strength	
	Strength in (MPa)	Normalized Strength
R0	40.6	1.00
R50	34.1	0.84
R100	30.2	0.74
R50 N0.4	37.5	0.92
R50 N0.8	40.3	0.99
R50N1.2	41.0	1.00
R100N0.4	32.0	0.79
R100N0.8	34.2	0.84
R100N1.2	35.1	0.86

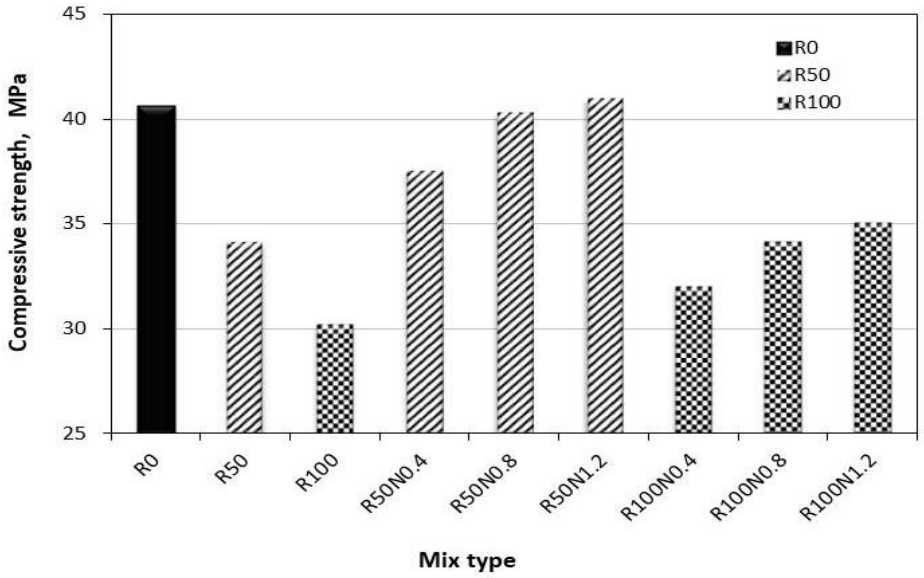

FIGURE 2. Compressive strength of all mixes

As expected, the compressive strength of the RAC mixes (R50, R100) is lower than that of the control mix (R0), as can be seen in Table 2 and Figure 2. This is mainly due to the heterogeneous nature of the recycled aggregate which is characterized by a weak and cracked surfaces resulted from the crushing process of demolished concrete [3-4]. The compressive strength of RAC decreased by 16% and 26% when the natural aggregate was replaced by 50% and 100%, respectively.

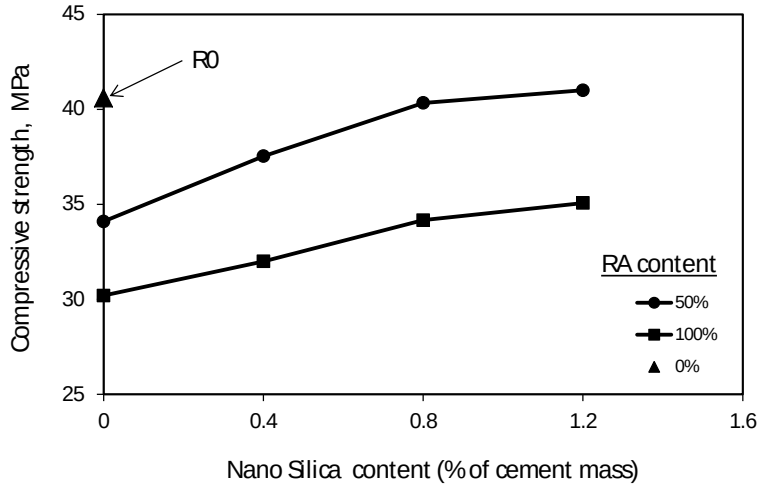

FIGURE 3. Effect of Nano silica particles content on the increase of compressive strength.

Figure 3. also shows that the addition of Nano SiO_2 enhanced the compressive strength of the mixes containing recycled aggregate. It is clear that the content of Nano particles affects the degree of strength enhancement. It can be seen that the compressive strength increases with the increase of content of Nano silica regardless

of the recycled aggregate content. For example, when the Nano silica is added at contents of 0.4%, 0.8% and 1.2%, the compressive strength increases by 10%, 18% and 20% for mixes containing 50% RA and by 6%, 13%and 16% for mixes made with 100% RA. The results also show that the increase in strength for mixes containing 50% RA is higher than those with 100% RA at all Nano silica contents. It seems that the addition of Nano silica at contents up to 0.8% (by mass of cement) to the RAC mixes is very beneficial and can result in comparable strength to that of the control mix R0 (mix with natural coarse aggregate). The mechanisms leading to this improvement is explained in the next section where the effect of adding the nanoparticles on the microstructure of the RAC is discussed.

3.2 MICROSCOPIC AND SCANNING ELECTRON MICROSCOPY (SEM) OBSERVATIONS

-Recycled aggregate specimens (particles)

The surface of some individual particles of the recycled aggregate with and without Nano silica was observed by a microscope to support and justify the gained enhancement in the compressive strength for the mixes made with recycled coarse aggregate. Also, SEM images for recycled aggregate concrete specimens were taken and used for the same purpose.

Figure 4a shows an image taken by a microscope with a magnification of 20x for the surface of a recycled aggregate particle. Microcracks and voids can be identified on the surface of the RA particle as can be seen in Figure 4b. These microcracks and voids are the main cause of the weakness of the RA which in turn results in low strength concrete [3,4]. A weak and cracked zone between the natural aggregate (NA) and the attached mortar (ITZ) can be observed. These microcracks and weak ITZ are usually caused by the process of the crushing of the demolished concrete [3]. Similarly, microcracks and weak ITZ can be identified in Figure 4c which shows an SEM image for the surface of a particle of RA.

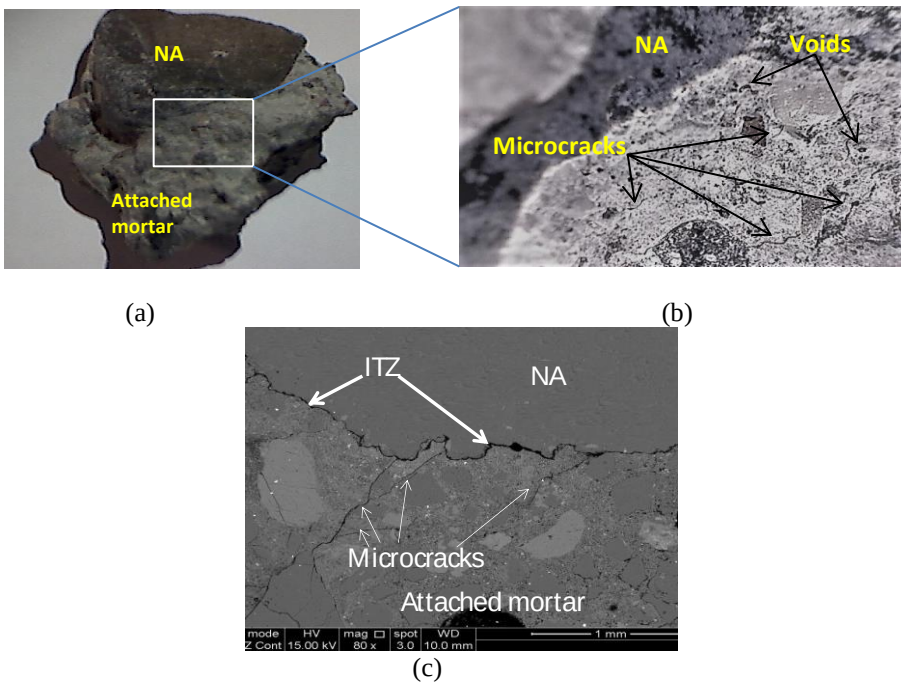

FIGURE 4. a- RA particle at 20x magnification b- RA surface at 200x magnification c- SEM image of the surface of a recycle aggregate particle.

To assess the effect of adding the Nano silica as a coat layer around the RA particles on their surfaces, microscopic images were taken for individual particles as can be seen in Figure 5. The effect of the nano silica on the surface of the RA particles is clear. The Nano silica modifies the surface by sealing all the microcracks and filling all the voids. This modification can partly explain the enhancement in the strength gained by adding the Nano silica to the mixes with RA.

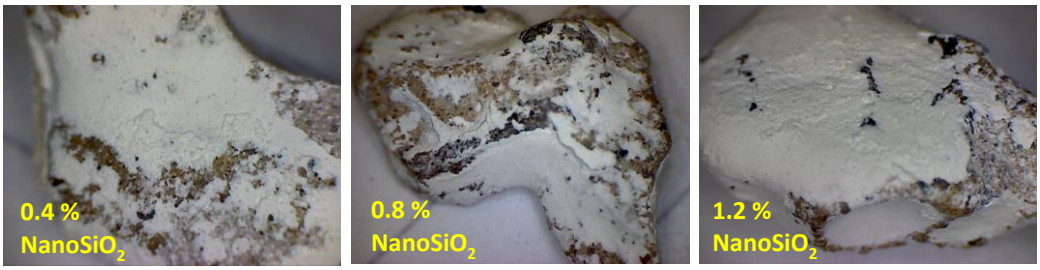

FIGURE 5. Effect of Nano silica content on the coating layer of RA particles

-Concrete specimens

The effect of using SiO_2 nanoparticles on the microstructure of RAC was also evaluated through observing concrete specimens with and without Nano SiO_2. The SEM images for the concrete specimens were taken and presented in Figure 6 and Figure7. Figure 6 shows SEM image for the RAC without SiO2 nanoparticles. The image clearly shows the fact that there are different ITZs in RAC: ITZ1 which exist

between the NA particle and the old attached mortar ; ITZ2 which lays between the NA particles and the new cement matrix (mortar) and ITZ3 which develops between the new and the old cement mortars. The existence of these ITZs with different microstructures increases the heterogeneous nature of RAC and hence results in a weak concrete in terms of both strength and durability aspects. Also, the image shows that ITZ3 is like the other two ITZs is porous and can be clearly identified by the very fine black line. The high porosity of this ITZ is due to the high concentration of $Ca(OH)_2$ resulted from the hydration of cement which is known for its high porosity.

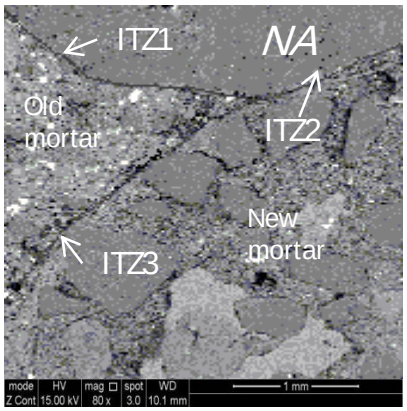

FIGURE 6. SEM image explains the ITZ s of in RAC sample without Nano silica

On the other hand, the ITZ3 in the RAC specimen (shown in Figure 7) included coated (with SiO_2 nanoparticles) RA particles cannot be clearly identified with a black line. Although, the old attached mortar and the new mortar can be recognized by their different porosity and microstructure, the two parts seems to be connected very well and the zone between them (which is the ITZ3) are very dense and refined (see Figure 6b). The densification of the microstructure of the ITZ3 can be attributed to the effect of adding the SiO_2 nanoparticles. These nanoparticles can result in a dense ITZ though two mechanisms: one is physical and the other is chemical. The latter is attributed to the chemical ability of the SiO_2 nanoparticles to react with the $Ca(OH)_2$ (one of the cement hydration products) and leading to the formation of more gel product, calcium silicate hydroxide (C-S-H) which is the product responsible of the strength of the concrete and dense microstructure of the ITZ in concrete [6,7]. The former, can be due to large surface area and the super-ultra-fine size of the nanoparticles. This small size of these particles help in filling up all the

micro/nano pores and voids exit in the attached mortar and the ITZ resulting in a more densefied microstructure of the cement matrix [7,8]. Hence, these two mechanisms seem to be the main reason behind the improvement in the strength of the RAC containing SiO_2 Nanoparticles.

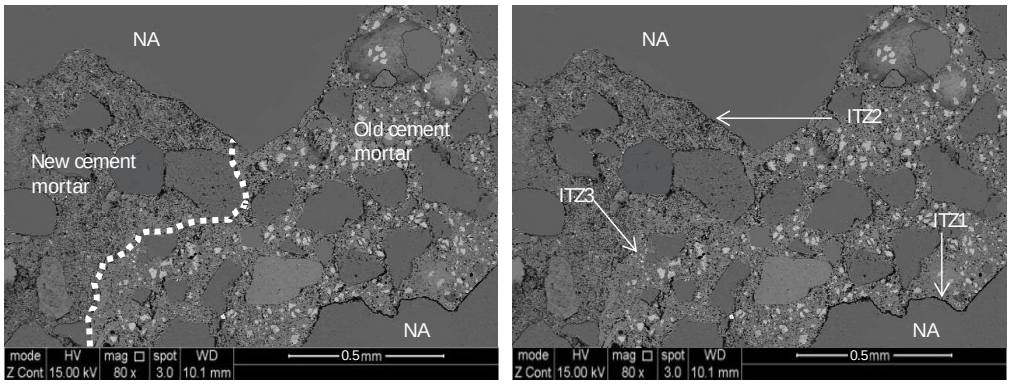

(a) (b)

FIGURE 7. a-SEM image of a concrete sample with Nano silica, b- image of the ITZ s of a concrete sample with Nano silica

4. CONCLUSIONS

. The following conclusions can be drawn based on the results and discussion:

- The addition of Nanoparticles of SiO_2 can improve the compressive strength of recycled aggregate concrete regardless of the content of RA.
- The increase in compressive strength depends on the content of the Nano SiO_2 content.
- The addition of nanoparticles of silica at contents of 0.4%, 0.8% and 1.2% , results in an increase in the compressive strength of 10%, 18% and 20% for mixes containing 50% RA and of 6%, 13%and 16% for mixes made with 100% RA, respectively.
- Microscopic and SEM observations revealed the heterogeneous nature of the RA particles which is characterized by weak and cracked attached mortar and porous ITZ.
- RAC microstructure can be positively modified though the addition of SiO_2 nanoparticles which can help densefy the microstructure RAC by phyiso-chemical mechanisms.
- RAC with Nanoparticles of SiO_2 can demonstrate comparable strength to that of NAC; hence, great enhancement in terms of sustainability and environmental effects of RA can be achieved.

REFERENCES

[1] Younis, K. H. and K. Pilakoutas, Strength prediction model and methods for improving recycled aggregate concrete. Construction and Building Materials, Vol. 49, No. 0, pp. 688-701, 2013.

[2] Tam, V.W., 2008. On the effectiveness in implementing a waste-management-plan method in construction. Waste management, 28(6), pp.1072-1080.

[3] Tam, V.W., Gao, X.F. and Tam, C.M., 2005. Microstructural analysis of recycled aggregate concrete produced from two-stage mixing approach. Cement and Concrete Research, 35(6), pp.1195-1203.

[4] Katz, A. (2004). "Treatments for the improvement of recycled aggregate." Journal of Materials in Civil Engineering 16(6): 597-603.

[5] Berndt, M. L. (2009). "Properties of sustainable concrete containing fly ash, slag and recycled concrete aggregate." Construction and Building Materials 23(7): 2606-2613.

[6] Sanchez, F. and Sobolev, K., 2010. Nanotechnology in concrete–a review. Construction and building materials, 24(11), pp.2060-2071.

[7] Said, A.M., Zeidan, M.S., Bassuoni, M.T. and Tian, Y., 2012. Properties of concrete incorporating nano-silica. Construction and Building Materials, 36, pp.838-844.

[8] Shaikh, F.U.A., Odoh, H. and Than, A.B., 2014. Effect of nano silica on properties of concretes containing recycled coarse aggregates. Proceedings of the Institution of Civil Engineers-Construction Materials, 168(2), pp.68-76.

[9] IQS No. 45/1984 ‘’Iraqi Specification for Cement’’ (1984)

[10] BS EN 12390-3, Testing hardened concrete Part 3: Compressive strength of test specimens. British Standard Institution, London, UK, 2009.

EMPLOYING SMARTPHONE AND COMPACT CAMERA IN BUILDING MEASUREMENTS

Haval A. Sadeq

Salahaddin University-Erbil
haval.sadeq@su.edu.krd

doi:10.23918/iec2018.11

ABSTRACT

This paper investigates the possibility of implementing images from smartphones and compact cameras for building measurement, such as archaeological buildings, for documentation purposes based on point cloud produced via photogrammetric technique. Images of the object are first captured from different positions. Then, the images are processed for the interior and exterior orientations to produce point cloud. For object registration, one distance is measured at the site, which is assigned to the model and used for scaling. The generated point cloud is subsequently exported into various software, such as AutoCAD, to take measurements or for any architectural studies. Two types of smartphone with different camera resolutions and two types of compact camera are used in the test. Results are validated by comparing several real measurements from the site. The quality of the data is proven to be accurate up to centimetre accuracy.

Keywords: smartphone camera, compact camera, point cloud, photogrammetry, archaeological, accuracy.

1. INTRODUCTION

Traditional building measurement using tapes is considered to be time consuming, especially at high-altitude areas or areas that have restricted access due to risks, such as ruined archaeological sites. By contrast, using equipment, such as laser scanning, total stations and theodolites, are considered to be expensive because they are time consuming and are designed on specialized people. The task has become difficult because it requires to measure architectural buildings that have complex architectural objects.The evolution of compact digital cameras and smartphone technology, which is accompanied by high-resolution and small size charge-coupled device (CCD) and complementary metal-oxide semiconductor (CMOS), has increased the demand for such equipment. In addition, the decrease in their size and the ease of image capturing have enabled users to carry them in the pocket. This paper focuses on using photogrammetry to generate the model for the building based on point cloud using compact and mobile phone camera. Considering the popularity of photogrammetric software, people can easily process the images for model generation and use it for measurement purposes.Close range photogrammetry is widely used to produce orthomaps for the front view of buildings using metric camera. Subsequently, metric cameras are used to capture image for the purpose of façade reconstruction with the introduction of digital photogrammetry. The development of off-the-shelf and built-in mobile cameras has resulted in the popularity of this system, which is only used for photography. Different studies have been conducted for the purpose of 3D reconstruction, and a method is suggested for interactive 3D model reconstruction based on mobile phones using photogrammetric techniques [1]. Smartphones are used in 3D model generation for the purpose of updating 3D urban maps and detailed enhancements [1]. The accuracy of mobile phone sensors is compared with off-the-shelf cameras, which showed positive results for photogrammetric product implementation [2]. An algorithm least square model image fitting is also [3] implemented by using built-in GPS and image orientation from smartphones as initial values to enhance the exterior image orientation for photogrammetric products that can be used in building construction. [4] assessed the possibility of using mobile phone cameras in UAV for DEM and orthophoto generation. In this study, the images of three buildings are captured using smartphone and compact camera, and point cloud is automatically generated using

CapturingReality software https://www.capturingreality.com/, which is considered for its simplicity. The process is started by loading the captured images in the software, and the photogrammetric process is automatically started to produce point cloud.This paper is structured as follows. Section 1 presents the introduction. Section 2 describes the study area, and Section 3 depicts the implemented camera. Section 4 shows the geometric processing and the result analysis is in Section 5. Finally, Section 6 provides the conclusion.

1. STUDY AREA

In this study, three study areas are selected that are located in Erbil-Iraq. The first study area shown in FIGURE 1(a) is referred as study area-1, which is located in Erbil Citadel and represents the rear side of the grand gate at Erbil citadel. This object is considered difficult for surveyors to take measurements at the upper side of the building because it is considered to have high altitude and is difficult to access the top of the building. Study area-2 shown in FIGURE 1(b) is also located in Erbil citadel, which is considered to be an old archaeological building although it has been renovated. The area is displayed for tourists but with limited accessibility, as shown in the figure. A warning tape surrounds this area, and people can only view it because it is considered to be a ruined area. Thus, images are captured at a distance without the users entering the site. These sites are under the supervision of the High Commission for Erbil Citadel Revitalization (HCECR), which is authorized with the control and renovation of the historical building in Citadel. Study area-3 shown in FIGURE 1(c), is considered to be a modern building with different architectural objects and textures. This study area is considered to have smooth surfaces that enable the easy identification of points.

(a) (b) (c)

FIGURE 1. Selected study areas (a) study area-1, citadel gate is considered to be high altitude (b) study area-2 represents the renovated area that has been restricted for users to access (c) study area-3, modern house with different architectural materials and styles.

2. IMPLEMENTED SMARTPHONE CAMERA

In this research, four different types of cameras are used for image capture, as shown in FIGURE 2. Two different types of smartphone cameras are used, namely, Samsung smartphone model GT-I9060I with 5 MP and Samsung smartphone J730F Galaxy with 13 MP. In addition, two different compact cameras are used, namely, Canon camera IXUS160 with 20 MP and Sony camera model HX60V with 20.3 MP resolution. These cameras are known as off-the-shelf cameras because they are not specified for photogrammetric purposes and are designed for amateur users.

(a) (b) (c) (d)

FIGURE 2. used mobile phones (a) Samsung smartphone model GT-I9060I resolution 5 MP (b) Samsung smartphone J730F Galaxy 13 MP (c) Canon compact camera IXUS160 resolution 20 MP (d) Sony Compact Camera HX60V resolution 20.4 MP.

As shown in Table 1, two different types of sensors, namely, CCD and CMOS, are adopted in the camera. The two sensors are functioning with similar principle, which is to convert light into electrons, and they are invented at the same period of time. These mobile phones are considered to have small sensor size, which is known

as CMOS. CCD images are considered to have low-noise ratio and less susceptible to noise than CMOS. CMOS sensors are also considered to be less sensitive to light than CCD sensors because they have several transistors located next to them and are considered to consume low battery life, which made them dominant over CCD sensors in mobile phones. Thus, the future of CMOS sensors is the focus of the company [5].

TABLE 1.
Specification of smartphone and compact cameras

Item	Samsung smartphone model GT-I9060I	Samsung smartphone J730F Galaxy	Canon camera IXUS160 Compact Camera	Sony camera HX60V Compact Camera
Sensor resolution	5 MP	13 MP	20 MP	20.4 MP
Sensor type	CMOS	CMOS	CCD	CMOS
Image format (pixels)	2560 x 1920	4160 x 3120	5152 x 3864	5184 x 3888
Focal length (mm)	2.6	3.71	5	4.3–129
Pixel size(µm)	*	1.133	1.196	1.188
Sensor size(mm)	*	4.73 x 3.49	6.16 x 4.62	6.16 x 4.62
Crop factor	*	7.37	5.62	5.62

*Indicates that the information is unavailable.

The number of captured images is varied and is based on the complexity and arrangement of the structure. For instance, the number of captured images in study area-1 is 40 images because the object is façade of building. For study area-2, 96 images are used because the area has different objects, which are considered to be larger than other objects. The captured objects behind the warning tape are shown in FIGURE 1 (b). For study area-3, 60 images are captured because the area is identified to be the façade of the building and has less details than study area-2.

3. GEOMETRIC PROCESSING

This stage represents the photogrammetric process, which is achieved in CapturingReality software. At this stage, the images are processed to determine the camera parameters, real position and attitude of images and point cloud generation.

3.1. INTERIOR ORIENTATION

Interior orientation is the process that determines the internal geometry of the camera as it used during image capturing, which is designed for calibrated focal length, principal point location, lens the distortion, and sensor size. These parameters are necessary to calculate the actual location of the image space and

remove all the distortions from the image. The parameters of metric camera are obtained at the lab through specific test. For the off-the-shelf camera (used in this paper), two main methods are used for determining the camera parameters, which are known as field test or pre-calibration or through self-calibration [6]. According to the literature, the result of self-calibration can provide more accurate result than pre-calibration [7-10] because it is included in the bundle adjustment process during aerial triangulation. The camera parameter used in this research is based on self-calibration. For the calculation, the initial values are used, such as focal length, image format, ISO speed, and aperture. The initial values of the camera are saved in image metadata known as exchangeable image file format. The cameras used in this study, which are either smartphone or compact camera, are considered to have these parameters. In FIGURE 3, the interior orientation of Samsung SM-J730F is determined, and the lens distortion is plotted on the image, as shown in FIGURE 3(a). The tie point, which is used in parameters determination via self-calibration, is marked. This condition shows that the point is marked on the objects, as shown in FIGURE 3 (b). The parameters of the camera Samsung SM-J730F are shown in FIGURE 3 (c), which are related to focal length, principal point location and lens distortion. The focal length of Samsung SM-J730F is 3.71 mm. However, the value of 27.736067 mm in the determined calibration is based on 35 mm focal length and is equivalent to (35 mm). These equivalent values are selected to compare the viewing angles between different cameras. Camera industries have introduced the term ‘35 mm focal length camera’ [11]. This value can be determined by multiplying the focal length of the camera by focal length multiplier, crop factor or format factor, which is provided by manufacturers (7.37 from TABLE 1). Thus, the calibrated focal length is 3.76 mm.

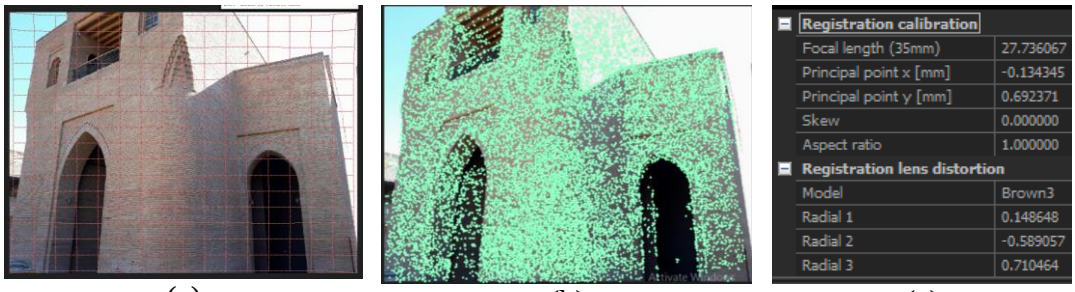

(a) (b) (c)

FIGURE 3. Interior orientation process using camera Samsung SM-J730F for study area-1 (a) shows the amount of distortion that has been affected on the image (b) detected tie point used in calibration (c) screenshot showing the determined parameters of interior orientations.

The model used in this study for the determination of image distortion model is represented in Equation (1), and is used in image correction ascribed by Brown [12]. The model is known as an eight-parameter physical model that is originally developed for film cameras. However, this model is valuable for digital cameras.

$$\begin{aligned} \Delta x &= -x_0 - \frac{\bar{x}}{c}\Delta c + \bar{x}r^2K_1 + \bar{x}r^4K_2 + \bar{x}r^6K_3 + (2\bar{x}^2 + r^2)P_1 + 2P_2\overline{xy} + b_1\bar{x} + b_2\bar{y}; \\ \Delta y &= -y_0 - \frac{\bar{y}}{c}\Delta c + \bar{y}r^2K_1 + \bar{y}r^4K_2 + \bar{y}r^6K_3 + 2P_1\overline{xy} + (2\bar{y}^2 + r^2)P_2; \end{aligned} \quad (1)$$

where Δx and Δy represent the corrections in x and y directions, respectively; $\bar{x}\ and\ \bar{y}$ are distances from a point to the principal point with respect to x and y directions; r is the radial distance from a point to the principal point; $K_1, K_2\ and\ K_3$ are radial distortion coefficients; $P_1\ and\ P_2$ are coefficients for decentring distortion; and $b_1\ and\ b_2$ represent the affinity of non-orthogonal parameters.

3.2. EXTERIOR ORIENTATION

At this stage, the position of images (X, Y and Z) and attitudes ($\omega,\ \varphi,\ k$) are determined. In general, the solution of airborne images for exterior orientation has reached a high precision level, especially with the attached GNSS/IMU information, which subsequently minimized the required GCPs [10, 13, 14]. However, the close-range images are considered challenging, because they rarely have GNSS/IMU instruments attached to the camera due to cost and load issues. Although this condition exists in mobile phones or several cameras, they are considered to have low accuracy, and they can be used as initial values. Thus, different approaches

should be integrated because of the instability of camera calibration process [15, 16]. Although providing data for exterior orientation in close-range photogrammetry is challenging, the images can be processed without providing any information about the image position or orientation. In addition, these approaches can be used to deal with images that are considered to be randomly captured and without sequences. These approaches can process images that have different illuminations and different perceptive views, which are captured from different non-calibrated or non-metric cameras [17-19]. Self-calibration technique is applied to the current photogrammetric tasks, in which the interior orientation is achieved during project implementation or exterior orientation. In this technique, the object points combined with the unknown feature point of interest that appeared in different photos are used in the process [20]. Self-calibration is introduced in Bundle Block adjustment. Thus, camera parameters, such as lens distortion and others, are collectively determined via determination of the object coordinates, which provide more accurate results than test-field calibration [21]. In the photogrammetric process of model registration or absolute orientation (i.e. scaling and georeferencing), seven parameters, namely, three translations, three rotations and one scale parameter [20], are required. This research focuses on distance measurement and does not require the coordinates of the points. Therefore, the model is only adjusted. The distance is measured in the model using tape instrument and is assigned in the model, as shown in FIGURE 4. The same procedure is applied to other study areas.

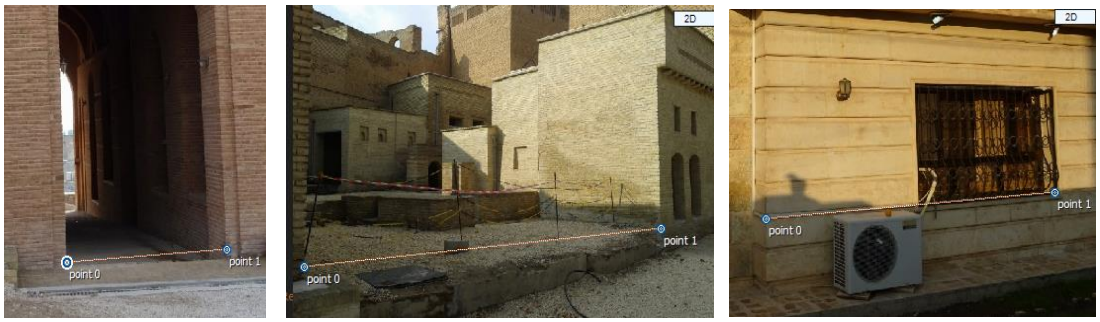

FIGURE 4. Defined distance is shown for the purpose of scaling the models.

3.3. POINT CLOUD GENERATION

Apart from image triangulation, images are available for point cloud construction. Point cloud is the result of image matching, which is obtained via collinearity equations. Image matching is considered as the main critical stage in photogrammetry. Different image matching techniques have been developed [22-27]. The technique used in this study is based on the technique that is available in the reality capture software, which is robust for the production of a point cloud, as shown in

FIGURE 5. The technique is not revealed for confidentiality purposes. The common technique that is considered to provide acceptable result is the least square matching, which is based on signal matching that depends on grey values [10]. However, a robust technique, which is called semi-global matching, has been developed. This technique can produce accurate results for 3D object reconstruction. This method requires large overlapping areas [28].

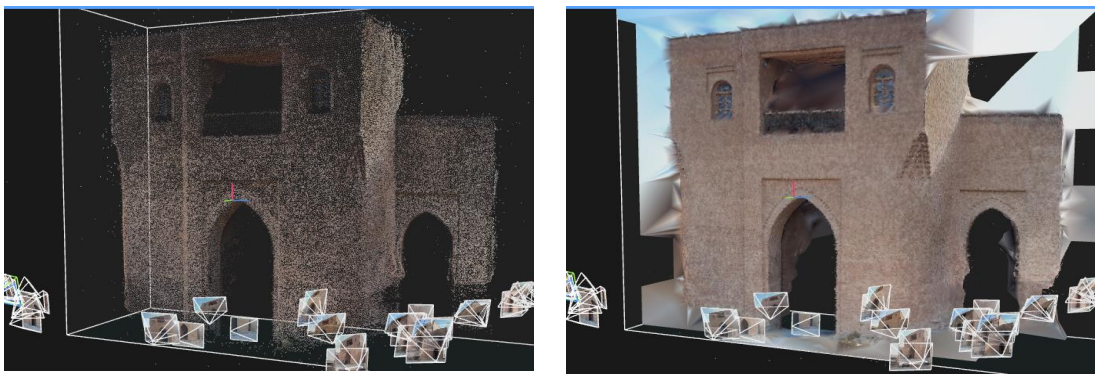

FIGURE 5. Produced point cloud (left image) and rendered object using images from Samsung J7 in study area-1(right image) with camera pose location.

For good visibility, point cloud is rendered for better visualization. The rendering issue is not related to the accuracy of quantity measurement. However, this issue is considered an important requirement for architects to produce realistic views of the object and for good analysis. FIGURE 6 shows the result on study area-2 that has rendered the models from four cameras samples, which shows that all objects are represented. In the rendering model, the roofs of buildings are not generated due to missing photos from the top of the buildings.

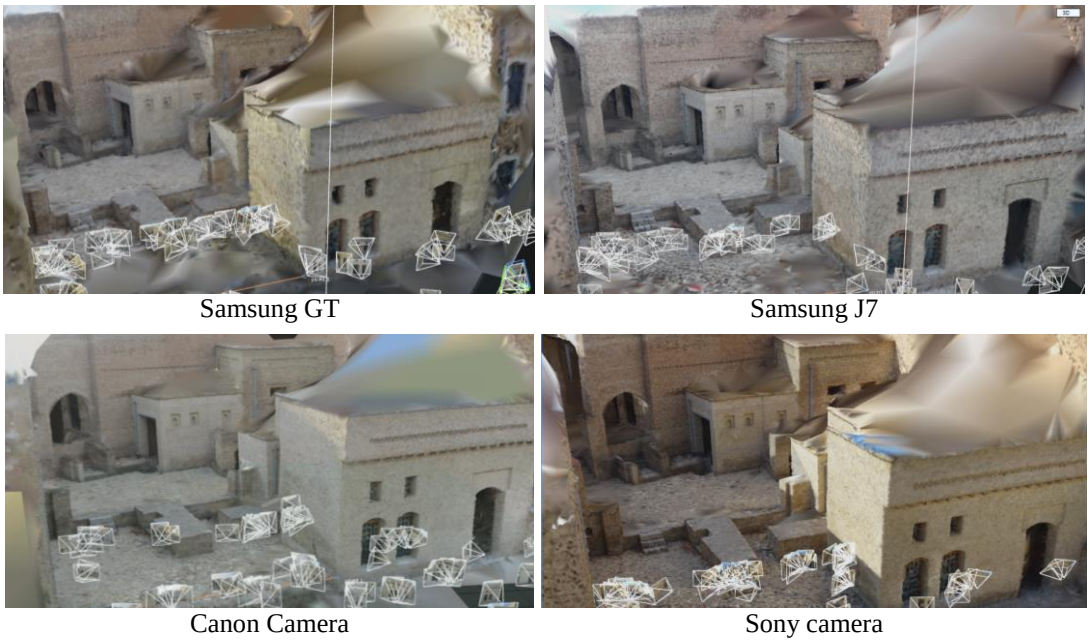

FIGURE 6. Rendered study-area-2, four different rendered models produced from smartphone and compact cameras with the camera pose location.

The produce point cloud model can be used for measurement and documentation purposes to produce a plan view. As shown in FIGURE 7, the top view of study area-2 with all details should produce a map for the site or building layout. The camera did not reach all the areas and has captured images only from one side. However, all the distant walls have been clearly produced.

FIGURE 7. Top view of study area-2 obtained from point cloud, which shows the captured image area and the logo of the ‘reality capturing software’.

4. RESULT ANALYSIS

For the model analysis, a set of measurements is selected at three locations. For the assessment, overall 55 different planemetric measurements are used to assess the accuracy of the obtained point cloud. At the site, the distances are obtained from different directions (i.e. in the X, Y and Z directions). Then it is compared with the measurements that are obtained from point cloud using ReCap, as shown in

FIGURE 8. ReCap is built in AutoCAD software, which is designed for laser scanning point cloud measurement. For good point selection of dimensions, the available colour feature in point cloud is clearly represented, which is similar to the point cloud available in laser scanning.

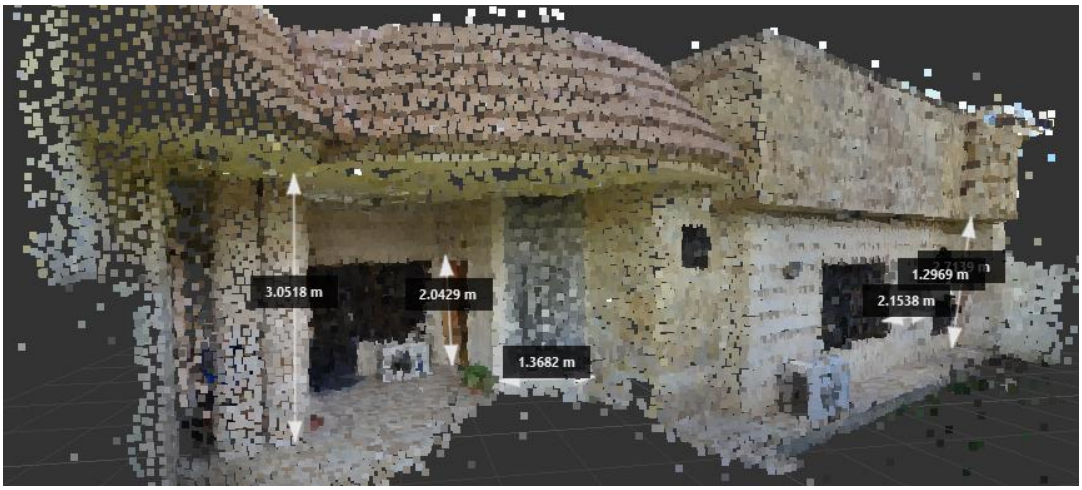

FIGURE 8. Generated point cloud in study area-3 with Sony camera with several measured distances on Autodesk ReCap-2014.

For qualitative analysis, a statistical analysis is applied to the residual. The achieved analysis tests are mentioned in Equations (2), (3) and (4) to obtain the accuracy of the obtained point cloud from each of the mentioned devices in three Study areas, as follows:

$$\mu = \frac{1}{n} \sum_{i=1}^{n} \Delta h_i; \tag{2}$$

$$\sigma = \sqrt{\frac{1}{(n-1)} \sum_{i=1}^{n} (\Delta h_i - \mu)^2}; \tag{3}$$

$$RMSE = \sqrt{\frac{1}{n} \sum_{i=1}^{n} \Delta h_i{}^2}; \tag{4}$$

where Δh_i represents the residual or error between the measured distance on point cloud and actual distance, and $\boldsymbol{n}$ represents the number of measurements.

The statistical analysis is listed in TABLE **2**, which shows that the accuracy of point cloud increases with the increase in the resolution of the image. The accuracy in the worst case is less than 0.08 m using smartphone camera. The accuracy is increased to 0.051 in the worst case and 0.35 in the best case with the increase in resolution by using J7. Compact cameras showed better performance than smartphone cameras in terms of study areas 1 and 2, and they are not much different, which is in the worst case less than 0.045 m. For the standard deviations and biases, all the samples for the worst case is 0.61 m and −0.022m, respectively. With the increase in the resolution of sensors, such as Samsung J7 and compact camera, the standard deviation and bias is improved to 0.51 and 0.22 m.

TABLE 2.

Obtained statistical data in analysing the accuracy of point cloud, the accuracy is in in the three directions X,Y, Z.

	Statistical test	Samsung smartphone model GT-I9060I	Samsung smartphone J730F Galaxy	Canon camera IXUS160	Sony camera HX60V Compact Camera
Study area-1	RMSE (m)	0.079	0.044	0.033	0.033
	STD (m)	0.055	0.027	0.032	0.028
	Bias (m)	0.001	−0.017	−0.002	−0.022
Study area-2	RMSE (m)	0.068	0.051	0.044	0.038
	STD (m)	0.061	0.051	0.026	0.033
	Bias (m)	0.008	0.007	0.015	−0.002
Study area-3	RMSE (m)	0.046	0.035	0.044	0.034
	STD (m)	0.044	0.036	0.049	0.038
	Bias (m)	0.013	−0.010	0.005	−0.014

5. CONCLUSIONS

An efficient technique to obtain the measurements of buildings with reasonable accuracy by using sensors is proposed. This technique is inexpensive and easy-to-use rather than using expensive devices, such as specific photogrammetric cameras. Any type of camera can be used although Samsung mobile phone and Canon Power Shot camera are used in the test. As shown in the result, as the quality of the camera increases the accuracy of the model is increased. The analysis showed that CMOS technology provided better accuracy than CCD under the same resolution. Modern technology has focused on the predominance of CMOS on imaging devices and has obtained more support for improvement from mobile companies.

The technique used in this study can minimize the work needed in documentation. The technique can help obtain quick measurements in the area. In addition, a real 3D model of the object can be obtained and can be used to produce the site layout. The attached colour to the point cloud will help the user identify the points accurately.

ACKNOWLEDGEMENTS

The author would like to appreciate the CapturingReality company for their cooperation in providing a redeem license to export the data. The author would like to acknowledge HCECR for permitting the access to measure the dimensions of the implemented study area.

REFERENCES

[1] B. Sirmacek and R. Lindenbergh, "Accuracy assessment of building point clouds automatically generated from iphone images," ISPRS - International Archives of the Photogrammetry, Remote Sensing and Spatial Information Sciences, vol. XL-5, pp. 547-552, 2014.

[2] A. Gruen and M. D. Akca, "Mobile photogrammetry," Vorträge Dreiländertagung SGPBF, DGPF und OVG, vol. 16, pp. 441-451, 2007.

[3] S. Wang, "Toward Automated FAÇADE Texture Generation for 3d Photorealistic City Modelling with Smartphones or Tablet Pcs," ISPRS-International Archives of the Photogrammetry, Remote Sensing and Spatial Information Sciences, pp. 351-354, 2012.

[4] J. Kim, S. Lee, H. Ahn, D. Seo, S. Park, and C. Choi, "Feasibility of employing a smartphone as the payload in a photogrammetric UAV system," ISPRS Journal of Photogrammetry and Remote Sensing, vol. 79, pp. 1-18, 2013.

[5] D. Durini, High performance silicon imaging: fundamentals and applications of cmos and ccd sensors: Elsevier, 2014.

[6] E. Edwards, E. Fey, P. A. Jones, R. K. Jungquist, A. G.LAreau, J. Lebarron, et al., "Cameras and sensing systems," in Manual of Photogrammetry, J. C. McGlone, Ed., ed: American Society for Photogrammetry and Remote Sensing, 2013.

[7] J. S. Aber, I. Marzolff, and J. Ries, Small-format aerial photography: Principles, techniques and geoscience applications: Elsevier, 2010.

[8] S. Harwin, A. Lucieer, and J. Osborn, "The Impact of the Calibration Method on the Accuracy of Point Clouds Derived Using Unmanned Aerial Vehicle Multi-View Stereopsis," Remote Sensing, vol. 7, pp. 11933-11953, 2015.

[9] D. Herrera, C. J. Kannala, and J. Heikkila, "Forget the checkerboard: Practical self-calibration using a planar scene," pp. 1-9, 2016.

[10] T. Rosnell and E. Honkavaara, "Point cloud generation from aerial image data acquired by a quadrocopter type micro unmanned aerial vehicle and a digital still camera," Sensors (Basel), vol. 12, pp. 453-80, 2012.

[11] R. Sheppard, Digital photography: top 100 simplified tips & tricks vol. 25: John Wiley & Sons, 2010.

[12] W. Forstner, B. Wrobel, F. Paderes, C. S. Fraser, J. Dolloff, E. M. Mikhail, et al., "Analytical Photogrammetric Operations," in Manual of Photogrammetry, J. D. McGlone, Ed., Sixth Edition ed Bethesda: American Society of Photogrammetry and Remote Sensing (ASPRS), 2013.

[13] G. Buyuksalih and Z. Li, "Practical experiences with automatic aerial triangulation using different software packages," The Photogrammetric Record, vol. 18, pp. 131-155, 2003.

[14] J. Kremer and E. Kruck, "Integrated Sensor Orientation–Two Examples to show the Potential of simultaneous GPS/IMU and Image Data Processing," Theory, Technology and Realities of Inertial/GPS Sensor Orientation, 2003.

[15] K. Gutjahr, P. Hafner, M. Ofner, K. Längauer, M. Wieser, and N. Kühtreiber, "Performance of GNSS/IMS integration methods in context of a near real-time airborne mapping platform," EuroCOW10, Commission III, WG, vol. 3, 2010.

[16] K.-W. Chiang, H.-W. Chang, C.-Y. Li, and Y.-W. Huang, "An artificial neural network embedded position and orientation determination algorithm for low cost MEMS INS/GPS integrated sensors," Sensors, vol. 9, pp. 2586-2610, 2009.
[17] S. Agarwal, Y. Furukawa, N. Snavely, I. Simon, B. Curless, S. M. Seitz, et al., "Building rome in a day," Communications of the ACM, vol. 54, pp. 105-112, 2011.
[18] M. Brown and D. G. Lowe, "Automatic Panoramic Image Stitching using Invariant Features," International Journal of Computer Vision, vol. 74, pp. 59-73, 2006.
[19] I. Stamos and P. E. Allen, "3-D model construction using range and image data," vol. 1, pp. 531-536, 2000.
[20] K. Kraus, Photogrammetry: geometry from images and laser scans, 2nd ed.: Walter de Gruyter, 2007.
[21] T. A. Clarke and J. G. Fryer, "The development of camera calibration methods and models," The Photogrammetric Record, vol. 16, pp. 51-66, 1998.
[22] N. Haala, "Comeback of digital image matching," in Photogrammetric Week, 2009, pp. 289-301.
[23] W. Tao, Y. Lei, and P. Mooney, "Dense point cloud extraction from UAV captured images in forest area," pp. 389-392, 2011.
[24] F. Leberl, A. Irschara, T. Pock, P. Meixner, M. Gruber, S. Scholz, et al., "Point Clouds," Photogrammetric Engineering & Remote Sensing, vol. 76, pp. 1123-1134, 2010.
[25] A. Gruen, "Development and Status of Image Matching in Photogrammetry," The Photogrammetric Record, vol. 27, pp. 36-57, 2012.
[26] E. Gülch, "Advanced matching techniques for high precision surface and terrain models," in Photogrammetric Week, 2009, pp. 303-315.
[27] M. Pohanka, K. Musilek, and K. Kuca, "Evaluation of aflatoxin B1--acetylcholinesterase dissociation kinetic using the amperometric biosensor technology: prospect for toxicity mechanism," Protein Pept Lett, vol. 17, pp. 340-2, Mar 2010.
[28] H. Hirschmuller, "Stereo processing by semiglobal matching and mutual information," IEEE Trans Pattern Anal Mach Intell, vol. 30, pp. 328-41, Feb 2008.

AN APPROACH FOR DESCRIPTION OF ELASTIC PARAMETERS OF CROSS-ANISOTROPIC SATURATED SOILS

Ahmed Mohammed Hasan

Salahaddin University-Erbil
ahmed.hasan@su.edu.krd or ahmedunsat2014@gmail.com

doi:10.23918/iec2018.12

ABSTRACT

The processes of deposition and consolidation in natural soils or compaction in fill materials will typically produce soils that are initially cross-anisotropic (also known as transversely isotropic or orthotropic) in terms of both small strain elastic behaviour and large strain plastic behaviour. For small strain elastic behaviour, five elastic parameters are required to fully describe cross-anisotropic soils such as two Young's moduli (E_v in vertical direction and E_h in horizontal direction), two Poisson's ratios (v_{vh} horizontal strain due to vertical strain and v_{hh} horizontal strain due to horizontal strain) and an independent shear modulus such as G_{hv} (a shear wave horizontally transmitted with vertically polarised). These five elastic parameters have been expressed in different fashions in the literature. In this paper results from derivations showed that it is possible to express the elastic parameters for cross-anisotropic soils in a different way than that expressed in the literature using as a function of independent measurements of two shear moduli and two constrained moduli from three pairs of bender/extender elements BEEs fitted on a cross-anisotropic soil sample in a triaxial apparatus and measuring or assuming the value of v_{hh} using combination of triaxial testing system and bender/extender element testing system,

Keywords: elastic parameters, cross-anisotropic soils, bender/extender elements, shear and constrained moduli.

1. INTRODUCTION

For a shear wave, the direction of motion of the soil particles (the wave polarisation) is perpendicular to the direction of wave transmission, as shown in Figure 1 [1]. Hence, different shear wave velocities can be measured, depending upon the direction of the wave transmission and the direction of the wave polarisation, e.g. V_{svh} , V_{shv} and V_{shh} (see Figure 2 [2,3]), where the second subscript gives the wave transmission direction, the third subscript gives the wave polarisation direction and *v* and *h* represent vertical and horizontal respectively. For compression waves, the direction of particle motion (wave polarisation) is the same as the direction of wave transmission (see, Figure 1). By transmitting compression waves in vertical and horizontal directions, compression waves velocities V_{pv} and V_{ph} can be measured (see Figure 2).

The importance of anisotropy of very small strain behaviour has been investigated by many authors [4-7]. They showed, using numerical analysis, that including anisotropy of *G* during the prediction of deformations of tunnelling in stiff clays (such as London clay) appeared to play a vital role.

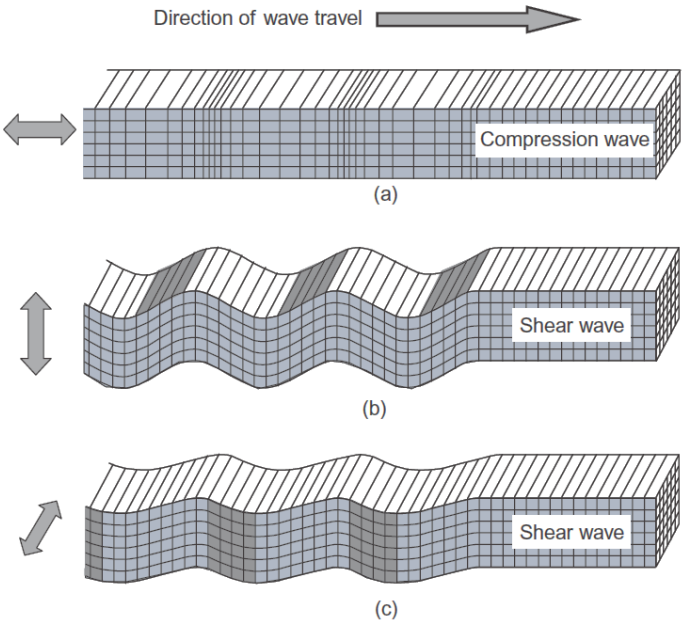

FIGURE 1. Compression and shear wave travel: (a) Compression wave with horizontal transmission, V_{ph} (b) Shear wave with horizontal transmission and vertical polarisation, V_{shv} (c) Shear wave with horizontal transmission and horizontal polarisation, V_{shh} [1]

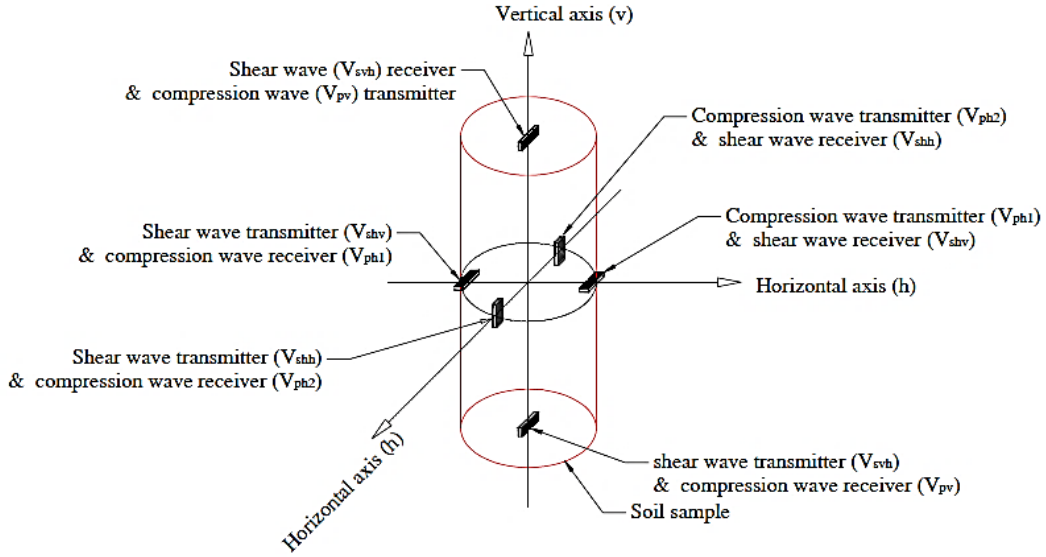

FIGURE 2. Multi-directional pairs of BEEs fitted on a triaxial soil sample [2,3]

This anisotropy of soil fabric can evolve during plastic straining, leading to changes in the anisotropy of mechanical behaviour. These changes of anisotropy caused by changes of soil fabric are therefore termed strain induced anisotropy [8]. The 5 independent elastic constants of cross-anisotropic soils have been expressed using different techniques in the literature. For example, two of them are presented here. Stokoe et al. [9] and Fioravante & Cappoferri [10] showed that the 5 independent elastic constants of cross-anisotropic soils could be measured with bender/extender elements if an additional extender element was used to determine a constrained modulus M in an oblique direction. Alternatively, Pennington [11] showed how all 5 independent constants could be determined by combining bender element testing (to measure G_{hv} and G_{hh}) with local strain measurement on triaxial samples (to measure E_v, E_h and ν_{vh}). This does, however, have the drawback of combining two different types of measurement (at two different strain amplitudes). The main objective of this paper is to express the elastic parameters for cross-anisotropic saturated soils in a different fashion than those have been presented in the literature. The current expressions use a combination of triaxial testing system and bender/extender element testing system whereas other expressions employ, for example, either a triaxial testing system with local strain measurement on triaxial samples [11] or a cubical calibration chamber with geophone systems [9]. It means that additional equipment (i. e. bender/extender element testing system) in the geotechnical

laboratory can be used to measure independent elastic constants and then express them.

1. BENDER/EXTENDER ELEMENT TESTING

Bender/extender elements are piezoelectric transducers that can transmit and receive shear waves and compression waves in order to determine shear wave velocity V_s and compression wave velocity V_p . These wave velocities can then be used to determine very small strain elastic values of shear modulus G and constrained modulus M as follows Biot [12].:

$$G = \rho V_s^2 \tag{1}$$

$$M = \rho V_p^2 \tag{2}$$

where ρ is the bulk density of the soil. In all cases, the wave velocity V (i.e. V_s or V_p) is determined from a measurement of travel time t and the known tip-to-tip distance L_{tt} between transmitter and receiver elements [13]:

$$V = \frac{L_{tt}}{t} \tag{3}$$

2. ELASTICITY THEORY

3.1 ELASTIC MODULI OF ISOTROPIC SATURATED SOILS

At very small strains, the behaviour of saturated soils can be treated as elastic. If the soil is isotropic, the elastic behaviour can be represented by two independent elastic properties, which are normally selected either as Young's modulus E and Poisson's ratio ν or as shear modulus G and bulk modulus K [14], where:

$$G = \frac{E}{2(1+\nu)} \tag{4}$$

$$K = \frac{E}{3(1-2\nu)} \tag{5}$$

For saturated soil, it can be helpful to choose to express the elastic properties in terms of G and K (rather than E and v), because shear modulus G should be the same for both drained and undrained behaviour, and K is often considered as infinite for undrained behaviour. For linear elastic behaviour, G and K are constants, but soils often show non-linear elastic behaviour, with G and K varying with stress, strain or soil state.

Constrained modulus M is the elastic modulus (applied normal stress increment divided by normal strain increment in the same direction) for a condition where strain is prevented in both perpendicular directions. For an isotropic elastic soil, M can be expressed in terms of E and v , or in terms of G and K [14]:

$$M = \frac{E(1-v)}{(1-2v)(1+v)} \tag{6}$$

$$M = K + \frac{4}{3}G \tag{7}$$

Equations (1) and (2) show that the shear wave velocity V_s and compression wave velocity V_p measured in bender/extender elements BEE tests depend upon G (Equation 4) and M (Equation 6 or 7), respectively.

3.2 ELASTIC MODULI OF ANISOTROPIC SATURATED SOILS

Love [15] showed that thermodynamic considerations mean that the stiffness matrix (and compliance matrix) of an elastic material must be symmetric. This means that the most general form of linear anisotropic elastic behaviour involves 21 (rather than 36) independent elastic constants, for example see Graham and Houlsby[16]. For a cross-anisotropic elastic material, with the same properties in all horizontal directions but different properties in vertical directions, symmetry of the stiffness and compliance matrices implies that [15]:

$$\frac{v_{hv}}{E_h} = \frac{v_{vh}}{E_v} \tag{8}$$

where E_h and E_v are the Young's moduli in horizontal and vertical directions respectively, v_{hv} is the Poisson's ratio giving the ratio of vertical to horizontal strain increment caused by a uniaxial stress increment in the horizontal direction, and v_{vh} is the Poisson's ratio giving the ratio of horizontal to vertical strain increment caused by a uniaxial stress increment in the vertical direction. Thermodynamic considerations also imply that for this cross-anisotropic material, the shear moduli G_{vh} , G_{hv} and G_{hh} are given by [15]:

$$G_{hv} = G_{vh} \tag{9}$$

$$G_{hh} = \frac{E_h}{2(1+v_{hh})} \tag{10}$$

This means that, as shown by Graham & Houlsby [14], the behaviour of a cross-anisotropic elastic material involves only 5 independent elastic constants, which can be taken as E_v , E_h , v_{vh} , v_{hh} and G_{vh}. The stress-strain relations of this cross-anisotropic elastic material can then be expressed as [15]:

$$\begin{bmatrix} \Delta\varepsilon_{xx} \\ \Delta\varepsilon_{yy} \\ \Delta\varepsilon_{zz} \\ \Delta\gamma_{xy} \\ \Delta\gamma_{yz} \\ \Delta\gamma_{zx} \end{bmatrix} = \begin{bmatrix} \frac{1}{E_h} & \frac{-v_{hh}}{E_h} & \frac{-v_{vh}}{E_v} & & & \\ \frac{-v_{hh}}{E_h} & \frac{1}{E_h} & \frac{-v_{vh}}{E_v} & & & \\ \frac{-v_{vh}}{E_v} & \frac{-v_{vh}}{E_v} & \frac{1}{Ev} & & & \\ & & & \frac{1}{G_{hv}} & & \\ & & & & \frac{1}{G_{hv}} & \\ & & & & & \frac{2(1+v_{hh})}{E_h} \end{bmatrix} \begin{bmatrix} \Delta\sigma'_{xx} \\ \Delta\sigma'_{yy} \\ \Delta\sigma'_{zz} \\ \Delta\tau_{xy} \\ \Delta\tau_{yz} \\ \Delta\tau_{zx} \end{bmatrix} \tag{11}$$

For the conditions of the triaxial test, Equation (11) gives:

$$\Delta\varepsilon_v = \frac{1}{E_v}\Delta\sigma'_{\mathrm{v}} - \frac{2v_{vh}}{E_v}\Delta\sigma'_{\mathrm{h}} \tag{12}$$

$$\Delta\varepsilon_h = \left(\frac{1}{E_h} - \frac{v_{vh}}{E_h}\right)\Delta\sigma_{\mathrm{h}}^{'} - \frac{v_{vh}}{E_v}\Delta\sigma_{\mathrm{v}}^{'} \qquad (13)$$

where *x* and *y* are horizontal directions, *z* is the vertical direction, $\Delta\sigma'_{xx}$, $\Delta\sigma'_{yy}$ and $\Delta\sigma'_{zz}$ are normal stress increments, $\Delta\varepsilon_{xx}$, $\Delta\varepsilon_{yy}$ and $\Delta\varepsilon_{zz}$ are corresponding normal strain increments, $\Delta\tau_{yz}$, $\Delta\tau_{zx}$ and $\Delta\tau_{xy}$ are shear stress increments and $\Delta\gamma_{xy}$, $\Delta\gamma_{yz}$ and $\Delta\gamma_{zx}$ are corresponding shear strain increments.

3. DERIVATION OF EXPRESSIONS FOR E_H , E_V AND v_{VH}

4.1 EXPRESSIONS FOR M_v

If a stress increment $\Delta\sigma_v^{'}$ is applied in a vertical direction, to produce a corresponding strain increment $\Delta\varepsilon_v$ in that direction, while strains are prevented in the horizontal direction (i.e. $\Delta\varepsilon_h$=0). Equation 13 can be re-arranged to give:

$$\Delta\sigma_h^{'} = \frac{E_h}{E_v}\frac{v_{vh}}{(1-v_{vh})}\Delta\sigma_{\mathrm{v}}^{'} \qquad (14)$$

By inserting Equation 14 into Equation 12:

$$\Delta\varepsilon_v = \left(\frac{1}{E_v} - \frac{2v_{vh}}{E_v}\frac{E_h}{E_v}\frac{v_{vh}}{(1-v_{hh})}\right)\Delta\sigma_{\mathrm{v}}^{'} \qquad (15)$$

For this situation of no horizontal strain, the vertical constrained modulus M_v is defined by [17]:

$$\Delta\varepsilon_v = \frac{\Delta\sigma_{\mathrm{v}}^{'}}{M_v} \qquad \text{m(16)}$$

Comparing Equation 15 and 16:

$$M_v = \frac{E_v}{1-2v_{vh}\dfrac{E_h}{E_v}\dfrac{v_{vh}}{(1-v_{hh})}} \qquad (17)$$

This simplifies to the standard result for the constrained modulus of an isotropic elastic material (see Equation 6) if $E_v = E_h = E$ and $v_{vh} = v_{hh} = v$.

4.2 EXPRESSIONS FOR M_h

Consider a situation where a stress increment $\Delta\sigma'_{xx}$ is applied in one horizontal direction (x), to produce a corresponding strain increment ($\Delta\varepsilon_{xx}$) in that direction, while strains are prevented in the other horizontal direction ($\Delta\varepsilon_{yy}=0$) and in the vertical direction ($\Delta\varepsilon_{zz}=0$). Equation 11 now gives:

$$\Delta\varepsilon_x = \frac{1}{E_h}\Delta\sigma'_{\mathrm{x}} - \frac{\nu_{vh}}{E_h}\Delta\sigma'_{\mathrm{y}} - \frac{\nu_{vh}}{E_v}\Delta\sigma'_{\mathrm{z}} \tag{18}$$

$$\Delta\varepsilon_y = -\frac{\nu_{hh}}{E_h}\Delta\sigma'_{\mathrm{x}} + \frac{1}{E_h}\Delta\sigma'_{\mathrm{y}} - \frac{\nu_{vh}}{E_v}\Delta\sigma'_{\mathrm{z}} = 0 \tag{19}$$

$$\Delta\varepsilon_z = -\frac{\nu_{vh}}{E_v}\Delta\sigma'_{\mathrm{x}} - \frac{\nu_{vh}}{E_v}\Delta\sigma'_{\mathrm{y}} + \frac{1}{E_v}\Delta\sigma'_{\mathrm{z}} = 0 \tag{20}$$

Solving the two simultaneous equations of Equations 19 and 20 for $\Delta\sigma'_y$ and $\Delta\sigma'_z$ gives:

$$\Delta\sigma'_{\mathrm{y}} = \left[\frac{\nu_{hh}E_v + \nu_{vh}^2E_h}{E_v - \nu_{vh}^2E_h}\right]\Delta\sigma'_{\mathrm{x}} \tag{21}$$

$$\Delta\sigma'_{\mathrm{z}} = \left[\frac{(1+\nu_{hh})\nu_{vh}E_v}{E_v - \nu_{vh}^2E_h}\right]\Delta\sigma'_{\mathrm{x}} \tag{22}$$

Inserting for $\Delta\sigma'_{\mathrm{y}}$ and $\Delta\sigma'_{\mathrm{z}}$ from Equations 21 and 22 in Equation 18 and re-arranging:

$$\Delta\varepsilon_x = \left[\frac{(1-\nu_{hh}^2)E_v - 2\nu_{vh}^2(1+\nu_{hh})E_h}{E_h(E_v - \nu_{vh}^2E_h)}\right]\Delta\sigma'_{\mathrm{x}} \tag{23}$$

For this situation of zero strain in the y (horizontal) and z (vertical) directions, the horizontal constrained modulus M_h is defined by:

$$\Delta\varepsilon_x = \frac{\Delta\sigma_x^{'}}{M_h} \tag{24}$$

Comparing Equations 23 and 24:

$$M_h = \frac{E_h(E_v - 2\nu_{vh}^2 E_h)}{(1-\nu_{hh}^2)E_v - 2\nu_{vh}^2(1+\nu_{hh})E_h} \tag{25}$$

This simplifies to the standard result for the constrained modulus of an isotropic elastic material (Equation 6) if $E_v = E_h = E$ and $\nu_{vh} = \nu_{hh} = \nu$.

4.3 EXPRESSIONS FOR E_h , E_v AND ν_{vh}

One of the five independent elastic moduli of a cross-anisotropic soil ($G_{hv} = G_{hv}$) can be measured directly from one of the measurements provided by the standard arrangement of three BEE pairs. None of the other 4 independent elastic moduli of a cross-anisotropic soil (E_h , E_v , ν_{vh} and ν_{hh}) can be determined from this standard arrangement of three BEE pairs, however if the value of one of them (say ν_{hh}) is known or assumed, then it is possible to determine the values of the other three (say E_h , E_v and ν_{vh}) from the other three parameters measured by the standard arrangement of three BEE pairs (G_{hh} , M_v and M_h).

Re-arranging Equation 10 gives:

$$E_h = 2(1+\nu_{hh})G_{hh} \tag{26}$$

Inserting Equation 26 into Equation 17 and re-arranging:

$$(1-\nu_{hh})(M_h - E_v)E_v = 4\nu_{vh}^2(1+\nu_{hh})M_h G_{hh} \tag{27}$$

Similarly, inserting Equation 26 into Equation 25:

$$[(1-\nu_{hh})M_h - 2G_{hh}]E_v = 4\nu_{vh}^2(1+\nu_{hh})(M_h - G_{hh})G_{hh} \tag{28}$$

If G_{hh} , M_v and M_h are known, and v_{hh} is either known or assumed, Equations 28 and 29 form two simultaneous equations in 2 unknowns (E_v and v_{vh}). Solving:

$$E_v = \frac{(1+v_{hh})M_v G_{hh}}{(1-v_{hh})(M_h - G_{hh})} \tag{29}$$

$$v_{vh} = \frac{1}{2(M_h - G_{hh})}\left[\frac{M_v\left((1-v_{hh})M_h - 2G_{hh}\right)}{(1-v_{hh})}\right]^{1/2} \tag{30}$$

Equations 26, 29 and 30 provide expressions for the independent elastic moduli E_h , E_v and v_{vh} in terms of three of the moduli measured by the standard arrangement of three BEE pairs (G_{hh} , M_v and M_h) and the final independent elastic modulus v_{hh} , the value of which must be either known independently or assumed.

It is clear that BEE tests using the conventional arrangement of three pairs of BEEs (one transmitting vertically and two transmitting horizontally) provide only 4 independent measurements and hence cannot be used to determine all 5 independent elastic constants for a cross-anisotropic soil.

4. CONCLUSION

Based on the preceding derivations, it can be concluded that it is possible to use a combination of triaxial testing system and three pairs of bender/extender elements BEEs fitted on a cross-anisotropic soil sample, to express elastic parameters for cross-anisotropic soils in a different fashion than those have been expressed in the literature. Expressions for the independent elastic moduli E_h , E_v and v_{vh} are derived in terms of three of the moduli measured by the standard arrangement of three BEE pairs (G_{hh} , M_v and M_h) and the final independent elastic modulus v_{hh} , the value of which must be either known independently or assumed.

REFERENCES

[1] C., Clayton, "Stiffness at small strain: research and practice", *Géotechnique*, 61 (1), 5-37, 2011.

[2] A. M. , Hasan, "Small strain elastic behaviour of unsaturated soil investigated by bender/extender element testing", PhD dissertation, University of Glsgow, UK, 2016.

[3] A. M. Hasan, and S. J. Wheeler, "Influence of compaction procedure on elastic anisotropy" *Proc. 5th International Conference on Unsaturated Soils, Sydney, Australia,* 2014, Vol. 1, pp. 285-289.

[4] K. M., Lee, and R., Rowe, "Deformation caused by surface loading and tunnelling: the role of elastic anisotropy", *Géotechnique*, 39 (1), 125-14, 1989.

[5] B. Simpson, J. H. Atkinson, and V. Jovicic, "The influence of anisotropy on calculations of ground settlements above tunnels", *Proceedings of the international symposium on geotechnical aspects of underground construction in soft ground, Rotterdam: Balkema*, 1996, 591-594.

[6] J. Wongsaroj, K. Soga, S. Yimsiri, and. M. R. J., "Stiffness anisotropy of London clay and its modelling: laboratory and field", *Advances in geotechnical engineering: the ICE, Proceedings of the Skempton conference, 1, London, UK*, 2004.

[7] A. Grammatikopoulou, F. C. Schroeder, A. Gasparre, N. Kovacevic, and V. Germano, "The influence of stiffness anisotropy on the behaviour of stiff natural clay", *Geotechnical and Geological Engineering*, 32, 1377-1387, 2014.

[8] V. Jovicic, and M. Coop, "The measurement of stiffness anisotropy in clays with bender element tests in triaxial apparatus", *Geotechnical Testing Journal*, 21 (1), 3-10, 1998.

[9] K. H. Stokoe, S. K. Hwang, N. K. J. Lee, & R. D. Andrus, "Effect of various parameters on the stiffness and damping of soils at small to medium

strains", *Keynote Lecture. Proc. 1st Int. Symp. on Pre-Failure Deformation of Geomaterials, Hokkaido*, 1995, 2, 785-816.

[10] V. Fioravante, and R. Capoferri, "On the use of multi-directional piezoelectric transducers in triaxial testing", *Geotechnical Testing Journal*, 24 (3), 243-255, 2001.

[11] D., Pennington, "The anisotropic small strain stiffness of Cambridge Gault clay", PhD dissertation, University of Bristol, UK, 1999.

[12] M. A., Biot, "Theory of propagation of elastic waves in a fluid saturated porous solid", *Journal of Acoustical Sociaty of America* . 28, No. 2,168-178, 1956.

[13] J. Viggiani, and J. H. Atkinson, "Interpretation of Bender Element Tests" *Géotechnique*, 45 (1), 149-154, 1995.

[14] L.D. Landau, and E.M. Lifshitz, "*Theory of Elasticity*", Course of Theoretical Physics. (2nd Ed), Pergamon: Oxford, 7, 13, 1970.

[15] A. Love, *A treatise on the Mathematical theory of elasticity*, University Press, Cambridge, 1927.

[16] J. Graham, and G. T. Houlsby, "Anisotropic elasticity of a natural clay" *Géotechnique*, 33 (3), 354-354, 1983.

[17] W. Powrie, *Soil Mechanics concepts and applications*, 3rd. ed. Abingdon, UK: Taylor and Francis group, 2014.

HYDROLOGICAL STUDY AND ANALYSIS OF TWO FARM DAMS IN ERBIL GOVERNORATE

Basil Younus Mustafa[1]

[1]*Erbil Polytechnic University, Erbil Technical Engineering College*
[1]*Ishik University*
[1]*basil.younus@epu.edu.krd*

doi:10.23918/iec2018.13

ABSTRACT

This research presents hydrological study and analysis for two proposed farm dams (Chaluk and Zurgazraw) located in Erbil Governorate - Iraqi Kurdistan Region. Many site visits were made to the Chaluk and Zurgazraw areas to select the most suitable site for the farm dams. The area and properties of the catchment area for both farm dams were measured by arc GIS software and were equal to 1.99, and 3.97 km^2 for Chaluk and Zurgazraw farm dams, respectively. The topographic study and surveying of the selected sites aimed to construct the contour maps of the sites, determine the capacity of the reservoir for different heights of the farm dam embankment, and locate the centerline of the dam and spillway. In the hydrological analysis, as the proposed farm dam's streams are ungauged streams with no runoff data records, the U.S. Soil Conservation Service (SCS) method was used to find the annual runoff yield. This method depends on physical parameters of the catchment area and daily rainfall depth data taken from Erbil Meteorological station; the calculated minimum, maximum, and average runoff yield were equal to 16556, 233407, and 103957 m^3 for Chaluk, and 33030, 456641, and, 207393 m^3, Zurgazraw farm dam. The Australian (ARR) organization method was used to determine the 50 year return period peak discharge for the farm dams catchment area, which were equal to 14.71, and 24.07 m^3/sec for Chaluk, and Zurgazraw farm dams, respectively. Based on the calculated average annual inflow and calculated annual sediment inflow into farm dams by Universal Soil Loss Equation, the dead, and live storages elevations, and volumes were fixed to be equal to 411, and 418 m.a.s.l. (meters above sea level) and 7741, and 103425 m^3 for Chaluk, and 404, and 412 m.a.s.l 20863, and 293822m^3 for Zurgazraw farm dam.

Keywords: Farm dam, Runoff, Catchment area, Peak discharge, Curve number, Sediment inflow

1. INTRODUCTION

Kurdistan region of Iraq is frequently subjected to a severe drought, which causes shortages, as the available water resources do not satisfy water demands for domestic, livestock consumption, agriculture, tourism and environment requirements. Therefore, the water resources management becomes one of the most important facility to solve the drought issues. Water harvesting is a useful practice to capture runoff and utilize it in situ for various uses especially supplemental irrigation during drought spells [1].

Investigations and studies started for water harvesting through the construction of small reservoirs (farm dams) everywhere feasible, that aims at collection of excess rainfall water and conservation of the eroded soil, in addition to groundwater recharge. Two locations near Chaluk and Zurgazraw villages in Erbil Governorate were proposed for conducting the feasibility studies and design of small reservoirs (farm dams) in order to reclaim water resources in the region. The present study is a part of feasibility study and design of Chaluk and Zurgazraw farm dams, and was conducted at the request of International Center for Agriculture Research in the Dry Areas (ICARDA).

2. GENERAL DATA

2.1 SITE SELECTION

Many site visits were made to the Chaluk and Zurgazraw areas to select the most suitable site for the farm dams; three potential locations were selected for each area to construct the farm dam in it. For each area, the selection of the suitable one, among the three locations, has been done based on the followings [2]:

a. Topography and storage capacity: For economic feasibility of storage project, it is necessary that the length of the farm dam embankment body should be as small as possible and for a given height it should store a maximum volume of water, this factor was taken into consideration in the selection of both farm dams site.
b. Catchment Area and Hydrology: The catchment area upstream the farm dam location is sufficient catchment and it is expected that it will bring enough amount of water to fill the reservoir. To be sure about this factor, the hydrological study of the catchment area has been being prepared.

c. Foundation: A good foundation for the farm dam embankment body will be provided after a geotechnical investigation of the selected site, it is very important to find the soil permeability, the location of bedrock and to know whether the foundation is pervious or impervious.
d. The availability of the materials for construction: It is very important for the economic feasibility of the project to have a suitable material for construction near the selected site to minimize the cost of the project, which has been ensured for both areas of studies.
e. Spillway Location: The selected site of the farm dam has a suitable location for the spillway structure to release surplus water during the floods.
f. Irrigation Command: The selected site is suitable for irrigation purposes; the site is upstream of the cultivated areas, hence these areas can be easily irrigated during the drought days, so the supplementary irrigation technique can be easily provided to the area.

The Topographic study and surveying of the selected sites aimed to construct contour maps of the sites, determine the capacity of the reservoir for different heights of the farm dams' embankment and locate the axes of the lake and spillway. Two reference points were taken GPS; then, data were collected using total station (Topcon GTS235) every 10 to 15m for the construction of topographic maps and surface details. Chaluk and Zurgazraw villages (farm dams' locations) are situated to the South and South East of Erbil city, Iraqi Kurdistan region. Additional details for the farm dams' locations are listed in the Table (1), and shown in the prepared counter maps in Figure (1).

TABLE 1.
Coordinates for the Proposed Farm Dams

No.	Farm Dam and Village Name	Sub- District to which they belong	UTM Coordinates		
1	Chaluk	Khabat	X	Y	Z
	BM1		383599.55	4010641.7	415.97
	BM2		383485.42	4010675.3	419.62
	BM3		383604.82	4010537	417.8
2	Zurgazraw	Shamamik			
	BM1		397310.08	3974029	416.85
	BM2		397454.12	3973812	415.12
	BM3		397253.14	3973890.2	412.08

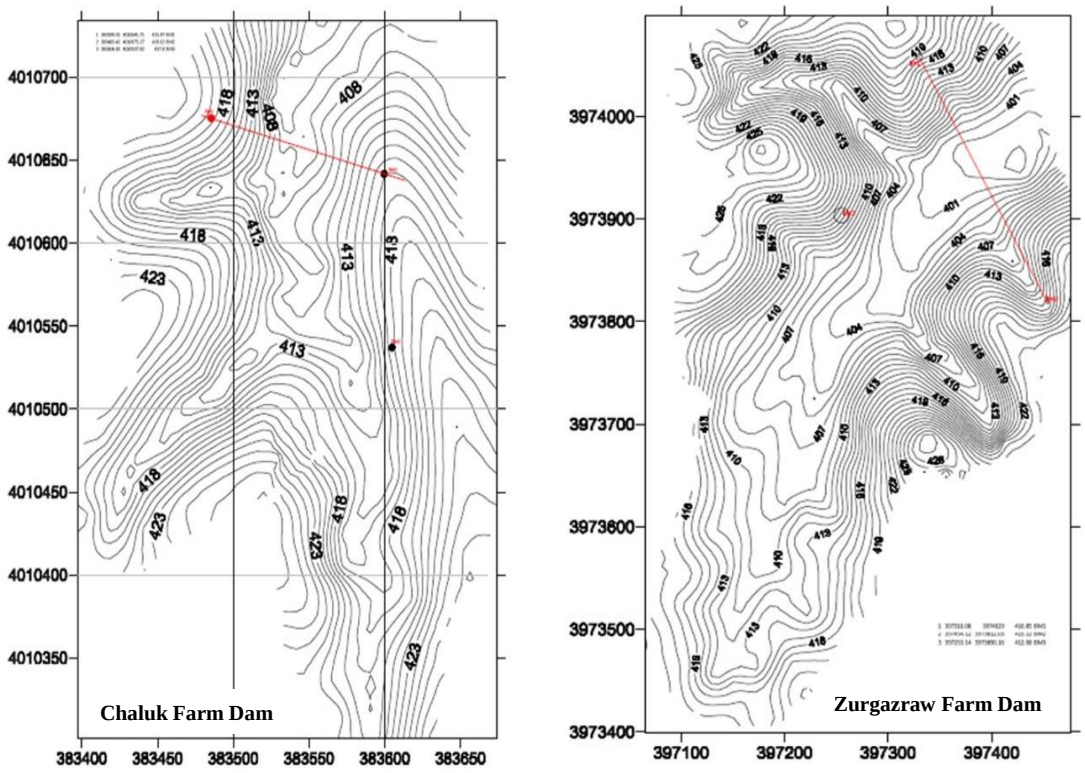

FIGURE 1. Contour Maps of Proposed Farm Dams

2.2 CLIMATE

The Chaluk farm dam site is situated 25 km west of Erbil city and 3.5 km east of Khabat District, and the Zurgazraw farm dam site is situated 30 km South of Erbil city. The farm dams are located in a semi-arid zone, with hot summer and cold winter, and the rainfall occurs from October to May. Full and complete meteorological data records for the areas are available at Erbil meteorological station; this is because there is no closer meteorological station near the farm dams' sites. Erbil Metrological station has records for the daily rainfall data for the period from 1992-1993 to 2010-2011, and the maximum 24hr rainfall depths the period from 1975-1976 to 2010-2011. The recorded minimum and maximum monthly temperature in Erbil metrological station for the period 1993-2010 is 4.1 C^o in January, and 41.8 C^o in July. The recorded average annual evaporation for the period 2001–2010 was 2485.3 mm, and the minimum and maximum average monthly humidity for the period 2000-2010 are 26.5%, in July and 68.8% in January, respectively. The average annual rainfall depth for the period from 1941-1942 to 2010-2011 is 403 mm, and the max 24hr rainfall depth for the period from 1975-1976 to 2010-2011 is 75.7 mm, which occurred in February,1995 [3].

2.3 TARGET BENEFICIARIES

Villages downstream of the farm dams will benefit from the stored water of the farm dam for supplemental irrigation, and livestock watering. Table (2) shows general Socio-Economic data of the proposed farm dams.

TABLE 2.
General Socio-Economic Data for Proposed Farm Dams

No.	Hill Lake Name	Beneficiary Village	No. of Families	Population	No. of Animals		Agriculture (ha)
					Small	Large	
1	Chaluk	Chaluk	80	400	900	105	50
2	Zurgazraw	Zurgazraw	45	225	500	255	125

3. HYDROLOGICAL ANALYSIS

3.1 CATCHMENT AREA

The catchment area shape and properties of the proposed farm dams, measured by arc GIS software, are shown in figure (2) and table (3). In general, the catchment areas shape has rather a hilly topography, very little flat land with steep slopes at some parts of the basin. The rainfall-runoff take places in the valleys in winter, but no historical flow measurements are available for the streams of the catchment area.

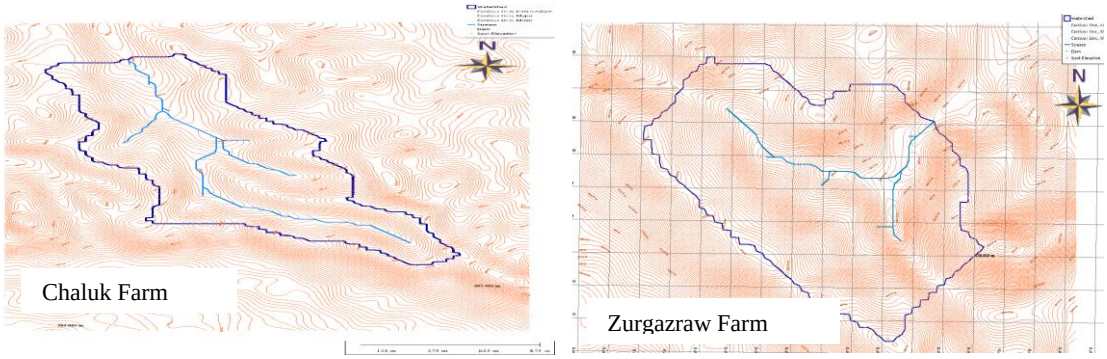

FIGURE 2. Proposed Farm Dams Catchment Area

TABLE 3.
Farm Dams Catchment Properties

Farm Dam Name	Chaluk	Zurgazraw
Basin Area	1.99 km^2	3.97 km^2
Basin Length	2722.76 m	11750.88 m
Basin Slope	0.0923 m/m	0.0819 m/m
Basin Perimeter	9256.43 m	5733.16 m
Basin Shape Factor	3.73 mi^2/mi^2	1.28 mi^2/mi^2
Mean Basin Elevation	431.39 m	411.99 m
Maximum Stream Length	3315 m	4550m
Maximum Stream Slope	0.03016 m/m	0.034 m/m

3.2 ESTIMATING THE CATCHMENT ANNUAL YIELD FROM SURFACE RUNOFF

The most readily available source of water is the surface water in rivers and lakes. This water is usually stored in dams. In certain parts, fortunate farmers have 'run of the river' schemes, that is, they do not need storages because the flows in the rivers are so reliable that they can meet all requirements. This is the situation in areas of consistently high rainfall.

The proposed farm dams' streams are ungauged streams with no runoff data records. There are many methods to calculate the runoff yield for ungauged streams; they depend on the stream catchment area characteristics and measured annual rainfall depth. The variability of rainfall limits the accuracy of forecasting, and hence, the reliability of these methods. It therefore follows that, despite the most careful calculations, it is difficult to guarantee that a farm dam will always meet requirements. However, a method of estimating the potential catchment yield must be adopted so that a farm water supply scheme can be planned on a reasonably sound basis. Usually, the most accurate method for estimating the yield of the ungauged streams is SCS (Soil Conservation Services); this method is used for the calculation of the daily runoff by using daily recorded rainfall data for the farm dam site and catchment area characteristics. In 1954 [4], SCS derived the following equation for calculating surface runoff depth in (mm):

$$\mathrm{SRO} = \frac{(\mathrm{P}-0.2\mathrm{S})^2}{(\mathrm{P}+0.8\mathrm{S})} \quad \ldots\ldots\ldots (1)$$

Where:

P is daily rainfall depth in (mm), and

S is a potential maximum retention in (mm), that can be calculated from the following equation:

$$\mathrm{S} = \frac{25400}{\mathrm{RCN}} - 254 \quad \ldots\ldots\ldots (2)$$

RCN: is runoff coefficient called runoff curve number, which depends on the soil type, land use and infiltration rate.

The Runoff Curve Number (RCN) technique has been proven to be a very useful tool for evaluating effects of changes in land use and treatment on surface runoff. It is

the procedure most frequently used within the SCS and by hydrologists worldwide to estimate surface runoff from ungauged watersheds. The infiltration rate is the rate at which water enters the soil at the surface and which is controlled by surface conditions. The hydrologic soil groups, as defined by SCS soil scientists according to infiltration rate, are: A type Soils having high infiltration rates (greater than 0.76 cm/hr), B type Soils having moderate infiltration rates (between 0.38 – 0.76 cm/hr), C type Soils having slow infiltration rates (between 0.13 – 0.38 cm/hr), and D type soils having very slow infiltration rates (less than 0.13 cm/hr). SCS gives RCN corresponding to above soil groups in tables [5].

In the SCS method of runoff estimation, the effects of the surface conditions of a watershed are evaluated by means of land use and treatment classes. Land use is the watershed cover and it includes every type of vegetation suggested by SCS [4].

SCS prepared a table gives RCN corresponding to the land uses. The tabulated RCN values are for normal soil moisture conditions which are referred to as Antecedent Moisture Condition II (AMC-II). AMC-I has the lowest runoff potential and the watershed soils are dry. AMC-III has the highest runoff potential as the watershed is practically saturated from antecedent rainfall. The following equations shall compute RCN for AMC-I or AMC-III [6]:

$$\mathrm{RCN(I)} = \frac{4.2\ \mathrm{RCN(II)}}{10 - 0.058\ \mathrm{RCN(II)}} \quad \ldots\ldots\ldots (3)$$

$$\mathrm{RCN(III)} = \frac{23\ \mathrm{RCN(II)}}{10 + 0.13\ \mathrm{RCN(II)}} \quad \ldots\ldots\ldots (4)$$

For each Farm dam catchment area, the runoff curve number (RCN) was calculated from SCS tables based on the hydrologic soil groups and the nature of the antecedent moisture condition for AMC-II group (weighted mean) without dividing the area into sub-areas; as the areas are not large. In the calculation, the following were assumed:

a- Soil cover of the Farm dam catchment areas are Loam soil, type C, Soils having slow infiltration rates.

b- The land use of the Farm dam catchment areas is Small grain, Straight row.

c- Months October and November are regarded as AMC-I condition because the land is at its lowest moisture content, a period of starting rainfall, the duration between two rainfalls are almost long then the probability of runoff is low. Months December,

January, and February are considered to be AMC-II condition; this is because the soil moisture increases, the duration between two successive rainfalls is short and the probability of runoff increases. Months March, April and May are considered as AMC-III due to the fact that the soil is almost saturated and the possibility of runoff is at the maximum level.

Based on the above steps and conditions, the runoff curve numbers for the farm dam catchment areas were found to be equal to 84, 68.8 and 92.4 for groups AMC-II, AMC-I and AMC-III, respectively.

Based on the daily rainfall data for the interval from (1992-1993) to (2010-2011) and using Equations (1) and (2), the daily, monthly, and annual runoff depth were calculated as summarized in Table (4). Based on this table, the average annual runoff depth is found to be 52.24 mm, and by multiplying the runoff depth by the catchment area of each farm dam, the annual inflow volume in (m^3) is calculated, as shown in the Table (5).

TABLE 4.
Summery of average, minimum, and maximum annual surface runoff calculation

Month	Oct.	Nov.	Dec.	Jan.	Feb.	march	April	May	Total
Year	Runoff (mm)	Runoff (mm)	Runoff (mm)	Runoff (mm)	Runoff (mm)	Runoff (mm)	Runoff (mm)	Runoff (mm)	Runoff (mm)
1992-1993	0.0	12.9	11.4	6.5	3.4	11.9	57.1	14.1	117.3
1993-1994	0.0	0.0	2.5	10.0	11.6	52.8	16.0	0.4	93.2
1994-1995	0.9	1.6	6.9	9.8	46.3	22.9	13.3	0.0	101.8
1995-1996	0.0	1.6	0.0	7.0	0.1	20.4	6.1	0.0	35.1
1996-1997	0.0	0.0	7.2	10.9	2.5	15.5	11.9	0.0	48.1
1997-1998	0.0	0.0	9.4	11.3	0.0	16.2	4.6	0.0	41.5
1998-1999	0.0	0.0	0.7	1.8	4.0	1.3	0.4	0.0	8.3
1999-2000	0.0	0.0	6.3	2.4	0.2	2.2	1.6	0.2	13.0
2000-2001	0.0	0.0	2.4	1.7	3.1	44.2	11.1	0.0	62.5
2001-2002	0.0	0.0	1.1	8.7	0.2	32.9	9.4	0.0	52.3
2006-2007	0.4	0.0	0.6	4.5	14.6	7.0	3.2	0.4	30.8
2007-2008	0.0	0.0	0.0	0.1	1.4	31.5	0.0	0.0	33.1
2008-2009	2.2	0.0	0.1	0.0	0.2	22.3	1.8	0.1	26.7
2009-2010	0.0	0.0	6.9	0.3	9.2	26.0	2.3	2.8	47.4
2010-2011	0.0	0.0	0.9	11.2	2.0	5.9	52.2	0.4	72.5
Total	3.5	16.1	56.2	86.1	98.9	313.2	191.2	18.4	783.6
Average	0.2	1.1	3.7	5.7	6.6	20.9	12.7	1.2	52.2
max	2.2	12.9	11.4	11.3	46.3	52.8	57.1	14.1	117.3
Min	0.0	0.0	0.0	0.0	0.0	1.3	0.0	0.0	8.3

TABLE 5.
Catchment yield from surface runoff for the both proposed farm dams

No.	Farm dam name	Annual Runoff Depth (SRO) in (mm)			Catchment area (A) in (Km^2)	Runoff yield volume (V) in (m^3)		
		Max.	Min.	Avg.		Max.	Min.	Avg.
1	Chaluk	8.32	117.29	52.24	1.99	16,556	233,407	103,957
2	Zurgazraw	8.32	117.29	52.24	3.97	33,030	465,641	207,393

3.3 PEAK (FLOOD) DISCHARGE CALCULATION

The peak flood is the maximum flood to be expected from a catchment following a rainfall of estimated intensity and duration for a selected return period. In many parts of the Iraqi Kurdistan region, information is not available or smaller streams are not gauged to allow estimation of such floods for spillway design purposes. A very approximate peak flood estimate can be made by taking the highest daily rainfall figure for the catchment and making the assumptions that all farm dams in the same catchment is 100 percent full, the ground is saturated, and 100 percent run-off will occur. An important element in designing spillways of a farm dam is to establish run-off within a specified return period (recurrence interval). Selection of a return period depends on the economic balance between cost of periodic repair or replacement and the cost of providing additional capacity to reduce the cost of repair or replacement. Most spillways on farm dams are cut into the earth because concrete is too expensive but concrete lined spillways are more resistant to flood current erosion and more stable than earth type spillway. The generally accepted flood frequency return periods used for Minor dams and farm dams are (depending on consequences of overtopping) 10-50 years [2].

As the farm dams' catchment area streams are ungauged streams (no data record for flood discharges), the Peak (flood) discharges were calculated using empirical methods, which depends on the maximum rainfall depth and catchment area characteristics. The main methods are:

1- **SCS Unit Hydrograph method** [7]

This method involves determining the peak rate of runoff (Qp) expressed in (m^3/sec) per cm of runoff from a given drainage area. This (Qp) is primarily a function of the time it takes for runoff to travel through the basin to the design point. Once this rate of runoff is determined, it can be multiplied by the amount of runoff to produce a discharge. The SCS model can be considered the most suitable for medium and large catchment areas.

2- **Run-off (ARR)-A Guide to Flood Estimation** [2]

This method is used for small to medium-sized ungauged rural catchments for an Average Recurrence Interval (Return period) of 50 years especially for farm dam spillway discharge design. This method is developed in Australian (ARR) organization takes into consideration rainfall intensity, catchment characteristics and size, the average slope of the waterway and its length from source to the Farm dam site. The formula is:

$$Q_Y = 0.278 * C_Y * I_{TC} * A \quad \ldots\ldots (5)$$

Where Q_Y is the flood discharge for 50 years return period (m^3/sec), C_Y is run-off coefficient (dimensionless) depends on return period (Y) for 50 years return period is equal to 0.25 [1], I_{Tc} is average rainfall intensity (mm/hr) for design duration of (T_c), and A is area of catchment (km^2).

$$I_{TC} = \frac{P_T}{T_C} \quad \ldots\ldots (6)$$

Where Tc is the design duration or concentration time in (hr), for ungauged watersheds. it can be worked out by the California formula, which is:

$$T_C = \left(\frac{0.871L^3}{\Delta H}\right)^{0.385} \quad \ldots \ldots (7)$$

Where T_c in (hr), L is the length in (km) of the particular flow path and ΔH is the maximum elevation difference in the catchment area. Table (6) shows the calculation of T_c for all proposed farm dams catchment areas.

TABLE 6.
Calculation of time of concentration (T_c)

No.	Farm Dam Name	Length (m)	ΔH (m)	T_c (hr)
1	Chaluk	3315	100	0.643
2	Zurgazaw	4550	155	0.784

P_T is maximum 24hr design rainfall depth. As the Normal practice in this method is to use 24 hours as the design rainfall duration, the current study is based on the available recorded 24 hr max rainfall depth in the Erbil meteorological station for 36 years' period from (1975-1976) to (2010-2011).

Using the frequency analysis by Gumble distribution Equations (8), (9), (10), (11), and (12) below [8], the max. 24 hr rainfall amount for return periods (2, 3, 4,5,10, 25, and 50) years were obtained for the farm dams catchment area under study as shown in the Table (7).

$P_T = P` + K_T\sigma$ …… (8)

Where P_T is 24hr max. rainfall depth for any return period (T) (mm), P` is Average values of 24hr max. Rainfall depth data σ is Standard Deviation of 24hr max, which is calculated using Equation (9):

$$\sigma = \sqrt{\frac{\sum(Pi-P`)^2}{(n-1)}} \quad \ldots\ldots (9)$$

$$P` = \frac{\sum Pi}{n} \quad \ldots\ldots (10)$$

Where n is No. of recorded rainfall data,

$$K_T = -(0.779) * (0.577 + y) \ldots\ldots\ldots (11)$$

$$y = \ln\{\ln(\frac{T}{T-1})\} \ldots\ldots\ldots (12)$$

TABLE 7.
24hr max. Rainfall calculation by Gumble distribution

T (year)	2	3	5	10	25	50
y = -ln{-ln(1-1/T)}	0.367	0.903	1.500	2.250	3.199	3.902
K_T	-0.164	0.254	0.720	1.305	2.044	2.592
P_T in (mm)	35.0	40.1	45.7	52.8	61.7	68.4

Using the values of T_c and P_T obtained in Tables (6) and (7), the rainfall intensity in (mm/hr) from Equation (6), and the flood discharge (Q_Y) in (m^3/sec) from Equation (5) for (50) years return period were calculated for both farm dams' catchment area, as shown in Table (8).

TABLE 8.
Flood discharge by (ARR) Method for both proposed farm dams

Farm Dam Name	P_T (mm)	Tc (hr)	I (mm/hr)	C_Y	A (Km^2)	$(Q)_T$ (m^3/ sec) for T= 50 years
Chaluk	68.40	0.643	106.38	0.25	1.99	14.71
Zurgazraw	68.40	0.784	87.24	0.25	3.97	23.07

4. FARM DAMS CHARACTERISTICS

4.1 FARM DAMS SEDIMENTATION

The loss of soil by erosion in the farm dams' catchment area was calculated using Universal Soil Loss Equation [9]:

$$A = R * LS * K * C * P \ldots\ldots\ldots (13)$$

Where: A is mean annual soil loss (ton/ hectare/ year), R is rainfall erosivity index, R value for the farm dams site is found from the iso-rodent map for northern Iraq

prepared by Nikolav, 1983 using the Wischmeir equation, 1962 [10], which is equal to 50. K is soil erodibility in the metric unit (Ton/hectare/unit of rainfall erosivity), K=o.5, is calculated from the map for northern Iraq prepared by Nikolav,1983 [10].

P is the soil conservation practice factor, which is defined as the ratio of soil loss from the field with supporting practices as contouring, strip cropping, minimum tillage or terracing to that with straight row farming up and downslope, depending on the land slope P value can be found from a table prepared by Nikolav, 1983 [10]. For the farm dams site, the average land slope is equal to 4%, and from Nikolav table, P would be equal to 0.5.

C is the cropping management factor, which is the ratio of soil loss from land cropped under the specified condition to the corresponding soil loss from tilled continuous fallow. C is equal to 0.16 for Biennial rotation (a common practice in Iraq) [10].

LS is the topographic factor for the site calculated as a function of the slope length (L) and slope steepness (S) from Equation (14) below, in which L is in meter and S is in percentage. The slope steepness (s) for the catchment area was taken as 4 % for average slope length (L=50 m), yielding LC to be equal to 0.52 from Equation (14) and A to be equal to 1.4 Ton/hectare/year from Equation (13).

$$LS = l^{0.5}(0.0138 + 0.00965 * S + 0.00138 * S^2 \quad \ldots\ldots\ldots \quad (14)$$

Table (9) presents the procedure to calculate the volume of the accumulated sediment for 50 years return period, which is the product of the multiplication of the catchment area, mean annual loss (A) and 50 years return period divided by the sediment density (1.6).

TABLE 9.
Mean annual soil loss for the farm dams

Farm Dam Name	Catchment Area (hectares)	A (mean annual soil loss) (ton/ha/year)	A (mean annual soil loss) (ton/year)	Sediment Density	A (mean annual soil loss) (m^3/year)	Volume of sediment for T=50 years (m^3)
Chaluk	199	1.04	206/96	1.6	114.97	6467.5
Zurgazraw	397	1.04	412.88	1.6	229.37	12900

4.2 FARM DAMS AREA - VOLUME CAPACITY TABLES

Based on contour maps of 1m contour interval (H) prepared for both surveyed farm dams, the volume between two successive contours has been calculated using the cone formula (Equation 17) based on the area of top counter (A_1) and the area of the bottom counter (A_2). Repeating these calculations for all counter intervals, the storage capacity table for each farm dams has been prepared as shown in Table (9).

$$V = \left(\frac{H}{3}\right) * (A_1 + A_2 + \sqrt{A_1 + A_2 + A_1 A_2}) \quad \ldots\ldots\ldots (17)$$

Based on the sediment volume calculations, Table (10) has been prepared to determine the elevations and the storage capacity for the proposed farm dams. The elevation and volume of the dead storage were fixed as 411 m.a.s.l., and 7741 m^3 for Chaluk, and 404 m.a.s.l., and 20863 m^3 for Zurgazraw farm dams, respectively. The normal water storage (spillway crest) and Embankment crest elevations were fixed at 418, and 420 m.a.s.l. for Chaluk, and 412, and 414 m.a.s.l. for Zurgazraw farm dams respectively. The live storage volume was calculated to be equal to 103425 m^3 for Chaluk, and 293822 m^3 for Zurgazraw farm dams respectively.

TABLE 10.
Farm Dams Elevation, Storage Capacity Calculation

Contour (m)	Area (m^2)	Volume (m^3)	Accumulative Volume (m^3)	Contour (m)	Area (m^2)	Volume (m^3)	Accumulative Volume (m^3)
407	123	41	41	401	1660	553	553
408	612	337	378	402	5224	3276	3829
409	1616	1074	1452	403	8498	6795	10625
410	3122	2328	3780	404	12084	10239	20863
411	4864	3961	7741	405	16449	14211	35074
412	6986	5893	13634	406	21227	18787	53862
413	9483	8203	21836	407	27363	24230	78092
414	12074	10753	32589	408	35149	31175	109267
415	15258	13635	46224	409	43363	39184	148451
416	19251	17216	63440	410	51450	47349	195800
417	23930	21548	84988	411	59287	55322	251123
418	28493	26178	111166	412	67936	63563	314685
419				413	67936	67936	382621
420				414			
Chaluk Farm Dam Elevation, Storage Capacity Table				Zurgazraw Farm Dam Elevation, Storage Capacity Table			

Based on the sediment volume calculations, Table (11) has been prepared to determine the elevations and the storage capacity for the proposed farm dams.

The elevation and volume of the dead storage were fixed as 411 m.a.s.l., and 7741 m^3 for Chaluk, and 404 m.a.s.l., and 20863 m^3 for Zurgazraw farm dams, respectively. The normal water storage (spillway crest) and Embankment crest elevations were fixed at 418, and 420 m.a.s.l. for Chaluk, and 412, and 414 m.a.s.l. for Zurgazraw farm dams respectively. The live storage volume was calculated to be equal to 103425 m^3 for Chaluk, and 293822 m^3 for Zurgazraw farm dams respectively.

TABLE 11.
Storages and Levels of Proposed Farm Dams

Item	Chaluk Farm Dam	Zurgazraw Farm Dam
Dead Storage Level (m.a.s.l)	411	404
Dead Storage Volume (m^3)	7,741	20,863
Dead Storage Flooded area (m^2)	4,864	12,084
Live Storage (Spillway Crest) Level (m.a.s.l)	418	412
Live Storage Volume (m^3)	103,425	293,822
Live Storage Flooded area (m^2)	28,493	67,936
Total Volume (m^3)	111,166	314,685
Embankment Bed level at the center line (m.a.s.l)	407	401
Embankment crest level (m.a.s.l)	420	414
Embankment height (m)	13	13

5. CONCLUSIONS

The purpose of Construction of the Chaluk and Zurgazraw proposed farm dams will be for supplemental irrigation, and livestock watering. The catchment area of the proposed Chaluk and Zurgazraw farm dams have been calculated by arc GIS software are, equal to 1.99, and 3.97 km^2, respectively. Based on the topographic study of the sites, the capacity of the reservoir for different heights of the farm dams' embankment determined.

The daily, monthly and annual runoff depth and volume have been calculated based on SCS equation for the farm dams' catchment areas using recorded daily rainfall depth in Erbil metrological station for the period from 1992-2011. The minimum, maximum, and average annual runoff volume have been found to be equal to 16556, 233407, and 103957 m^3 for Chaluk farm dam, and 33030, 465641, and 207393 m^3 for Zurgazraw farm dam, respectively.

The Peak (flood) discharges for the farm dams' catchment areas have been determined (using ARR method) based on the recorded maximum (24hr) rainfall depth in Erbil metrological station for the period from 1975-2011, which were found to be equal to 14.71, and 24.07 m^3/sec for the Chaluk and Zurgazraw farm dams, respectively.

The elevations of embankment crest were fixed at 420, and 414 m.a.s.l., and the normal water level at 418, and 412 m.a.s.l. for Chaluk and Zurgazraw farm dams, respectively. Based on the calculated sediment accumulation volume in the farm dams for 50 years return period, the dead storage elevation was fixed at 411, and 404 m.a.s.l., these elevations resulting a dead storage volume of 7741, and 12084 m^3, and live storage capacity equal to 103425, and 293822 m^3 for Chaluk and Zurgazraw farm dams, respectively.

REFERENCES

[1] Mark J. Hammer and Kenneth A., “Hydrology and quality of water resources", published by John Willey and Sons, 1981.

[2] Barry Lewis, “Farm dams Planning Construction and Maintenance “, National Library Cataloguing Publication, 2002.

[3] General Directorate of Water Recourses, Iraqi Kurdistan Region "Erbil Station Metrological Data for Period 1941-2011".

[4] Soil Conservation Service, “Urban Hydrology for Small Watersheds", Technical Release No. 55, U.S. Dept. of Agriculture, Washington, D.C., January 1975.

[5] U.S. Department of Agriculture, Soil Conservation Service, "Technical Release No. 55: Urban Hydrology for Small Watersheds", Washington, D.C., June 1986.

[6] Richard H. McCuen, "A Guide to Hydrologic Analysis Using SCS Methods", Prentice-Hall, Englewood Cliffs, N.J., 1982.

[7] B. Y. Mustafa, “Flood discharge calculation for ungauged watersheds in Erbil Governorate", Journal of Zanko, Salahaddin university/Erbil, Vol.19, No.2, 2007.

[8] Vector Miguel Ponce, "Engineering Hydrology Principles and Practice" Pub. by McGraw-Hill, 1998.

[9] White W.R.-Milli, "Sediment Transport Theories A review", Proc. Inst. Civ. Eng., part2,1975.

[10] Sando P. Nikolov, "Rainfall Erosion in Northern Iraq an Aid to Soil Conservation", Baghdad, 1983.

[11] Sherman, L.K., "Stream flow from rainfall by the unit-graph method", Eng. News Rec., Vol. 108, pp. 501-505, April, 1932.

[12] Richard C. Sorrel, P.E., "Computing Flood Discharges for Small Ungauged Watersheds" Geological and Land Management Division, Jul.2003.

[13] Soil Conservation Service, “Hydrology, Sec. 4 of National Engineering Handbook", U.S. Dept. of Agriculture, Washington, D.C., 1972.

INFLUENCE OF UPSTREAM BLANKET ON EARTH DAM SEEPAGE

Krikar M-Gharrib Noori[1], Hawkar Hashim Ibrahim[2], Dr.Ahmed Mohammed Hasan[3]

[1]Koya Technical Institute, EPU, Koya, KRG-Iraq
[2&3] College of Engineering, Salahaddin University-Erbil
[1]Krikar.bedary@epu.edu.krd, [2]hawkar.ibrahim@su.edu.krd, [3]ahmed.hasan@su.edu.krd

doi:10.23918/iec2018.14

ABSTRACT

Seepage is one of the main causes of earth dam failure. Concerning the failure, the control of seepage is required. In this study, the analyses of seepage problem were performed on Shiwashok earth dam body and its foundation. This study has concentrated on the efficiency of using upstream blanket to reduce seepage discharge and the uplift pressure of Shiwashok earth dam in Kurdistan region of Iraq. To meet the aims of this study, different clay blanket lengths and thicknesses were investigated. Two dimensional simulations of 23m high Shiwashok earth dam were carried out using the numerical analysis SEEP/W software using existing data of the geometrical and mechanical properties of the earth dam and its foundation. The outcomes showed that lengthening the clay blanket and increasing blanket thickness reduced the percentage of seepage amount and uplift pressure at the downstream side of the dam. It can be concluded from the results of the simulations that the optimum blanket length (BL) and the blanket thickness (t) were 80m, and 1m to 1.5m, respectively.

Keywords: Seepage Control, Clay Blanket, Shiwashok Earth Dam, SEEP/W.

1. INTRODUCTION

Embankment dams are primarily built from compacted soil or rock. They are the principal means of storing water[1]. When the embankment dams are impounded with water, they are subject to seepage through their embankments and foundations. Seepage is considered one of the common reasons that cause failure in earth dam [2]. There are many different methods to decrease and control the seepage discharge at the foundation of embankment dams such as grout curtain, concrete wall, slurry trench, cutoff wall, upstream blanket, filters, sand drains, and relief wells [3], [4]. The selection of the seepage control approaches is based on some aspects including material availability, cost, soil type, construction access, machinery availability, and construction access [5]. Each of these approaches has its own, technical, economical and practical limitations. For example, in a case that the reservoir head exceeds 200 ft (60.96m) upstream blankets should not be used because the hydraulic gradient acting across the blanket may result in piping and serious leakage [6]. Therefore, using any of the seepage control approaches or a combination of them can be provided with the foundation condition and the practical limitation considerations.

Rezk and Senoon [7] calculated the seepage problem of earth dam with upstream blanket analytically to evaluate the effect of the blanket length on each of seepage and head loss. It was recommended to apply mathematical solution to find seepage discharge and head loss for earth dam with upstream blanket. It was recommended to apply a mathematical solution to find seepage discharge and head loss for earth dam with the upstream blanket. It was found that the mathematical solution could be validly applied for the relative depth of the upstream impervious layer (d/L) ratio ranging from 0.014 to 0.164. In Goharnejad, et al. [8] study the effects of upstream clay blankets in terms of geometry, and dimensions were examined to reduce the seepage in the foundation of Farim Sahra Dam in Iran. According to the results, upstream blanket considerably decreases seepage discharge and the upstream clay blanket with 0.75 m thickness and 150 m length suggested. In this case, the seepage amount is about 73% less than the amount when there is no clay blanket, and the possible applied thickness is at least 0.75m, which might be changed according to the topographical situation.

This study concerns about investigating of Shiwashok earth dam, which has already designed without clay blanket, which is not constructed yet. To avoid failure of the

dam, before construction, checking stability and re-designing of the dam is crucial. For that reason, in this paper, the effects of various upstream blanket lengths and thicknesses on seepage discharge and uplift pressure were studied. Numerical simulation carried out using SEEP/W software used to study seepage in Shiwashok earth dam.

2. MATERIAL AND METHODS

2.1 SEEPAGE THEORY

SEEP/W is formulated on the basis that the flow of water through both saturated and unsaturated soil follows Darcy's Law [9]:

$$q = kiA \tag{1}$$

where q is the specific discharge, k is the hydraulic conductivity, i is the gradient of total hydraulic head and A is cross-sectional area of flow. The rate of underseepage may be estimated for pervious foundation, which is cut off by a clay blanket by [10]:

$$\frac{Q_o}{K_o\ H} = \frac{1}{0.88 + \left[\frac{B + BL}{D_f}\right]} \tag{2}$$

where Q_o is rate of underseepage in m/sec per running meter of dam, K_o is permeability of the foundation in m/sec., H is head of water in the reservoir in m, B is width of the base of the core in m, D_f is depth of the foundation in m, and BL is Blanket length.

2.2 NUMERICAL SIMULATION

In this study, for the purpose of seepage analysis through a heterogeneous earth dam, Shiwashok zoned earth dam was taken to model as a case study. It is 23 m height, its crest crown is 7 m wide and the base width of the dam is 136 m. The reservoir water level is 20 m high faces the upstream side. The upstream face of the dam has a slope of 1:2.75 while the downstream slope of the dam designed to have a 1:2.5 slope with 2 m berm and its height is 12 m from the base level. The downstream slope is flattened to 1:2.75 in the downward direction below the berm elevation. A cofferdam with 11 m high and 4 m width crest will be a part of the main dam body while its crest will be a berm for the upstream slope. The upstream face of the cofferdam has a slope

of 1:2.75, while the downstream slope of the cofferdam designed to have a 1:2.25 slope. The crest of the core is at 22 m high and its width is 4 m. It will expand with a slope 1:3.75 to the foundation to reach about 15 m at a lowest level of the dam. The filter material was used on the downstream side and extends along the downstream side foundation. The hydraulic conductivity of the dam components is described in Table 1.

TABLE 1.
The permeability of the materials used in the components of the dam

Types of materials	Permeability (k)
Shell	$1 * 10^{-6}$ m/sec
Core	$3 * 10^{-9}$ m/sec
Filter	$5 * 10^{-4}$ m/sec
Foundation	$1 * 10^{-6}$ m/sec

Using the numerical analyses of SEEP/W software and having the mechanical and geometrical properties of the dam and its foundation, two-dimensional simulation of Shiwashok earth dam with 25 m assumed alluvial foundation was carried out. The study was performed to investigate the effects of the upstream blanket with the same permeability of the core (k = 3*10-9 m/sec), on the seepage amount and uplift pressure. The parameters used in analyses are the thickness of the blanket (t), and the length of the blanket (BL). Figure 1 shows Shiwashok earth dam cross section with and without clay blanket.

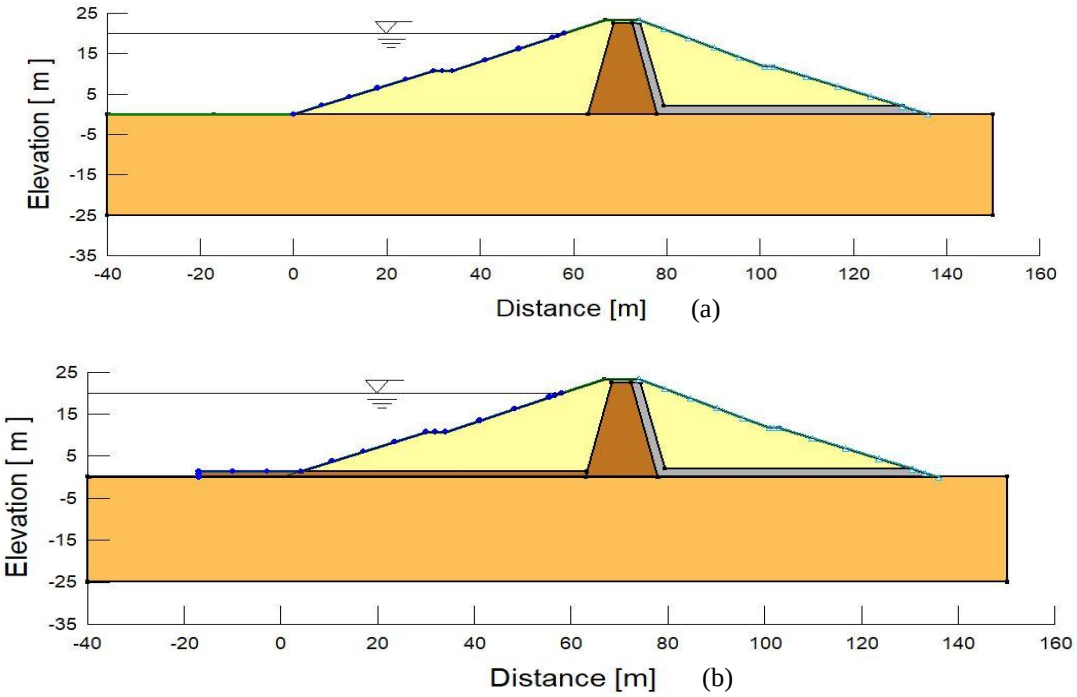

FIGURE 1. Cross section of Shiwashok earth dam used in this study
(a) without clay blanket (b) With clay blanket

3. RESULTS AND DISCUSSION

Seepage analysis performed, considering geometrical parameters and material properties of Shiwashok earth dam, using the SEEP/W software (GeoStudio 2007). To mesh the models, rectangular elements with 4-nodes as well as 3-node triangular elements were considered. Results from different models, compared and discussed extensively to select the best model. The results included the seepage reduction, the quantity of seepage through the dam, the pore water pressure distribution, and the effects upstream blanket. Since cutoff trenches are not essential or are quite costly, an upstream blanket tied into the core of the dam and was used to reduce underseepage. In order to investigate the effects of the clay blanket on the seepage reduction, and pore water pressure, various clay blanket lengths with different thickness were used. The blanket lengths that used in this study were (55m, 80m, 105m, and 130 m).

The study demonstrates that for a constant blanket thickness, the percentage of seepage amount reduced due to the increase in the length of the clay blanket. Lengthening the clay blanket caused an increase in the length of the water flow path and thus induced a decrease in the hydraulic gradient and uplift pressure at the downstream side of the dam. This, in turn, caused a reduction in the velocity and therefore a decrease in the discharge at the dam foundation.

Figure 2 shows the reduction of seepage as a result of an increase in the length of the blanket for different blanket thickness and compared with the curve plotted by the USBR [10]. It is clear that obtained curve from the SEEP/W for the blanket thickness of 2.5 m has slightly difference with the USBR (2014) designed curve but a great difference can be noticed for a dam with the thickness of 0.5 m . It is important to note that the blanket lengths with less than four times the reservoir water depth ($BL/H < 4$) reduce seepage considerably; however, it is also noticeable that the longer blanket length does not have a significant effect on the percentage of seepage quantities and seepage reduction. Hence, the determined length for upstream the blanket can be suggested as four times the water level height.

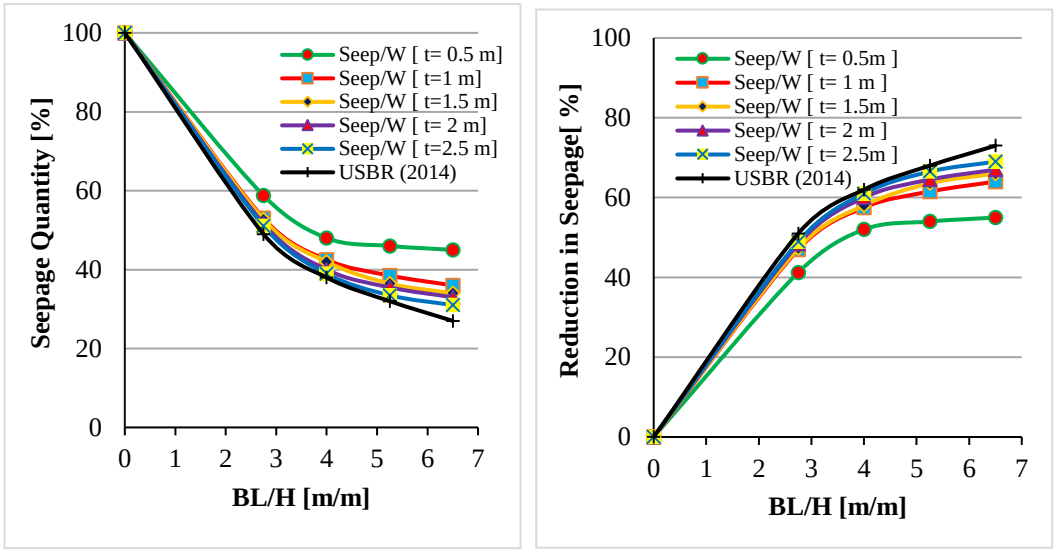

(a) (b)

FIGURE 2. Shows the relationship between the percentage of (a) seepage quantity and (b) seepage reduction with the ratio of blanket length to the water head (BL/H) for different blanket thicknesses compared to the curve plotted by [USBR [10]].

As far as the blanket thickness is concerned, five cases have been considered for the study. The outcomes indicated that increasing the blanket thickness could play a significant role to reduce the seepage discharge. Figure 3 explains the effect of the blanket thickness with different lengths in the reduction of seepage in the dam foundation. Subsequently, increasing in blanket thickness causes decrease the seepage discharge. It can be seen that the blanket thicknesses of more than 1.5 m do not have a considerable effect in seepage reduction. Therefore, it is important to note that the blanket thicknesses between 1m to 1.5m are a good choice for reducing seepage quantities.

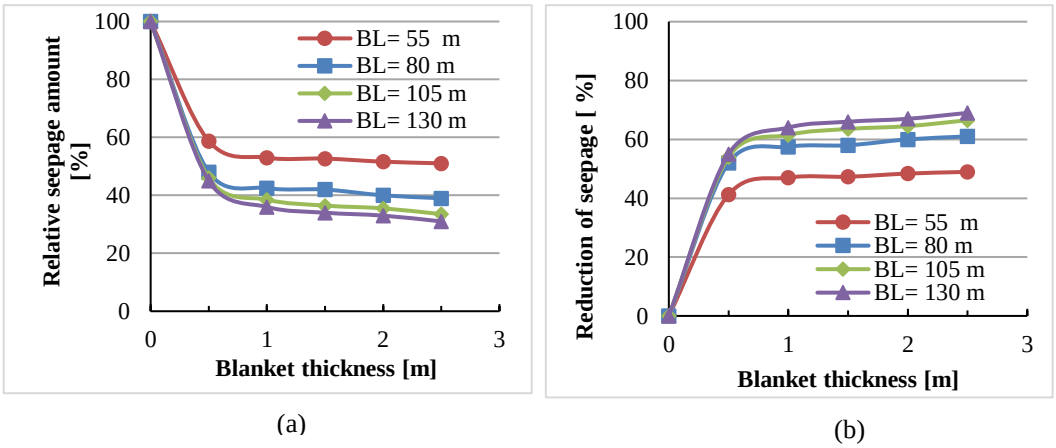

(a) (b)

FIGURE 3. Illustrates the relationship between the percentage of (a) seepage quantity and (b) seepage reduction with various blanket thickness (t=0.5m. 1m, 1.5m, 2m, 2.5m) for three different blanket length.

Figure 4 compares the effect of pore water pressure for the dam without and with upstream blankets with different lengths and thicknesses at the level directly under the embankment at the downstream side of the dam. It is obvious that the upstream blankets have the influence in decreasing the amount of pore water pressure. The amount of reducing of pore water pressure for the same thickness with different lengths are almost similar. This is because of existing of the filter at the downstream side of the dam. Whereas, when the lengths of the upstream blanket are increased the amount of pore water pressure slightly decrease.

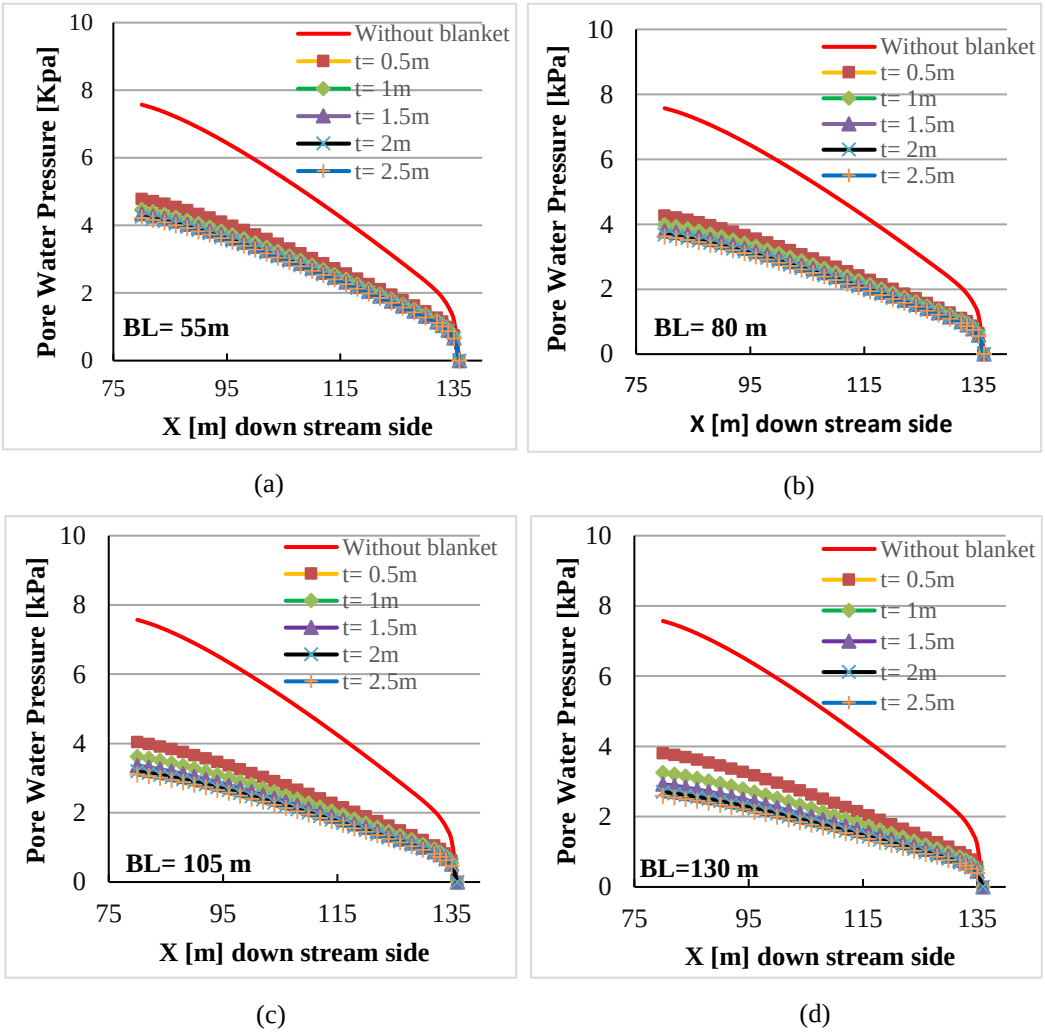

FIGURE 4. Shows the distribution of pore water pressure at the downstream side directly under the embankment due to the effects of the variation of blanket thickness and blanket length (a) BL= 55m, (b) BL= 80m, (c) BL= 105m, and (d) BL= 130 m.

Figure 5 compares the influence of pore water pressure for the dam without and with upstream blankets with different lengths and thicknesses at 4 m below under the embankment at the downstream side of the dam. It is important to note that the upstream blankets have considerable effect in decreasing the amount of pore water pressure. It is also noticeable that the differences are declined significantly from the centroid of the dam toward toe of the dam, particularly at the last 20 m. This is because there is a filter at the downstream side of the dam.

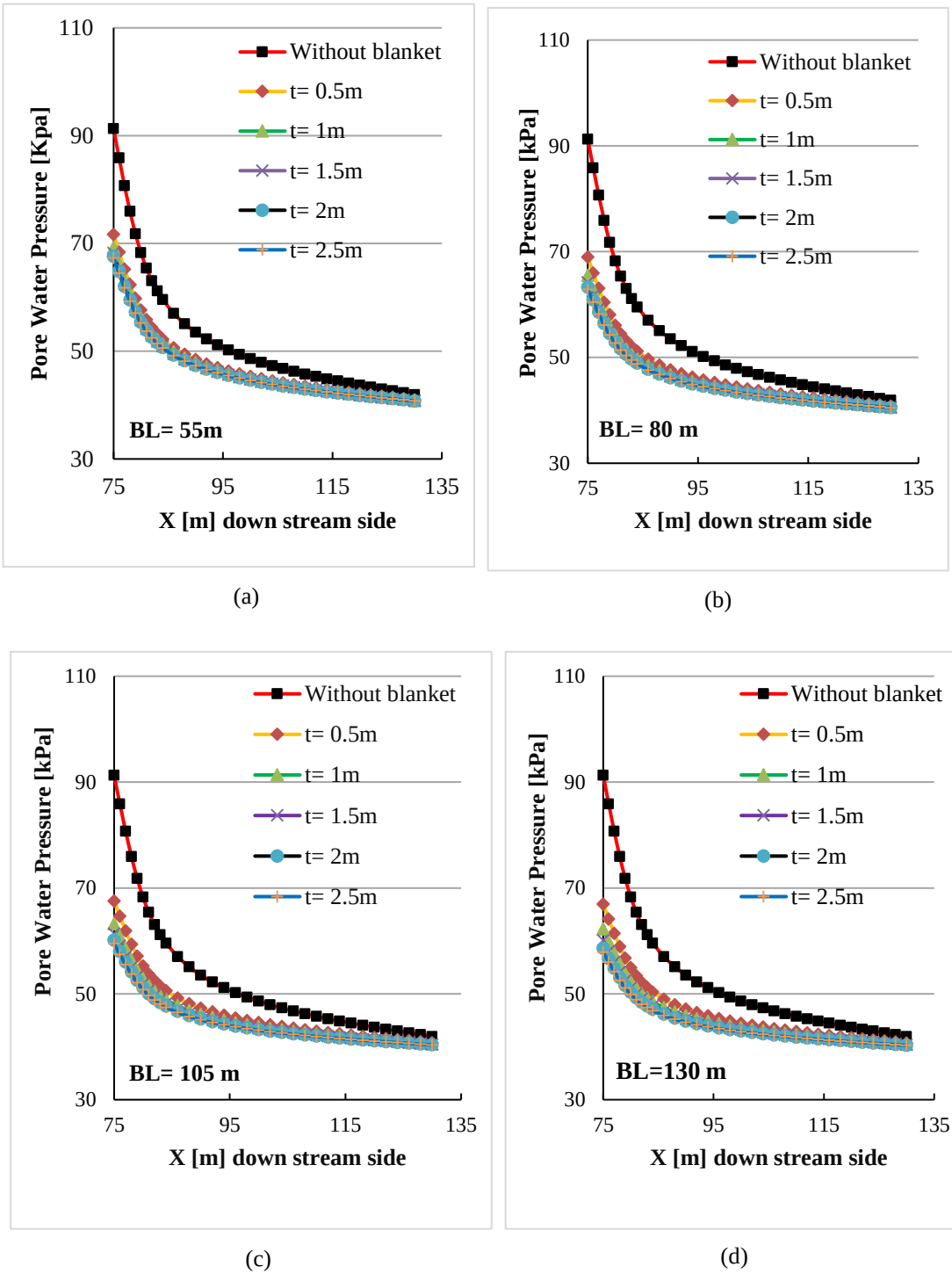

FIGURE 5. Shows the distribution of pore water pressure at the downstream side four meters under the embankment due to the effects of the variation of blanket thickness and blanket length (a) BL= 55m, (b) BL= 80m, (c) BL= 105m, and (d) BL= 130 m.

Comparing values of pore water pressure from Figure 4, with their corresponding values at the same distance in Figure 5 (i.e. at the same distance of X[m] downstream side), it is clear that the trend of reduction of the pore water pressure is substantially different. This is probably attributable to the existing of the filter at the level of 0 m (see Figure 1) and not at the level of -4 m which helps the pore water pressure to quickly reach to zero.

4. CONCLUSION

In this paper, to reduce the underseepage and pore water pressure, the effects of the upstream blanket with different lengths and thicknesses tied to the core were investigated. Based on the analyses performed of the results using SEEP/W software using the existing data, it can be concluded that the blanket length of 80 m and thickness of 1 m to 1.5 m can be recommended to be preferably utilized in a real construction. This means that the blanket length is four times greater than water head. The blanket thickness more than 1.5 m is not quite effective in the reduction of seepage and pore water pressure. The Shiwashok earth dam has not been constructed yet by the Kurdistan Regional Government (KRG) due to economic crisis. The final proposed design of the Shiwashok dam did not include a clay blanket (see Figure 1a), therefore this study recommends to add a clay blanket with the details presented in this paper, in order to increase safety and avoid possible failure to the dam.

REFERENCES

[1] D. P. Coduto, M.-C. R. Yeung, and W. A. Kitch, Geotechnical engineering : principles and practices. Upper Saddle River: Pearson, 2011.

[2] S. United, Army, and E. Corps of, Engineering and design. general design and construction considerations. [Washington, D.C.]: U.S. Army Corps of Engineers, 1994.

[3] P. Peter, "Canal and river levees. Developments of civil engineering. Vol. 29," ed: Elsevier/North-Holland, Inc., New York, 1982.

[4] James L. Sherard, Richard J. Woodward, and Stanley F. Gizienski, Earth and earth-rock dams : engineering problems of design and construction. Ann Arbor (Mich.): UMI, 1992.

[5] B. Tatone, C. Donnelly, D. Protulipac, and C. Clark, "Evaluation of the hydraulic efficiency of a newly constructed plastic concrete cut-off wall," in Proc., 2009 Canadian Dam Association Annual Conf, 2009.

[6] E. Williams, "Seepage Analysis and Control for Dams," Department of the Army US Army Corps of Engineers, Washington, 1986.

[7] M. A. E.-R. M. Rezk and A.-A. A. A. Senoon, "Analytical solution of earth dam with upstream blanket," Alexandria Engineering Journal, vol. 51, pp. 45-51, 2012/03/01/ 2012.

[8] H. Goharnejad, M. Noury, A. Noorzad, A. Shamsaie, and A. Goharnejad, "The effect of clay blanket thickness to prevent seepage in dam reservoir," Res. J. Environ. Sci. Research Journal of Environmental Sciences, vol. 4, pp. 558-565, 2010.

[9] GEO-SLOPE, Seepage Modeling with SEEP/W 2007. Calgary, Alberta, Canada: GEO-SLOPE International Ltd, 2008.

[10] USBR, Embankment Dams, Chapter 8: Seepage Washington, D.C.: U.S. Department of the Interior, Bureau of Reclamation, 2014.

SELF-COMPACTING CONCRETE REINFORCED WITH STEEL FIBERS FROM SCRAP TIRES: RHEOLOGICAL AND MECHANICAL PROPERTIES

Khaleel H. Younis[1], Fatima Sh. Ahmed[2] , Khalid B. Najim[3]

[1]Erbil Polytechnic University (EPU), Erbil, Kurdistan-Iraq
[2&3]University of Anbar - Anbar, Iraq.
[1]Ishik University, Erbil, Kurdistan-Iraq
[1]Knowledge University, Erbil, Kurdistan-Iraq
[1]khaleelyounis@epu.edu.krd, [2]fatimashafia2@gmail.com,[3]khalidnajim@uoanbar.edu.iq

doi:10.23918/iec2018.15

ABSTRACT

The aim of this study is to evaluate the rheological behavior and the mechanical performance of SCC with different contents and lengths of recycled steel fiber (RSF) recovered from scrap tires. The rheological properties investigated in this study include: slump flow, J-ring, L-box, and V-funnel tests. The mechanical properties include: compressive and flexural strength. The parameters of the study are fiber content and length. In total, thirteen self-compacting concrete (SCC) mixtures were prepared. Three fibers contents 30, 60 and 90 kg/m^3 were investigated and for each fiber contents W_f, four mixes were prepared with four different fiber lengths (L_f) (10, 15, 25, 35 mm). A control mix (plain SCC) was also prepared for comparison reasons. The results showed that the addition of RSF decreased the slump flow, slowed down the flow rate and increased the V-funnel time but maintained the requirement of SCC up to 60 kg/m^3 fiber content. Shorter fibers had less effect on the rheological behavior of SCC than long fibers. Both RSF content and length affected the compressive strength and the flexural strength of SCC. Long RSF reduced compressive strength but increased the flexural strength.

Keywords: Recycled steel fiber; SCC, Rheological properties; compressive strength; flexural strength.

1. INTRODUCTION

Both developed and developing countries are suffering from the enormous number of tires accumulated every year. Billions of tires are discarded every year worldwide [1]. The disposal of such huge number of waste tires has a large impact on the environment. Also, waste tires can cause serious issues to the human health and increase fire hazards in the case of burning or illegal dumping [2, 3]. The utilization of such huge waste of tires in the production of self-compacting concrete (SCC) is a decent and sustainable solution to mitigate serious environmental issues [2]. Self-compacting concrete (SCC) is a type of concrete, which has unique properties that enable it to be placed and compacted during casting without any external aid saving time needed for construction [4]. The use of recycled steel fiber (RSF) recovered from scrap tires as reinforcement in SCC can be a valuable solution for the aforementioned issues associated with the disposal of waste tires. This will also enhance the sustainability of SCC and make this type of concrete eco-friendly. The characteristics of SCC in the fresh state are vital since SCC should have the ability to consolidate, pass the reinforcing rebars and fill all form's parts and corners with no segregation [4]. The addition of manufactured steel fibers to SCC mixtures affects its properties in fresh and hardened states [5,6]. Previous studies [5-7], have reported that the use of manufactured steel fibers in SCC may have an adverse effect on the rheological properties of SCC. Manufactured steel fibers can reduce the flowability, increase the viscosity (decrease the passing ability), increase the risk of segregation and decrease the density of the fresh SCC. However, studies on the effect of use of RSF in SCC mixtures on the fresh properties are rare. The use of discontinuous manufactured steel fibers in different length and content by randomly distributing them in a concrete member may be useful to improve the tensile, flexural, shear, impact strength and reducing shrinkage. Due to the ability of these steel fibers to arrest and slow down the crack growth, these fibers can limit the cracks at early stage of loading history (microcracks) [5,6]. The effect using RSF on the mechanical properties of normal concrete has been reported by several studies [2, 8-11]. It has been reported that RSF can show performance similar to that of manufactures steel fibers [2,9,10].

Therefore, it can be used as alternative to the expensive manufactured steel fibres. Nonetheless, studies that tackle the influence of RSF on the mechanical performance of SCC are rare. Hence, this article is part of a research aims at assessing the properties of SCC with different content and length of RSF in both fresh and hardened conditions. This article describes the experimental program, presents the experimental results and analyses the effect of different content and length of RSF on the rheological and mechanical properties of SCC.

2. EXPERIMENTAL WORK

2.1 MATERIALS

Portland Cement (type I) produced by AL-MAS cement factory (42.5 R – B.S) 12/96 in Kurdistan-Iraq was used in this study. The specific gravity and specific surface area of cement were 3.12 and 314 m^2/kg, respectively. The adopted cement conforms to the Iraqi specification No.5/1984 [12] The silica fume used in this study was in the form of a gray powder having a specific gravity of 2.2. Its commercial name is Sika Fume-HR. It was used in all mixes as a partial replacement of cement with 10% by weight.

Natural rounded river aggregate was used as coarse aggregate with a maximum size of 14 mm. and specific gravity of 2.65.Natural river sand was used as fine aggregate with a maximum size of 4.75 mm. The specific gravity and fineness modulus are 2.67 and 2.8, respectively. High water reduction admixture (HWRA) as super plasticizer (SP) was used to provide high workability that essentially required for SCC. Sika viscocrete super E4-S was used in this study in this study, the RSF was collected from a factory of recycling scrap tires located near Erbil city. The factory is recovering rubber from the scrap tires while the steel wires were discarded as waste as shown in Figure 1. In this study, those wires were collected and prepared to be reused as concrete reinforcement. These steel wires were cleaned from remaining rubber and burned carbon existing on the surface of these wires to provide a good adhesion with concrete, as seen in Figure 2. After cleaning, the steel wires were cut into four different lengths (10, 15, 25 and 35 mm) using plate cutting machine. The scrap steel wires were separated manually into

fibers to form recycled steel fibres (RSF) before adding them to the concrete mixture (see Figure 2). The RSF had a diameter of 0.25 mm and a tensile strength of around 1000 MPa.

(a) (b)

FIGURE 1. A- Recycled steel wires a-before cleaning , b- after cleaning.

FIGURE 2**.** Sample of the **r**ecycled steel fibers used in current study (for fibers with length =35mm)

2.2 MIX PROPORTIONS AND PREPARTION OF SPECIMNES

There is no standard SCC mix design method; therefore, trial and error approach should be followed until the appropriate proportions of materials that verify SCC requirements are reached. In this study, thirteen SCC mixtures were prepared with the same total binder content and water to cement ratio as presented in Table 1 which shows the code and mix proportions of all mixes. As can be seen, the parameters of the study are fiber content and length: three fibers contents 30, 60 and 90 kg/m^3 were investigated and for each fiber contents, four mixes were prepared with four different

fiber lengths (L_f) (10, 15, 25, 35 mm). A control mix (plain SCC) was also prepared for comparison reasons. In the study, all mixes have been prepared by following European guidelines of SCC EFNARC [4]. A 0.04 m^3 mechanical rotary mixer was employed in the production of concrete mixtures. Three (100 mm) cubes and three prisms 100×100×500 mm, were cast for each mix. After casting, the specimens were then covered by plastic sheets and allowed to cure for 24 hours before being demoulded. Then, the specimens were kept in water tanks for 27 days for further curing.

TABLE 1.

Code of mixes and mix proportions in kg/m^3.

mix name	W_f kg/m^3	L_f mm	Cement kg/m^3	SF kg/m^3	Water litre/ m^3	Sand kg/m^3	Gravel kg/m^3	SP litre/ m^3
M0	--	--	405	45	170	850	810	11.25
M1	30	10	405	45	170	850	810	11.25
M2		15	405	45	170	850	810	11.25
M3		25	405	45	170	850	810	11.25
M4		35	405	45	170	850	810	11.25
M5	60	10	405	45	170	850	810	11.25
M6		15	405	45	170	850	810	11.25
M7		25	405	45	170	850	810	11.25
M8		35	405	45	170	850	810	11.25
M9	90	10	405	45	170	850	810	11.25
M10		15	405	45	170	850	810	11.25
M11		25	405	45	170	850	810	11.25
M12		35	405	45	170	850	810	11.25

2.3 TEST METHODS

Rheological properties

Slump flow, T_{50} flow time, J-ring, L-box, BJ, TJ, and V-funnel were conducted to assess the fresh properties of the SCC mixes. These tests were undertaken following the specifications and guidelines of European Federation of National Associations Representing producers and applicators of specialist building products for Concrete (EFNARC) for SCC [4]. The sequence of performing the fresh concrete tests was the same with all mixes. The fresh properties were conducted immediately after the completion of concrete mixing.

Mechanical properties

The compressive strength was obtained at age of 28 days using the (100 mm cubes) and BS EN 12390-3 [13]. The flexural strength was obtained at 28 days using (100×100 ×500) mm prisms. All prisms were tested in two-point loading over a span of 300 mm following the recommendations of the BS EN 12390-5 [14].

3. RESULTS AND DISCUSSIONS

3.1 RHEOLOGICAL PROPERTIES

To evaluate the effect of the use of RSF on the performance of SCC mixtures, the rheological behavior of all mixes was quantified by assessing: 1- flow, viscosity and filling ability of concrete by slump flow and V-funnel tests; 2- the passing ability of concrete by j-ring and L-box tests (see Figure 3). The results of all fresh concrete properties and the limits of EFNARC are presented in Table 2. In general, it can be seen that the rheological properties of SCC showed a gradual degradation with the addition of RSF. It was shown that both RSF content (W_f) and length (L_f) affected the rheological of SCC.

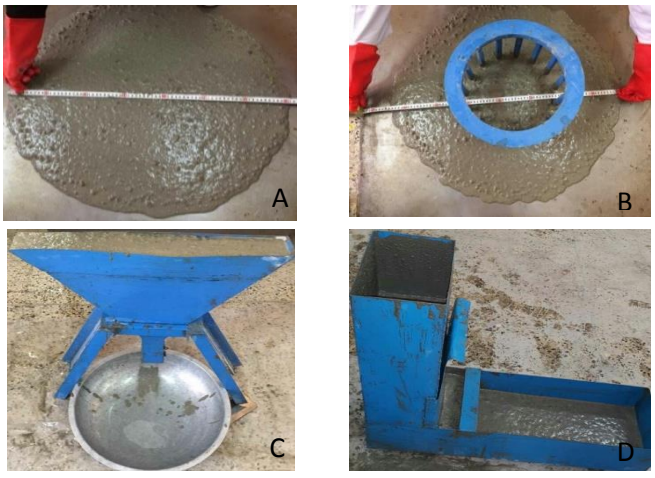

FIGURE 3. Rheological properties tests: a- slump flow, b- j-ring , c-V-funnel, d- L-box,

TABLE 2.

Result of rheological properties of all mixes.

Mix code.	W_f, kg/m^3	L_f, mm	Slump Flow		J-Ring		V-Funnel, sec	L-box %
			Flow, mm	T_{500}, sec	Flow, mm	B_J		
M0	-	-	788	2.25	760	0.65	8	0.95
M1	30	10	755	2.3	740	0.975	8.3	0.9
M2		15	745	2.47	720	1.35	8.35	0.85
M3		25	725	2.7	700	1.45	8.46	0.833
M4		35	720	3	695	2.125	8.68	0.82
M5	60	10	720	2.35	715	1.22	9.4	0.87
M6		15	700	2.38	710	1.5	10.5	0.82
M7		25	665	3.38	655	1.625	11.45	0.78
M8		35	645	4.6	615	2.15	11.6	0.76
M9	90	10	670	2.8	650	1.7	12	0.82
M10		15	660	3.4	630	1.95	13.5	0.814
M11		25	575	5	540	4.75	15.6	0.77
M12		35	560	6.3	495	8.25	17	0.75
Limits of EFNARC			650-800, mm	2-6, sec	650-800,mm	0-20	8-12, sec	0.8-1%

-Slump flow and J-ring tests

For the slump flow test results, as can be seen in Table 2 and Figure 4, the flow characteristics decreased proportionally with increasing RSF content. The reduction in flow properties was clearly observed when long fibers is used rather than short ones.

The control mix M0 which is plain SCC (without RSF) showed a 788 mm slump flow and 2.25sec. flow time (T_{500}). For mixes having 30 kg/m^3 fibers content, a marginal effect on slump flow and fluidity was observed compared to the control mix M0. Where, the slump flow of M1, M2, M3 and M4 reduced by only 4.2 %, 5.5 %, 8.0% and 8.6%, for fiber lengths of 10, 15, 25 and 35 mm, respectively. The reduction in slump flow clearly increased when fiber content increased to 60 kg/m^3. Table 2 shows that the reduction in slump flow of M5, M6, M7 and M8 compared to M0 was 8.6%, 11.1%, 15.6 %, and 18.1%, respectively. Additionally, at higher fibers content 90 kg/m^3, the reduction in slump flow significantly increased, particularly with long fibers. In

comparison to M0, the slump flow of mixes M9, M10, M11 and M12 declined by 15.0%, 16.2%, 27% and 28.9%, respectively.

All mixes of the fiber contents of 30 and 60 kg/m^3 fulfill the EFNARC requirements [4] of slump flow as can be seen in Figure 4. This means that these mixes still maintain the characteristics of SCC. However, for mixes with 90 kg/m^3 content, the slump flow of the mixes with long fibers (25mm and 35mm) does not meet the requirements of EFNARC,

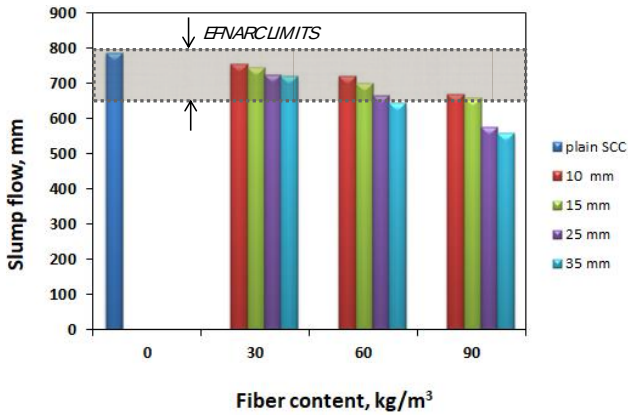

FIGURE 4. Effect of RSF content on slump flow.

This reduction in slump flow due to the addition of RSF could be attributed to the resistance to flow that develops because of the presence of RSF ; hence increasing the internal friction between aggregate particles and fibers [5,6]. The increasing in the internal friction proportionally increased with fiber content (Wf). The high stiffness (modulus of elastic) of steel fibers could be one of the sources for a likely increase in inter-particle friction under the free flow [5,15] with a possible absorbing of the moving energy [11]. In terms of RSF length, regardless of the fiber content, the tangle of long fibers caused reduction in slump flow more than short fibers.

As far as the results of flow time, j-ring (flow and Bj) are concerned, similar behavior to that of the slump flow was observed for the mixes containing RSF. The increase in the fiber content and length adversely affected the results of flow time and j-ring tests. The reduction in flow time and j-ring flow is an indication of the high viscosity of the mixes with RSF. Despite the negative effect of the RSF on the results of flow time and j-ring

tests, all mixes with RSF (apart from M11 and M12) conform with the limits of EFNARC [4]as can be seen in Table 2.

V-funnel and L-box tests

The results of V-funnel test, as can be seen in Table 2, show that the mixes incorporating of RSF exhibited an increase in V-funnel time compared to the plain SCC. The V-funnel time gradually increased with RSF content and length. The addition of RSF with 30 kg/m3 showed little effect on passing ability of concrete through the V-funnel. At this RSF content, time recorded in V-funnel test in comparison to M0 decreased by 3.75%, 4.4%, 5.75% and 8.5% for M1, M2, M3 and M4, respectively. The time needed by RSF mixes to pass through the V-funnel increased with RSF content at 60 kg/m^3 by 17.5%, 31.25%, 43.12% and 45% for M5, M6, M7 and M8 compared to the control mix M0; Figure 5. As the fibers content increased to 90 kg/m^3, V-funnel test results exceeded the upper limit of EFNARC guidelines [4]. Much higher increase 50%, 68.7%, 95% and 112.5% in the V-funnel time was recorded for mixes M9, M10, M11 and M12, respectively, compared to the control mix. This could be due to the same reasons mentioned previously related to the increased internal friction between aggregate particles and RSF leading to high viscosity and increased flow time through V-funnel [15]. Additionally, the long fibers prevent the aggregate particle from the free movement causing delay in flow [15]

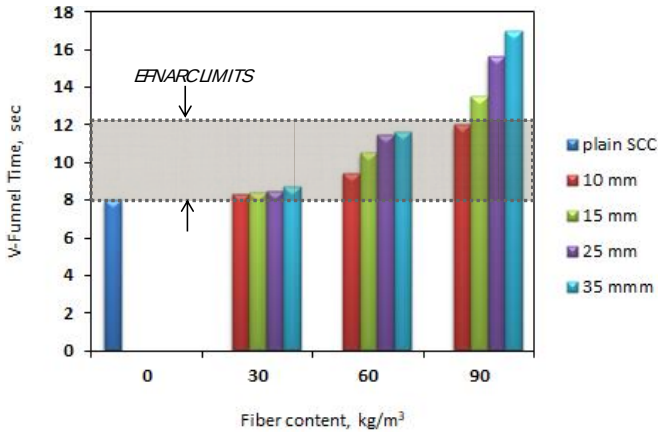

FIGURE 5. Effect of RSF content on V-funnel time (sec).

L-box test was performed to assess passing ability of all SCC mixes, and the results of which are shown in Table 2. The results showed that the incorporation of RSF negatively affected the passing ability of mixes with RSF. It is clear that this reduction in blocking ratio depends on both the fiber content W_f and fiber length L_f. The higher the RSF content the higher the reduction in the passing ability of the mixes. Also, the passing ability decreased when the length of the fibers increased. However, all mixes with RSF (apart from M11 and M12) meet the requirements of EFNARC [4]as can be seen in Figure 6. The reduction in passing ability can be attributed to the presence of fibers which work as obstacles and de-accelerate the movement. The influence of adding RSF is significantly appearing with high contents (90 kg/m^3) and with long fibers. Long fibers could lead to a reduction in the internal energy needed for the mix to move freely.

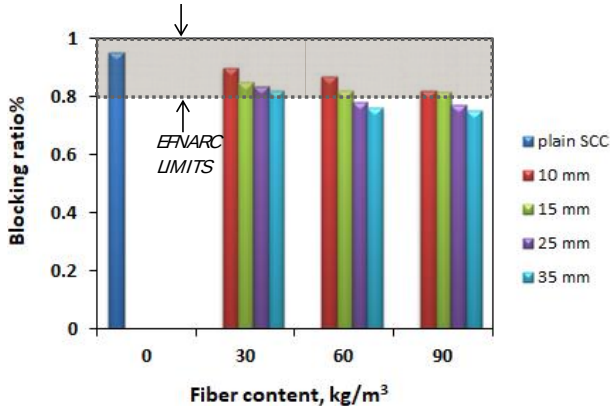

FIGURE 6. Effect of RSF content on blocking ratio (L-box test)

From the results of the rheological properties, it seems that the RSF can be used up to 60 kg/m^3 content with no effect on the properties of being SCC as all requirements of EFNARC can be satisfied. Higher contents such as 90 kg/m^3 can be used but the length of the RSF should not exceed 15 mm.

3.4 MECHANICAL PROPERTIES

The results of the mechanical properties including compressive strength and flexural strength for all mixes are presented in Table 3. The results are the average of three specimens.

TABLE 3.

Result of compressive and flexural strength of all mixes

Mix code	W_f, kg/m^3	L_f, mm	Compressive strength, MPa	Flexural strength, MPa
M0	0	-	55	6.2
M1	30	10	62	6.88
M2		15	61	7.24
M3		25	59	7.86
M4		35	56	7.9
M5	60	10	58	7.88
M6		15	56	8.05
M7		25	52	8.15
M8		35	50	8.33
M9	90	10	54	7.3
M10		15	53	7.34
M11		25	50	7.98
M12		35	48	8.1

-Compressive strength

The inclusion of RSF doesn't show significant effect on compressive strength of SCC mixtures. From test results presented in Table 3, mixes show either a slight increase or decrease in compressive strength comparing to the control mix (plain SCC).

The results show that the two parameters (fiber content and length) examined in this study affected the compressive strength of SCC mixes containing RSF. The effect of these parameters is shown in Figure 7. It can be seen that for low fiber content (30 kg/m^3) the compressive strength increases (for all RSF lengths) up to 12.7% compared to the control mix; whereas for high fiber content (90 kg/m^3), the strength decreases (for all RSF lengths) by up to 12.7% compared to the control mix. However, for moderate fiber content (60 kg/m^3) the compressive strength slightly increased for short fibers (10 and 15mm) and slightly declined for long fibers (25 and 35mm).Same results were concluded by researchers [7,15] but for manufactured steel fibers. For all fiber contents,

the compresive strength increased with the decrease of the length of the fibers which means shorter fibers exhibited better performance in terms of comreessive strength.

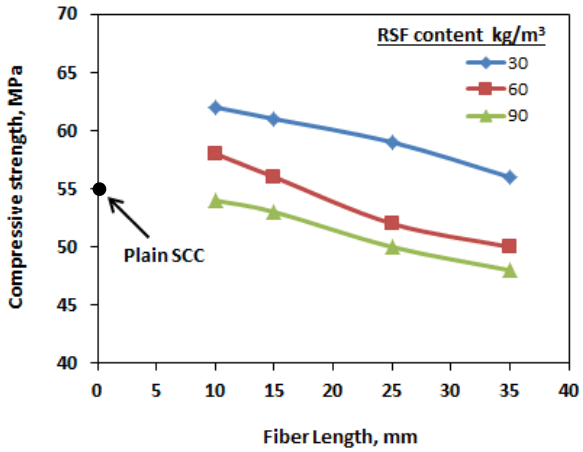

FIGURE 7. Effect of RSF length and content on the compressive strength of SCC.

The increase in compressive strength for low content and short fibers could be due to the ability of short fibers in delaying the propagation of microcracks and slowing down the development of microcracks to macrocrcks and; thus delaying the failure of concrete [2,8]. Also, the incorporation of RSF could transfer the compression failure from collapse/ brittle to ductile failure [8] which also lead to higher strength before failure. This result were in a compatibility with previous results [15],

The reduction in compressive strength for high contents and long fiber might be due to a reduction in rheological of RSFSCC mixes as mentioned in the presvius section. Furthermore, adding RSF could increase the pososity of concrete due to the increase in the entrapped air voids which considered as concrete defect [2]. During mixing and casting, fibres may entrap large air voids especially with high content of fibres [2]. Moreover, the reduction in strength can be attributed to the existence of long fibers ineffective in arresting microcracks [11]. Additionally, the existence of long RSF could increase the entrapp air voids due to balling and tangle of fibers. This would result in accelerating the propagation of cracks and failure.

-Flexural strength

Table 3 also shows the results of the flexural of all SCC mixes. The performance of SCC mixes with RSF under compression loading is not the same as under bending loading. Regardless of the fiber content, all SCC mixes with RSF show higher flexural strength than that of the plain SCC. Additionally, for the same fiber content, the higher the fiber length the higher the flexural strength as can be seen in Figure 8. For example, the flexural strength increased by 11.0%, 16.8%, 26.8% and 27.4% for mixes M1, M2, M3 and M4 compared to M0, respectively. It was expected that mixes with 90 kg/m^3 RSF content would show the best flexural performance; however, these mixes exhibited less flexural strength enhancement compared with the 30 kg/m^3 fiber content. This could be due to the same effect related to the development of air voids at high contents of RSF which is mentioned earlier. The best flexural performance is shown by mixes with 60 kg/m^3 fiber content. At this fiber content, enhancements in the flexural strength of up to 34% were observed.

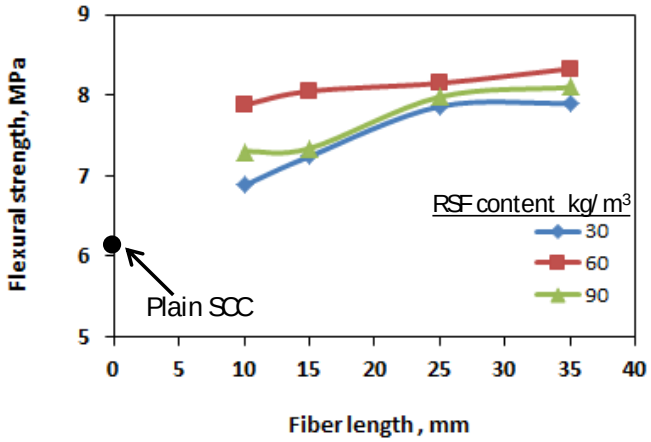

FIGURE 8. Effect of RSF length and content on the flexural strength of SCC.

The enhancement in flexural strength due to RSF incorporation can be mainly attributed to the role of fibers in bridging the microcracks and arresting the sides of the macrocracks in concrete body and hence delaying the occurrence of concrete failure [2, 15,11]. Also, this behavior could be partly due to the pull-out resistance of fibers [11]which increases with the increase of fiber length. This can result in a significant increase in fracture resistance and thus increasing the ductility of SCC mixes [11].

4. CONCLUSIONS

The discussion of the results can lead to the following conclusions:

- The use of RSF reduced the slump flow and J-ring flow and decelerated the flow rate (T_{500}) of SCC mainly due to the increase in inter-particle friction under the free flow. However, all mixes with RSF (apart from mixes with high content 90 kg/m^3 and long fibers 25 and 35 mm) maintain the EFNARC requirement of slump flow and flow rate.
- Mixes with RSF exhibited higher viscosity and lower passing ability than that of plain SCC as the V-funnel time increased and the blocking ratio decreased with the increase of RSF content and length. Nonetheless, all mixes with RSF (apart from mixes with high content and long fibers) comply with EFNARC requirements.
- For low fiber content (30 kg/m^3) the compressive strength increased (for all RSF lengths) up to 12.7% compared to the control mix; whereas for high fiber content (90 kg/m^3), the strength decreased (for all RSF lengths) by up to 12.7% compared to the control mix. However, for moderate fiber content (60 kg/m^3) the compressive strength slightly increased for short fibers (10 and 15mm) and slightly declined for long fibers (25 and 35mm).
- All SCC mixes with RSF showed higher flexural strength than that of the plain SCC by up to 34%. For the same fiber content, the higher the fiber length the higher the flexural strength.
- The utilization of RSF in SCC can lead to an innovative, sustainable and cost-effective self-compacting fibre reinforced concrete.

REFERENCES

[1] Thomas, B.S. and R.C. Gupta, Properties of high strength concrete containing scrap tire rubber. Journal of Cleaner Production, 2016. 113: p. 86-92.

[2] Younis, K. H., (2016) "Mechanical perfromance of concrete reinforced with recycled steel fibres extracted from post-consumer tyres)" Proceedings of the 2nd International Engineering Conference on Developments in Civil Engineering and Computer Applications (2nd IEC2016) 20 – 22 February, Erbil-Kurdistan-Iraq.

[3] Thomas, B.S., and R. C. Gupta. "A comprehensive review on the applications of waste tire rubber in cement concrete." Renewable and Sustainable Energy Reviews 54 (2016): 1323-1333.

[4] EFNARC (2005) "The European Guidelines for self-compacting concrete: specification, production, and use" http://www.efnarc.org/(Accessed on August 2016)

[5] A. S. El-Dieb and M.M.R. Taha, *flow characteristics and acceptance criteria of fiber-reinforced self-compacting concrete (FR-SCC).* Construction and Building Materials, 2012. **27**: p. 11.

[6] Gencel, O., et al., Workability and mechanical performance of steel fiber-reinforced self-compacting concrete with fly ash. Composite interfaces, 2011. 18(2): p. 169-184.

[7] Madandoust, R., et al., Assessment of factors influencing mechanical properties of steel fiber reinforced self-compacting concrete. Materials & Design, 2015. 83: p. 284-294.

[8] Younis, K. H. and K. Pilakoutas, Strength prediction model and methods for improving recycled aggregate concrete. *Construction and Building Materials*, Vol. 49, No. 0, pp. 688-701, 2013.

[9] Tlemat, H., Steel fibres from waste tyres to concrete: testing, modelling and design. PhD.thesis, The University of Sheffield, UK, 2004.

[10] Pilakoutas, K., K., Neocleous, Tlemat, H., Reuse of steel fibres as concrete reinforcement. *Engineering Sustainability*, Vol. 157, No. ES3, pp. 131-138, (2004)

[11] Centonze, G., M. Leone, and M. Aiello, Steel fibers from waste tires as reinforcement in concrete: A mechanical characterization. Construction and Building Materials, 2012. 36: p. 46-57.

[12] IQS No. 45/1984 ''Iraqi specification for aggregate'' (1984).

[13] BS EN 12390-3, *Testing hardened concrete Part 3: Compressive strength of test specimens.* British Standard Institution, London, UK, 2009.

[14] BS EN 12390-5:2009, *Testing hardened concrete Part 5: Flexural strength of test specimens.*British Standard Institution, London, UK, 2009.

[15] Khayat, K. and Y. Roussel, Testing and performance of fiber-reinforced, self-consolidating concrete. Materials and Structures, 2000. 33(6): p. 391-397.

MECHANICAL PROPERTIES OF CONCRETE USING IRON WASTE AS A PARTIAL REPLACEMENT OF SAND

Krikar M-Gharrib Noori[1] , Hawkar Hashim Ibrahim[2]

[1] *Koya Technical Institute, EPU*
[2]*Salahaddin University-Erbil*
[1] *Krikar.bedary@epu.edu.krd,* [2] *hawkar.ibrahim@su.edu.krd*

doi:10.23918/iec2018.16

ABSTRACT

The utilising of iron waste in concrete as a partial replacement of sand is attaining enormous significance nowadays, mostly because of the improvement in the strength of concrete and environmental benefits. The aim of this study is to assess the possibility of applying iron waste in different percentages (6%, 12%, 18%, 24%, and 30%) as fine aggregate replacement of sand to increase the strength of concrete. For this purpose, the mix proportion was designed as (1:2.12:2.37) for giving 33 MPa of compressive strength of concrete at 28 days of curing. In order to achieve the goal of the study, laboratory experiments, compressive strength, and flexural tensile strength were conducted to determine the influence of iron waste on the strength of concrete. Thus, based on this study, the progress of strength with the percentages of iron waste in different time was plotted. According to the results, it can be found that 12% of iron waste is more efficient than the other percentages in both compressive and flexural strength because it obtains the maximum strength in the shortest time, and it seems that increasing iron waste more than 12% leading to decrease the strength of the concrete.

Keywords: Concrete, Sand Replacement, Iron Waste, Compressive Strength, Flexural Tensile Strength.

1. INTRODUCTION

Nowadays, one of the most commonly expended construction material in the world is concrete. It consists of cement, sand, gravel, and water. Additional materials could be supplied to the mixture. The concrete comprises amount of entrapped air and may have knowingly entrained air attained using an admixture or air-entraining cement [1]. Sand as fine aggregate is more extensively consumed in concrete construction. Hence, numerous developing countries have nowadays faced a struggle in providing the quantity of natural sand so that encounter the enhancing desires of infrastructural development in recent years [2]. In this regard, sand could be replaced by different waste materials, which might be able to improve plasticity, workability, and increase concrete strength to enhance durability [3]. In terms of waste materials environment impact, advancements in technology enhance not only human comforts but also damages the environment [4]. Although industrialization is one of the key factors for growing economy, also it has led to serious troubles that leading to environmental pollution. Waste materials, discharged in large quantities by industries, create serious environmental problems. To lowest possible environmental impact, the reusing of these waste materials will become an essential standard to protect the environment [5]. Regarding this, reusing unwanted remaining materials will be a popular substitute for disposaling the waste, in this waste utilization, possible pollution problems and cost are reduced or even the pollution is removed along with the achievement of environment protection. However, to use available materials most efficiently, the consideration of utilization strategy should be combined with the considerations of energy and environment [6]. Iron waste is one of the materials discharged in great amounts by-product of the steel industry in Kurdistan Region of Iraq. Disposing this waste impact negatively on the environment. Iron waste, due to its high strength and durability, might be able to increase a concrete strength in terms of compressive strength and flexural tensile [3]. The presented work studies the effective of iron waste on compressive strength and flexural tensile strength of concrete based on laboratory tests. According to the past literature, during the history of the industries of iron and steel, different methods have been attempted to create operational use of the waste materials of iron and steel. Various studies have been done to use the waste material in the concrete mixture for improving concrete properties and preventing the environment from

these unwanted materials. In this study, some of them will be reviewed. Dubey, et al. [7] considered using the blast furnace slag powder to determine its effect on compressive strength of concrete. In this study, blast furnace slag was partially used as a replacement of cement in different percentage 5 to 30%. It has been discovered, from the experimental investigations, that the optimum substitution of Ground Granulated Blast Furnace Slag Powder to cement is 15% without changing much the compressive strength. Ugama, et al. [8] examined determining the appropriateness of using iron ore tailing (IOT) to partly replace fine aggregate for concrete which it is utilized for rigid pavement. The control mix composites a normal mixture of concrete which only sand functioned as fine aggregate, while the replaced sand in the other mixes was by 20%, 40%, 60%, 80% and 100% iron ore tailing (IOT). Strength and consistency tests were studied on all samples of concrete. It was noticed that increasing the ratio of iron ore tailing in the mixture, leads to decrease in the concrete workability. The results for tests of compressive and indirect tensile strength at twenty eight days were 43.67 N/mm^2 and 2.69 N/mm^2, respectively. They were attained for concrete when 20% iron ore tailing (IOT) was used, then the results equated to compressive strength and indirect tensile strength outcomes of 45.02 N/mm^2 and 2.64 N/mm^2 respectively, gained at 28 days as only sand as a fine aggregate was used. Alzaed [9] studied the effect of iron filings on concrete strenth as one of the portions of the concrete mixture. In the paper, the iron filing was supplied to the concrete mix in four different percentage, to detrmine the difference, which might be gained in compression and tensile concrete strengths at twenty eight days. In the study, numerous standard cubes and cylinders were fabricated and tested using 0% (control), 10%, 20% and 30% of iron filing in the concrete mix. It was determined that when iron filing supplemented to the concrete mix, the compressive strength of concrete increased steadily while the tensile strength showed a minor effect as the ratio of iron filing applied more than 10%. As a result, two formulas were suggested, which might be utilized to expect the quantity of increasing corresponding to each percentage of iron filing contributed to the concrete mix. Ghannam, et al. [3] carried out an experimental investigation to explore the possibility of using the iron powder (IP) and granite powder (GP) to partially replace to fine aggregate in concrete mixture. The percentages 5%, 10%, 15%, and 20% of GP and IP were added to replace sand by weight. It was found that the most

effective replacement percentage of sand with granite powder in concrete was 10% by weight in increasing the compressive and flexural strength compared to other ratios. The test results showed that the compressive strength increased nearly 30%, as sand partly replaced to 10% of GP in concrete, compared with normal concrete. Similar results were also found for the flexure. It was moreover remarked that substituting of sand with up to 20% of iron powder by weight in concrete resulted in increasing in compressive and flexural strength of the concrete.

2. STUDY IMPLICATION

Iron waste is an industrial by-product that is produced as a result of producing steel from the steel factory. This waste material can be applied as partial replacement of sand in concrete. The aim of this study is to evaluate the suitability of using iron waste as a partial replacement of fine aggregate and to observe that iron waste leads to increase the compressive strength, and flexural strength of concrete, as used in certain proportions. The experimental research considered in this study displayed the mechanical properties of concrete have enhanced as sand was replaced partially by iron waste in certain proportions. Furthermore, recycling of this by-product and employing it in concrete will decrease its effect on the environment and its health hazards. The usage of iron waste instead of sand will reduce using of sand in the construction industry hence maintaining more of this natural resource.

3. EXPERIMENTAL INVESTIGATION

The experimental program included preparing concrete cubes and beams with and without iron waste replacement. The concrete mixture consists of Portland cement, sand, coarse aggregates, iron waste, and water. The cubes were prepared to evaluate the concrete compressive strength and the beams were equipped to assess the flexural strength.

4. MATERIALS AND METHODOLOGY

4.1 MATERIALS

Materials that used for this study comprised of cement, fine aggregates (sand), coarse aggregates (gravel), iron waste, and water. According to ASTM codes, necessary tests were carried out for the materials.

4.1.1 CEMENT

Cement is a binder substance that can bind other materials together. Physical properties of Ordinary Portland cement was found and compared with the code specification (ASTM C 150) which is shown in Table 1. The results are compatible with the code specification.

TABLE 1.

Properties of cement with the code specification

No	Parameters	Values	Code Specification ASTM C150
1	Fineness	0.04	0.01 – 0.06
2	Specific gravity	3.1	around 3.15
3	Consistency	28 %	26% – 30 %
4	Initial Setting time (minutes)	70	≥ 45
5	Final Setting time (minutes)	290	≤ 375

4.1.2 FINE AGGREGATE (SAND)

Sand is a naturally occurring granular material composed of finely material particles. The fine aggregate passed through sieve #4 (4.75 mm) and predominately retained on sieve # 200 (75 μm) was used. The sand has a specific gravity of 2.67, bulk density 1647 kg/m^3 and the fineness modulus equal to 2.6.

4.1.3 COARSE AGGREGATE (GRAVEL)

Coarse aggregate is one of the main components of concrete composite materials. The maximum size of coarse aggregate was 12.5 mm used. The gravel has a specific gravity of 2.74, bulk density 1600 kg/m^3 and the fineness modulus equal to 6.2.

4.1.4 IRON WASTE

Iron waste is a by-product material. When the waste material is disposed of, it will affect the environment. Over the past few years, the amount of this material have been increased by steel factories in the Kurdistan region of Iraq. In order to reduce the impact of waste materials on the environment, iron waste could be used instead of sand concrete mixture. The iron waste has a specific gravity, bulk density and the fineness modulus with 3.56, 2168 kg/m3, and 2.3, respectively. It should be noted that there is a difference between the density of the sand and the iron waste that will be expected to affects the density of the concrete. Furthermore, the waste material was accumulated in a steel factory in Bazyan related (Sulaymani Province).The quantities of this waste material will be increase and it will effect on our environment. Therefore, it is crucial to use this material to improve concrete properties.

4.1.5 WATER

A clean water is used for mixing process and curing. The used water should be applied according to the mix proportion design.

4.2 METHODOLOGY

4.2.1 WORK PLAN

As it is described previously that using iron waste in concrete as replacement of sand might increases its strength. To find out that experimental method was used, both flexural tensile strength and compressive strength of concrete were considered to be tested. Regarding this, the research is planned as firstly ordinary concrete with only cement, sand, aggregate, and water as control was prepared. Then fine aggregate sand is partially replaced by iron waste in different percentage. The percentages were as follows: (6%, 12%, 18%, 24%, and 30%) for compressive strength and for flexural tensile strength. For each percentage, nine cubes and nine beams were made up. Overall, total samples were 54 cubes and 54 flexural beams. The cubes with dimensions of (100*100*100) mm samples were used for the compressive strength test, and utilizing beam specimens with dimensions of (100 ×

100 × 500mm) for the flexural tensile strength test. The samples were tested after three different times of curing (7, 14, 28) days.

4.2.2 CONCRETE MIX DESIGN

The mix proportions are important to a strong and durable concrete. The mix design should achieve the desired workability of concrete to prevent segregation and allow for ease of placement. In this regard, using the standard mix design according to Dixon, et al. [1], the mixture was designed for giving compressive strength of concrete of 33 MPa after 28 days of curing. The mix proportion was prepared as (1:2.12:2.37). Table 2 shows the weight of mixture components. The percentages of iron waste (0, 6, 12, 18, 24, and 30 %) were used instead of sand.

TABLE 2.
Quantities of materials used in kg/m3

Iron Waste Percentage %	Cement kg/m^3	Iron Waste kg/m^3	Sand kg/m^3	Aggregate kg/m^3	Water kg/m^3	Water/ cement
0%	385	0	818	912	200	0.52
6%	385	49.08	768.92	912	200	0.52
12%	385	98.16	719.84	912	200	0.52
18%	385	147.24	670.76	912	200	0.52
24%	385	196.32	621.68	912	200	0.52
30%	385	245.4	572.6	912	200	0.52

4.2.3 LABORATORY TESTS

The concrete slump test is a practical test to measure the consistency of the concrete to check the workability of fresh concrete. In this regard, slump tests according to ASTM C143 were carried out for all mix ratios. Figure 1 (a) shows the slump test. Compression tests and flexural tests were implemented on concrete cubes, and concrete beams respectively. Compressive strength is the capacity of a material or structure to withstand loads tending to reduce size. The compressive strength samples were prepared according to ASTM C39 [10], concerning this, nine standard compressive concrete cube specimens (100 × 100 × 100mm) were fabricated to be tested for zero percent and each proportion of iron waste. Meanwhile, the flexural strength (modulus of rupture) samples were prepared according to ASTM C293 [11]. A plain concrete beam (100 x 100 x 500 mm) was loaded in flexure at the third points of 300-mm span until it fails due to cracking on the tension face. Modulus of rupture is computed as [12]:

$$R = \frac{3PL}{2bd^3} \tag{1}$$

where; R is the modulus of rupture [MPa], P is a maximum applied load indicated by testing machine [N], L is the span length [m], b is the average width of specimen [mm] and d is the average depth of specimen [mm]. the samples were cured for 7 days, 14 days, and 28 days under standard conditions. Then the tests of the specimens were implemented. The test of the samples for a compressive strength by MPa and flexural strength by KN at 7 days, 14 days, and 28 days were carried out. Figure 1 (b) & (c) show the compression test and flexural test respectively. Regarding preparing the samples, fifty-four cubes were prepared for compressive strength, every eighteen samples were tested at 7 days, 14 days and 28 days for control and other proportions. Meanwhile, fifty-four beams were tested for the flexural strength test. Similarly, for the flexure, every eighteen samples were tested at 7 days, 14 days and 28 days for control and other proportions. Moreover, the test results of the cubes, and beams, of concrete made with IP were equated to the test results of the normal concrete (control) specimens.

(a) (b) (c)

FIGURE 1. (a) Slump Test, (b) & (c) display compressive and flexure strength specimen test

5. RESULTS AND DISCUSSION

5.1. SLUMP TEST

The outcomes show that the slump decreased slightly and gradually as iron waste increased. This means that the workability of the concrete is in an acceptable range with a good durability of concrete. Figure 2 displays the slump test for all mixing ratio.

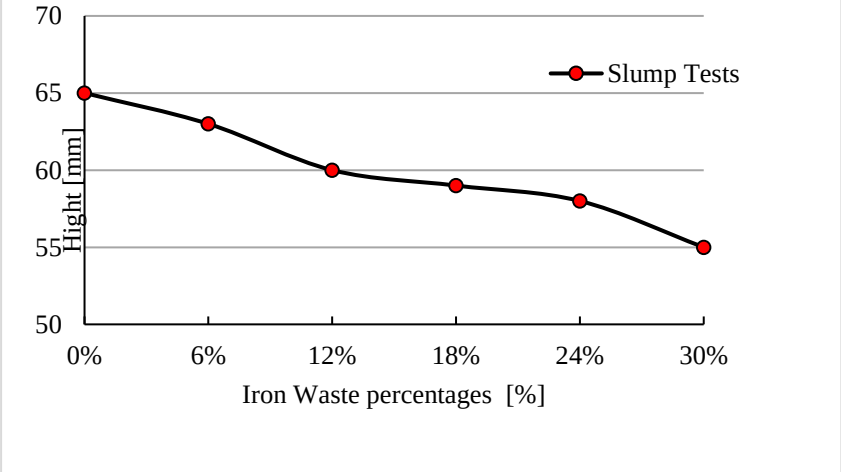

FIGURE 2. Presents the slump test for all mixing ratio

5.2. COMPRESSIVE STRENGTH TEST

Compressive strength test was carried out to evaluate the strength progress of concrete, comprising different percentages of iron waste at the age of 7, 14, 28 days, respectively. It is shown in Figure 3 that increasing the iron waste leading to

gradually gains in the compressive strength. It is observed that increasing the iron waste to 12% gives the highest strength among the results, which from this point onwards increasing the amount of iron waste decreases the strength of concrete. It can be realized that using 12% iron waste in concrete will give 15% more compressive strength in 28 days than normal concrete (control).

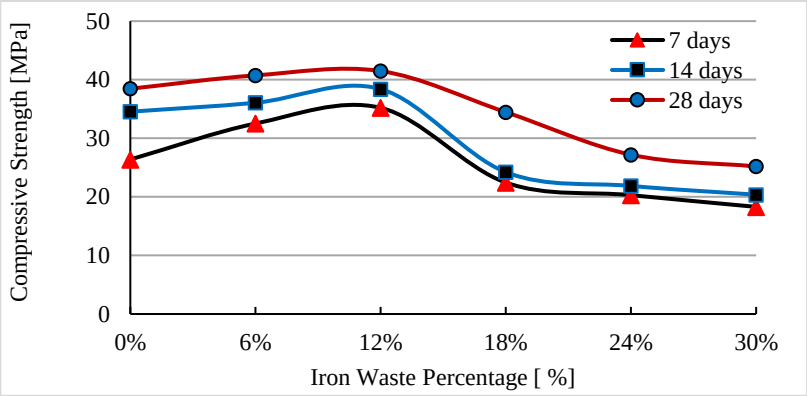

FIGURE 3. Compressive strength of different iron waste percentages for different time of curing

5.3. FLEXURAL TENSILE STRENGTH TEST

Regarding the flexural tensile strength, flexural samples were tested to evaluate the strength of concrete, containing various ration of iron waste. Based on the results shown in Figure 4, the flexural tensile strength gradually increases as the iron waste percentage reaches 12%. It is clear from the figure that increasing iron waste more than 12% leads to falling down the flexural tensile strength. Therefore, it can be said that iron waste can be limitedly used to be effective as a replacement of sand to increase the strength of concrete. As a result, it can be concluded that using waste materials are the benefit in terms of not only preserving the environment, but also improving the structural properties of concrete.

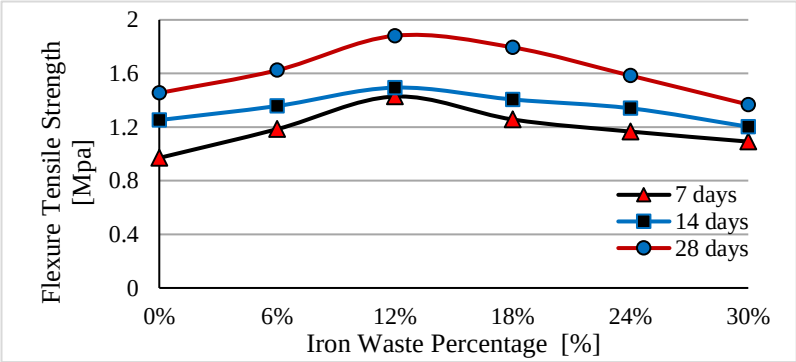

FIGURE 4. Shows the flexural tensile strength of different iron waste percentages for different time of curing

6. CONCLUSIONS

In conclusion, the workability of the concrete is slightly and gradually decreased by increasing iron waste. The strength of concrete increased while curing was prolonged. The compressive and flexural tensile strength slightly increased by increasing iron waste ratio until 12%. It can be noted that using 12% iron waste in concrete gave 15% more compressive strength in 28 days than normal concrete. It should be significantly concentrated on that the mix ratio was basically designed to gives 33 MPa at 28 days but more than this can be obtained at 7 days by adding 12% of iron waste which was about 35 MPa. So in case, the concrete needs to reach the maximum compressive strength in the shortest time, 12% iron waste can be recommended to use in the concrete.

7. ACKNOWLEDGMENT

The authors would like to thank Koya University for its help in providing the necessary facilities needed to perform this research.

REFERENCES

[1] D. E. Dixon, J. R. Prestrera, G. R. Burg, E. A. Abdun-Nur, S. G. Barton, L. W. Bell, et al., "Standard Practice for Selecting Proportions for Normal, Heavyweight, and Mass Concrete (ACI 211.1-91)," 1991.

[2] S. Raman, M. Safiuddin, and M. Zain, "Non-destructive evaluation of flowing concretes incorporating quarry waste," Asian journal of civil engineering (Building and Housing), vol. 8, pp. 597-614, 2007.

[3] S. Ghannam, H. Najm, and R. Vasconez, "Experimental study of concrete made with granite and iron powders as partial replacement of sand," Sustainable Materials and Technologies, vol. 9, pp. 1-9, 2016.

[4] R. Joshi, "Effect of using selected industrial waste on compressive and flexural strength of concrete," International Journal of Civil and Structural Engineering, vol. 4, p. 116, 2013.

[5] A. Jayaraman, N. Karthiga Shenbagamn, and V. Senthilkumar, "Eco Friendly Building Materials Used for High strength and high performance Concrete," International Journal of ChemTech Research, vol. 10, pp. 23-28, 2017.

[6] B. Bahoria, D. Parbat, P. Naganaik, and U. Waghe, "Comprehensive literature review on use of waste product in concrete," International journal of Application or Innovation in Engineering & Management, vol. 2, pp. 387-394, 2013.

[7] A. Dubey, R. Chandak, and R. Yadav, "Effect of blast furnace slag powder on compressive strength of concrete," International Journal of Scientific & Engineering Research, vol. 3, pp. I094-I098, 2012.

[8] T. Ugama, S. Ejeh, and D. Amartey, "Effect of iron ore tailing on the properties of concrete," Civil and Environmental Research, vol. 6, p. 7, 2014.

[9] A. Alzaed, "Effect of iron filings in concrete compression and tensile strength," International Journal of Recent Development in Engineering and Technology, vol. 3, pp. 121-125, 2014.

[10] A. Standard, "ASTM C39 Standard Test Method for Compressive Strength of Cylindrical Concrete Specimens," ASTM International, 2015.

[11] M. American Society for Testing, C. o. C. Committee, A. Concrete, and A. S. C. o. T. f. Strength, Standard test method for flexural strength of concrete (using simple beam with center-point loading). Philadelphia, Pa.: ASTM International, 2010.

[12] D. A. Fanella, Reinforced concrete structures : analysis and design, 2016.

EFFICIENT TECHNIQUES TO MINIATURIZE THE SIZE OF PLANAR CIRCULAR MONOPOLE ANTENNA

Y. A. Fadhel[1],R. M. Abdulhakim[2]

[1]*University of Duhok*

[2]*Nawroz University*

[1]*revinkmasoud@gmail.com*, [2]*yasser.fadhel@uod.ac*

doi:10.23918/iec2018.17

ABSTRACT

Recently different techniques have been adopted by many researcher to minimize the size of antennas being employed in compact devices. In this paper miniaturization of a planar circular monopole antenna (PCMA) has been introduced while maintaining its working range of frequencies covering the UWB range (3.1~10.6 GHz). Two different techniques are suggested; firstly, the PCMA radiator has been modified by eliminating areas with least concentrated current distribution, which led to generation of a crescent-shape radiator and the overall size reduction reached 11.76% of the original size. Secondly, the edge of the circular radiator has been corrugated according to some suggested formulas, which increased the size reduction to about 42.6%. Another advantage has been achieved for the corrugated PCMA by extending the upper limit of its impedance bandwidth to 13.85 GHz. All designed antennas have been fabricated and verified via practical experimental measurements. Simulated and measured results have shown that both techniques were succeeded in miniaturizing the overall size of PCMA antenna, but precisely, corrugation technique was more efficient.

Keywords: Miniaturized Antennas, PCMA, Crescent-Shaped, Corrugation, UWB.

1. INTRODUCTION

Since adopting the UWB standard by Federal Communication Commission (FCC) in 2002 [1] for short-range peer-to-peer ultra-fast communication, researchers competed in designing different types of antennas that obey the wideband range of frequencies (3.1 GHz ~ 10.6 GHz) which is required by this technology. Some of these antennas were planar and others were non-planar. Concerning to the planar microstrip antennas the main challenge was represented in its narrow band feature, which has been overcame via designing of a certain shapes of antennas having different aspect lengths in the way of the exciting current to be resonating with different wavelengths which in turn widening the range of frequencies to cover the UWB range. Among these shapes were; the triangular, elliptical, circular, ring, etc. [2, 3]. It has been concluded in [4] as a common silent characteristic for all designed antenna shapes that; the impedance bandwidths of these antennas will be wider as much as the edges of their radiating elements are having a round or smoothly curved shapes. In turn, this will be more convenient for their features with UWB requirements.

In spite of the complexity in designing of these UWB antennas but the challenges were raised up when different techniques suggested for miniaturizing them. For instance, symmetrical exponential corrugations have been introduced in the radiator of tapered slot antenna (TSA) by [5] which enables the antenna to resonate at lower frequencies with comparably smaller size structure. The depth of these corrugation slots has been selected to be less than quarter of the effective wavelength at the lowest operation frequency, and this presents an inductive reactance against the passing wave which in turn increases the effective electrical length of the structure. Although the TSA antenna in general, is characterized by its directional radiation pattern, but omnidirectional TSA has also been introduced as that in [6], where some corrugations have been made to miniaturize its size. In addition to these

aforementioned benefits of corrugations in miniaturization of planar antennas, it has been shown in [7] that adding the corrugation slots could improve the antenna gain very efficiently, where several corrugation shapes like; rectangular, saw tooth and cosine shapes have been used. Therefore, corrugation technique has been suggested in this paper to modify the circular radiator of PCMA which gives 42.6% of reduction compared to the original antenna size. This miniaturization will be achieved via some suggested formulas Another technique of miniaturization is depending on the current distribution analysis to suggest elimination for some metallization areas of that antenna, like that performed in [8], in which a crescent-shape has been introduced as a miniaturized shape of original elliptical shape radiator. Another work by [9] evolved the crescent-shape antenna from elliptical shape by carving a circular hole inside the radiator symmetrically, which succeeded to remove 40% of the metallization and 60% of the ellipse area. But these aforementioned works have failed to make reduction in the overall size. Unlike other design in [10] which modified a slot antenna that enabled up to 63% of overall size miniaturization after removing some areas but the modification here was associated with major changes in the shape of the antenna by changing the U-shape radiator to cactus shape, and also the modified antenna has not stay slot antenna anymore .The elimination of undesired areas is also introduced in this paper due to the aforementioned reasons but with minor changes in the shape of the original antenna, in a trial to enhance the design procedure that might be extended to other shapes of planar antennas. The miniaturization process suggested here is considered as a complementary process for the main design procedure. The original antenna to be designed will be a PCMA as one of the common UWB antennas, and its current distribution will be simulated, to figure out the undesired or least current distributed areas. Then these areas will be eliminated to generate the planar crescent-shape monopole antenna (PCSMA) which will achieve a

reduction in the overall size by not less than 11.76% while almost maintaining the same characteristics as that of the original antenna.

2. ANTENNA DESIGN

A PCMA antenna has been selected to be designed as one of the common and simple planar monopole antennas that covers the entire UWB frequency range. Figure 1 shows the PCMA antenna designed here, and the dimensions have been designed according to the relations suggested by [11] as follows:

$$f_L = \frac{c}{\lambda} = \frac{7.2}{(L + r + P) * k}\ GHz \qquad (1)$$

Where f_L is the lower band-edge frequency, r and L are deciding the size of a virtual cylindrical monopole antenna which corresponding to the values of its radius and effective height, respectively. The area of this virtual antenna is considered to be equal to the radiator area of PCMA antenna. And accordingly, they could be calculated as follow [11]:

$$L = 2\,R \qquad (2)$$

$$r = R/4 \qquad (3)$$

where R is the radius of the circular radiator, also one can say that P is the neck length in cm for the 50 Ω microstrip feed line between the radiator element and the ground plane, the width of the microstrip feed line is W_T, the value of $k = \sqrt{\varepsilon_{eff}}$ and P will be omitted or included in the L_C dimension as shown in figure 1. The approximated value of ε_{eff} has been calculated as [12]:

$$\varepsilon_{eff} \approx \frac{\varepsilon_r + 1}{2} \qquad (4)$$

The whole planar antennas designed here were using FR4 substrate with thickness of 1.6 mm, and ε_r = 4.3 which gives ε_{eff} = 2.65, accordingly k is

1.627. This value is suggested by [13] to be taken 1.15 as an empirical value. Therefore if the lower frequency is chosen to be 2 GHz, then R will be equal to 11.7 mm, but it has been taken as R = 12.5 mm to ensure earlier starting for the working band of frequencies.

Other

TABLE 1.
Design parameters of PCMA antenna.

Parameter	Dimension (mm)
P	0.5
R	12.5
W_S	40
W_T	2.8
L_S	51
L_G	22.7
L_C	13

parameters were L_G = 22.7 mm, L_C = 13 mm and W_T = 2.8 mm. The all aforementioned design parameters are shown in the Table 1.

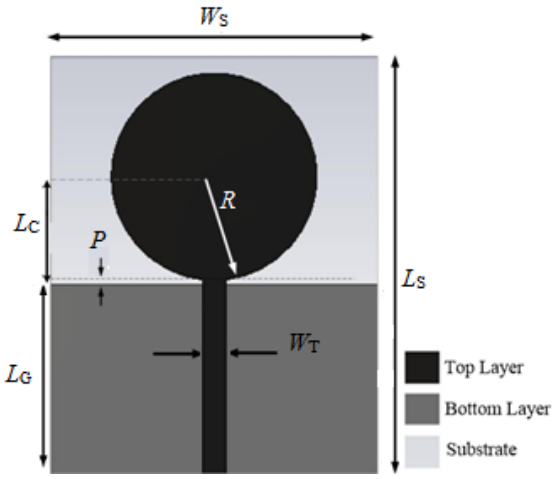

FIGURE 1. Geometry of the simulated PCMA antenna.

3. MINIATURIZATION

After designing the PCMA antenna, it is necessary to miniaturize it while preserving its features almost unchanged. The miniaturization process has been performed by two different methods. The first technique was achieved through eliminating the areas with least distributed surface current which generates a crescent-shaped radiator to decrease the overall height of the radiator while preserving those areas with most distributed surface current. Therefore the overall height has been reduced physically while the most important areas have been preserved in a trail to keep same antenna features as those of the original antenna. Figure 2 shows the PCSMA antenna and all of its parameters are listed in Table 2. The dimensions of this antenna have been optimized to get closer features to the parent antenna, and the overall size is reduced to 88.2% (40*45/40*51=0.882) of the original antenna.

TABLE 2.
Design parameters of PCSMA antenna.

Parameter	Dimension (mm)
L_{C1}	13
L_{C2}	19
L_S	45
L_G	22.75
W_S	40
W_T	2.8
P	0.5
R_1	12.5
R_2	11

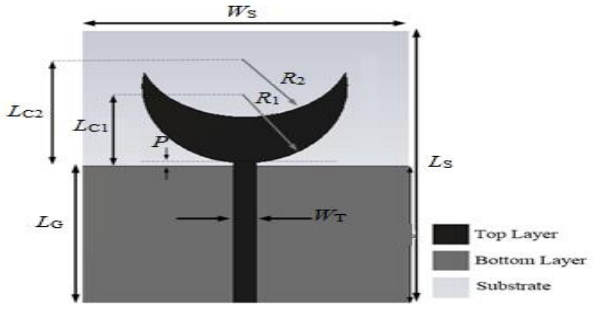

FIGURE 2. Geometry of the simulated PCSMA antenna.

The second technique of miniaturization for the PCMA antenna is performed by corrugating the edges of the circular radiator in somehow to get repeated slots around its round edge as depicted in figure 3. Due to the fact that the current flowing through the radiator will mainly be distributed at the edges, therefore the required electrical length of the circumference for the circular radiator of PCMA will be compressed physically via corrugations that maintains the same effective circumference electrical length as that of the original PCMA. Figure 4 shows a zoomed portion of the corrugated structure, and the required size of these corrugations could be calculated by equating the circumference of the circular radiator of PCMA antenna with that of the corrugated PCMA antenna as follow:

$$2\pi\, R_o = 2\pi\, R_1 - N\, R_1\, d\phi + 2\, N\, L_{Slot} + N\, R_2\, d\phi \qquad (5)$$

where R_o is the radius of the original PCMA before miniaturization, N is the number of corrugation slots, and the other parameters R_1, R_2 and $d\phi$ are as shown in Figure 4. The depth of corrugated slots is defined as L_{Slot} and could be calculated from R_1 and R_2 as:

$$L_{Slot} = R_1 - R_2 \qquad (6)$$

Performing some simplification on equation 5 then R_1 will be equal to:

$$R_1 = R_o - \frac{N\, L_{Slot}(2 - d\phi)}{2\pi} \qquad (7)$$

where $d\phi$ is in radians while other parameters are all in (mm). The number of corrugated slots N will not be related directly with $d\phi$ because in the case of this design two additional slots will be hidden within the microstrip feedline side therefore:

$$(N + 2) = \frac{2\pi}{d\phi} \quad (8)$$

Now if N is taken as 28, R_o = 12.5 mm, L_{Slot} = 0.65 mm, then equation 8 gives $d\phi$ = π/30 (rad) which is equal to (6°) and equation 7 gives R_1 = 7.01 mm, which has been taken 7 mm in this design. The all design parameters are listed in Table 3. It is worthy to mention that for different number of corrugated slots more or less than 28 that used here then the number of hidden slots will be changed and equation 8 will be changed accordingly.

If it is desired to make the depth of the corrugated slots equal to their width which is the arc length then L_{Slot} will be given as:

$$L_{Slot} = R_1\, d\phi \quad (9)$$

Accordingly, if equations 8 & 9 are substituted into equation 7, then R_1 will be:

$$R_1 = \frac{2\pi\, R_o}{6\pi - 2\pi\, d\phi - 4\, d\phi + 2\, d\phi^2} \quad (10)$$

This technique has reduced the original size of the radiator while kept the required electrical length of the circumference unaffected via the compressing taken place in the corrugated circumference. Accordingly, the important characteristics of the antenna have been preserved while the overall size is reduced to 57.4% ((30*39/40*51)*100%=57.35%) of the original antenna size.

TABLE 3.

Design parameters of corrugated PCMA antenna.

Parameter	Dimension (mm)
L_C	7.65
L_{Slot}	0.65
L_S	39
L_G	22.75
W_S	30
W_{Slot}	1
W_T	2.8
P	0.5
R_1	7
R_2	6.35

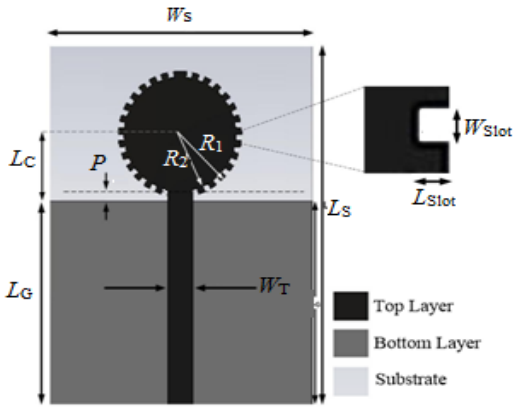

FIGURE 3. Geometry of the simulated corrugated PCMA.

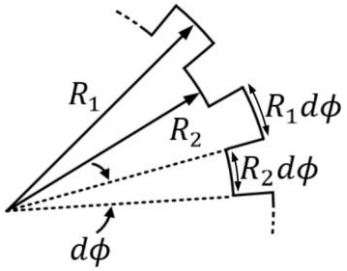

FIGURE 4. Details of the corrugated structure.

4.RESULTS AND DISCUSION

PCMA has been designed as one of the common UWB antennas with dimensions and geometry as mentioned in previous section, then two different techniques have been used; firstly, by eliminating the undesired or least current distributed areas to generate a planar crescent-shaped monopole antenna (PCSMA), secondly by corrugating the round edge of the circular radiator to miniaturize its circumference. All the designed UWB antennas have been simulated using CST Microwave Studio™ software package. Figure 5 shows the simulation results of the return loss curves versus frequency for the PCMA, PCSMA, and Corrugated PCMA. It shows that all of these designed antennas are maintaining their working which covered the entire UWB. Investigating the surface current distributions for the three designed antennas are shown in figures 6 to 8 and they were plotted for 5 and 9 GHz of frequencies. The PCSMA will offer the required area of metallization in least size compared to the PCMA. Therefore, it has been concluded that the current will be concentrated at this miniaturized area which is almost distributed at the lower side edges of the radiator. While in corrugated PCMA the current will follow a corrugated path offered by the radiator edge and it will cross the required path with least height compared to PCMA, which validates the technique of eliminating the undesired areas.

After completing the design and simulation of the aforementioned antennas, the all three antennas have been fabricated as shown in figures 9 to 11, and tested via Rohde & Schwarz® ZVL13 VNA. The return loss data has been measured for the all three antennas and plotted in comparison with their simulation one as shown in figures 12 to 14. The measurement results are almost agreed with the simulation results except some shifting due to imperfection in the fabrication. However, the practical experimental measurements validate the design and its modification which performed to miniaturize the size of the PCMA. Therefore the miniaturized antennas will

be working with almost the same features with least size which satisfy the goal of this research.

The simulated and measured radiation patterns in E and H planes for the three antennas are shown in figures 15 to 17 for 5 and 9 GHz of frequencies. Measured radiation patterns are almost meet the simulated patterns. And also the miniaturization techniques have nearly not affected the radiation pattern that performed by PCSMA nor corrugated PCMA. Finally, the simulated realized gain curves for PCMA, PCSMA and corrugated PCMA have been plotted as shown in figure 18. For PCMA it is noticed that almost the gain is increased with increments in the frequency, which is common in UWB antennas, while for corrugated PCMA and in spite of the great miniaturization occurred in its size but its gain (not less than 2 dB) was still having a reasonable value comparing to the gain of half wave dipole antenna (*i.e.* 2.15 dB), and getting up to (4.8 dB at 9.5 GHz). Although the miniaturization ratio in corrugated PCMA is greater than that of PCSMA but its gain still better than the gain of PCSMA, and this may back to the circumference length in the corrugated PCMA that has been maintained via corrugated edge, while it is truncated in PCSMA.

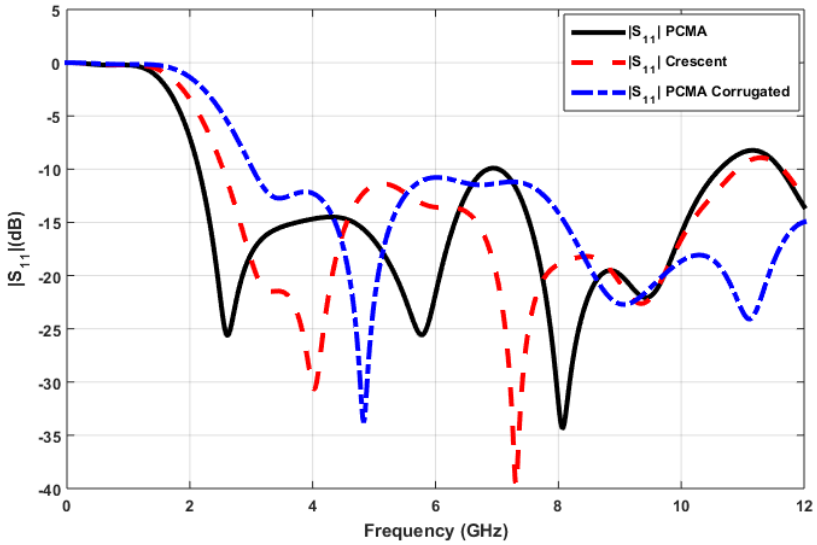

FIGURE 5. Comparison of simulated return loss curves for the PCMA, PCSMA and corrugated PCMA

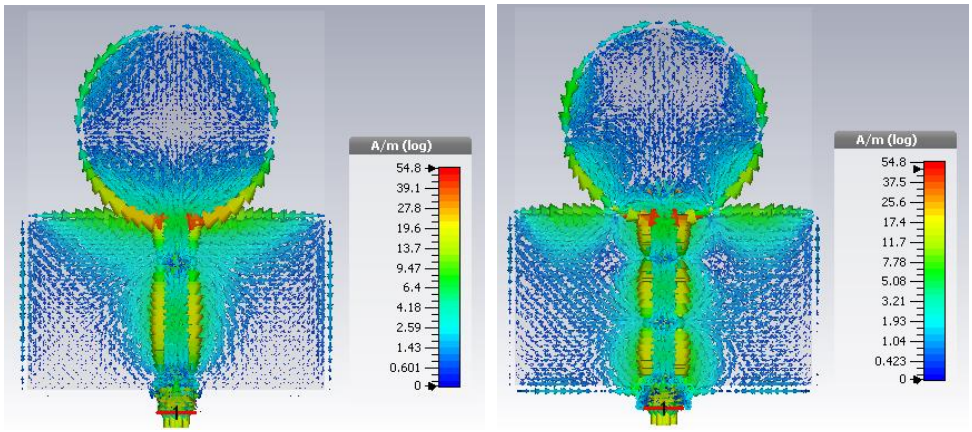

(a) (b)

FIGURE 6. Surface current distribution for the PCMA at (a) 5 GHz, and (b) 9 GHz.

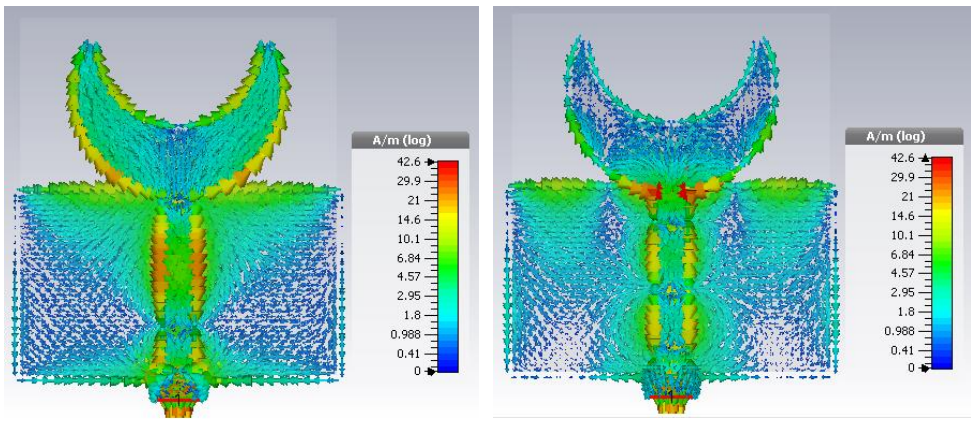

(a) (b)

FIGURE 7. Surface current distribution for the PCSMA at (a) 5 GHz, and (b) 9 GHz.

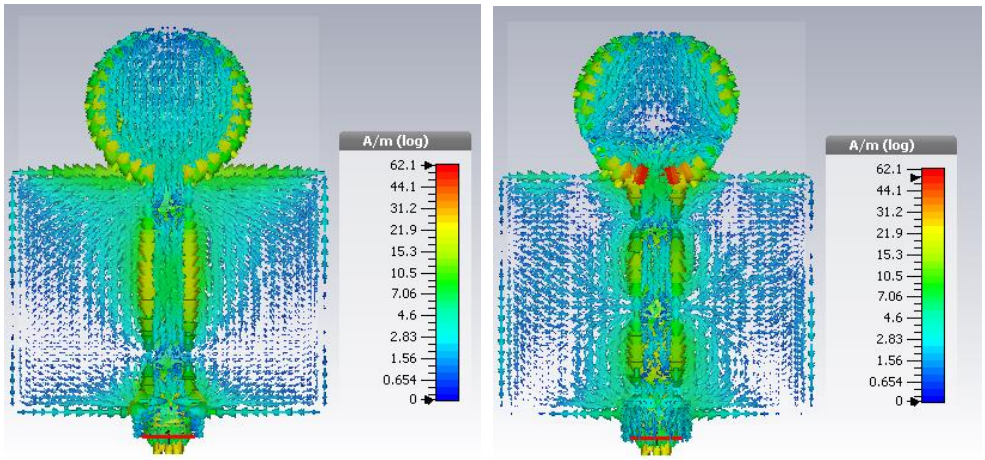

(a) (b)

FIGURE 8. Surface current distribution for the Corrugated PCMA at (a) 5 GHz, and (b) 9 GHz.

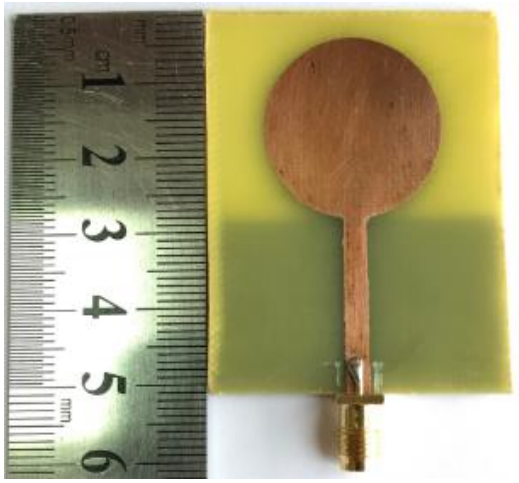

FIGURE 9. Fabricated PCMA.

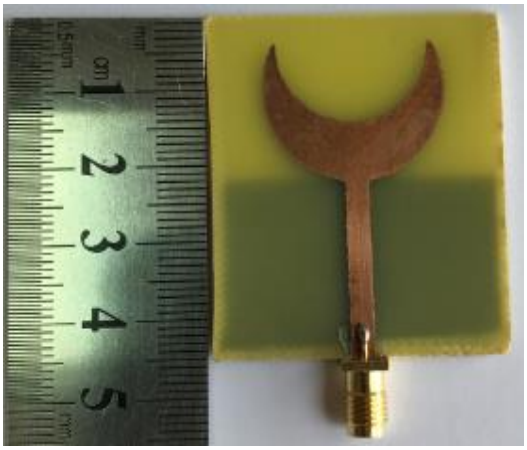

FIGURE 10. Fabricated PCSMA.

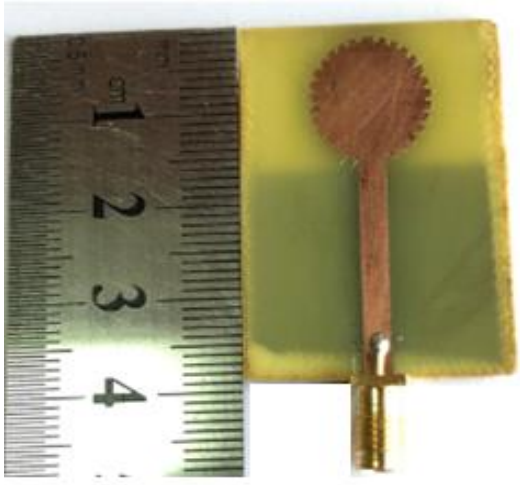

FIGURE 11. Fabricated corrugated PCMA.

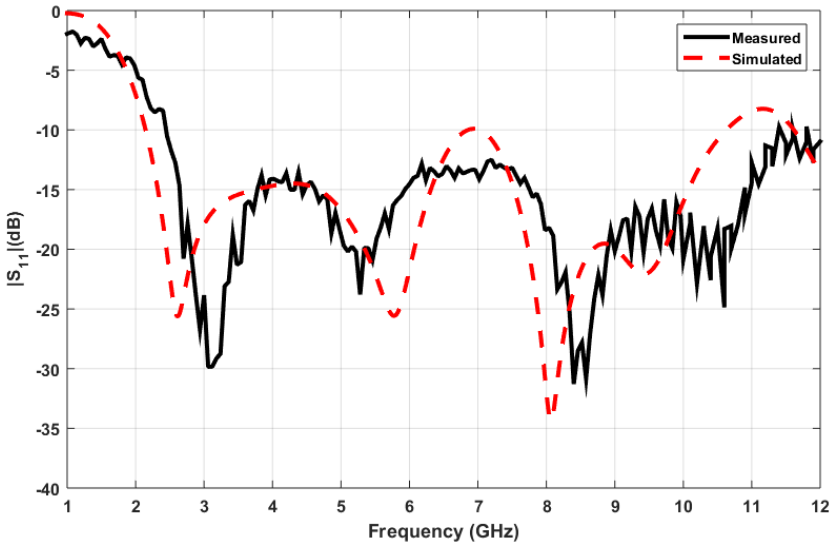

FIGURE 12. Return loss curves (measured and simulated) for the PCMA.

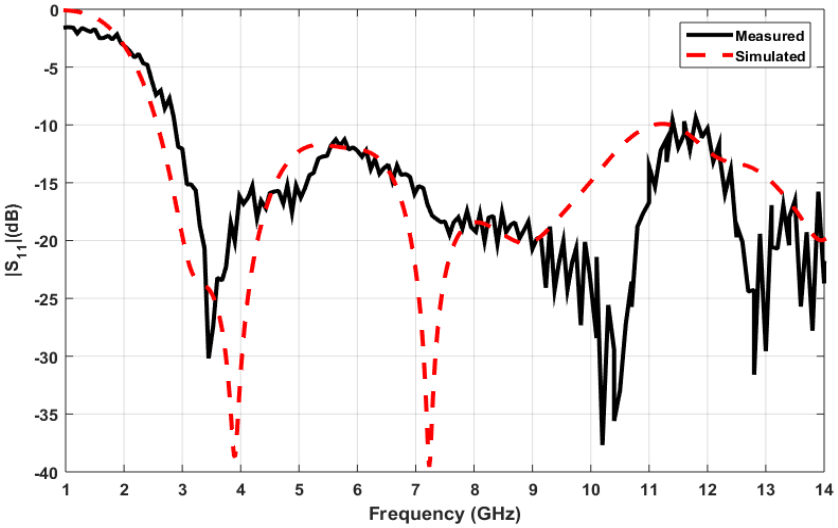

FIGURE 13. Return loss curves (measured and simulated) for the PCSMA.

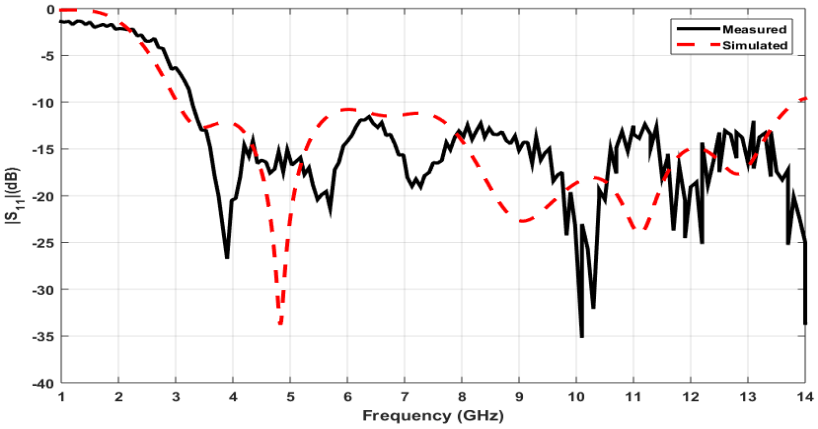

FIGURE 14. Return loss curves (measured and simulated) for the Corrugated PCMA.

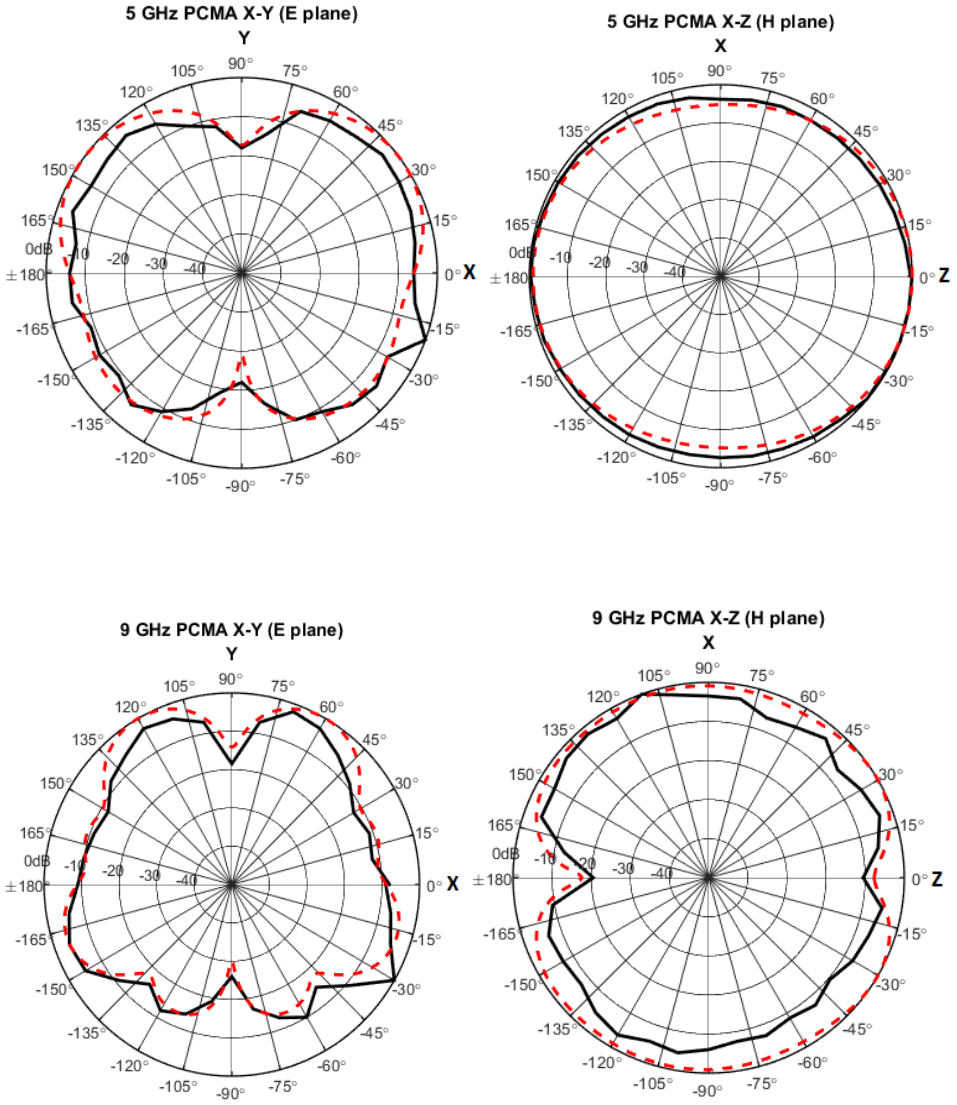

FIGURE 15. Radiation patterns simulated (- - -) and measured (—) of the PCMA in H and E planes, for frequencies of 5 and 9 GHz.

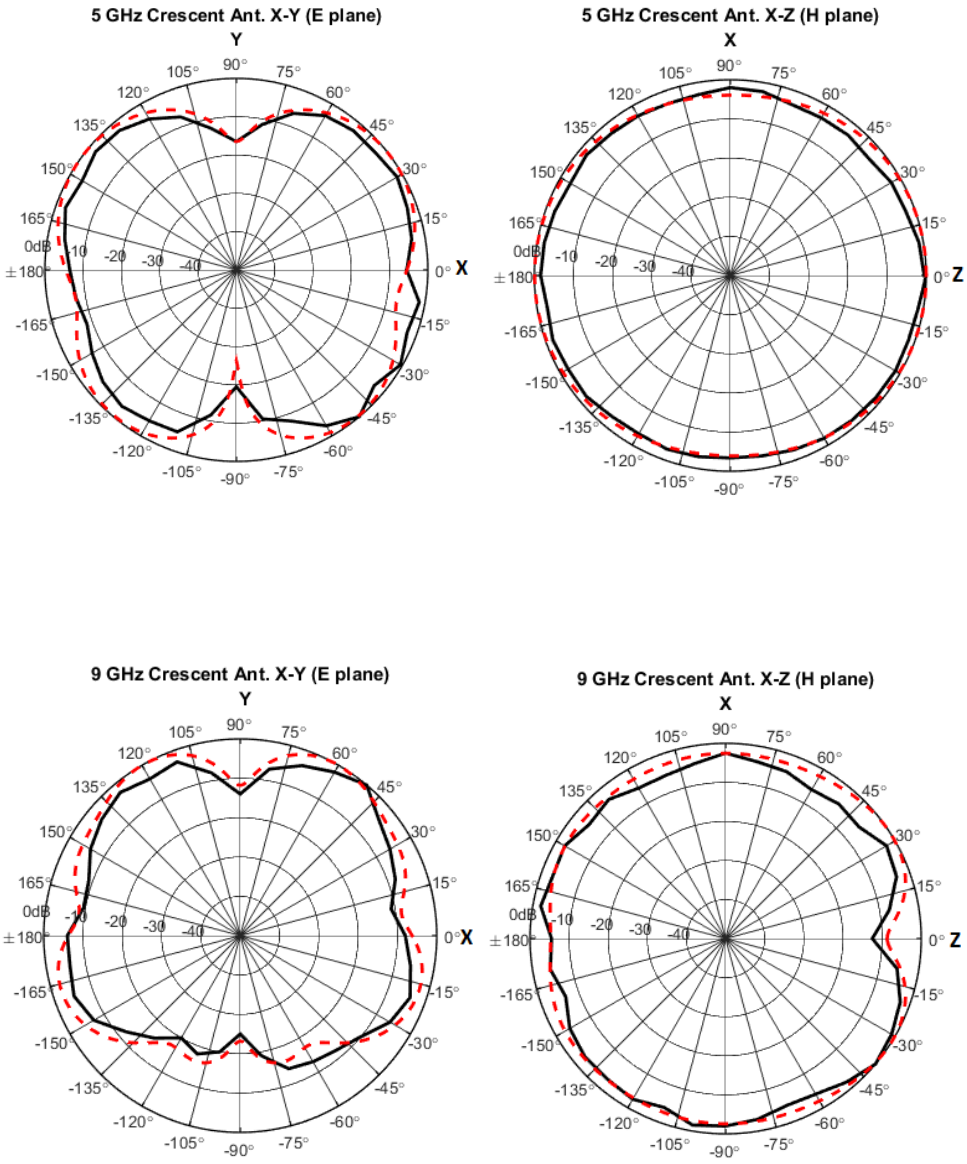

FIGURE 16. Radiation patterns simulated (- - -) and measured (—) of the PCSMA in H and E planes, for frequencies of 5 and 9 GHz.

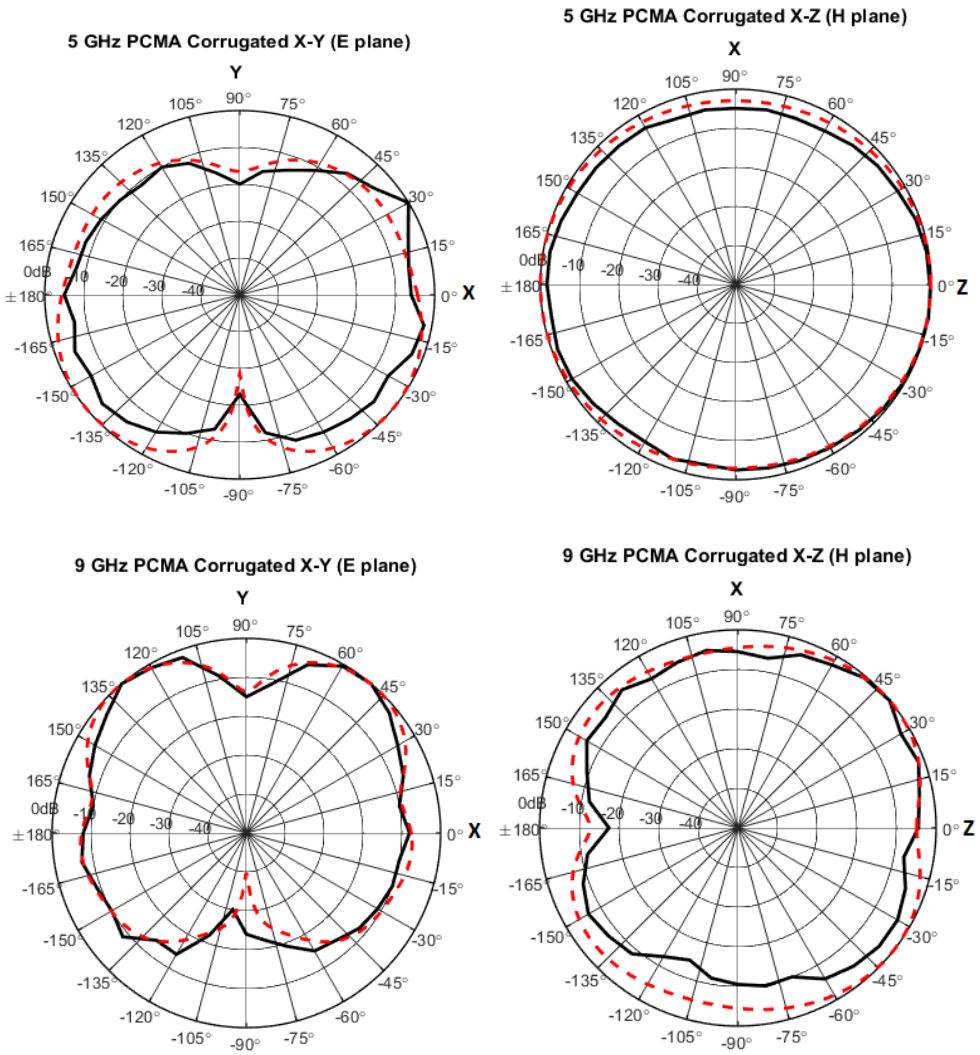

FIGURE 17. Radiation patterns simulated (- - -) and measured (—) of the Corrugated PCMA in H and E planes, for frequencies of 5 and 9 GHz.

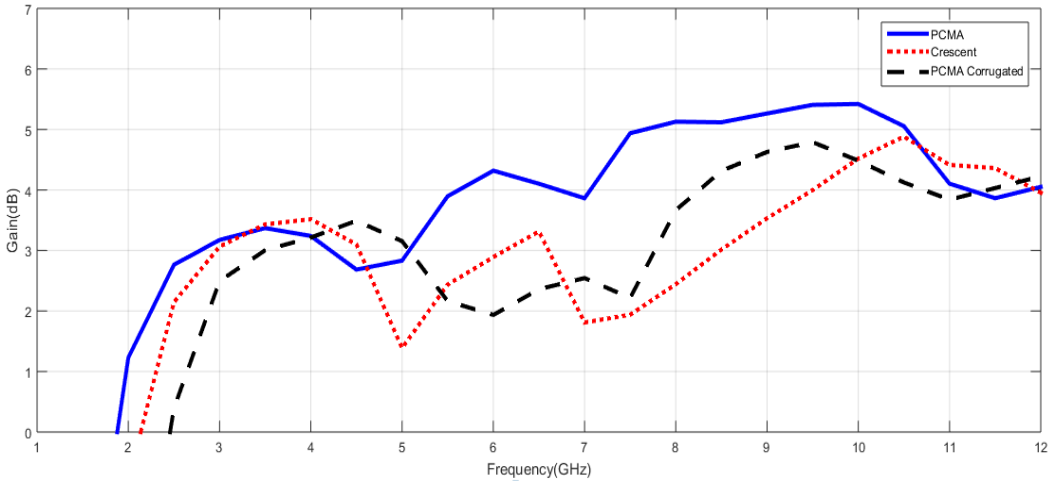

FIGURE 18. Comparison of simulated realized gain curves for the PCMA, PCSMA and corrugated PCMA.

5. CONCLUSIONS

Two techniques have been suggested here to miniaturize the overall size of PCMA; the first technique has been performed by eliminating the least current distributed areas, which resulted in a crescent-shaped radiator. While the second technique introduces corrugated slots around the round edge of the PCMA radiator, in which a 57.4% of overall size reduction has been achieved while its gain was still maintaining more than (2 dB), which is comparable with that of half wave dipole antenna. Results shown that corrugation technique was more efficient due to the reduction in size was 42.6% which is more than 11.76% for the other techniques, also the upper limit of the impedance bandwidth for the corrugated PCMA has been extended to 13.85 GHz. Another advantage of the corrugation technique has been shown that the gain characteristics was better than that of area eliminating technique, and the reason may back to maintaining the perimeter electrical length in corrugated PCMA as much as that of the original PCMA antenna, while in PCSMA a certain portion of the perimeter's upper side has been truncated. However, both miniaturized antennas are still having the required characteristics just like the original parent PCMA antenna that obey the UWB requirements.

REFERENCES

[1] First Report and Order (FCC 02-48), "New Public Safety Applications and Broadband Internet Access Among Uses Envisioned by FCC Authorization of Ultra-Wideband Technology," Action by the Commission Feb. 14, 2002.

[2] Sayidmarie, K. H., & Fadhel, Y. A., "Self-Complementary Circular Disk Antenna for UWB Applications," Progress In Electromagnetics Research C, Vol. 24, 111-122, 2011.

[3] Sayidmarie, K. H, and Fadhel, Y. A., "Design Aspects of UWB Printed Elliptical Monopole Antenna with Impedance Matching", Loughborough Antennas & Propagation Conference LAPC2012, UK, Nov. 2012.

[4] Fadhel, Y. A., "Design and Implementation of Ultra Wide Band Antennas for Imaging Applications," PhD Thesis, University of Mosul, July, 2013.

[5] Beada'a, J. M., Abbosh, A. M., Mustafa, S., and Ireland, D., "Microwave System for Head Imaging," IEEE Transactions on Instrumentation and Measurement, Vol. 63, No. 1, 117-123, 2014.

[6] Bialkowski, M. E., Abbosh, A. M., Wang, Y., Ireland, D., Bakar, A. A., and Mohammed, B. J., "Microwave Imaging Systems Employing Cylindrical, Hemispherical and Planar Arrays of Ultrawideband Antennas," Proceedings of the Asia-Pacific Microwave Conference APMC2011, pp. 191-194, Dec., 2011.

[7] Chareonsiri, Y., Thaiwirot, W., and Akkaraekthalin, P., "Design of Ultra-Wideband Tapered Slot Antenna by Using Binomial Transformer with Corrugation," De Gruyter, Frequenz 2017, Journal of RF-Engineering and Telecommunications, 2017.

[8] Chen, M. S., Weng, W. C., & Wang, S. T. (2013, February), "Design of the Crescent-Shape Planar Ultra-wideband Antenna with a Band-notch

Structure," IEEE 2nd International Symposium on Next-Generation Electronics (ISNE), pp. 271-274, Kaohsiung , Taiwan, Feb., 2013.

[9] Azenui, N. C., and Yang, H. Y. D., "A Printed Crescent Patch Antenna for Ultrawideband Applications," IEEE Antennas and Wireless Propagation Letters, Vol. 6, 113-116, 2007.

[10] Nikolaou, S., and Abbasi, M. A. B., "Miniaturization of UWB Antennas on Organic Material," International Journal of Antennas and Propagation, Vol. 2016, 12 pages, Article ID 5949254, 2016.

[11] Ray, K. P., "Design Aspects of Printed Monopole Antennas for Ultra-wide Band Applications," International Journal of Antennas and Propagation, Vol. 2008, 8 pages, Article ID 713858, 2008.

[12] Balanis C. A., "Antenna Theory Analysis and Design," John Wiley & Sons Inc, 3rd ed., 2005.

[13] Matin, M. A., "Ultra Wideband Communications: Novel Trends– Antennas and Propagation", Published by InTech, Croatia, pp. 177-183, July, 2011.

ANALYSIS OF ELASTIC BEAMS ON LINEAR AND NONLINEAR FOUNDATIONS USING FINITE DIFFERENCE METHOD

Saad Essa

Erbil Polytechnic University ,Ishik University,
saad_khalis@epu.edu.krd, saad.essa@ishik.edu.iq

doi:10.23918/iec2018.18

ABSTRACT

An approximate method is developed to analyze the deflection in beams and beam-column by solving the differential equation for the elastic deformation of beam and beam-column. The analysis is performed using the central difference of finite difference method for the Euler-Bernoulli beam and beam-column supported on an elastic, nonlinear foundation with rigid or elastic discrete supports. To make a verification of the results, Laplace Transformation method is used to solve the elastic differential equation of beam and beam-column based on linear elastic supports and the results are compared with the finite difference method. Two types of beams are selected, simply supported and fixed-fixed with five elastic supports of an idealized soil. In the nonlinear idealization, the division of force into many levels are assumed and based on these forces, the equivalent displacements are obtained from an assumed power law equation by using the finite difference method. Central finite difference scheme has a second order is used throughout the numerical analysis with five nonlinear behavior of springs separated by an equal distance between them.

Keywords: Finite difference method, Euler-Bernoulli beam, Laplace transformation.

1. INTRODUCTION

Beams on an elastic foundation has been solved by many researchers and analytical solutions of the differential equation have been proposed [1-2]. The geometric stiffness matrix was formulated and derived for beams on elastic foundation by Eisenber et al. [3]. Many authors used a finite element technique to find an approximate solution. Two-parameter elastic foundations were formulated to analyze beams based on exact displacement function [4]. Analysis of finite element beam column on elastic Winkler foundation was carried out using exact stiffness matrix terms [5]. Lower order of finite strip method developed for the analysis of soil-iteration models. At the early stage, the model was used for soil layered under vertical load with uniform soil properties. The change of soil properties in the longitudinal direction was included in the research by Cheung et al. [6] and Oskoorouchi et al. [7]. Mixing between finite strip method and soil spring system has been developed and applied to study the plate vibration responses on elastic foundation with different boundary conditions [8-9]. Vallabhan and Das [10] estimated a non-dimensional third parameter using iterative procedure to represent the distribution displacement of beams rested on elastic foundation. Omurtag et al. [11] used a mixed-type formulation based on Gateaux differential for the derivation of Kirchhoff plate-elastic foundation interaction. Binesh [12] used a mesh-free method for the analysis of a beam on two parameter elastic foundation. Sato et al. [13] obtained an exact solution for beam on elastic foundation in static and free vibration problems based on equidistant elastic supports. Jumel et al. [14] proposed a first order correction to take into account of interface elasticity and transverse anticlastic curvature of flexible substrate. Borak and Marcian [15] used modified Bettis theorem to develop an alternative analytical solution of beams on an elastic foundation. The calculation was based on the determine of beam's deflection on an elastic foundation from the deflection of a reference beam which is topologically equivalent. In this paper, the nonlinear assumption of soil behavior is used to analyze Euler-Bernoulli elastic beam and beam-column under compression load rested on it. Numerical method based on the finite difference method is used for the analysis of fourth-order linear ordinary differential equation of beam and beam-column. The constants in this equation are determined by using the boundary conditions of simply supported and fixed-fixed ends. In addition, closed form

solution based on the Laplace transformation method is used to get the results under the same conditions. Numerical examples are illustrated for both elastic beam and beam-column on the nonlinear soil behavior and the results are showed in figures and tables.

2. MODELLING OF SOIL MECHANICAL PROPERTIES AND ALGORITHM

Throughout analysis of any foundation, soil is not a linear material and for modeling it as a linear material could cause a considerable error. Soil actually behaves as a hyperbolic curve in relationship of stress-strain [3]. Load deflection relationship curve might be assumed to exist, as shown in Figs. 1-5 when modelling the reaction of a soil foundation. In every iteration of the force level, the tangent of the curve is obtained which means the slope of the force-displacement curve of soil. In this study, this curve is obeyed according to the nonlinear behavior of soil that defined in Eq. (1)

$$P = 0.5 P_u \varepsilon^n \tag{1}$$

where P_u is the ultimate soil bearing capacity of the soil in kN/m^2 and ε is the strain of soil underneath the footing. n is the power law variation that changes with the applied force and displacement. Here, the strain equals to the actual displacement because the length is assumed for one meter. Five nodes are idealized for the nonlinear soil reaction using the finite difference method to find the displacements. The load per unit area of foundation is plotted with displacement for each spring as shown in Figs 1-5. For each figure, the corresponding deflection are selected based on five loads chosen as 0.1, 0.25, 0.5, 0.75, and 1.0. These curves behavior which are represented the soil mechanical activities are working based on Eq. (1). The value of power n in Eq. (1) goes to decline with increasing of load step from 0.1 to 1.0. The differential equation that describing the elastic deflection curve of Euler-Bernoulli beam-column on a nonlinear elastic foundation under the action of a distributed load is governed by Eq. (2)

$$\frac{d^2}{dx^2}\left[EI \frac{d^2 y}{dx^2} \right] + P_\alpha \frac{d^2 y}{dx^2} + k(x) y = w(x) \tag{2}$$

where $y(x)$ is the deflection of the beam, E is the modulus of elasticity of the material made for the beam, I is the moment of inertia of the cross-section, P_α is the axial load applied at the ends to the beam, $w(x)$ is the applied distributed load and $k(x)$ is the foundation modulus. In the linear analysis of foundation, $k(x)$ is taken as a constant number while in the nonlinear foundation analysis varies in its values with respect to its position.

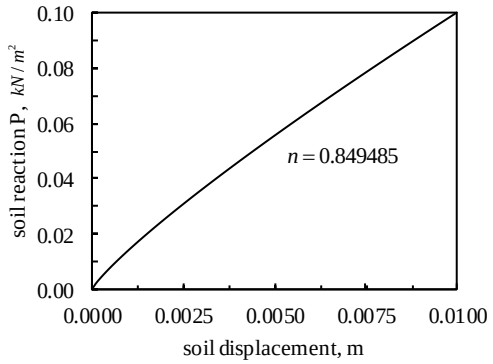

FIGURE 1. Load-displacement curve of soil at $P = 0.10 kN/m^2$

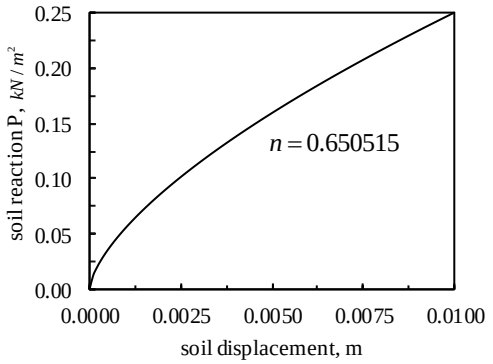

FIGURE 2. Load-displacement curve of soil at $P = 0.25 kN/m^2$

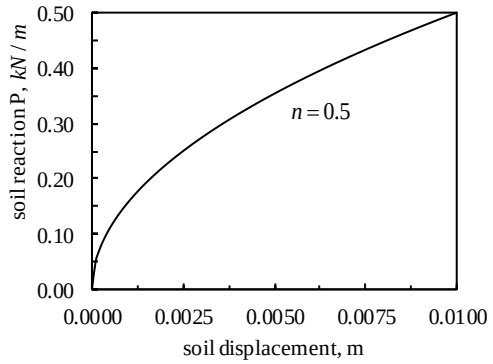

FIGURE 3. Load-displacement curve of soil at $P = 0.50 kN/m^2$

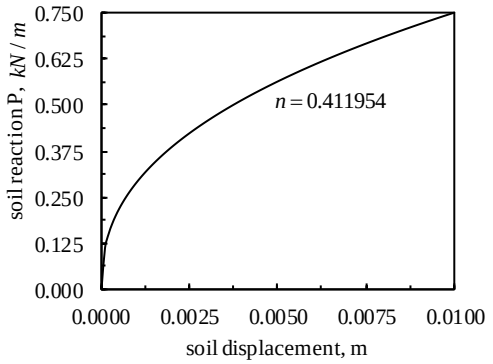

FIGURE 4. Load-displacement curve of soil at $P = 0.75 kN/m^2$

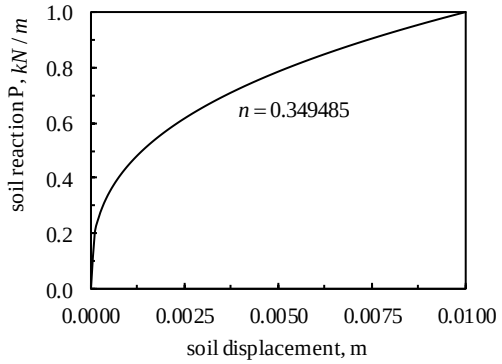

FIGURE 5. Load-displacement curve of soil at $P = 1.0 kN/m^2$

With applying finite difference scheme, Eq. (2) can be written for the elastic beam-column on nonlinear foundation as

$$y_{i+2} - 4y_{i+1} + 6y_i - 4y_{i-1} + y_{i-2} + \frac{P_\alpha}{EI}(y_{i+1} - 2y_i + y_{i-1})h^2 = \frac{w_i h^4}{EI} - \frac{k_i y_i h^4}{EI} \qquad (3)$$

In the case of elastic beam on nonlinear foundation can be calculated in the same Eq. (3) with $P_\alpha = 0$. The second and fourth order derivatives in Eq. (2) are substituted by second order central difference approximation in the finite difference equation (Eq. (3)). The finite difference grid is used for the analysis of beam and beam-column rested on elastic nonlinear foundation with taking a limit number of idealized springs. The distances between the springs are taken an equal and the axial load as a compression load at the ends. In the conventional finite difference analysis, the geometric and boundary conditions of the equilibrium differential equation are considered. The condition that y' and y'' are zero at station i is approximated using Eq. (4) and Eq. (5) respectively, as

$$y_{i+1} - y_{i-1} = 0 \qquad (4)$$

$$y_{i-1} - 2y_i + y_{i+1} = 0 \qquad (5)$$

Figure 6 shows the simply supported beam-column on five nonlinear idealized springs with equal distances between them.

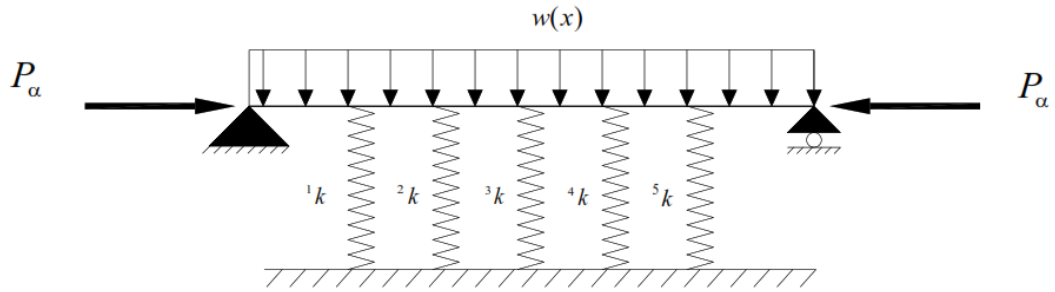

FIGURE 6. Simply supported beam-column rested on five springs.

The algorithm processes in this study are followed as the following steps: In the first load step ($P=0.1$) with the constant last strain ($\varepsilon=0.01$), the power n is determined to equal 0.849485 according to the Eq. (1) with taking $P_u=10.0$. After then, the stiffness (k) is equal to the slope of the load-deflection curve by assuming the deflection equals to the strain for idealized springs. Then the k values for the five springs are approximately linear for this step and equal to 10.0 because the exact values in this step can't be determined without present the springs deflection. By applying the finite difference technique (Eq. (3)), values of the springs deflection can be determined based on the constant value of stiffness ($k=10.0$) for all assumed nodes. For the second step ($P=0.25$), the value of power n can be determined with constant final strain ($\varepsilon=0.01$). In this step, with determining the values of deflections from the first step, the new stiffness (k) for all five nodes can be calculated by substituting the deflection values in the derivative of Eq. (1) ($4.24743/\varepsilon^{0.150515}$) which considers the slope of the load-deflection curve then the corrected deflections can be evaluated by applying the same equation of finite difference method. For the third step ($P=0.5$), the same procedures are applied from calculating the power n and evaluating the stiffness based on the second step deflections to reach the new corrected deflections. The processes are repeated for the fourth step ($P=0.75$) and fifth step ($P=1.0$). The observation of this algorithm is the load-deflection curve goes from linear at the first step to nonlinear behavior ending with the power $n=0.349485$. The soil beneath the beam or beam-column behaves actually according to the mentioned five steps. The reason to stop of these processes at the last step is the small difference between the values of numerical method (finite difference method) and the exact solution (Laplace Transformation).

2.1 LAPLACE TRANSFORMATION METHOD

In this section, the Laplace transformation method is used to find the deflections of beam rested on linear elastic foundation. To apply this method, the basic principle is defined as $F(s)$ be a given function. The Laplace transform $F(s)$ of function $f(t)$ is defined by

$$\mathrm{L}\{f(x)\} = \int_0^\infty e^{-sx} f(x)dx,\ s > 0 \tag{6}$$

By rearranging the fourth order differential equation in Eq. (2), the equation can be written as

$$y^{(4)}(x) + 4\beta^4 y(x) + \alpha^2 y''(x) = \frac{w(x)}{EI} \tag{7}$$

where, $4\beta^4 = k/EI$ (k is the foundation modulus) and $\alpha^2 = P_\alpha / EI$ (P_α is the axial applied load at the beam ends). By taking the Laplace transformation for the fourth order differential equation in Eq. (7) under constant value of the distributed load $w(x)$, the equation becomes

$$f(s) = \frac{EIs\left(\left(\alpha^2 + s^2\right)\left(sy(0) + y'(0)\right) + sy''(0) + y'''(0)\right) + w}{(EIs)\left(4\beta^4 + s^4 + \alpha^2 s^2\right)} \tag{8}$$

For simply supported beam rested on elastic foundation under axial load at the ends of the beam, the boundary conditions at the ends which satisfying the Eq. (8) are deflection and moment equal to zero ($y(0) = y(l) = y''(0) = y''(l) = 0$) and Eq. (8) can be written as

$$f(s) = \frac{w + EIs\left(c_2 + c_1\left(s^2 + \alpha^2\right)\right)}{EIs\left(s^4 + s^2\alpha^2 + 4\beta^4\right)} \tag{9}$$

where $c_1 = y'(0)$ and $c_2 = y''(0)$. In addition, by applying the boundary conditions for the fixed-fixed beam with axial load at the ends with taking the deflection and slope at the ends equal to zero ($y(0) = y(l) = y'(0) = y'(l) = 0$), Eq. (8) can be written as

$$f(s) = \frac{w + EIs(c_2 + c_1 s)}{EIs(s^4 + s^2\alpha^2 + 4\beta^4)} \tag{10}$$

where $c_1 = y''(0)$ and $c_2 = y'''(0)$.

3. NUMERICAL EXAMPLES

The aim of this section is to validate the solution procedure for the determination of the beam deflection rested on elastic foundation. To do so, several examples of the analysis of beam columns are illustrated based on the analytical and numerical solutions. The first example explains beam ($\alpha = 0.0$) and beam-column ($\alpha = 1.0$) with simply supported on elastic foundations while the second one is treating with beam and beam-column with fixed ends. For the both examples, the parameters are selected as a following data: $k = 1.0$, $k = 2.0$, $EI = 1.0$, $P_u = 10.0$ and $L = 1.0$. The constants for simply supported and fixed-fixed respectively are $c_1 = 0.0412493$, $c_2 = 0.0412493$ and $c_1 = 0.0831848$, $c_2 = -0.499307$. These constants are used for Laplace transformation method in Eqs. (9) and (10). The results in the Figs. 7-14 show deflection by using analytical method for both beam and beam-column in the case of simply supported and fixed-fixed conditions. Tables (1) and (2) show the numerical deflection of beam and beam-column on elastic foundation for both simply supported and fixed-fixed, respectively based on central difference of finite difference method. Tables (3) and (4) represent stiffness values and corresponding deflection which should be used in the tangent equation at each level for simply supported beam. In addition, tables (5) and (6) show the stiffness values and corresponding deflection for fixed-fixed beam rested on nonlinear foundation, respectively.

TABLE 1.

Numerical deflection of simply supported beam and beam-column on elastic foundation (m).

Divided length, m	Deflection $k=1,\ \alpha=0$	Deflection $k=2,\ \alpha=0$	Deflection $k=1,\ \alpha=1$	Deflection $k=2,\ \alpha=1$
0.0	0.000000	0.000000	0.000000	0.000000
1/6	0.006680	0.006611	0.007437	0.007351
2/6	0.011451	0.011330	0.012760	0.012611
3/6	0.013168	0.013029	0.014679	0.014506
4/6	0.011451	0.011330	0.012760	0.012611
5/6	0.006680	0.006611	0.007437	0.007351
6/6	0.000000	0.000000	0.000000	0.000000

TABLE 2.

Numerical deflection of fixed-fixed beam and beam-column on elastic foundation (m).

Divided length, m	Deflection $k=1,\ \alpha=0$	Deflection $k=2,\ \alpha=0$	Deflection $k=1,\ \alpha=1$	Deflection $k=2,\ \alpha=1$
0.0	0.000000	0.000000	0.000000	0.000000
1/6	0.001123	0.001120	0.001148	0.001145
2/6	0.002566	0.002559	0.002634	0.002627
3/6	0.003175	0.003167	0.003263	0.003255
4/6	0.002566	0.002559	0.002634	0.002627
5/6	0.001123	0.001120	0.001148	0.001145
6/6	0.000000	0.000000	0.000000	0.000000

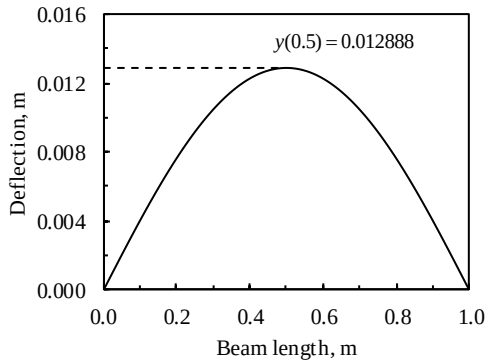

FIGURE 7. Analytical deflection of simply supported beam on linear elastic foundation with $k=1$ and $\alpha=0$.

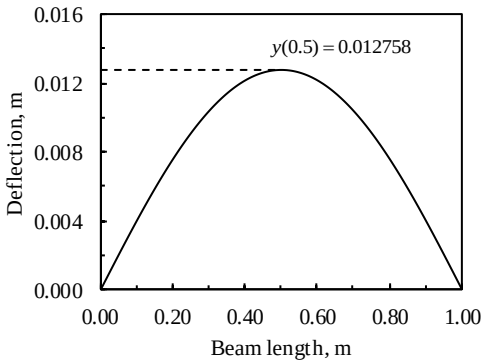

FIGURE 8. Analytical deflection of simply supported beam on linear elastic foundation with $k=2$ and $\alpha=0$.

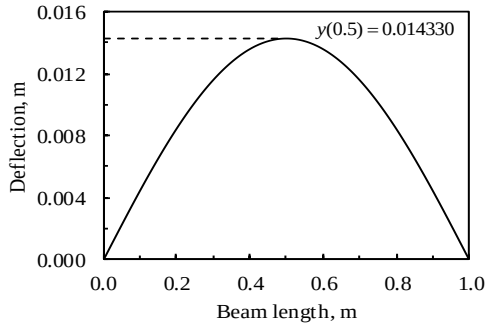

FIGURE 9. Analytical deflection of simply supported beam-column on linear elastic foundation with $k=1$ and $\alpha=1$.

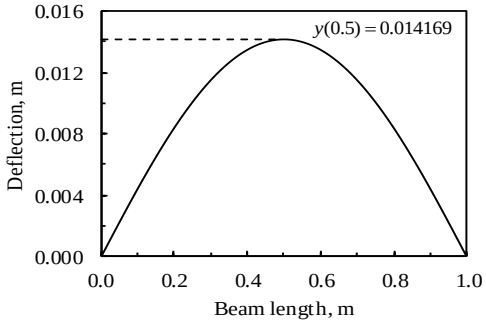

FIGURE 10. Analytical deflection of simply supported beam-column on linear elastic foundation with $k=2$ and $\alpha=1$.

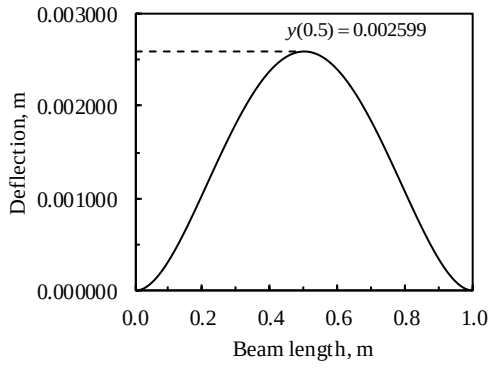

FIGURE 11. Analytical deflection of fixed-fixed beam on linear elastic foundation with $k=1$ and $\alpha=0$.

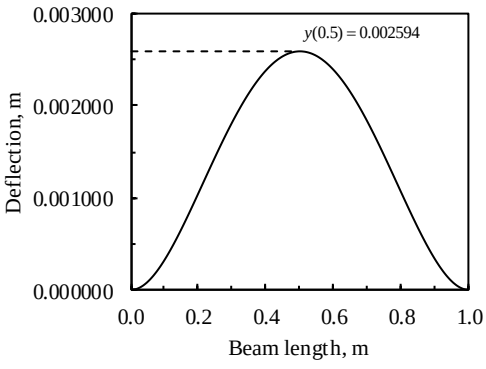

FIGURE 12. Analytical deflection of fixed-fixed beam on linear elastic foundation with $k=2$ and $\alpha=0$.

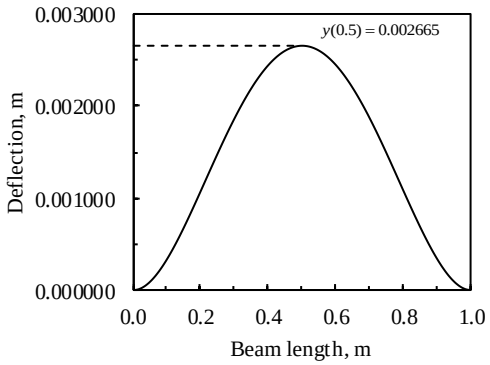

FIGURE 13. Analytical deflection of fixed-fixed beam on linear elastic foundation with $k=1$ and $\alpha=1$.

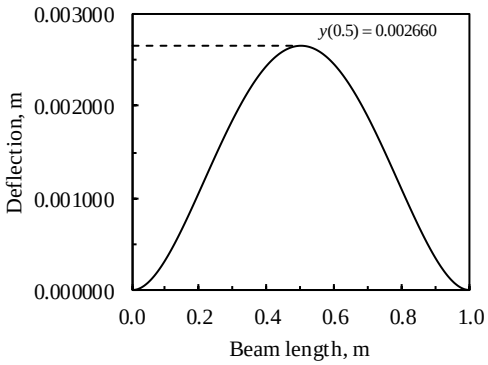

FIGURE 14. Analytical deflection of fixed-fixed beam on linear elastic foundation with $k=2$ and $\alpha=1$.

TABLE 3.

Stiffness of load per unit area and deflection curve for simply supported beam (kN/m^2).

Beam length, m	${}^1k$	${}^2k$	${}^3k$	${}^4k$	${}^5k$
0.10	10.0000	43.2154	71.7068	60.8176	70.5617
0.25	10.0000	35.8092	54.8407	44.3825	49.7651
0.5	10.0000	34.1072	51.1660	40.9110	45.4655
0.75	10.0000	35.8092	54.8407	44.3825	49.7651
1.00	10.0000	43.2154	71.7068	60.8176	70.5617

TABLE 4.

Deflection of simply-supported beam rested on nonlinear foundation for five iterations (m).

Beam length, m	${}^1u$	${}^2u$	${}^3u$	${}^4u$	${}^5u$
0.10	0.000610	0.001216	0.003161	0.003396	0.004345
0.25	0.001045	0.002078	0.005401	0.005808	0.007432
0.5	0.001201	0.002387	0.006204	0.006674	0.008540
0.75	0.001045	0.002078	0.005401	0.005808	0.007432
1.00	0.000610	0.001216	0.003161	0.003396	0.004345

TABLE 5.

Stiffness of load per unit area and deflection curve for fixed-fixed beam (kN/m^2).

Beam length, m	^1k	^2k	^3k	^4k	^5k
0.10	10.0000	16.7481	57.3219	110.6000	145.3530
0.25	10.0000	14.7920	42.9680	73.3240	89.7250
0.5	10.0000	14.3261	39.8927	65.9587	79.2439
0.75	10.0000	14.7920	42.9680	73.3240	89.7250
1.00	10.0000	16.7481	57.3219	110.6000	145.3530

TABLE 6.

Deflection of fixed-fixed beam rested on nonlinear foundation for five iterations (m).

Beam length, m	^1u	^2u	^3u	^4u	^5u
0.10	0.000110	0.000272	0.000511	0.000718	0.000925
0.25	0.000251	0.000620	0.001162	0.001632	0.002102
0.5	0.000310	0.000767	0.001437	0.002016	0.002596
0.75	0.000251	0.000620	0.001162	0.001632	0.002102
1.00	0.000110	0.000272	0.000511	0.000718	0.000925

4. CONCLUSIONS

In this study, a finite difference method for the analysis of beam and beam-column resting on nonlinear elastic foundation is formulated based on the iterative procedure. In addition, to control the accuracy of the numerical method, exact solution for beam and beam-column of Euler-Bernoulli on a nonlinear elastic foundation is investigated based on the proposed formula in Eq. (1). The nonlinear load-displacement curve of the soil is plotted at each of the load step with determining the power n at each of load level. With applying the finite difference procedures at each load level, the displacements corresponding to it are determined then used in Eq. (3) to find the next level displacements under the equal of point

load at each of the five interior nodes. The iterative procedure converges rapidly to the solution after the fifth trail because the value of the power n decreases with the advance steps and the curve approaches to the ideal curve path of soil. The final strain of the soil behavior at all levels is selected as a constant value ($\varepsilon = 0.01$) and the value of the power (n) is determined at each load level. Accuracy is controlled by using the Laplace Transformation method with the inverse Eq. (10) which refer to the closed form solution. Two examples are solved for both beam and beam-column based on Euler-Bernoulli theory which show the characteristic features for applying the both methods. The analytical method using Laplace transformation is idealized in the figures with evaluating maximum displacement for all cases. It is shown that, for a twice stiffness value of beam and beam-column, the foundation deflections are reduced for simply supported and fixed-fixed ends. On the other hand, the deflections increase in the case of beam-column which refers to presence of axial load ($\alpha = 1$) than in the case of beam only ($\alpha = 0$). Moreover, the deflection of foundation rested on nonlinear soil behavior and the effect of compression axial with simply supported ends is greater than that for the fixed-fixed ends.

ACKNOWLEDGEMENTS

The author wishes to thank Associate Prof. Dr. Hakan Argeso from the Department of Manufacturing Engineering at Atilim University, Ankara-Turkey, for his valuable help and support.

REFERENCES

[1] R. D. Cook, Concepts and applications of finite element analysis, John Wiley & Sons, 2007.

[2] Miyahara, F., & Ergatoudis, J. G., "Matrix analysis of structure-foundation interaction," Journal of the Structural Division, vol. 102, no. 1, pp. 251-265, 1976.

[3] Eisenberger, M., Yankelevsky, D. Z., & Clastornik, J., "Stability of beams on elastic foundation," Computers & structures, vol. 24, no. 1, pp. 135-139, 1986.

[4] Zhaohua, F., & Cook, R. D., "Beam elements on two-parameter elastic foundations," Journal of Engineering Mechanics, vol. 109, no. 6, pp. 1390-1402, 1983.

[5] Yankelevsky, D. Z., & Eisenberger, M., "Analysis of a beam column on elastic foundation," Computers & structures, vol. 23, no. 3, pp. 351-356, 1986.

[6] Cheung, Y. K., Tham, L. G., & Guo, D. J., "Applications of finite strip and layer methods in micro-computers," in International Conference on Numerical Methods in Geomechanics (ICONMIG), 1985.

[7] Oskoorouchi, A. M., Novrouzian, B., De Roeck, G., & Van Den Broeck, J., "Zoned finite strip method and its applications in geomechanics," Computers and Geotechnics, vol. 11, no. 4, pp. 265-294, 1991.

[8] Huang, M. H., & Thambiratnam, D. P., "Analysis of plate resting on elastic supports and elastic foundation by finite strip method," Computers & Structures, vol. 79, no. 29, pp. 2547-2557, 2001.

[9] Chow, Y. K., Swaddiwudhipong, S., & Phoon, K. F., "Finite strip analysis of strip footings: Horizontal loading," Computers and Geotechnics, vol. 8, no. 1,

pp. 65-86, 1989.

[10] Vallabhan, C. G., & Das, Y. C., "Parametric study of beams on elastic foundations," Journal of engineering mechanics, vol. 114, no. 12, pp. 2072-2082, 1988.

[11] Omurtag, M. H., Özütok, A., Aköz, A. Y., & OeZCELİKOeRS, Y. U. N. U. S., "Free vibration analysis of Kirchhoff plates resting on elastic foundation by mixed finite element formulation based on Gateaux differential," International Journal for Numerical Methods in Engineering, vol. 40, no. 2, pp. 295-317, 1997.

[12] Binesh, S. M., "Analysis of beam on elastic foundation using the radial point interpolation method," Scientia Iranica, vol. 19, no. 3, pp. 403-409, 2012.

[13] Sato, M., Kanie, S., & Mikami, T., "Mathematical analogy of a beam on elastic supports as a beam on elastic foundation," Applied Mathematical Modelling, vol. 32, no. 5, pp. 688-699, 2008.

[14] Jumel, J., Budzik, M. K., & Shanahan, M. E., "Beam on elastic foundation with anticlastic curvature: Application to analysis of mode I fracture tests," Engineering Fracture Mechanics, vol. 78, no. 18, pp. 3253-3269, 2011.

[15] Borák, L., & Marcián, P., "Beams on elastic foundation using modified Betti′ s theorem," International Journal of Mechanical Sciences, vol. 88, pp. 17-24, 2014.

EXPERIMENTAL STUDY ON HARDENED PROPERTIES OF HIGH STRENGTH CONCRETES CONTAINING METAKAOLIN AND STEEL FIBER

Barham Haidar Ali[1], Arass O. Mawlod[2], Ganjeena Jalal Khoshnaw[3], Junaid Kameran[4]

[1,3&4]*Ishik University, Erbil, KRG, Iraq*
[2]*University of Raparin, KRG*
[3]*ErbilPolytechnic University*
[1]*Barham.haydar@ishik.edu.iq,* [2]*aras.omar@uor.edu.krd,* [3]*ganjeena.jalal@ishik.edu.iq*

doi:10.23918/iec2018.19

ABSTRACT

In this paper the outcomes of an experimental research on mechanical properties of conventional concrete and a concrete incorporated metakaolin (MK) with and without steelfiber. One of the ingredients of the concrete mixture was metakaolin; Portland cement was partially substituted with metakaolin (MK) as 10% by weight of the total binder content. Steel fibers with length/aspect ratios of 60/80 and hook ended was embedded into the concrete to make fiber reinforced concretes. Value of water/binder ratios (w/b) was 0.35. To know the impacts of MK and steelfiber, the mechanical behaviors of the concrete were investigated such as: compressive, flexure, and bonding strength of the concretes. At the age of 28 days in room temperature, tests were held. The level of the significance of the variance on the hardened properties of concrete was achieved through the calculation of the experimental results.

Keywords: Bonding strength; Compressive strength concrete; Metakaolin; Steel fiber; Flexure strength.

1. INTRODUCTION

Concrete is the most commonly used building material all over the world because of its versatility and availability. Especially reinforced concrete structural elements have been indispensable parts of construction works due to the ease in erection and relatively lower cost than the other structural materials. The proper adherence between reinforcingbars and concrete is the most desired feature because of the fact that structural capacity of reinforcedconcrete members depends on the monolithic behavior. The prominent component controlling the competence of the bond is mostly the quality of concrete. Because the reinforcing steel bars are obtained from a fixed manufacturing process and the properties do not significantly fluctuate compared to concrete. However, structural concretes have many different characteristics depending mainly on the amount and type of the ingredients [1]. It is reported that concrete with improved mechanical property has superior adherence with reinforcing steel bars [2]. apart from its excellent properties, concrete shows a rather low performance when subjected to tensilestress. For this reason, the utilization of fibers to provide enhancement in tensile strength behavior of concrete has attracted the interest of the researchers [3-9]. Mechanicalproperties of concrete can be improved by exploitation of reinforcement with randomlyoriented short separated fibers, which obstruct and/or control initiation and propagation of cracks. Fiber reinforced concrete (FRC) can keep on resisting much amount of loads even at deflections. The characteristics and performance of FRC varies depending on matrix properties as well as the fibermaterial, fiber concentration, fiber geometry, fiberorientation, and distribution of fiber [8]. in order to enhance the mechanical properties, particularly compressive strength, use of some pozzolanic materials has been studied by researchers for many years [10-16]. Pozzolans, like silica fume and fly ash, are the most usual known mineral admixtures utilized in manufacturing of high-strength concrete. These materials grant extra performance to the concrete by reacting with Portland cement hydration products to form secondary C-S-H gel, the main function part of the paste are providing strength for concrete [17].In previous two decades, there has been a growing attraction in the beneficiation of metakaolin (MK) as a supplementary cementing material in concrete to enhance its features. MK is an ultrafine pozzolana, manufactured by calcination of purified kaolin clay at a temperature ranging from 650 to 900 ^{o}C to separate the chemically bound water and

ruin the crystalline structure [18-19]. Unlike other industrial by-product materials, MK needs a thorough process of manufacturing. It has to be carefully refined to remove inert impurity and ground to particles of micron size. Research has shown that concrete mixtures containing high-reactivity MK present comparable performance to the ones with other mineral admixtures in terms of mechanical properties as well as permeability and durability properties [20-28]. Moreover, the use of this material is also environmentally friendly due to the reduction of CO_2 emission to the atmosphere by decreasing Portland cement consumption.

In this study, the integrated impact of MK and steel fiber on mechanical properties of concretes was examined through an experimental program. One water/binder (w/b) ratio has been applied to manufacture the concretes. For steel fiber reinforced concretes, steel fiber with length/aspect ratios of 60/80 was used. The steel fibers were supplemented to concrete with 0.25% and 0.75% of the volume of the concrete. The mechanical properties of the concretes were measured through compressive and flexural tensile strength testing at the end of 28 days of curing. Moreover, adherence between reinforcing steel bar and concrete were evaluated by means of bonding strength examine at the same age.

2. METHODOLOGY

2.1. MATERIALS

2.1.1 CEMENT

CEM I type Portland cement having specific gravity of 3.14 and Blaine fineness of 328 m^2/kg was used for making ready the concrete examine samples utilized indetermination of mechanical properties. The chemical composition of the cement as it is seen in Table 1.

2.1.2 Metakaolin

The metakaolin utilized in this research is a white powder with a Dr. Lange whiteness value of 87. It has a specific gravity of about 2.60, and specific surface area (Nitrogen BET Surface Area) of 18000 m2/kg. Physical and chemical properties of MK used in this research are also shown in Table 1. The source for obtaining the MK is from Czech Republic.

TABLE 1.

Features of Portlandcement and metakaolin.

	Item	Portland Cement	Metakaolin
Chemical properties	CaO (%)	62.58	0.5
	SiO_2 (%)	20.25	53
	Al_2O_3 (%)	5.31	43
	Fe_2O_3 (%)	4.04	1.2
	MgO (%)	2.82	0.4
	SO_3(%)	2.73	-
	K_2O	0.92	-
	Na_2O	0.22	-
	LOI (%)	1.02	0.4
Physical properties	Specific gravity	3.14	2.60
	Fineness (m^2/kg)	327*	18000**

* Blaine specific surface area
** BET specific surface area

2.1.3 AGGREGATE

Fine aggregate was a mix of river sand and crushed sand whereas the coarse aggregate was river gravel with a maximum particle size of 22 mm. Aggregates were gained from local sources. Properties of the aggregates are given in Table 2. Grading of the aggregate mixture was kept constant for all concretes. Figure 1. shows the gradation of aggregate.

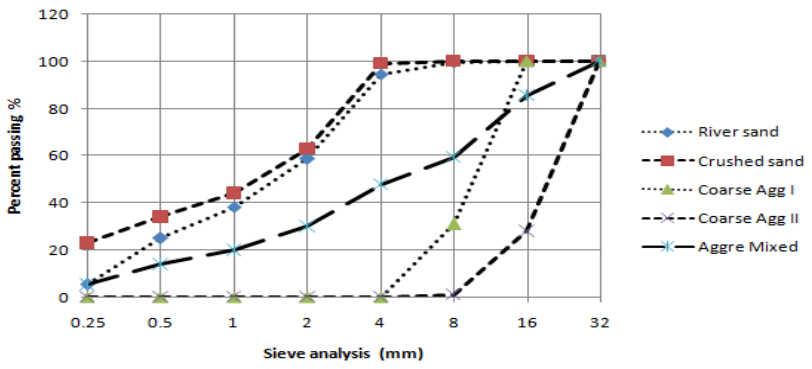

FIGURE 1. Grading of aggregate.

TABLE 2.

Sieveanalysis and physicalproperties of aggregates.

	Sievesize, (mm)	Passing (%)			
		FineAggregate		CoarseAggregate	
		River Sand	Crushed Sand	No I (4-16 mm)	No II (16-22 mm)
Sieve Analysis	31.5	100	100	100	100
	16.0	100	100	100	27.7
	8.0	99.7	100	31.5	0.6
	4.0	94.5	99.2	1.0	0.1
	2.0	58.7	63.3	0.5	0.0
	1.0	38.2	43.7	0.5	0.0
	0.50	24.9	28.4	0.5	0.0
	0.25	5.4	16.4	0.4	0.0
	Fineness modulus	2.87	2.57	5.66	6.72
Physical Properties	Specific gravity	2.79	2.42	2.72	2.73
	Absorption, %	0.55	0.92	0.45	0.42

2.1.4 SUPERPLASTICIZER

Sulphonated naphthalene formaldehyde based high range water-reducing admixture with specific gravity of 1.19 was employed to achieve slump value of 14±2 cm for the ease of handling, placing, and consolidation in all concrete mixtures. The superplasticizer was adjusted at the time of mixing to obtain the specified slump.

2.1.5 STEEL FIBER

One sorts of commercially available hooked end steel fibers (Dramix 60/80) was used for manufacturing of steel fiber reinforced concretes. The geometrical properties and aspect ratios of the steel fiber is given in Table 3.

TABLE 3.
Features of steel Fiber

Designation of the steel fibre	Diameter D (mm)	Length L (mm)	Aspect ratio (L/D)
SF	0.75	60	80

2.1.6 STEEL BAR

16 mm diameter of reinforcing ribbed steel bars used. The yield strength of 420 MPa were used for preparing the reinforced concrete samples to be utilized for examining the bonding strength.

2.2 . MIX PROPORTION

A series of concrete mixture with water-to-binder ratios of 0.35 was designed to manufacture plain and MK containing concretes. MK modified concretes were manufactured by 10% substitute of the cement with MK by the weight. For manufacturing of steel fiber (SF) reinforced concretes, a type of (SF) was supplemented to the concrete by 0.25% and 0.75% of the total concrete volume. Therefore, 6 various sorts of concrete mixtures were made for testing the mechanical properties of the concretes. The specification of the concrete mixtures are shown in Table 4. the designations of each mix were produced based on containing of MK , sort of steel fiber, and volume fraction of steelfiber. For instance, 10M 0.75SF name stands for the concrete containing 10% MK and 0.75% steel fiber (SF). Freshly poured concrete samples were enclosed with plastic sheet and stocked in laboratory at 21±2 ^{o}C for 24 hours. Then, the samples were removed from the mold and transferred to a water tank for curing up to 28th day.

2.3 . EXAMINING THE SAMPLES

The concrete samples having different dimensions were used for examining. Cubic samples having 150x150x150 mm were used for compressive strength. For three point flexural tensile strength testing, prismatic samples with 100x100x500 mm dimensions were used to ensure 450 mm span length for examining. Bonding strength between concrete and reinforcement was examined on cubic reinforced concrete sample. To ensure uniform load distribution, a smooth surface is required. So, the top surface of the pullout samples were capped with gypsum coating. The details and dimensions of the pullout examining samples are shown in Figure 2. For each examine, three samples were used. Each experimental variance was defined by averaging the results gained from those samples. All of examines were held at the end of 28 day curing period.

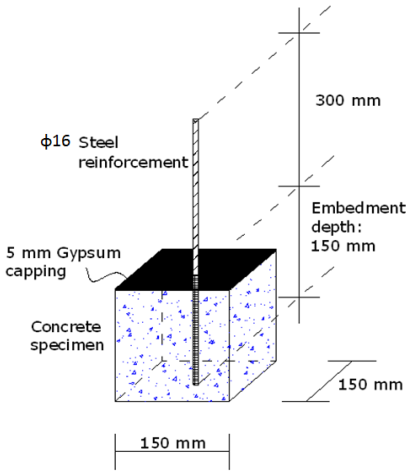

FIGURE 2. Details of the bondingstrength examined samples.

TABLE 4.

Plain and steel fiber reinforced concretes containing metakaolin (kg/m^3)

Mix ID	w/b ratio	Water	Cement	Metakaolin	FineAggregate		CoarseAggregate		SteelFiber	SP*
					Natural sand	Crushed sand	No I (4-16 mm)	No II (16-22 mm)	SF	
Control I	0.35	157.5	450	0	663.1	284.2	568.4	378.9	0 19.62 58.85 0 19.62 58.85	11.25
M0-25SF		157.5	450	0	663.1	284.2	568.4	378.9		12.5
M0-75SF		157.5	450	0	663.1	284.2	568.4	378.9		13.75
Control II		157.5	405	45	660.0	282.9	565.7	377.2		10
M10-25SF		157.5	405	45	660.0	282.9	565.7	377.2		11.25
M10-75SF		157.5	405	45	660.0	282.9	565.7	377.2		13

*SP:Superplastizer

2.4 . TEST METHODS

The compression test fitting to ASTM C39 [29] was held on the samples by a 3000 KN capacity testing machine. Three-point flexural tensile strength complying with ASTMC293 [30] was implemented to the prismatic samples through 100 kN capacity bending frame. Bonding strength of the concretes was found according to RILEM RC6 [31]. According to the standard the bonding strength, τ, is measured by dividing the tensile force by the surface area of the steelbar embedded in concrete (Equation 1). For this examine, a special modified test apparatus was established to 600 kN capacity universaltesting machine.

$$\tau = \frac{F}{\pi \times d \times L} \qquad \text{(Equation 1)}$$

Where F is the tensile load at failure (N), d and L are the diameter (mm) and embedment length (mm) of the reinforcing steel bar, respectively. In this research d and L are 16 mm and 150 mm, respectively.

3. RESULT AND DISCUSSION

In this paper, the mechanical properties of concrete are investigated the results are shown in the Table 5. each compressive strength, bond strength, and flexural strength are discussed in the following paragraphs.

TABLE 5.

Test results of the compressive, bond, flexural, and tensile strength.

w/b	Mixes	Com. Str. (MPa)	Bond Str. (MPa)	Flex. Str. (MPa)
0.35	0MK0SF	62.7	11.7	5.8
	0MK0.25SF	66	13.1	7.1
	0MK0.75SF	72	16	7.4
	10MK0SF	62.3	12.6	7.1
	10MK0.25SF	72.4	14	7.6
	10MK0.75SF	75.7	16.9	7.9

3.1. COMPRESSIVE STRENGTH

Figure 3.Shows the changes in compressive strength of the plain and MK contained concretes with the increase in the quantity of fiber reinforcement. Table 5, shows that the plain concretes compressive strength values were between 62.7 MPa and 72 MPa

for specified w/b ratios of 0.35, while MK contained ones had compressive strength values between 62.3 MPa for the previous and 75 MPa for the latter. The compressive strength results revealed that containing of MK had a slight impact on the compressive strength of the concretes. Same outcomes have been reported by previous authors [9, 22-27]. For instance, in the research of Güneyisi et al. [24] concretes containing 5% and 15% substitute level of MK yielded relatively recorded a higher value of strength than that of plain concretes. As it shown from the Figure 3, Rising the amount of SF concluded in ascending of the compressive strength of the concretes without depending on the addition of MK. Nili and Afroughsabet [8] stated that 28 day compressive strengths of plain concrete produced with w/b ratio of 0.46 were 41.30 MPa, 46.35 MPa, and 47.25 MPa for steel fiber volume fractions of 0%, 0.5%, and 1.0%, respectively. Moreover, the impact of steel fiber is also obviously illustrated in Figure 3. The higher the percentage of steel fiber, the higher the ascending in compressive strength was monitored, especially for MK contained ones. Forinstance, the plain concretes made with steel fiber volume fraction of 0.25% and 0.75% had 66 MPa and 72 MPa, respectively. However MK contained concretes with the same parameters and percentage of steel fiber had 72.4 MPa and 75.7 MPa, respectively.

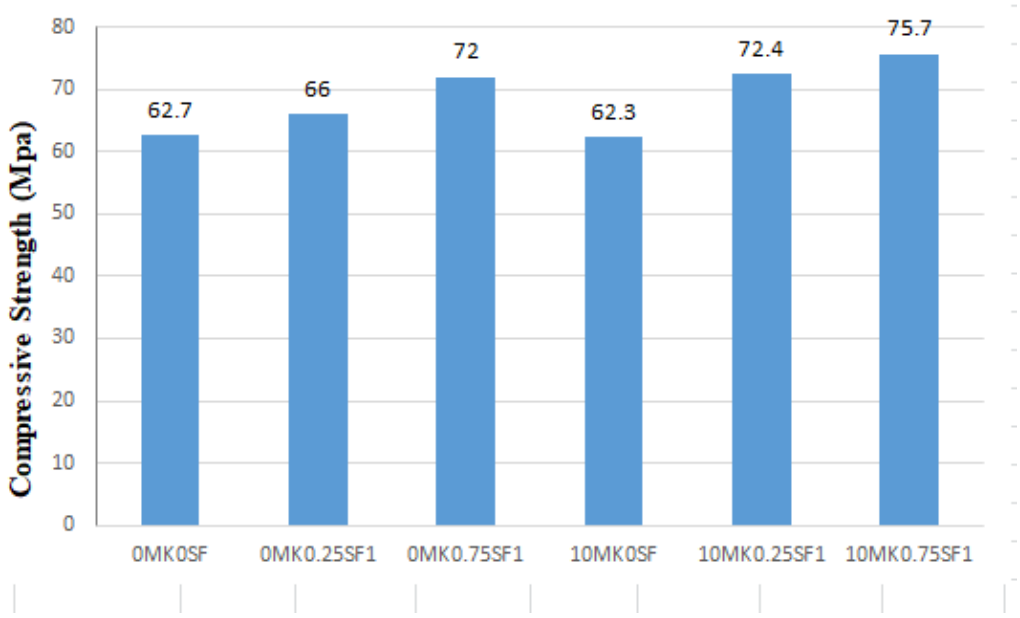

FIGURE 3. Effect of steel fiber and MK incorporated concretes on the compressive strength.

3.2 . TENSILE STRENGTH

The tensile strength of plain and MK included concretes were monitored with respect to flexure tensile strength. The test outcomes of flexural tensile strength examines are presented in Table 5, and figure 4 , respectively, to demonstrate the effectiveness of steel fiber reinforcement. It was stated that the main and importance contribution of the steel fibers was caused in increasing of flexural tensile strength capacity of the concrete [32]. Another distinguishable result from the tensile strength examining is that unlike previous results, the contribution MK with increasing SF was observed to be better. This condition may be attributed to the distribution of the steel reinforcement within the cement matrix. Namely, the short steel fiber, the more homogenous distribution may be achieved. Sanal and Özyurt [33] investigated the effect of orientation of steel fibers on the mechanical performance of the concretes. They reported that, short-cut steel fibers have a tendency to align in the flow direction and greater orientation density in the pouring direction resulted in a greater flexural toughness.

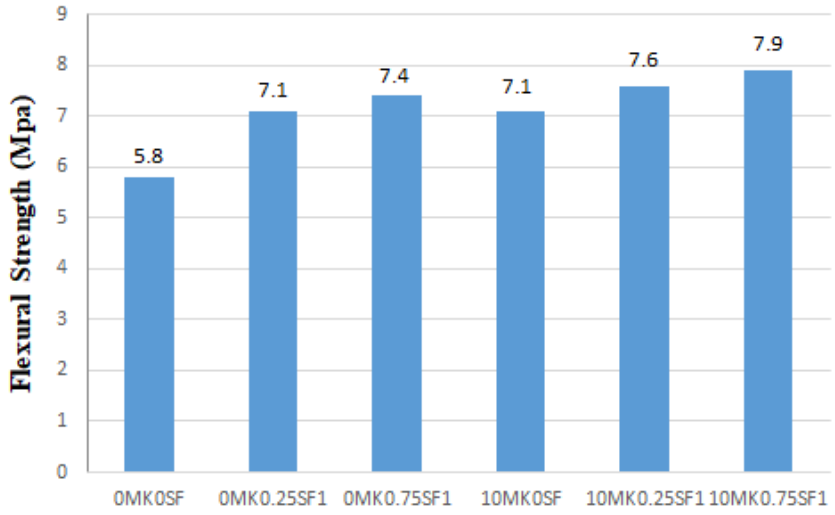

FIGURE 4. Effect of steel fiber and MK incorporated concretes on the three-point flexural strength.

3.3. BONDIN GSTRENGTH

Bonding strength of the concretes versus the amount of the steel fiber reinforcement is showed in Table (5) and plotted Figure 5. The figure depicted that the ascending in the volume fraction of SF concluded in great change in the bonding strength. The observation seems to be applicable to 0% and 0.75% use of steel fiber. Nevertheless, inclusion of MK to the concretes imparted additional performance in terms of bonding strength. For instance, the highest bonding strength for MK modified concretes was monitored as 16.9 MPa, while the minimum value for plain concrete was monitored as 12.5 MPa. Therefore, 35% improvement in bonding strength capacity was achieved by combined inclusion of MK and steel fibers. Baran et al. [34] stated that steelfibers improve the pull-out resistance of strands by controlling the crack growth inside concrete blocks. They reported that, by this method, the grade of confinement at the strand-concrete interface was ascended, which concluded in enhancement in both friction and mechanical bond components of the resistance. Their outcomes also displayed that more than 30% ascending was acquired in pull-out strength due to fiber reinforcement. Being one of the most known mineral admixtures MK is known to have comparable contribution to the mechanical and durability performance of concretes as silica fume does [22, 24, 25]. However, the studies regarding the effect of inclusion of MK on the bonding strength between concrete and steel bars has not yet attracted the adequate attention. The former outcomes introduced for silica fume included steel fiber reinforced concretes may underlined the impact of usage of MK for this purpose. In the research of Chan and Chu [35], the impact of silica fume on the bond properties of steel fiber in matrix of reactive powder concrete (RPC) were investigated. They carried out pullout tests in their experimental program, with the silica fume inclusion as the parent variable. They pointed out that the inclusion of silica fume in RCP matrix greatly improve the fiber–matrix bond. Abu-Lebdeh et al [36] also brought to light that the quality of matrix has pronounced significance on the bonding and tensile strain capacity of steel fibers in high strength concrete. Consequently, owing to its superior increment in cemen tmatrix as an outcome of pore size refinement [28], MK assured enhancement in the pullout capacity of the reinforced concretes.

Photographic views of the pullout samples examined in this research are presented in Figure 6. As it is shown, after failure, the reinforcing steel bars were separated from

the concretes without steel fiber, whereas steel fiber reinforced concretes did not extricate the steel bars.

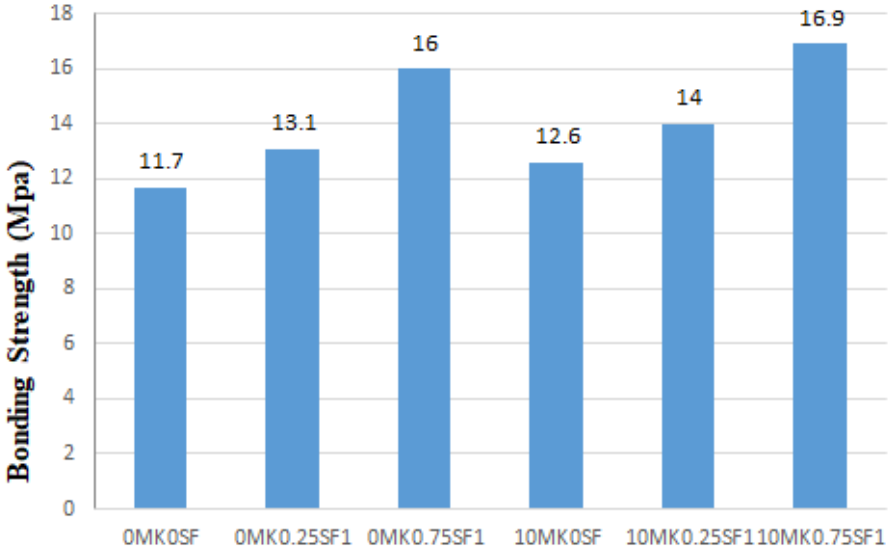

FIGURE 5. Effect of steelfiber and MK incorporated concretes on the bondstrength.

(a) (b)

FIGURE 6. Typical failurepatterns of concretes a) without fiberreinforcement and b) withfiber reinforcement.

3. CONCLUSION

The following outcomes are achieved according to the experimental outcomes presented above.

- The use of MK as a substitute material resulted in enhanced mechanical properties of concretes compared to plain ones for the given w/b ratios. The outcomes show that the incorporating of MK mainly impacts on increasing of bonding strength. A slight impact of MK incorporation is recorded for compressive and flexural tensile strength. The content of steel fibers also contributed to the compressive strength. The steel fibers (SF) provided higher compressive strength improvement with ascend in volume fraction. The grade of enhancement was more prominent for MK concretes than plain ones.
- By incorporation of steel fibers significant enhancement in bonding and tensile strength capacities of the concretes were observed. The steel fibers with higher volume fraction of steel fibers (SF) demonstrated higher development in bonding strength. These impacts of steel fiber reinforced concretes may be attributed to the dispersion and orientation of the steel fibers within the concrete.

REFERENCES

[1] Mehta PK, Monteiro PJM. (2006).Concrete: Microstructure, Properties, and Materials. 3rd Edn, McGraw-Hill, USA.

[2] Ersoy U, Özcebe G, Tankut T. (2003). Reinforced concrete. METU Press. Ankara, Turkey.

[3] Bentur A, Mindess S, Diamond S. (1985). Pull out processes in steel fiber reinforced cement, International Journal of Cement Composites & Lightweight Concrete . 7(1), 29-38.

[4] Barros JAO, Cruz JS. (2001). Fracture energy of steel fiber-reinforced concrete. Mechanics of Composite Materials and Structures. 8 (1), 29–45.

[5] Banthia N, Trottier JF. (1995). Concrete reinforced with deformed steel fibres. Part II: Toughness characterization. ACI Materials Journal. 92 (2), 146-154.

[6] Khayat KH, Roussel Y. (2000). Testing and performance of fiber reinforced, self-consolidating concrete. Materials and Structures. 33, 391 – 397.

[7] Quian CX, Stroeven P. (2000). Development of hybrid polypropylene-steel fibre reinforced concrete. Cement and Concrete Research. 30, 63-69.

[8] Yurtseven AE. (2004). Determination of mechanical properties of hybrid fiber reinforced concrete. MSc thesis, METU, Ankara, Turkey.

[9] Nili M, Afroughsabet V. (2012). Property assessment of steel–fibre reinforced concrete made with silica fume. Construction and Building Materials. 28, 664–669.

[10] Güneyisi E, Gesoğlu M, Mermerdaş K. (2008). Improving strength, drying shrinkage, and pore structure of concrete using metakaolin. Materials and Structures. 41, 937-949.

[11] Al-Khaja WA. (1994). Strength and time-depended deformations of silica fume concrete for use in Bahrain. Construction and Building Materials. 8, 169-172.

[12] Brooks JJ, MegatJohari MA, Mazloom M. (2000). Effect of admixtures on the setting times of high-strength concrete. Cement Concrete Composites. 22 ,293-301.

[13] Hooton RD. (1993). Influence of silica fume replacement of cement on physical properties and resistance to sulfate attack, freezing and thawing, and alkali silica reactivity. ACI Material Journal. 90, 143–151.

[14] Chindaprasirt P, Homwuttiwong S, Sirivivatnanon V. (2004). Influence of fly ash fineness on strength, drying shrinkage and sulfate resistance of blended cement mortar. Cement and Concrete Research. 34, 1087-1092.

[15] Khatri RP, Sirivivatnanon V, Yu LK. (1997). Effect of curing on water permeability of concretes prepared with normal Portland cement and with slag and silica fume. Magazine of Concrete Research. 49, 162-172.

[16] Ramezanianpour AA, Malhotra VM. (1995). Effect of curing on the compressive strength, resistance to chloride ion penetration and porosity of concretes incorporating slag, fly ash, or silica fume. Cement Concrete Composites. 17, 125–33.

[17] Neville AM.(1996). Properties of Concrete, 4th and final ed., Addison Wesley Logman, England.

[18] Kakali G, Perraki T, Tsivilis S, Badogiannis E. (2001). Thermal treatment of kaolin: the effect of mineralogy on the pozzolanic activity. Applied Clay Science. 20, 73-80.

[19] Al-Akhras NM. (2006). Durability of metakaolin concrete to sulfate attack. Cement Concrete Research. 36, 1727–1734.

[20] Coleman NJ, Page CI. (1997). Aspect of the pore solution chemistry of hydrated cement pastes containing metakaolin. Cement Concrete Research. 27, 147-154.

[21] Brooks JJ, Johari MAM. (2001). Effect of metakaolin on creep and shrinkage of concrete. Cement Concrete Composites. 23, 495-502.

[22] Boddy A, Hooton RA, Gruber KA. (2001). Long-term testing of the chloride-penetration resistance of concrete containing high-reactivity metakaolin. Cement Concrete Research. 31, 759-765.

[23] Ding JT, Li Z. (2002). Effects of metakaolin and silica fume on properties of concretes. ACI Materials Journal. 99, 393-398.

[24] Güneyisi E, Mermerdaş K. (2007). Comparative study on strength, sorptivity, and chloride ingress characteristics of air-cured and water-cured concretes modified with metakaolin. *Materials and Structures*. 40, 1161-1171.

[25] Güneyisi E, Gesoğlu M, Karaoğlu S, Mermerdaş K. (2012). Strength, permeability and shrinkage cracking of silica fume and metakaolin concretes. Construction and Building Materials. 34, 120-130.

[26] Poon CS; Kou SC, Lam L. (2006). Compressive strength, chloride diffusivity and pore structure of high performance metakaolin and silica fume concrete, Construction and Building Materials. 20 (10), 858-865.

[27] Kim HS, Lee SH, Moon HY. (2007). Strength properties and durability aspects of high strength concrete using Korean metakaolin. Construction and Building Materials. 21, 1229-1237.

[28] D.S. Klimesch, A. Ray, (1998). Autoclaved cement– quartz pastes with metakaolin additions. Advanced Cement Based Mater. 7, 109–118.

[29] ASTM C39/C39M-12. (2012). Standard test method for compressive strength of cylindrical concrete specimens annual book of ASTM Standard, Vol. 04-02, 7 pages. Philadelphia, USA.

[30] ASTM C293/C293M-10 (2012). Standard test method for flexural strength of concrete (Using simple beam with center-point loading) Annual Book of ASTM Standard, Vol. 04-02, 3 pages. Philadelphia, USA.

[31] RILEM RC 6, (1996). Recommendations for the testing and use of constructions materials bond test for reinforcement steel. 2. Pull-out test, 3 pages

[32] KayaliO, Haque MN, Zhu B. (2003). Some characteristics of high strength fiber reinforced lightweight aggregate concrete. Cement and concrete composites .25, 207–213.

[33] Sanal İ, Özyurt N. (2010). Effects of formwork dimensions on the mechanical performance of fiber-reinforced cement based materials,9th International Congress on advances in civil engineering, 27-30 Karadeniz Technical University, Trabzon, Turkey.

[34] Baran E, Akis T, Yesilmen S. (2012). Pull-out behavior of prestressing strands in steel fiber reinforced concrete. Construction and building materials. 28, 362–371.

[35] Chan Y, Chu S. (2004). Effect of silica fume on steel fiber bond characteristics in reactive powder concrete. Cement Concrete Research. 34.1167–1172.

[36] Abu-Lebdeh T, Hamoush S, Heard W, Zornig B. (2011). Effect of matrix strength on pullout behavior of steel fiber reinforced very-high strength concrete composites. Construction and Building Materials. 25, 39–46.

PREDICTION OF CBR AND MR OF FINE GRAINED SOIL USING DCPI

Alle A. Hussein[1],Younis M. Alshkane[2]

[1&2]*University of Sulaimani, Kurdistan Region, Iraq*
[1]*alle.hussein@univsul.edu.iq*

doi:10.23918/iec2018.20

ABSTRACT

Determining the in-situ engineering properties such as Modulus of Resilient (Mr), California Bearing Ratio (CBR) and for some subgrade materials in road construction has always been an economic challenge for geotechnical engineers. Therefore, a number of in-situ tests have been developed to overcome this challenge. One of the most adaptable techniques that can be used to predict geotechnical properties of soils economically is Dynamic Cone Penetration Index test (DCPI). It is accomplished by dropping 8-kg hammer over a height of 575mm and assessing the penetration depth of a 60° cone tip with 20 mm base diameter into the ground per blow for each tested depth. In this paper, the empirical equations to predict CBR and Mr of fine-grained soil using DCPI were reviewed and revised based on data obtained from the literature review. Based on the statistical analysis, two empirical equations were proposed to predict CBR and Mr. The obtained results verify the reliability of the modified equations. Also, the correlation between DCPI and dry density of fine-grained soils was studied.

Keywords: DCPI, CBR, Resilient Modulus, Dry Unit Weight, Water Content, Cohesive Soil.

1. INTRODUCTION

CBR and Mr of subgrade materials are crucially required to design subbase and base of road constructions. Usually, the values of these parameters are determined from the laboratory tests. However, laboratory tests demand a significant effort as well as time consuming. The simple alternative method is to use the Dynamic Cone Penetration Index (DCPI). A comprehensive undisturbed sample can be defined as a soil with an in-place structure that is absolutely unchanged. Such samples are vital for the laboratory tests that examine the structures of the soil. Yet, several issues make it practically incredible to obtain a justly undisturbed sample. In concern to those issues, various techniques have been developed to conduct in-situ tests such as dynamic cone penetrometer device (DCP), which is initially developed by Scala [1]. DCPI has been used to characterize sites of pavement layers and subgrades. The degree of compaction, water content, California bearing ratio and resilient modulus (Mr) are the major technical keys that significantly affect the for subgrade's resistance to deformation[2,3,4]. DCP device is well-known for its easiness to operate with low costs, superiority to provide consistent results, and rapid assessment of soil properties. It is significantly cheaper and faster than digging bore holes, mainly when the depth of examination is low and the soils being explored are not gravel materials [5, 6]. Nevertheless, sometimes false values are obtained in the field when piston tip rests on a small stone unit or pebble. Furthermore, it should always be kept in mind that DCP measured parameters are gained at natural water content. when relating these values back to those determined in the laboratory, the mentioned circumstances must be taken into consideration.

2. CBR PREDICTION FROM DCP

CBR is measured by converting pavement unbound material strength values which result from cone penetration resistance [7]. In 1969, the results of DCPI were correlated with CBR values by Van Vuuren [7]. The United States Army Corps of Engineers (USACE) [8] found a relationship between CBR) and DCPI* that was generally used by geotechnical engineers.

$$CBR = 292/(DCPI)^{1.12} \quad (1)$$

Webster et al. [8] as reported by Mejías-Santiago et al. [7] developed the following Equations (2 and 3) to take into account the plasticity of soils as high plasticity (CH) clays and low plasticity clays (CL) of CBR values smaller than 10%:

$$CBR = 1/ (0.017019 \times DCPI)^2 \quad \text{for CL soils CBR<10} \quad (2)$$

$$CBR = 1/ (0.002871 \times DCPI) \quad \text{for CH soils} \quad (3)$$

These empirical equations are accepted by many agencies and experts. These equations are used in ASTM D6951 for predicting CBR using DCPI. Similar relationships are found in literature based on both laboratory and field measurements of CBR. Table 1 presents the empirical equations to estimate CBR from DCPI value.

TABLE 1.
DCP and CBR relationships obtained from literature [7]

References	Correlation (DCPI in mm/blow)	Type of study
Livneh [9]	$\log CBR = 2.20 - 0.71 (\log DCPI)^{1.5}$	Lab
Harison [10]	$\log CBR = 2.81 - 1.32 \log DCPI$	Lab
Gabr et al. [11]	$\log CBR = 1.4 - 0.55 \log DCPI$	Both
Abu-Farsakh et al [12]	$CBR = 1{,}161.1/(DCPI)^{1.52}$	Both
George et al. [13]	$\log CBR = 1.68 - 0.78 \log DCPI$	Field
Patel and Patel [14]	$CBR = 24.903/(DCPI)^{1.331}$	Lab

*Some references use the abbreviation (PR) instead of (DCPI).

3. PREDICTION OF Mr FROM DCPI

Determining resilient modulus from laboratory tests is time consuming, expensive and involves high-quality undisturbed samples. As an alternative, the DCPI is a suitable method to estimate the modulus value in the field because of its simplicity and portability. Literature found many empirical correlations that connect the value of CBR to value of DCPI. Heukelom and Klomp [15] proposed the linear equation as given by Equation 4 for cohesive soils having a CBR value of less than or equal to 10. Powell et al. [16] suggested Equation 5 as an alternative one between CBR and resilient modulus which is suitable for CBR values of 2 to 12. Various relationships were found by researchers are presented in Table 2.

$$M_r\ (MPa) = 10.34\ CBR \quad (4)$$

$$M_r\ (MPa) = 17.58\ CBR^{0.64} \quad (5)$$

TABLE 2.

DCP and Mr relationships obtained from literature [7]

Reference	Correlation DCPI in mm/blow and Mr in MPa	Type of study
Chen et al. [17]	$M_r = 338/DCPI^{0.39}$	Field
Chen et al. [18]	$M_r = 537.76/DCPI^{0.66}$	Field
Abu-Farsakh et al. [12]	$\ln(M_r) = 2.35+(5.21/\ln(DCPI))$	Field
Herath et al. [19]	$M_r = 16.28+(928.24/DCPI)$	Both
Nazzal et al. [20]	$M_r =5,301.54/(DCPI^{1.44}+8.31)$	Field
Mohammad et al. [21]	$M_r =151.80/DCPI^{1.10}$	Both
George et al . [13]	$M_r =600.61/DCPI^{1.31}$	Field

4. METHODOLOGY

Data collected from the literature review was subjected to a statistical analysis so as to develop new empirical equations to estimate values of CBR and Mr of subgrade and base materials using DCPI. The study focused on CBR and Mr data. In addition, moisture content and dry unit weight corresponding to DCPI was studied. This process was made possible by using data from earlier studies and then graphing them to understand how each parameter impacted on the results obtained by other authors. Data from different references through (2005 and 2017) is presented in Table 3.

5. DYNAMIC CONE PENETRATION TEST (DCPI)

5.1 DCP INSTRUMENT

Figure 1 shows the DCP equipment that was adopted by ASTM under the fixed term D6951/D6951M. It comprises of two 16-mm (5/8-inch) diameter shafts coupled at a near midpoint, and a handle which is located at the upper part of the device. The mass of the hammer is 8-Kg that can be dropped freely from a height of 575 mm to transfer energy through the lower shaft to the tip of cone. The lower shaft contains an anvil and a pointed tip sloped at 60 degrees. The tip is driven into the soil by

dropping the hammer into the anvil which serves as the lower stopping mechanism for the hammer. By measuring the penetration of lower shaft into the soil after each hammer drop the underlying soil strength is determined. This value is recorded in millimeters per blow and is known as dynamic cone penetration index (DCPI) (ASTM). By plotting the DCPI versus depth, thickness and strength of different soil layers can be obtained.

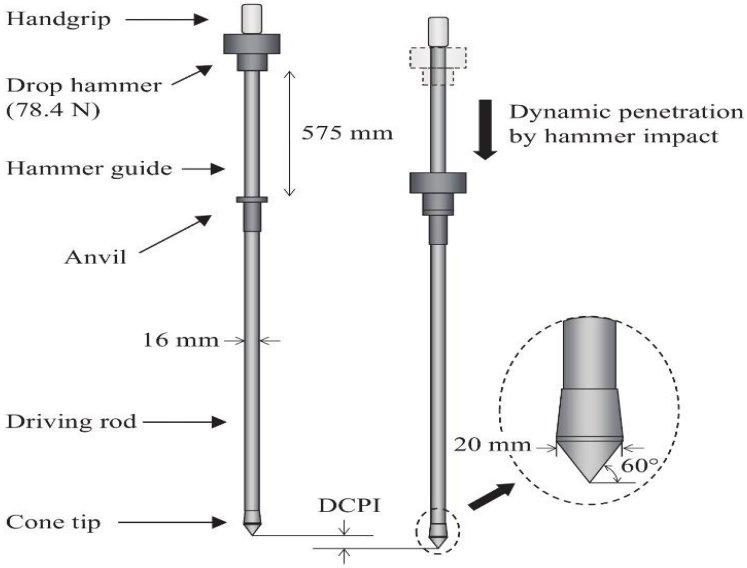

FIGURE 1. The dynamic cone penetrometer device [22]

5.2 SUMMERY OF DCP TEST

The DCP tip can be pushed into soil under consideration by bracing the sliding hammer to the handle then releasing it.Figure 2 shows the test setup. The net penetration for a given number of blows can be measured in mm/blow and named as DCPI. This value can be correlated with geotechnical properties such in situ CBR, shear strength, dry unit weight and Mr [23].

FIGURE 2. DCP test operation [24]

TABLE 3.

Literature review on DCP data corresponding to different parameters

Reference	Soil type	DCPI (mm/ blow)	CBR %	Mr MPa	W%	γdry (KN/m^3)	Remarks
Abu-Farsakh et al., [12]	CM and MC	6.52 - 11.83	24.22 - 62.5	--	--	--	The results showed a good correlation between the DCP-PR and the CBR value with R^2 of 0.84
Mohammad et al., [26]	Clay and Clayey Silt	9 - 65.2	---	7.5 - 91.7	12 - 36.7		A good agreement was obtained between the M_r predicted using DCPI
George et al.,[13]	SM and SC	1 - 18.3	3.9 - 50	---	5.8 - 19	8.23 - 22.68	The best fit curve obtained followed a logarithmic model
Sahoo and Reddy, [25]	ML and CL	6.82 - 105	1 - 46.18	---	7.2 - 11.4	19.2 - 20.8	logarithmic relationships have been developed correlating the Laboratory DCP values with the corresponding CBR values
Patel et al.,[14]	Sandy Soils, Sandy-Clay soils and Clayey soils	16.6 - 29.4	9.5 - 3.5	---	8 - 10.2	19 - 20.5	Good relationship observed between DCPI and CBR with R^2 greater than 0.8

TABLE 3.

(continued)

Reference	Soil type	DCPI (mm/blow)	CBR %	Mr MPa	W%	γdry (KN/m^3)	Remarks
Herath et al.,[19]	CL, CL-ML and CH	*6.54 - 63.7	38.8 - 106	--	8.5 - 32.8	13.1 - 18.9	A good correlation was obtained between the predicted and measured Mr using DCPI.
Mohammad et al.,[21]	Silt and Clay	9 - 65.2	--	7.6 - 87.4	5 - 60	--	A Good relationship was found to predict Mr using DCPI
Singh et al., [27]	CL, ML-CL and SM	12 - 21.33	3 - 9.07	---	4.9 - 14.6	---	Increase in PI of soil adversely affect the performance of the subgrade
Sisodia and Amin, [28]	Clayey, Silt and Sandy Soils	9.8 - 32.52	3.4 - 8.2	---	9.8 - 13.6	18 - 20.3	Logarithmic relationship was observed among DCPI and CBR with an R^2 of 0.88
Current study	Fine grained soil	1 - 105	1 - 48.14	7.5 – 91.4	4.9 – 14.6	17.9 – 20.9	Power relation was observed between DCPI and both CBR and Mr,
Remarks	Different types of fine grained soils were investigated	DCPI data varies from 1 to 105 mm/blow	CBR varies from 1 to 106 percent	Mr varies from 7.5 to 91.7 MPa	W% ranged from 4.9 to 60 percent	Dry unit weight varies from 8.23 to 22.68	CBR, Mr, W% and dry unit weight have been studied

6. RESULTS AND DISCUSSION

Geotechnical properties (CBR and Mr) of fine grained soil were the main aim in this research. A data of 132 data was collected from literature where DCPI and in situ CBR values were conducted. A data of 146 was collected from literature in which DCPI and lab data were analyzed. Furthermore, collected data points for DCPI corresponding to moisture content and dry unit weight were (55 and 44) points, respectively, are presented in Table 4. In the statistical analysis, the simple regression analysis was utilized and the coefficient of correlation (R) is used to determine the suitability of the fit. It describes the relative correlation between the predicted and actual results. The guide proposed by Smith (1993) was adopted as follows: (a) a robust correlation exists between two sets of variables if R=>0:8; (b) correlation exists between two sets of variables if 0:2 < R=< 0:8; (c) a weak correlation occurs between two sets of variables. If R=< 0:2.

TABLE 4.
Data collected in this research

Parameter	No. of collected data	References
CBR	132	Wu and Sargand, [7] ; George et al., [13] ; Patel et al., [14]; Singh et al., [27]; Sisodia and Amin, [28]
Mr	146	Mohammad et al., [21] ; Mohammad et al., [26]; Herath et al., [19]
W%	55	Patel et al., [14]; Singh et al., [27]; Sisodia et al., [28]
Dry unit weight	44	Patel et al., [14]; Sisodia et al., [28]

After analyzing the collected data, the relationships between each of CBR, Mr, W%, and dry unit weight with DCPI were obtained. On one hand, a power relationship was found between DCPI and each of CBR, Mr, and dry unit weight. However, the value of the R^2 varied in the developed relationships. The values of R^2 were 0.64, 0.77 and 0.58 for CBR, Mr, and dry unit weight, respectively, as shown in Figures (3, 4, and 5). On the other hand, the DCPI has a logarithmic relationship with W% with an R^2 of 0.36 (see, Figure.6).

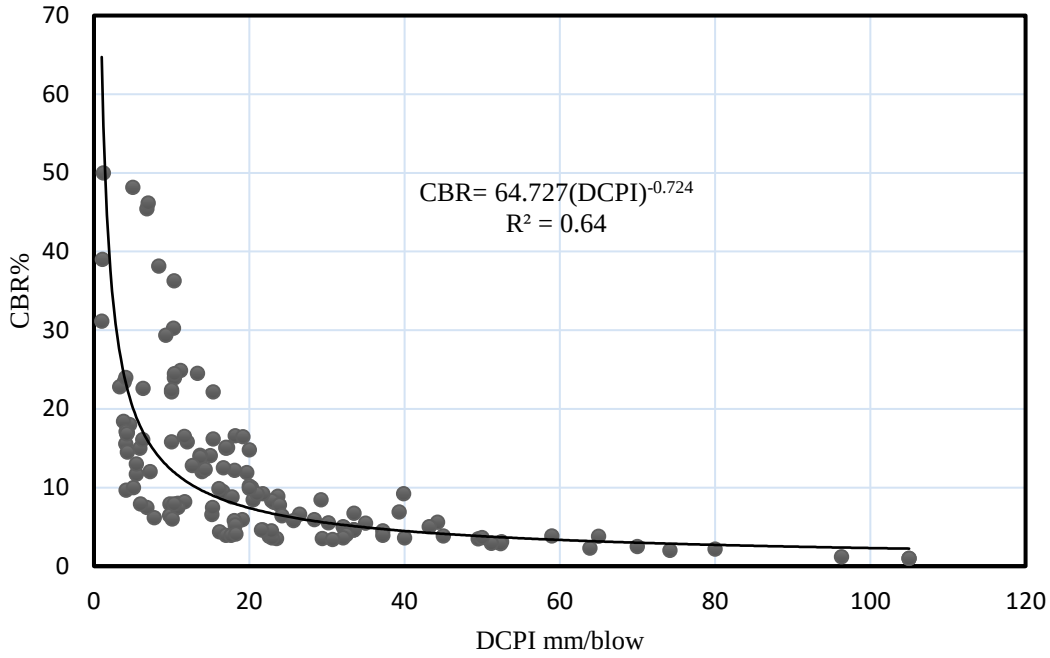

FIGURE 3. Relationship between DCPI and CBR

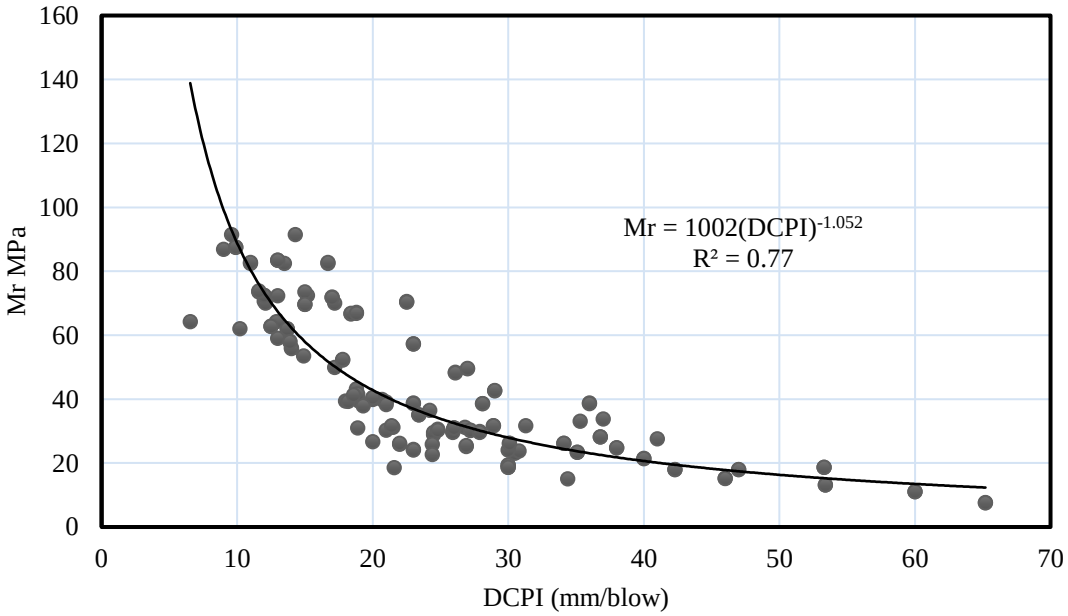

FIGURE 4. Relationship between DCPI and Mr

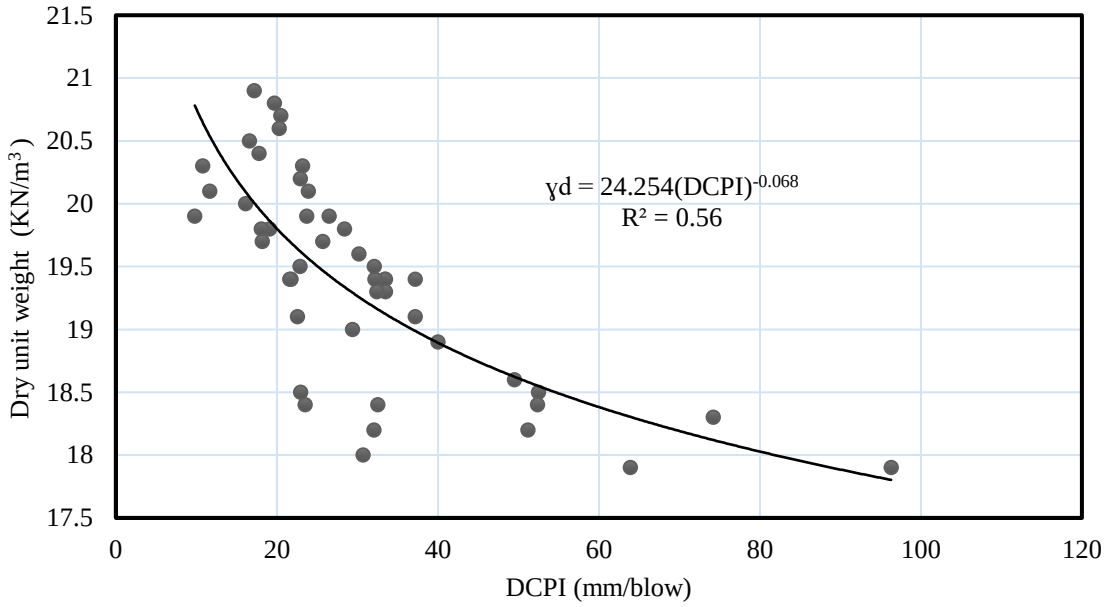

FIGURE 5. Relationship between DCPI and dry unit weight

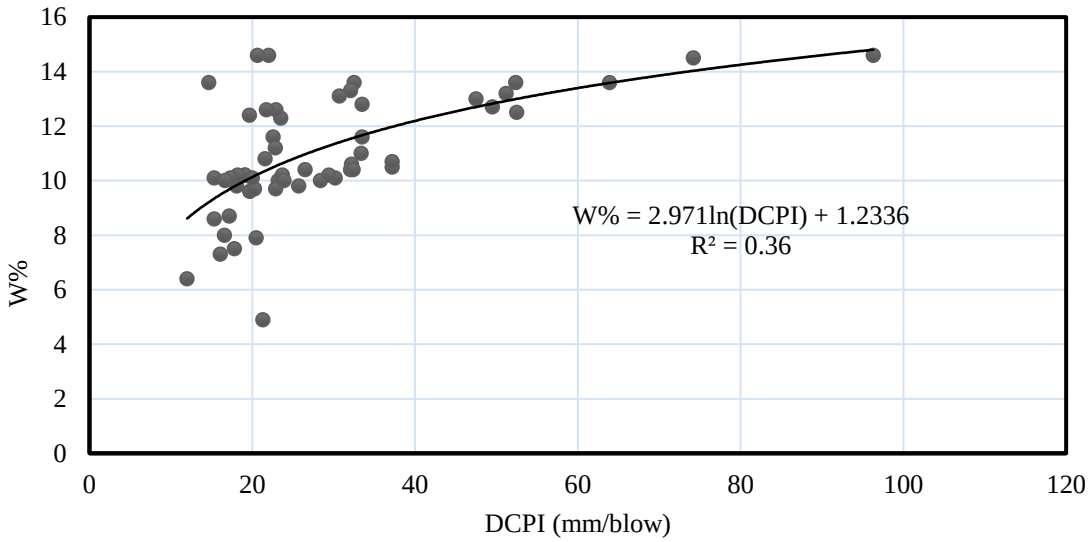

FIGURE 6. Relation between DCPI and W %.

From the analysis, the following empirical equations are proposed to estimate CBR, Mr, γdry, w% from DCPI value:

$$CBR = 64.727*(DCPI)^{-0.724} \quad (R^2 = 0.64) \quad (6)$$

$$Mr = 1002*(DCPI)^{-1.052} \quad (R^2 = 0.77) \quad (7)$$

$$\gamma dry = 24.254(DCPI)^{-0.068} \quad (R^2 = 0.56) \quad (8)$$

$$W\% = 2.971*\ln(DCPI) + 1.2336 \quad (R^2 = 0.36) \quad (9)$$

It would be interesting to study the reliability of the empirical equation developed in the literature and in this study using extensive statistical analysis.

8. CONCLUSIONS

In this study the empirical equations to predict CBR and Mr values using DCPI were modified using data obtained from literature, the study focused on fine grained soil. According the statistical analysis of the collected data, the following conclusions are made:

1. A power relationship was found between Mr and DCPI with coefficient of determination(R^2) of 0.77
2. A power relationship was found between CBR and DCPI with coefficient of determination (R^2) of 0.64.
3. A poor correlation was found between dry unit weight and DCPI with R^2 of 0.56 whereas a very poor correlation was found between water content and DCPI value ($R^2 = 0.36$).
4. Resilient modulus and CBR values are influenced by the moisture content and dry unit weight, Theses values decreased with an increase of moisture content and increased with an increase of dry unit weight.
5. Dynamic cone penetrometer test (DCP) can be recommended devise to predict the geotechnical properties of soils.

REFERENCES

[1] A. J. Scala, "Simple methods of flexible pavement design using cone penetrometers," New Zealand Engineering, vol. 11, (2), 34, 1956.

[2] C. E. Cary, and C. E. Zapata, "Resilient modulus for unsaturated unbound materials," Road Materials and Pavement Design, vol. 12, (3), pp. 615-638, 2011.

[3] C. W. Ng, C. Zhou, Q. Yuan, and J. Xu, "Resilient modulus of unsaturated subgrade soil: experimental and theoretical investigations," Canadian Geotechnical Journal, vol. 50, (2), pp. 223-232, 2013.

[4] B. Yang, R. Zhang, X. Zha, C. Liu, and Q. Pan, "Improved testing method of dynamic cone penetrometer in laboratory for evaluating compaction properties of soil subgrade," Road Materials and Pavement Design, vol.17, (2), pp. 487-498, 2015.

[5] A. Sawangsuriya, and T. B. Edil, "Evaluating stiffness and strength of pavement materials," Proceedings of the Institution of Civil Engineers-Geotechnical Engineering, vol. 158, (4), pp. 217-230, 2005.

[6] S. D. Mohammadi, M. R. Nikoudel, H. Rahimi, and M. Khamehchiyan, "Application of the dynamic cone penetrometer (DCP) for determination of the engineering parameters of sandy soils," Engineering Geology, vol. 101, (3), pp. 195-203, 2008.

[7] Mejías-Santiago, M., García, L., & Edwards, L. "Assessment of Material Strength Using Dynamic Cone Penetrometer Test for Pavement Applications'' In Airfield and Highway Pavements ASCE, 2015, pp. 837-848.

[8] S. L. Webster, R. H. Grau, and T. P. Williams, "Description and application of dual mass dynamic cone penetrometer," Instruction report, U.S. Army Engineer Research and Development Center, Vicksburg, Mississippy, U.S.A, 1992.

[9] M. Livneh, "The correlation between dynamic cone penetrometer (DCP) and CBR values," Transportation Research Institute, Technion, Israel Institute of Technology, 1987.

[10] J. A. Harison, M. Grant, A. Nataatmadja, and G. Woodman, "Correlation between California bearing ratio and dynamic cone penetrometer strength measurement of soils," Proceedings of the Institution of Civil Engineers, vol. 87, (1), pp. 119-125,1989.

[11] M. A. Gabr, K. Hopkins, J. Coonse, and T. Hearne, "DCP criteria for performance evaluation of pavement layers," Journal of performance of constructed facilities, vol. 14, (4), pp. 141-148, 2000.

[12] M. Abu-Farsakh, M. Nazzal, K. Alshibli, and E. Seyman, "Soil parameters for pavement design and subgrade resilient modulus: Application of dynamic cone penetrometer in pavement construction control," Transportation Research Record: Journal of the Transportation Research Board, pp. 52-61, 2005.

[13] V. George, N. C. Rao, and R. Shivashankar, "PFWD, DCP and CBR correlations for evaluation of lateritic subgrades," International Journal of Pavement Engineering, vol. 10, (3), pp. 189-199, 2009.

[14] M. A. Patel, H. S. Patel, and G. Dadhich, " Prediction of subgrade strength parameters from dynamic cone penetrometer index, modified liquid limit and moisture content," in Procedia-Social and Behavioral Sciences, pp. 245-254, 2013.

[15] W. Heukelom, and A. Klomp, "Dynamic testing as a means of controlling pavements during and after construction," In International Conference on The Structural Design of Asphalt Pavements, Vol. 203, (1), 1962.

[16] W. D. Powell, J. F. Potter, H. C. Mayhew, and M. E. Nunn, "The structural design of bituminous roads," Report, Transport Research Laboratory, Crowthorne, Berkshire, U.K, 1984.

[17] J. Chen, M. Hossain, and T. Latorella, "Use of falling weight deflectometer and dynamic cone penetrometer in pavement evaluation," Transportation Research Record: Journal of the Transportation Research Board, pp. 145-151, 1999.

[18] D. H. Chen, D. F. Lin, P. H. Liau, and J. Bilyeu, "A correlation between dynamic cone penetrometer values and pavement layer moduli," Geotechnical Testing Journal, vol. 28, (1), pp. 42-49, 2005.

[19] A. Herath, L. N. Mohammad, K. Gaspard, R. Gudishala, and M. Y. Abu-Farsakh, "The use of dynamic cone penetrometer to predict resilient modulus of subgrade soils," Geo-Frontiers 2005, Geotechnical Special Publication ASCE, Reston, 2005.

[20] M. Nazzal, M. Abu-Farsakh, K. Alshibli, and L. Mohammad, "Evaluating the light falling weight deflectometer device for in situ measurement of elastic modulus of pavement layers," Transportation Research Record: Journal of the Transportation Research Board, pp. 13-22, 2007.

[21] L. N. Mohammad, A. Herath,, M. Y. Abu-Farsakh, K. Gaspard, and R. Gudishala, "Prediction of resilient modulus of cohesive subgrade soils from dynamic

cone penetrometer test parameters," Journal of Materials in Civil Engineering, pp. 986-992, 2007.

[22] W. Hong, and J. Lee, "Application of a nondestructive method to evaluate the active layer in a cold region," (Sciences in Cold and Arid Region), [online] 2018, http://www.scar.ac.cn/fulltext/2017/3/20170305.htm (Accessed: 4 February 2018).

[23] American Association of State Highway, & Transportation Officials. AASHTO Guide for Design of Pavement Structures, Vol. 1, 1993.

[24] Sitetestingservices, I2Analytical,[online], http://www.i2analytical.com/services/geotechnical-testing/site-testing-services/ (Accessed: 4 February 2018).

[25] P. K. Sahoo, and K. S. Reddy, "Evaluation of subgrade soils using dynamic cone penetrometer," International Journal of Earth Sciences and Engineering, vol. 2, (4), pp. 986-992, 2009.

[26] L. N. Mohammed, K. Gaspard, A. Herath, and M. D. Nazzal, "Comparative evaluation of subgrade resilient modulus from non-destructive, in-situ, and laboratory methods,"Instruction report, Louisiana Department of Transportation and Development, Louisiana, U.S.A, 2007.

[27] D. Singh, J. N. Jha, and K. S. Gill, "Evaluation of existing alluvial soil subgrade using dynamic cone penetrometer and index properties," International Journal of Current Advanced Research, vol. 6, (7), pp. 4669-4675, 2017.

[28] M. Sisodia, and A. Amin, "Sub-grade soil assessment using correlation between dynamic cone penetration indexes (DCPI) unconfined compressive strength (UCS)," International Journal for Research in Applied Science and Engineering Technology, vol. 5, (8), 2017.

[29] Smith, M. , "Neural Networks for Statistical Modeling'', John Wiley &;Sons, Inc, 1993.

EVALUATION OF WASTEWATER CHARACTERISTICS IN THE URBAN AREA OF SULAIMANYAH GOVERNORATE IN KURDISTAN-IRAQ

Abdulfattah Ahmad Amin

Erbil Polytechnic University / Erbil Technology Institute
Ishik University - Erbil
abdulfattah14ahmad@yahoo.com

doi:10.23918/iec2018.21

ABSTRACT

The population of Iraqi Kurdistan region is increasing rapidly. This has increased pressure on water supply and waste water management in the region. The Sulaimanyah city and other cities of Iraqi Kurdistan region are facing serious challenges in this regard. the present paper is aimed to study the characteristics of waste water in Sulaimanyah city, its harmful effects on environment and how to deal with these problems in order to safeguard the city from environmental pollution. All important parameters such as biological oxygen demand, chemical oxygen demand, total suspended solid, turbidity and phosphorus of waste water study were found higher than standard value. Only pH value was found in a standard range. Two types of samples of waste water were collected (stagnant and running) from three different places in Sulaimanyah. The values of different parameters for these samples are: pH range was 7.57-7.06, conductivity range is 190- 813 μS/cm, turbidity range was 37-250 mg/L, dissolved oxygen (DO) range is 3.25-6.5 mg/L, biological oxygen demand (BOD_5) range was 18-58 mg/L, chemical oxygen demand (COD) range was 10-110 ppm, phosphorous range was 3.48 -6.26 ppm and total suspended solid (TSS) 84-284 mg/L. Such type of water is not suitable for vegetation and other agricultural purposes.

Keywords: wastewater, BOD_5, COD, conductivity, TSS, pH**.**

1. INTRODUCTION

Today is an important time for criticizing waste water effluent and thinking about water shortages, both occur with the ramifications of continuous population growth. In urban areas, the poor management of water use, and waste water management strategies might cause shortage of water [1]. Environmental pollution will be unquestionably one of the major significant problems due to human activities, and waste water will be an important part of major threat for pollution in the affected area. The globally billions of citizens lack access to safe drinking water and face waste water sanitation problems [2]. The Iraqi Kurdistan region might sewerage system problem. However, poor practices of using water raises serious question on how water is supplied to different cities including Sulaimanyah that has a sewerage network system. waste water is produced from human activities. Volume of waste water has been increased by domestic, industrial and commercial activities. Improved living conditions, and urbanization also play vital role in this regard. Scientific study reveals that waste water consists of 99.9% of clean water, but only 0.1% of solids or undesirable species [3]. In this paper, physiochemical characteristics of waste water from Sulaimanyah city are studied in order to determine their organic load and impact on environment. one of the difficulties to implement an appropriate waste water treatment and management system is the current economic situation in the region. Lack of interest by relevant authorities in understanding the problems associated with waste water, its treatment and management might be another reason for what has been observed as a result of this study.

2. STUDY AREA

Sulaimanyah city is the second biggest city in Iraqi Kurdistan region. Geographically it is located between latitude 45° 20' east and longitude north 35° 30'. Waste water enters into the Tanjero River from the southeast of Sulaimanyah city. This river runs for more than 20 km and passes through several villages and country sides before it sinks into Darbandikhan. The waste water samples were collected from Tanjero, Qaragull, and Tapilkarm sites of Sulaimanyah city. These samples were collected from stagnant and running waste water.

3. SAMPLING AND METHODOLOGY

18 samples were collected in total from three different (Tanjero, Qaragull, and Tapilkarm) sites during July-September 2017. Among these, nine samples were collected from stagnant waste water and nine from the running waste water. The pH, electrical conductivity, turbidity, dissolved oxygen, BOD_5 were measured with the help of pH, turbidity and DO, and BOD_5 meter in the Ministry Lab of Natural Resources.

4. RESULTS AND DISCUSSIONS

In this paper, eight parameters of physicochemical characteristics were checked. Three destinations of Sulaimanyah were selected which include Tanjero, Qaragull, and Tapilkarm. Also, from each station, two types (stagnant and running) of waste water samples were collected.

TABLE 1.

Physicochemical characteristics of stagnant waste water samples collected from different sites of Sulaimanyah city.

S. No.	Parameters	Tanjero	Qragull	Tapikarm
1	pH	7.06	7.57	7.13
2	Conductivity (µs/cm)	361	813	195
3	Turbidity (NTU)	37	155	180
4	TSS (ppm)	44	187	168
5	COD (mg/L)+	61	110	45
6	Phosphorus(ppm)	5.76	5.93	6.26
7	BOD_5 (mg/L)	58	40	42
8	DO (mg/L)	4.1	2.1	3.2

TABLE 2.

Physicochemical characteristics of running waste water samples collected from different sites of Sulaimanyah city.

S. No.	Parameters	Tanjero	Qragull	Tapikarm
1	pH	7.12	7.03	7.26
2	Conductivity (µs/cm)	290	290	390
3	Turbidity (NTU)	104	250	67
4	TSS (ppm)	89	284	84
5	COD (mg/L)	10	53	35
6	Phosphorus(ppm)	3.66	4.38	3.48
7	BOD_5 (mg/L)	29	30	19
8	DO (mg/L)	5.66	4.45	7.26

The pH value also tells about the main sources of the growth of microorganisms in waste water. Generally, it requires a pH between 6.5 and 7.5 for optimal growth. The pH value higher than 8.5 and lower than 5 directly influences the growth of microorganisms [4, 5]. The pH value in waste water samples from Sulaimanyah city were found to fall in the range of 7 to 7.5.

BOD_5, "Higher BOD, means higher organic matter "Microorganisms use water, which is dissolved by the atmospheric oxygen for biochemical oxidation of organic matter [6]. In stagnant waste water samples from Tanjarow (Sulaimanyah city), BOD_5 is found in high amount, which is 58 mg/l. While in running waste water sample from the same destination BOD_5 is 28 mg/l. High BOD_5 is due to central sewerage system which contains black and gray water. Also, the lower range of BOD_5 in samples of running water at the third destination (TapiKarm) 18 mg/l was noticed. This clearly shows that waste water in Sulaimanyah does not undergo any treatment.

Phosphate is the main form of total phosphorus in water and waste water body. It is found two forms in waste water bodies. The first one is organic and the second one is inorganic form. High concentration of phosphate form of phosphorus compound may produce an issue of water bodies (algae). Phosphate concentration in waste water samples collected from for the direct discharge into the environment was found

higher. According to standard value of phosphate is (3 ppm) [7].The value in table indicates that in Sulaimanyah city, there is higher range because direct discharge of waste water. High concentration of phosphate recorded in the stagnant waste water samples as compared to the running waste water samples flow of wastewater at all three destinations.

Turbidity is the amount of suspended matter such as the clay, silt, inorganic matter and organic matter in water and waste water. The presences of these matters in water change the color and form of water. The turbidity measures the sprinkling of the light on the suspended particle in water and its value equivalent to 5 NTU is suitable for drinking [5]. Furthermore, the turbidity was found more in running waste water samples than in stagnant waste water samples.

Dissolved Oxygen is the most significant element in water quality control. The concentration of dissolved oxygen content of water is affected by the temperature. Reduction of the dissolved oxygen in water can encourage the microbial depletion of nitrate to nitrite. At 40ºC, the concentration is 10.05 mg/l, while at 8ºC dissolved oxygen in wastewater is (20.4 mg/l) [5].The samples collected from Sulaimanyah was found to contain dissolved oxygen between 3.25 to 6.71 mg/l.

COD is the amount of oxygen equal to organic matter. Also, it is the amount of oxygen required to oxidize the organic compound completely to CO_2 and H_2O [8]. It is the most important and rapidly measured variable for categorizing water bodies. The value of COD is higher than the value of BOD_5. Generally, this indicates that less number of compounds can be biologically oxidized than the number which can be chemically oxidized [9]. The COD is negatively correlated with CO_2, pH and nitrate and positively correlated with conductivity and turbidity. Water contamination can be categorized by the chemical oxygen demand value according to (EPA globally, 2000). It is assumed that, the range of COD between (4-8) ppm is low level and (12 -16) ppm is high level. COD in the waste water samples of Sulaimanyah indicates high level contaminations. Especially the Qaragull area waste water samples were found highly contaminated because of the waste water discharge from industry without any treatment.

TSS (Total suspended Solids) is the amount of composed algae, clay, and fine mineral. The human activities results in high concentration of TSS [10]. In samples from

Sulaimanyah higher concentration of TSS were noticed. In general 30ppm of TSS concentrations is considered suitable or acceptable in natural waters [11].The main reason of high TSS values is the centralized sewerage system is the in Sulaimanyah.

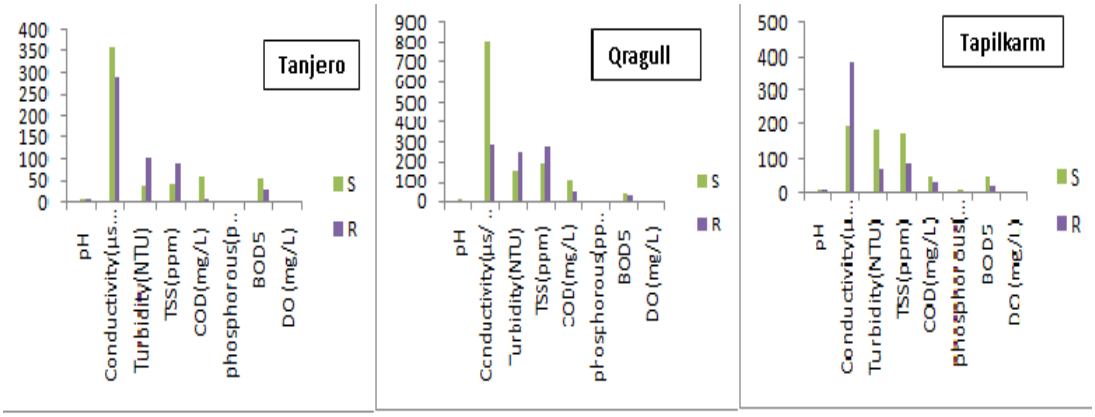

FIGURE 1. Above figure shows comparison of samples of stagnant waste water and samples of running waste water in Tanjero, Qargull and Tapikarm Sulaimanyah.

Note: S stands for stagnant waste water sample and R stands for running waste water sample.

The pH value observed is an optimum value and falls in the standard range. The observed value of pH is acceptable to be discharged into the environment without treatment. The value of TSS was observed much higher than the standard values. The use of waste water in industry, agriculture and recharging the ground water are the main purposes for treating wastewater. The high value of BOD_5 changes the color of waste water samples into gray and Black water. In order to reduce the pressure on fresh water resources and to reduce health risks, safe use of waste water needs to be ensured in the best possible way.

5. CONCLUSION

The waste water in Sulaimanyah city of Iraqi Kurdistan region is found unsuitable to be discharged into environment without treatment. These issues associated with waste water might cause serious problems to environment and public health. The pH or alkalinity value in waste water samples is in standard ranges but turbidity is exceeding permissible and standard value. The majority of the channel waste water is polluted by industry. BOD_5 for the stagnant waste water samples is higher than the waste water samples of running water. The higher values of BOD_5 in waste water samples indicate higher contaminations and effect the environment in a bad way. COD and electrical conductivity wastewater value were found in line with standard values. Such type of waste water can be used for irrigation purposes for growing crops but it is not suitable for vegetables.

RECOMMENDATION(S)

It is proposed to develop an overall system for waste water management with proper planning. Waste water is rich source of renewable energy if managed properly. In doing so, environment can be protected from pollution, more water will be available for irrigation, risks to public health could be minimized and agricultural land can be fertilized free of cost. It's the time to prepare and adapt a new strategic approach to find a suitable solution for waste water management in Sulaimanyah. More active and improved monitoring of waste water is required and a comprehensive check needs to be put in place on discharging waste water into environment.

REFERENCES

[1] H. M. Jasim, Yousaf. Y.A.A. Kurdi, F.H.I Al nidai," Environmental Issues in Erbil City," *International Journal of Engineering Trends and Technology*, 4(8), p. 7.2013.

[2] World Health Organization (WHO) Geneva, Addendum Microbiological agents in drinking water, 2nd edition, 2002.

[3] N.S.Topare, S.JAttar, M.M Manef ," Sewage/Waste Water Treatment Technologies: A Review, Scientific Review and Chemical Communication,1(1),18-24,2011.

[4] D. Bouknanaa, B. Hammoutia , R. Salghid , S. Jodehe , A. Zarrouka , I. Warade A. Aounitia , M. Sbaab ," Physicochemical Characterization of Olive Oil Mill Wastewaters in the eastern region of Morocco," J. Mater. Environ. Sci. 5 (4), 1039-1058, 2014.

[5] World Health Organization (WHO),Guideline for Drinking Water Quality. 3rd edition, Vol. 1, Recommendations, Geneva P. 512-520,2006.

[6] B. Y. Ammary, "Nutrients requirements in biological industrial wastewater treatment," African Journal of Biotechnology, vol. 3 (4), pp. 236-238, April 2004.

[7] J.Cleary, C. Slater, and D.Diamond," Analysis of Phosphate in Wastewater Using an Autonomous Microfluidics-Based Analyser," World Academy of Science, Engineering and Technology, vol 52, 196-199, 2009.

[8] G.Bitton," Waste water microbiology," Journal of Environmental Protection**,"** Vol.7, No.5, March 31, 2016.

[9] J. Kwak, B.Khang, E. Kim,and H .Kim, "Estimation of Biochemical Oxygen Demand Based on Dissolved Organic Carbon, UV Absorption, and Fluorescence Measurement," Journal of Chemistry, vol 2013, Article ID 243769, 9 pages,2013.

[10] D.Safari , G.Mulongo , D.Byarugaba and W.Tumwesigye ," Impact of Human Activities on the Quality of Water in Nyaruzinga Wetland of Bushenyi District – Uganda," Int. Res. J. Environment Sci, Vol. 1(4), 1-6, November 2012.

[11] ISO, Environmetal Management – life cycle assessment- principls and Framwork: International Standard 14040. International Standards Organisation, Geneva,2006.

EFFECT OF STEEL REINFORCEMENT ON THE MINIMUM DEPTH-SPAN RATIO

Mereen Hassan Fahmi Rasheed[1],Saad Essa[2]

[1] *Erbil Polytechnic University*
[2]*Ishik University*
[1]*mereen.akrawi@epu.edu.krd*,[2]*saad_khalis@epu.edu.krd*

doi:10.23918/iec2018.22

ABSTRACT

Building codes and standards include methods and provisions for deflection control and determining minimum thickness of slabs and beams, also determining the immediate and long or time-dependent deflection. The ACI code depth-span limitations tabulated for normal weight concrete and specified yield strength of steel, for other values of steel yield strength and lightweight concrete, correction factors are provided. In this study, correction factors are suggested to include the effect of tensile reinforcement on the depth-span ratio in addition to the ACI code correction factors.

Keywords: Deflection, Depth-span ratio, Deflection control.

1. INTRODUCTION

Deflection control of building codes and standards include methods and provisions for calculating deflection as minimum thickness of slabs and beams. There are two approaches to deflection control.

i. Indirect method, by assuming suitable upper limits on the depth-span ratio which is satisfactory for many cases of spans, loads, load distribution, member size and properties.
ii. Direct method by calculating the deflection for the actual case and compare the results with the specific limitations that permitted by the codes and standards.

Generally, the deflection is occurring during the normal service life of the member due to full dead load and some fraction of live load. The ACI code (ACI Committee, American Concrete Institute, & International Organization for Standardization, 2014) and other design codes and specifications calculate the deflection under loads up to the full-service load to ensure that stresses in the stream fiber in both steel and concrete remain within the elastic ranges, i.e. the un-cracked section properties are used in the calculations of the immediate deflection. Then the long term or time dependent deflection are calculated due to concrete creep and shrinkage along the life of the structure.

ACI code (ACI Committee, American Concrete Institute, & International Organization for Standardization, 2014), provides the minimum depth for one-way slabs and beams shown in table (1), for non-prestressed condition, normal weight concrete with density ($w_c = 145$ pcf or $2320\ kg/m^3$) and steel reinforcement yield strength ($f_y = 60000$ psi or 414 MPa). Correction factors are used for light weight concrete with density in the range $(90-115)$ pcf or $(1440\ -\ 1840)\ \mathrm{kg/m^3}$ and yield strength other than (60000 psi):

$$\lambda_w = 1.65 - 0.005\, w_c \geq 1.09 \quad (1)$$

$$\lambda_y = 0.4 + \frac{f_y}{100000} \quad (2)$$

TABLE 1.

Minimum thickness (h) ACI code limitation [1-10]

Support type	One-way slab	Beam
Simply supported	$L/20$	$L/16$
One end continuous (Propped)	$L/24$	$L/18.5$
Two ends continuous (Fixed ended)	$L/28$	$L/21$
Cantilever	$L/10$	$L/8$

The minimum thickness calculated by the code provisions to ensure that the beam or slab will be stiff enough and the deflection within the permissible range. Generally, deflections are influenced by load, span, beam cross section properties, material properties and support conditions (simply supported, fixed or free).

Elastic deflection can be expressed in the following general form (Nilson, A. H., Darwin, D., & Dolan, C. W., 2010; Wight, J. K., 2016; McCormac, J. C., & Brown, R. H., 2015):

$$\Delta = \frac{f\left(\text{load, span, support conditions}\right)}{EI} \tag{3}$$

Where:

$EI =$ the flexural rigidity of the member ($N.mm^2$).

$E =$ modulus of elasticity of the material (MPa).

$I =$ moment of inertia of the cross section (mm^4).

$f\left(\text{load, span, support conditions}\right)$ is a function of the load, span and support conditions, which is determined by elastic analysis, table (2) shows the maximum deflection of different type beams and loadings (Hibbeler, R. C., & Kiang, T., 2015; Spiegel, L., & Limbrunner, G. F., 2003; Ghali, A., Neville, A., & Brown, T. G., 2003). Factors affecting of reinforced concrete beams and slabs are loadings, material property E, section property I, boundary conditions or support conditions and time dependent factors due to creep and shrinkage on concrete, also the deflection can be controlled by addition of the steel reinforcement bars in tension and compression zones or using pre-stressing concrete. Lee et al (Lee, Y. H., Kim, M. S., Lee, J., & Scanlon, 2013) compared provisions of different codes and

standards about minimum thickness, they concluded that the CSA and ACI provisions have limited application and the proposed equation is recommended for calculation the minimum thickness. Beal (Beal, A. N., 1983) presented an approximated depth-span ratio for the preliminary design specifications in term of (M / bd^2) rather than (A_s / bd) to include the effect of steel design stress. Shehata et al (Shehata, I. A., Shehata, L. C., & Garcia, S. L., 2003) presented a theoretical study for the minimum steel ratio that are required for bending, shear and torsion for beams with different concrete strengths. Ho et al (Ho, J. C. M., Kwan, A. K. H., & Pam, H. J., 2004) developed a simplified method for providing minimum flexural ductility and evaluation of maximum values of tension steel ratio and neutral axis depth corresponding to the proposed minimum curvature ductility factor for various concrete grades and steel yield strengths. Akmaluddin (Akmaluddin, A., 2011) presented an improvement model of the effective moment of inertial to predict the short-term deflection of reinforced light weight concrete beam. The proposed model is verified and compared with experimental results of nine beams, good agreement is obtained with the experimental results and in some cases, have similar trend to the ACI and SNI provisions.

TABLE 2.

Maximum deflection of different types of loads and beams $= k\,w L^4 / EI$

Beam type	Loading	k
Simply supported	Uniform distributed load	5/384
One end continuous (Propped)	Uniform distributed load	1/185
Two ends continuous (Fixed ended)	Uniform distributed load	1/384
Cantilever	Uniform distributed load	1/8
Simply supported	Concentrated load at mid-span	1/48
One end continuous (Propped)	Concentrated load at mid-span	1/192
Two ends continuous (Fixed ended)	Concentrated load at mid-span	$1/48\sqrt{5}$
Cantilever	Concentrated load at tip	1/3

Un-cracked section property (I_{ut}) is used in the calculation of deflection up to cracking moment when the tensile stress at the extreme fiber reached to the tensile

strength of the concrete (f_r), but beyond this limit, effective moment of inertia (I_e) is used which is lied between cracking and un-cracked moment of inertia, as given in the following equation:

$$I_e = \left(M_{cr}/M_a\right)^3 I_{ut} + \left[1-\left(M_{cr}/M_a\right)^3\right] I_{cr} \quad (4)$$

where: $I_{cr} =$ cracked transformed section moment of inertia (mm^4).

$I_{ut} =$ un-cracked transformed section moment of inertia (mm^4).

$I_e =$ effective moment of inertia (mm^4).

$M_a =$ maximum bending moment due to the service load ($kN.mm$).

$M_{cr} =$ cracking bending moment due to the service load ($kN.mm$) and equal to:

$$M_{cr} = \frac{f_r\, I_{ut}}{y_t} \quad (5)$$

$f_r =$ modulus of rupture of the concrete (MPa).

$y_t =$ distance from the neutral axis of the section to the extreme fiber at the tension face (mm).

2. METHODOLOGY

In this study a modification factor is suggested on the depth-span ratio which is recommended in ACI code including the effect of the tension reinforcement on the determination of the moment of inertia taking f and E in equation (3) are constant. For rectangular section without reinforcement: $I_{ut} = bh^3/12$ while for beams with tension reinforcement:

$$y' = \frac{bh\left(\frac{h}{2}\right) + (n-1)\,A_s\,d}{bh + (n-1)\,A_s}$$

$$I_{ut} = bh^3/12 + bh\left(y' - h/2\right)^2 + (n-1)A_s\left(d - y'\right)^2$$

where: $b =$ width of the beam (mm).

$h =$ total depth of the beam (mm).

$d =$ effective depth of the beam (mm).

$A_s =$ area of the tension reinforcement (mm^2).

$y' =$ distance from the extreme fiber compression to the neutral axis of a concrete beam.

$n = E_s / E_c$

$E_s =$ Modulus of elasticity of steel $= 200000$ MPa .

$E_c =$ Modulus of elasticity of concrete (MPa) $= 4730\sqrt{f_c'}$

$f_c' =$ cylinder compressive strength of the concrete (MPa).

By equating the moment of inertia of the beam with tension reinforcement with the equivalent section without reinforcement which giving the same deflection, the new equivalent depth (h_1) is determined form the following equation:

$$bh_1^3/12 + bh_1\left[\frac{bh_1\left(\frac{h_1}{2}\right)+(n-1)(\rho bd_1)d_1}{bh_1+(n-1)(\rho bd_1)} - h_1/2\right]^2 + (n-1)(\rho bd_1)\left[d_1 - \frac{bh_1\left(\frac{h_1}{2}\right)+(n-1)(\rho bd_1)d_1}{bh_1+(n-1)(\rho bd_1)}\right]^2 = bh^3/12 \quad (6)$$

where: $d_1 = h_1 -$ central cover

$\rho =$ reinforcement index ratio $= A_s / bd$

Assuming ($d_1 = 0.85 h_1$), equation (6) leads to polynomial equation of 5th degree which is solved using Newton – Raphson method to find the value of the equivalent depth (h_1).

3. NUMERICAL EXAMPLE

Take a beam with the following dimensions:

$b = 10$ in $(250$ mm$)$, $h = 20$ in $(500$ mm$)$, $f_c' = 4000$ psi $(28$ MPa$)$ and $f_y = 60000$ psi (414 Pa) . Taking reinforcement $\rho = \rho_b$ (balance reinforcement index).

$$\rho_b = \left(\frac{0.85\beta_1 f_c'}{f_y} \right) \times \left(\frac{\varepsilon_u}{\varepsilon_u + \varepsilon_y} \right) \tag{7}$$

Substituting eq. (7) in eq. (6), the following equation is obtained:

$$h_1^5 + 11.77\, h_1^4 + 28.42\, h_1^3 - 8000\, h_1^2 - 54264\, h_1 - 92108.4 = 0 \tag{8}$$

this equation is solved to determine $h_1 = 18.69\,\text{in}\,(474.7\,\text{mm})$.

By applying the same procedures, the equivalent depth (h_1) is determined for different value of reinforcement ratio indices (ρ) as shown in table (3).

TABLE 3.

Results of Calculations of the numerical example.

ρ	ρ/ρ_b	h	h_1	$\alpha = h_1 / h$	% Reduction
0	0.00	20 in (500 mm)	20 in (500 mm)	1.000	0.00
$0.5\rho_b$	0.50	20 in (500 mm)	19.32 (490.73)	0.966	3.40
ρ_t	0.63	20 in (500 mm)	19.2 (487.68)	0.960	4.00
ρ_{max}	0.72	20 in (500 mm)	19.09 (484.89)	0.955	4.55
ρ_b	1.00	20 in (500 mm)	18.69 (474.73)	0.935	6.55

$$\rho_{max} = \left(\frac{0.85\beta_1 f_c'}{f_y} \right) \times \left(\frac{\varepsilon_u}{\varepsilon_u + 0.004} \right) \tag{9}$$

$$\rho_t = \left(\frac{0.85\beta_1 f_c'}{f_y} \right) \times \left(\frac{\varepsilon_u}{\varepsilon_u + 0.005} \right) \tag{10}$$

Figure (1) shows the relation between the ratio (h_1/h) and the reinforcement indices ratio (ρ/ρ_b), as shown the ratio (h_1/h) decreased as the reinforcement ratio (ρ/ρ_b) is increased, this mean that smaller depth is required as the tension reinforcement area is increased. The best fit equation obtained from figure (1) is:

$$(h_1/h) = (1 - 0.065\rho/\rho_b) \tag{11}$$

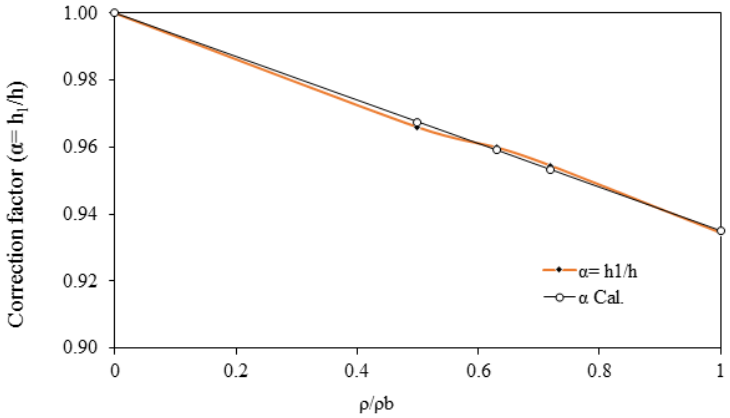

FIGURE 1. Effect of reinforced indices ratio on the correction factor (α)

Equation (11) represent the correction factor for the depth (h) which is determined form ACI code limitation table (1).

The above equation (11) can be written in another way:

$$h_1 = \alpha\, h_{ACI} \tag{12}$$

where (α) is the correction factor for the steel reinforcement effect as shown in table (4).

$$\alpha = (1 - 0.065\rho/\rho_b) \tag{13}$$

or

$$h_1 = (1 - 0.065\rho/\rho_b)\, h_{ACI} \tag{14}$$

The statistics properties from table (4) can be arranged like:

$R_{avg} = 0.99996$, Correlation $(r) = 0.99891$, Standard Deviation $= 0.02383$, Variance $= 0.00057$. The corrected total depth can be expressed in another form:

$$h_1 = \frac{L}{\beta N} \tag{15}$$

where: N is a constant depends on the support condition as shown in table (1) and L is the span of the beam.

Values of (β) are shown in table (5) for different values of (ρ/ρ_b). Figure (2) shows effect of the reinforcement indices ratio (ρ/ρ_b) of the correction factor (β),

as shown value of (β) increased as the ratio (ρ/ρ_b) is increased. This means that smaller total depth is required with increasing the steel reinforcement area as expected. The best fit equation obtained from figure (2) to predict (β) in term of reinforcement indices ratio (ρ/ρ_b) is shown below:

$$\beta = 1 + 0.069\,\rho/\rho_b \tag{16}$$

or

$$h_1 = \frac{L}{\left(1 + 0.069\,\rho/\rho_b\right) N} \tag{17}$$

The results of equations (13) and (16) are used to find the modified depth-span ratios including the effect of the tension reinforcement area for beams and slabs, as shown in tables (6a) and (6b).

TABLE 4.

Correction factor (α).

ρ	ρ/ρ_b	$\alpha = h_1/h$	α_{cal}	$R = \alpha_{cal}/\alpha$
0	0.00	1.0000	1.0000	1.0000
$0.5\rho_b$	0.50	0.9660	0.9675	1.0016
ρ_t	0.63	0.9600	0.9591	0.9991
ρ_{max}	0.72	0.9545	0.9532	0.9986
ρ_b	1.00	0.9345	0.9350	1.0005

TABLE 5.

Correction factor (β).

ρ	ρ/ρ_b	β	β_{cal}	$R = \beta_{cal}/\beta$
0	0.00	1.0000	1.0000	1.0000
$0.5\rho_b$	0.50	1.0352	1.0345	0.9993
ρ_t	0.63	1.0417	1.0435	1.0017
ρ_{max}	0.72	1.0477	1.0497	1.0019
ρ_b	1.00	1.0701	1.0690	0.9990

The statistics properties from table (5) can be arranged as the following:

$R_{avg} = 1.00039$, Correlation $(r) = 0.99842$, Standard Deviation $= 0.02542$, Variance $= 0.00065$.

TABLE 6A.

Modified minimum thickness (L/N) and N for beams.

ρ	ρ/ρ_b	Simply supported	One end continuous (Propped)	Two ends continuous (Fixed ended)	Cantilever
0	0.00	16	18.5	21	8
$0.5\rho_b$	0.50	16.563	19.151	21.739	8.282
ρ_t	0.63	16.667	19.271	21.875	8.333
ρ_{max}	0.72	16.763	19.382	22.001	8.381
ρ_b	1.00	17.121	19.797	22.472	8.560

TABLE 6B.

Modified minimum thickness (L/N) and N for slabs.

ρ	ρ/ρ_b	Simply supported	One end continuous (Propped)	Two ends continuous (Fixed ended)	Cantilever
0	0.00	20	24	28	10
$0.5\rho_b$	0.50	20.704	24.845	28.986	10.352
ρ_t	0.63	20.833	25.000	29.167	10.417
ρ_{max}	0.72	20.953	25.144	29.335	10.477
ρ_b	1.00	21.402	25.682	29.963	10.701

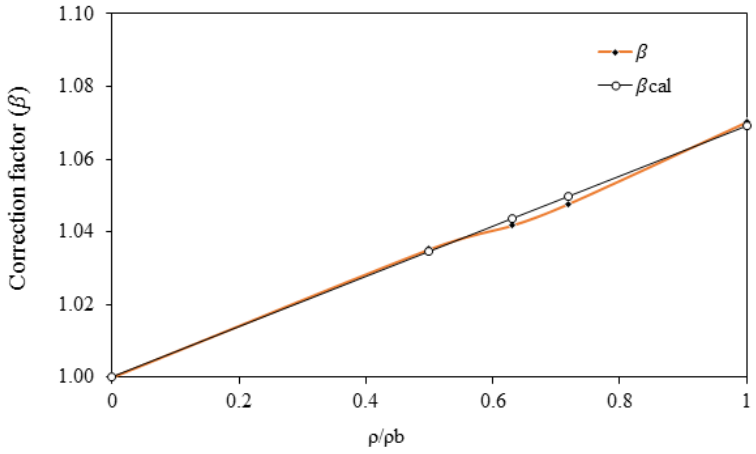

FIGURE 2. Effect of reinforced indices ratio on the correction factor (β)

4. CONCLUSIONS

1. A modification of the ACI code span-depth ratio is suggested in this study to include the effect of tension reinforcement area in addition to the correction for concrete type and yielding strength of steel bars.
2. The correction factors (α and β) are determined in term the reinforcement indices ratio (ρ/ρ_b).
3. The correction factor (α) decreased with increasing the value of the reinforcement indices ratio (ρ/ρ_b).
4. The correction factor (β) increased with increasing the value of the reinforcement indices ratio (ρ/ρ_b).
5. Suitable equations are proposed to predict value of (α) and (β).

REFERENCES

[1] ACI Committee, American Concrete Institute, & International Organization for Standardization. (2014). Building code requirements for structural concrete (ACI 318-14) and commentary. American Concrete Institute.

[2] Akmaluddin, A. (2011). Effect of Tensile Reinforcement Ratio on the Effective Moment of Inertia of Reinforced Lightweight Concrete Beams for Short Term Deflection Calculation. Journal of Engineering and Technological Sciences, 43(3), 209-226.

[3] Beal, A. N. (1983). Span Depth Ratios For Concrete Beams And Slabs. Structural Engineer-Part A, 61(4), 121-123.

[4] Ghali, A., Neville, A., & Brown, T. G. (2003). Structural analysis: a unified classical and matrix approach. Crc Press.

[5] Hibbeler, R. C., & Kiang, T. (2015). Structural analysis. Pearson Prentice Hall.

[6] Ho, J. C. M., Kwan, A. K. H., & Pam, H. J. (2004). Minimum flexural ductility design of high-strength concrete beams. Magazine of concrete research.

[7] Lee, Y. H., Kim, M. S., Lee, J., & Scanlon. (2013). Comparison of minimum thickness provisions for concrete beams in building codes and standards. Canadian Journal of Civil Engineering, 40(7), 595-602.

[8] McCormac, J. C., & Brown, R. H. (2015). Design of reinforced concrete. John Wiley & Sons.

[9] Nilson, A. H., Darwin, D., & Dolan, C. W. (2010). Design of concrete structures. New York, USA: McGraw-Hill Companies.

[10] Shehata, I. A., Shehata, L. C., & Garcia, S. L. (2003). Minimum steel ratios in reinforced concrete beams made of concrete with different strengths-Theoretical approach. Materials and Structures, 3.

[11] Spiegel, L., & Limbrunner, G. F. (2003). Reinforced concrete design. Prentice Hall.

[12] Wight, J. K. (2016). Reinforced concrete: mechanics and design. Pearson Education.

COMPRESSIVE STRENGTH AND WATER SORPTIVITY OF STEAM CURED LIGHTWEIGHT AGGREGATE CONCRETE

Junaid K. Ahmed[1], Arass O. Mawlod[2], Omer M.E. Taha[3], Barham H. Ali[4]

[1&4] Ishik university. Erbil. Kurdistan. Iraq.
[2]University of Raparin. Ranyah. Kurdistan. Iraq.
[3]Kirkuk university. Kirkuk. Iraq
[1]junaid.kameran@ishik.edu.iq ,[2]arass.omer@uor.edu.krd,[3]omer.muhie@ishik.edu.iq
[4]barham.haydar@ishik.edu.iq

doi:10.23918/iec2018.23

ABSTRACT

In this paper, compressive strength of concrete and water sorptivity of concrete partially replace aggregate by light weight fly ash aggregate in different ratio were studied. Different percentage of lightweight fine aggregate (LWFA) and a constant amount of lightweight coarse aggregate (LWCA) and were used to yield the concrete. Various amounts of LWFA were achieved by volumetric substitution of fine aggregate, six different replacement levels as, 0%, 25%, 50%, 75%, and 100% were utilized. Hence, in this experimental study six various concrete mixtures were produced. Steam curing method was applied to the concrete production. At first steam curing (SC) is exposed to concrete productions, and then the samples were moved to water until testing date. Enhancement of water sorptivity test was conducted at 28 days and 56 days. And enhancement of compressive strength test was applied over 56 days.

Keywords: *Fly ash, Lightweight Aaggregate, Sstrength development, Water Sorptivity***.**

1. INTRODUCTION

Fly ash is fabricated is massive volumes from coal-fired thermal power plants, but unfortunately, only a small quantity is utilized a cement replacement in concrete. The current disposal practice is to dump large amounts of fly ash in landfills and storage ponds. Fly ash has become one of the main causes of air and water pollution, which drives to problems of discarding as well as environmental damage. It is worth mentioning that in the recent past, fly ash and sintering aid powders were used in the advancement of new lightweight building materials. Physical features and strength of artificial lightweight sintered aggregates generated from different industrial by products were previously researched by Cheeseman and Virdi (2005), Cheeseman et al. (2005), Mangialardi (2001) and Wang et al. (2002). The conformity of fly ash for the pelletization and sintering process, on the other hand, is hard to guess because many physico-chemical factors are enclosed. The features of aggregates influenced by the types and amount of binder that did not change chemical composition but the microstructure of the aggregate, which is concluded by Ramamurthy and Harikrishnan (2006). Wasserman and Bentur (1997) reported that heat and polymer treatment change the structure and features of sintered fly ash lightweight aggregate (Lytag) to gain aggregates different in their strength, absorption and pozzolanic activity. Verma et al. (1998) investigated that producing of lightweight aggregate becomes a kind of trade in some countries such as USA, Russia, UK, Germany and Poland. The strength; stiffness and durability of concrete made with artificial lightweight aggregate studied by Al-Khaiat and Haque (1998), Al-Khaiat and Haque (1999), Kayali et al. (1999), Kayali et al. (2003),Yun et al. (2004) and ,Chiaia et al. (2010). Kockal and Ozturan (2010) revealed that durability transports very significant for concrete structures, with respect to the strength/weight ratio. Long-term durability is defined by the permeability of concrete. Permeable concrete is defenseless and can be effected by water and harmful substances, which in turn cause disintegrate of the concrete and reinforcement. The interferential transition zone between aggregate and the cement matrix effects on the strength, stiffness and durability of concrete.

Hanson (1963), Neville (1997), and Turkel and Alabas (2005) studied that when the steam is fabricated at atmospheric pressure, the temperature should be kept under 100ºC. Rajdy and Richards (1973), Taylor (1997) concluded that the pozzolanic reaction, thermo-activated by a high curing temperature, provided the development of C–S–H and conformed the phases to the damage of calcium hydroxide. The negative influence of steam curing may be due to the coarser pore structure, improved micro-cracking and delayed ettringite formation. The impact of curing temperature on the features of cement mortars and concretes has been the topic of several researches. It is commonly clarified that a high curing temperature directly after casting supports the development of mechanical features at early ages but adversely influences the strength at later ages. The findings of the study Mouret et al. (2003) showed that concrete cured at 35ºC had 10% less 28-day compressive strength when compared with the similar concrete cured at 20ºC. Verbeck and Helmuth (1968) pointed out that by increasing the curing temperature form 20ºC and 50ºC causes a 28% reduction in strength. Verbeck and Helmuth (1968) reported that the reduction at later age strength was referred to the rapid initial rate of hydration at higher temperature which retarded the subsequent hydration and produced a non uniform distribution of the hydration products. According to the study of Topcu and Toprak (2005), the increase in the curing temperatures of 20ºC, 40ºC, and 60ºC improved the strength at the early ages, but affected negatively the 28-day compressive strength of concrete made with river sand or crush stone sand. Baoju et al. (2005) exhibited the compressive strength of concrete containing ultrafine fly ash with or without slag effected by steam curing. They deduced that the concrete containing ultrafine fly ash (UFA) had much lower early strength after 13 h steam curing and the difference between the 28-day compressive strength of the 13 h cured steam concrete and that of the moist-cured concrete was significant. This finding indicated that the steam curing adaptability of UFA seemed to be rather poor. In another study Baoju et al. (2001), however, ultrafine fly ash composite was developed by adding some mineral powders into UFA. It was observed that concrete containing ultrafine fly ash composite and ground blast furnace slag gave the desired early compressive strength. Yazıcı et al. (2005) showed the usability of the fly ash in mixtures for the precast concrete industry. They revealed that steam curing enhanced the 1-day strength values of high volume fly

ash concretes from about 10 to 20 MPa. However, the ultimate compressive strength of steam-cured fly ash concrete was much lower than that of the standard-cured concrete. They concluded that the amount of bigger pores increased with increasing curing temperature associated with a rise in the mean pore radius, which was the reason for the difference in compressive strength at elevated temperatures compared to storage at 20^{o}C. Aside from the strength, the durability related features of the concretes were also negatively affected by curing at high temperatures. However, there is limited research on the durability performance of steam-cured concrete. According to Ho and Lewis (1992) and Ho (1998), steam-cured ordinary Portland cement concrete cover was poor in quality and equivalent to that achieved with only 2–3 days standard curing as showed by the water sorptivity tests. Ho et al.(1992) discovered the potential benefits of steam-curing on concrete mixes incorporating various combinations of fly ash, slag, and silica fume. It was explored that the steam-cured concretes were more porous as showed by their higher sorptivity compared with the standard cured specimens. Mixes with silica fume appeared to have the best performance with high early strength and low sorptivity.Ho and Cao (1994) studied that the quality of steam-cured concrete containing 20% fly ash was better than that with 28-days standard curing. Similar results were attained for blended cements containing 35% blast furnace slag by Ho et al. (1997) , Ho et al. (2003). According to the intensive research trials spent to increase the durability of steam-cured concrete. In recent years, the interest for using fly ash in the generation of lightweight aggregate has been a growing. The performance features of the lightweight concretes and the normal weight concrete were studied through compressive strength, representing the mechanical behavior, and through water sorptivity, representing the transport features of concrete. In the light of the findings revealed in the literature, the main aim of this paper is to examine the influences of lightweight fly ash aggregate (including fine and coarse) on the compressive strength, water sorptivity of the steam cured lightweight concrete which was kept for 17 h under high temperature about 70^{o}C.

2. EXPERIMENTALMETHODOLOGY

2.1Materials:

Portland cement, fine and coarse aggregates of crushed lime stone for control mixes, and artificial light weight aggregate made with fly ash including fine and coarse were used as materials in this study. To attain the required slump superplasticizer was used. CEM I-42.5R Portland cement (PC) complying with European Standards EN 197 (similar to ASTM C150 Type-1 cement) was used. Table 1 shows the physical properties and chemical composition of the PC. The maximum particle size of coarse aggregate was considered as 12 mm, and local aggregates were used. Pelletization disc in laboratory was used to produce the LWA including coarse and fine from fly ash. LWFA was substituted by fine normal weight crushed lime stone. A commercially available sulphonated naphthalene formaldehyde-based superplasticizer with a specific gravity of 1.22 was used to provide a consistent workability.

TABLE 1.
Properties of plain Portland cement (CEM I 42.5R)

Composition	Percentage
SiO_2(%)	19.79
Al_2O_3(%)	3.85
Fe_2O_3(%)	4.15
CaO (%)	63.84
MgO (%)	3.22
SO_3(%)	2.75
Na_2O(%)	-
K_2O(%)	-
Cl^-(%)	0.0063
Insoluble residue(%)	0.34
Loss on ignition(%)	0.87
Free lime(%)	1.28
Vicat time strat	2:42
(h:min) stop	3:44
Le chatelier (mm)	1
Fineness	15.3
(%) 90 µm	1.47
Specific surface (cm^2/gr)	3349
Specific gravity (gr/cm^3)	3.12

2.2 PRODUCTION OF LWFA AND LWCA

In the first stage of the experimental program lightweight fly ash aggregates (LWA) were produced through the cold bonding agglomeration process of fly ash and Portland cement in a tilted pan at ambient temperature. For this, 10% PC and 90% FA were mixed in powder form in the pelletizer shown in Fig. 1. After the dry powder mixture of about 10–13 kg was fed into the pan, the disc was rotated

at a constant speed to assure the homogeneity of the mixture. The amount of sprayed water used during pelletization process has been determined as the coagulant to form spherical pellets with the motion of rolling disc. The optimum water content required for each type of powder was determined according to ASTM D2216-10 [35]. Then, the water was sprayed on the mixture with a quantity of 22% by weight. The formation of pellets occurred between 10–12 min in trial productions. The total pelletization time was determined as 20 min for the compaction of fresh pellets. Finally, they were kept in sealed plastic bags for 28 days in a curing room in which the temperature and relative humidity were 21 _C and 70%, respectively. The curing method adopted in this study is a practical and simple method to fit the laboratory conditions. At the end of the curing period, hardened aggregates were sieved into fractions from 4 to 16 mm sizes to be used as coarse aggregate in concrete production [36].

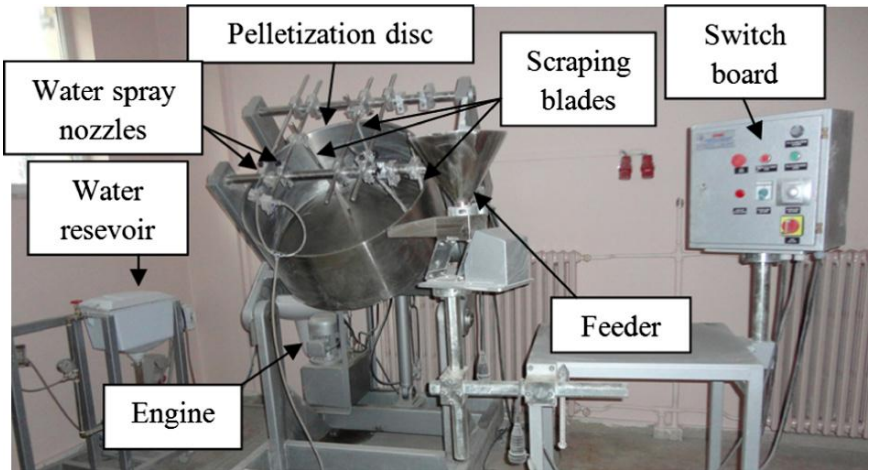

FIGURE 1. The general view of the pelletization disc.

2.3 CONCRETE MIXTURE DETAILS AND SPECIMENS

One set of controlmixtures with the same w/cm ratios of 0.35 with 450 kg/m^3 were designed. Steam curing was applied. In order to examine the impact of light weight fine aggregate fly ash was used as a parameter which replaced with (0%, 25%, 50%, 75%, and 100%) fine normal weight crushed stone aggregate (by weight). Six different mixtures were set in this experiment, and the details shown in Table 2. A constant of

aggregate grading mixture was used for all concretes. The mixtures shown in Table 2 were designed to have slump values of 150 ± 20 mm for w/cm ratios of 0.35 for the ease of handling, placing, and consolidation. To attain the required slump the superplasticizer was added at the time of mixing.

All concretes were mixed in accordance with ASTM C192 standard in a power-driven revolving pan mixer. For each mixture, eight 150 mm x 150mm x 150mm cubes for compressive strength testing, three Φ100x200-mm cylinders for determining water sorptivity testing and compacted by a vibrating table.

The samples after finishing and casting process, were put in a closed chamber for applying steam curing process and keeping for 17 h, after passing one, day all samples were demoulded and then were put in a water tank at 20 ±2 ^{0}C until the date of the tests age.

TABLE 2.
Mixture proportioning of the concrete Steam curing.

Description ID	w/c	Cement (kg/m3)	Coarse aggregate%		Fine aggregate %		SP*** (Gr/m3)
			NWA*	LWA**	NWA	LWA	
S0 (control)	0.35	450	100	0	100	0	12000
S-0	0.35	450	0	100	100	0	4086.96
S-25	0.35	450	0	100	75	25	3173.91
S-50	0.35	450	0	100	50	50	2000
S-75	0.35	450	0	100	25	75	900
S-100	0.35	450	0	100	0	100	500

* Normal weight aggregate
**Lightweight aggregate
*** Super plasticizer

2.4 CURING CONDITION

In steam-curing condition, fresh specimens within the moulds were placed in the steam chamber and subjected to the heat treatment cycle, as shown in Fig. 2. In this study, the

steam curing cycle had a total duration of 23 h inclusive of 2 h of preheating, 3 h of heating until the desired temperature of 70ºC was reached, which remained constant for 17 h, before the final cooling of the chamber which lasted 1 h. The steam curing chamber's humidity was above 90%. The samples were stripped and placed in water at 20 ± 2ºC in compliance with ASTM C192 until the date of testing.

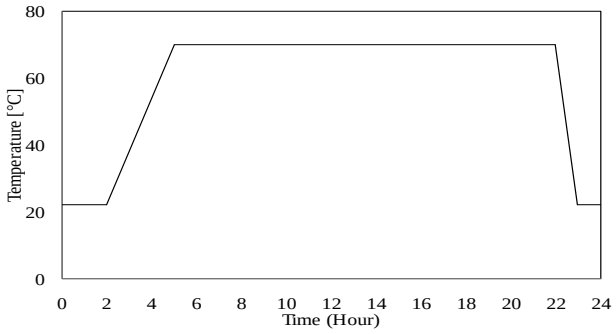

FIGURE 2. Schematic representation of steam curing procedure

2.4 TEST METHODS

2.4.1 COMRESSIVE STRENGTH:

The concrete cubes (150X150X150 mm) were tested under compression at one, three, 28, and 56 days after casting. The tests were performed by a 2000 kN capacitytesting machine in coincidence withASTM C39. For each mixture two specimens were tested in all testing age and results observation wastaken for the various amounts of LWFA replacements.

2.4.2 WATER SORPTIVITY:

The term of water sorptivity is used to characterize water entry into pores of unsaturatedconcrete due to capillarysuction. The rate of water absorption was measured according to ASTM C1585-04. For the test, twospecimens with dimensionsof (Ø100 x 85)mm cut from(Ø100 x 200) cylinders were utilized. At ages of 28days and 56days, the samples were dried first in an oven atabout 105^0C for one day till steady massand then allowedto cool to ambienttemperature in a closedcontainer. Then, the sides ofthe samples were painted with paraffin andthe sorptivitytest was performed byplacing the samples onglass rods in atray containingwater suchthat their bottomsurface was 5mm deep in water, thus allowing the water movement to be free through the bottomsurface.

The sampleds were weighed after they removed from the tray at different interval of times up to 1 h to evaluatethe massgain. The absorbed waters volume were determine by dividing the gained mass by the nominalsurface area of the sample andby the waterdensity. These values were plottedagainst the squareroot of time. The sorptivity coefficient of the concrete was defined as the slope of the best fit line. For each feature of the concrete, two specimens were tested and the average of them was reported as the sorptivity coefficient.

3. RESULTS&DISCUSSION

3.1 COMPRESSIVESTRENGTH*:*

Fig. 3shows values of compressivestrength ofthe LWCs subjected to steam curing, respectively. As clarified in Fig. 3, the decrease in compressivestrength considerably occurs by increasing the amount of replacement of LWFA. Since the changing in coarse aggregate was occurred from normal weight coarse aggregate of crushed lime stone into lightweight coarse aggregate fly ash, decrease in compressive strength can also be observed and this reduction continues with increasing amount of LWFA. A detailed comparison of the various LWFA replacements is shown in Table 3. By replacing the amount of light weight coarse aggregate fly ash fully instead of coarse aggregate crushed lime stone the decrease of strength was observed more clearly. But when the fine aggregate became variable and the coarse light weight fly ash aggregate kept constant for the remaining four mixes, strength of each mixes decreases by a small value by increasing the amount of LWFA replacement, as shown inFig. 4. Theexperimental results indicatedthat by increasing percentage of LWFA, the compressivestrength of the concretes is reduced.

TABLE 3.
Values of compressive strength.

Amount of LWFA* (%)	Compressive-strength (steam-curing)(MPa)			
	1day	3days	28days	56days
Control	47.245	51.324	54.471	57.52
0	31.90	32.60	38.15	38.27
25	28.88	30.92	35.76	35.95
50	23.86	25.47	31.79	32.95
75	23.45	24.66	30.06	31.20
100	21.31	23.35	28.46	28.66

*Lightweight Fly Ash Fine Aggregate

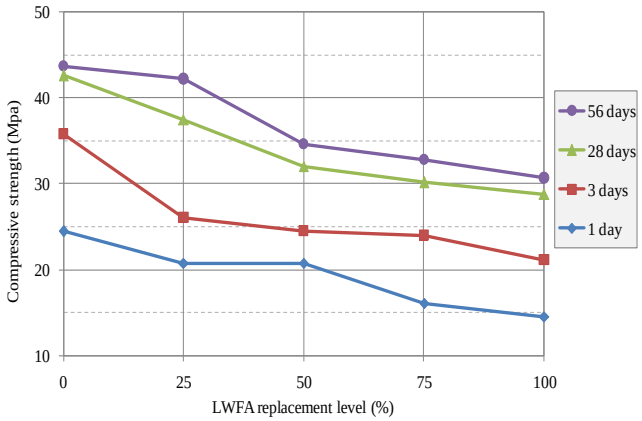

FIGURE 3. Compressive strength subjected to steam curing at different ages

3.2 WATER SORPTIVTY:

The differences in the sorptivity values, based on the amount of LWFA, are given in Fig. 4. The influence of LWFA, which causes the increased sorptivity of concretes, can clearly be seen. The sorptivity coefficients of the control concretes are small in value, as revealed in a comparison of the various LWFA replacements, due to replacing normal weight coarse aggregate into lightweight coarse aggregate fly ash and this rising of sorptivity value were continued with increased amount replacement of LWFA as shows in detail in Table 4. The replacemennt of LWFA at 0%, 25%, 50%, 75%, and 100%

resulted in the increasing value of the sorptivity coefficients by almost 8.5%, 20.28%, 30.93%, and 31%, respectively, for 28-days, and by 11.63%, 12.13%, 26.74%, and 25.14%, respectively, for 56-days for steam curing conditions. Moreover, increasing the amount of replacement of LWFA content increased the sorptivity associated with the strength reduction of the concrete for both steam curing conditions as aresult of thecoarser pore-structure, the result also achieved by Gu¨neyisi and Mermerdas (2007), Bai et al. (2002), and Erdogdu and Kurbetci (1998). The increase in the sorptivity of steam cured concretes may be attributed to the adverse effectof steam curingon the pore sizedistribution. According to Erdogdu, and Kurbetci (1998), heat treatment effect the porestructure of cementpaste by rising the amount of large pores in thecement paste.Similarly, Reinhardt ,and Stegmaier (2006) stated that increasing curingtemperature, the amountof biggerpores increased associated withthe rise in the meanpore radius.

TABLE 4.
Values of water sorptivity (mm/min1/2).

Amount of LWFA (%)	28 days	56 days
	Steam Curing	Steam Curing
Control	0.0765	0.0795
0	0.168	0.159
25	0.1815	0.1775
50	0.2175	0.215
75	0.284	0.2725
100	0.3685	0.341

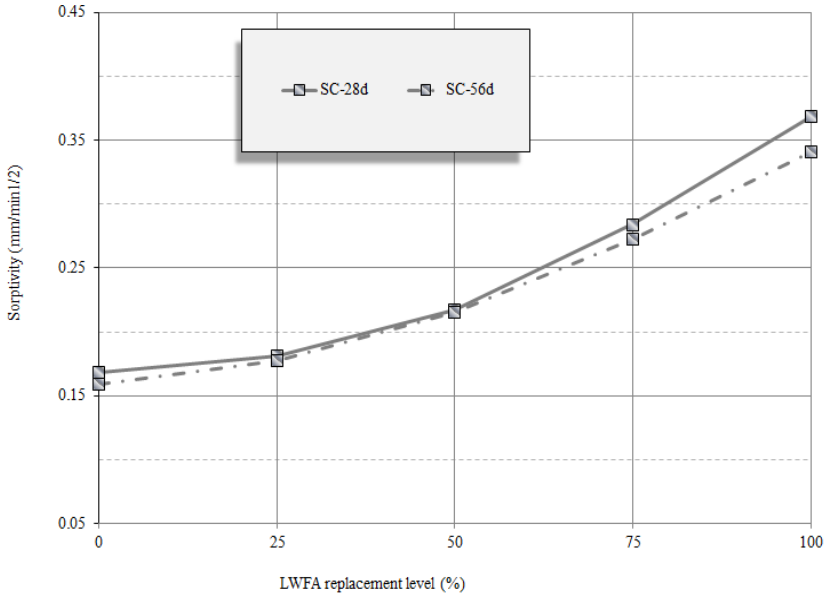

FIGURE 4. Water sorptivity coefficient of LWCs subjected steam curing at different ages

4. CONCLUSION

According to some evidences that were achieved in the current study, the following outcomes can be obtained:

1-The compressive strength at early age, for example at 1-day, is much more enough in gaining of strength as compared to the sample at the same age of moist cured. In the mass production of precast units such as blocks, pipe, pre-stressed units, etc., it is often desirable to hasten the process of hydration and hardening, so that the units may be installed within a few days after manufacture, and thus, avoiding storage problems.

2-Based on the test results achieved in this research (see Table 3), steam curing is preferable for lightweight concrete made with fly-ashaggregate since thedifference between compressive-strength at 1-day and at 56-days was insignificant.

3-The results also clearly show that increasing the amount LWFA replacement decreases compressive strength and increases in water sorptivity.

REFERENCES

[1] Al-Khaiat, H. & Haque, M.N., (1998) Effect of Initial Curing On Early Strength and Physical Properties Of A Lightweight Concrete. Cement Concrete Research, 28: 859–866.

[2] Al-Khaiat, H., and Haque, N., (1999). Strength and Durability of Lightweight and Normal Weight Concrete. Journal of Material Civil Engineering, 11: 231–235.

[3] Bai, J., Wild, S., and Sabir, B.B., (2002) Sorptivity and Strength of Air-Cured and Water-Cured PC-PFA-MK Concrete and the Influence of Binder Composition On Carbonation Depth. Cement Concrete Research, 32:1813–1821.

[4] Baoju, L., Youjun, X., and Jian, L., (2005) Influence Of Steam Curing On The Compressive Strength Of Concrete Containing Supplementary Cementing Materials. Cement Concrete Research, 35: 994–998.

[5] Baoju, L., Youjun, X., Shiqiong, Z. & Jian, L., (2001) Some Factors Affecting Early Compressive Strength Of Steam-Curing Concrete With Ultrafine Fly Ash. Cement Concrete Research, 31: 1455– 1458.

[6] Cheeseman, C.R., and Virdi, G.S. (2005) Properties And Microstructure Of Lightweight Aggregate Produced From Sintered Sewage Sludge Ash. Resource Conserv Recycle, 45 (1), 18–30.

[7] Cheeseman, C.R., Makinde, A. & Bethanis, S. (2005). Properties of lightweight aggregate produced by rapid sintering of incinerator bottom ash. Resource conserv recycle, 43 (2), 147–162.

[8] Chiaia, B., Van Mier, J.G.M & Vervuurt, A., (2010) Crack Growth Mechanisms in Four Different Concretes: Microscopic Observations and Fractal Analysis. Cement Concrete Research, 28: 103–114.

[9] Erdogdu, S., and Kurbetci, S., (1998). Optimum Heat Treatment Cycle for Cements of Different Type and Composition. Cement Concrete Researc, 28:1595–1604.

[10] Gu¨neyisi, E., and Mermerdas, K., (2007) Comparative Study On Strength, Sorptivity, And Chloride Ingress Characteristics Of Air-Cured And Water-Cured Concretes Modified With Metakaolin. J.Material Structure. 40:1161–1171.

[11] Hanson, J.A., (1963) Optimum Steam Curing Procedure in Precasting Plants. ACI J Proc, 60: 75–100.

[12] Ho, D.W.S., Chirgwin, G.J., & Mak, S.L. (1997). Water Sorptivity of Heat-Cured Concrete for Bridge Structures. In: Proceedings of Third CANMET/ACI International Conference on Advances in Concrete Technology Auckland, pp 97–108.

[13] Ho, D.W.S., Chua, C.W., & Tam, C.T., (2003) Steam-Cured Concrete Incorporating Mineral Admixtures. Cement Concrete Research, 33: 595–601.

[14] D.W.S., (1998) How Well Concrete Be Cured. In: Proceeding Of Fourth CANMET/ACI International Conference on Advances in Concrete Technology. Tokushima,Japan. pp 141– 151.

[15] Ho, D.W.S., & Cao, T. (1994) Water Sorptivity Of Steam Cured Concrete. CIA (NSW) Seminar on the Structural Use of Precast Concrete. Concrete Institute of Australia, 10 pp.

[16] Ho, D.W.S., and Lewis, R.K., (1992) Curing Techniques and Their Effectiveness. Concr Austria, 18: 3–7.

[17] Kayali, O., Haque, M.N., & Zhu, B., (1999) Drying Shrinkage of Fibre-Reinforced Lightweight Aggregate Concrete Containing Fly Ash. Cement Concrete Research, 29: 1835–1840.

[18] Kayali, O., Haque, M.N., and Zhu, B,(2003) Some Characteristics Of High Strength Fiber Reinforced Lightweight aggregate concrete. Cement Concrete Composite, 25: 207–213.

[19] Kockal, N.U, & Ozturan, T., (2010) Effects of lightweight fly ash aggregate properties on the behavior of lightweight concretes. J. Hazard Material, 179(1–3), 954–965.

[20] Mangialardi, T., (2001) Sintering Of Msw Fly Ash For Reuse As A Concrete Aggregate. J. Hazard Material, 87(B), 225–239.

[21] Mouret, M., Bascoul, A., & Escadeillas, G., (2003) Strength Impairment Of Concrete Mixed In Hot Weather Relation To Porosity Of Bulk Fresh Concrete Paste And Maturity. Mag Concrete Research, 55, 215–223.

[22] Neville, A.M., (1997). Properties of Concrete. London, UK. Pitman Publishing.

[23] Rajdy, F., & Richards, C., (1973) Effect of Curing and Heat Treatment History on the Dynamic Mechanical Response and The Pore Structure Of Hardened Cement Paste. Cement Concrete Research, 3: 7–21.

[24] Ramamurthy, K., and Harikrishnan, K.I., (2006) Influence of Binders on Properties of Sintered Fly Ash Aggregate. Cement Concrete Research, 8 (1), 33–38.

[25] Reinhardt. H.W and Stegmaier, M. (2006) Influence Of Heat Curing On The Pore Structure And Compressive Strength Of Self-Compacting Concrete (SCC). Cement Concrete Research, 36: 879– 885.

[26] Taylor, H.F.W. (1997) “Cement chemistry.” London, Thomas Telford.

[27] Topcu, I.B., and Toprak, .M.U., (2005) Fine Aggregate and Curing Temperature Effect on Concrete Maturity. Cement Concrete Research, 35: 758–762.

[28] Turkel, S., Alabas, V., (2005) The Effect Of Excessive Steam Curing On Portland Composite Cement Concrete. Cement Concrete Research, 35: 405–411.

[29] Verbeck, G.J., & Helmuth, R.H., (1968) Structures and Physical Properties of Cement Pastes. In: The Cement Association of Japan (Ed) Proceedings of the 5th International Symposium on the Chemistry of Cement. Tokyo,Japan. pp 1–32.

[30] Verma, C.L., Handa, S.K, Jain, S.K., & Yadav, R.K. (1998) Techno-Commercial Perspective Study For Sintered Fly Ash Light-Weight Aggregates In India. Construction Build Material. 12(6–7). 341–346.

[31] Wang, K.S., Sun, C.J., & Yeh, C.C., (2002). The Thermo Treatment of Msw Incinerator Fly Ash for Use as an Aggregate: A Study of the Characteristics of Size Fractioning. Resource Conserv Recycle, 35:177–190.

[32] Wasserman, R., & Bentur, A., (1997) Effect Of Lightweight Fly Ash Aggregate Microstructure On The Strength Of Concretes. Cement Concrete Research, 27(4), 525–537.

[33] Yazıcı, H., Aydın, S., Yig˘iter, H., & Baradan, B., (2005) Effect Of Steam Curing On Class C High-Volume Fly Ash Concrete Mixtures. Cement Concrete Research, 35:1122–1127.

[34] Yun, B., Ratiyah, I., & Basheer, P.A.M., (2004) Properties Of Lightweight Concrete Manufactured With Fly Ash, Furnace Bottom Ash And Lytag. In: International workshop on sustainable development and concrete technology. Beijing,Chine. 77–88.

[35] ASTM D2216-10, Standard Test Methods for Laboratory Determination of Water (Moisture) Content of Soil and Rock by Mass; 2010.

[36] Mehmet Gesog˘lu ,Erhan Guneyisi , Barham Ali and Kasım Mermerdas, (2013) Strength and transport properties of steam cured and water cured lightweight aggregate concretes. ELSEVIER Construction and Building Materials, Volume 49, December 2013, Pages 417-424

PROPOSED SUSTAINABILITY CHECKLIST FOR CONSTRUCTION PROJECTS

Bayan S. Al-Nu'man[1] , Thamir M. Ahmed[2]

[1&2]Ishik University

[1]*bayan.salim@ishik.edu.iq*,[2]*thamir.ahmed@ishik.edu.iq*

doi:10.23918/iec2018.24

ABSTRACT

Sustainability is a vital and effective contribution to control the use of natural resources in a scientific and accurate manner without wasting work and preserving these resources to meet the current and future needs of societies. The goal of achieving sustainability in construction projects requires procedures that start from design through the use of recyclable materials or reuse. To ensure this, the standards must be defined and implemented in a precise and practical manner. Sustainability criteria for construction projects are organized in sets of questions to be answered by the construction projects officials. These questions take focus on the main building construction steps .The checklist considers weighting the questions according to their level of effect on the sustainability measures. in the current work, 22 construction projects were evaluated in the province of Erbil / Kurdistan region of Iraq through the inclusion of a set of sustainability criteria in the form of questions addressed to the engineers and project managers. The results were analyzed to determine the implementation approaches of the sustainability criteria. Economic, social and environmental factors were included and construction steps were weighed in the questions of the checklist according to these factors. The results confirms the effectiveness of the proposed checklist for estimating a sustainability score for construction projects.the results show high variations in applying sustainability measures in the various construction steps in all of the construction projects. The reasons are due to the absence or weakness of binding laws and the lack of adoption of comprehensive designs based on the pillars of sustainability.

Keywords: Engineering Sustainability, Checklist, Construction Projects

1. INTRODUCTION

In the modern engineering and architectural culture, sustainable design and energy efficiency have become paramount in design and application for architects, engineers and users as civic requirements and financial limitations mount. In all areas of civil engineering, engineers are encouraged to ensure that projects have the maximum lifespan for their intended use and employ the least amount of natural resources (e.g., raw materials and energy required for their production) while still meeting client, economic, social demands and code requirements. ASCE adopted a Code of Ethics, which is the "model for professional conduct" for ASCE members (ASCE, 2006). Within this Code, ASCE has four fundamental principles and seven fundamental canons. Sustainability is mentioned in the first principle: "using [engineer's] knowledge and skill for the enhancement of human welfare and the environment." This principle directly addresses two of the three pillars of sustainability, social and environmental. This act by ASCE of including sustainable principles into their Code of Ethics enforces the commitment of the civil engineering community in understanding and incorporating sustainable practices into the field , (Charles J. Kibert, 2016), (Andrew Braham, 2017) .(Al-Nu'man and Ahmed) 2016, put a detailed checklist useful for construction officials to measure the sustainability condition of construction projects .The same authors (Al-Nu'man and Ahmed) 2016 , applied the developed guidelines on 16 large projects in Kurdistan. Approximately 50% was the score for the application of sustainability measures.

2. ASSUMPTION

The current study is based on the following hypotheses:

1. A questionnaire has been adopted and has included more than 95 questions related to most sustainability measures criteria.

2. The results of the study were based on the answers of the engineer or the project manager and no physical or field investigation have been made.

3. The questions were given different weight of importance. For questions thought to cover the three pillars of sustainability namely, the economic, the social and the environment dimensions, they were given the higher weight (Class A of 3 points). For questions thought to cover the two pillars of sustainability namely, the economic, and the social dimensions,

they were given the medium weight (Class B of 2 points). For questions thought to cover one pillar of sustainability namely, the environment dimensions, they were given the lower weight (Class C of 1 points).

3. QUESTIONNAIRE AND PROJECTS CONSIDERED

The questionnaires were submitted to the managers of these projects or the engineers. The response and interaction of the concerned parties in these projects was good and within the acceptable and useful limits. The accuracy of the responses is relative but sufficient to determine performance and performance indicators. the following is a detailed description of the format of the questions that have been approved and are classified according to the stages of construction workers and have covered most of the basic elements that reflect the implementation of the sustainability criteria.

The following are Questions presented to the projects officials.

"The answers required are only by (Yes/No).

The (Yes) means that sustainability measures are considered in a satisfactory way, the (No) means that sustainability measures are not considered. Reminding hereby that classes A, B and C were given to questions according to their greater impact on principle of sustainability, as mentioned in the assumptions.

1-Site and materials of Construction.

A1 - Avoid construction on main agricultural land

A2-Avoid building on undeveloped land that is environmentally sensitive.

A3-Avoid building on public gardens or adjacent lands to water bodies.

A4 - Choose a building that is well connected to existing public transport networks

A5 - Minimize the impact of the building and protect and promote natural vegetation.

A6 - Proper landscaping, use of contaminated rainwater, and recycled wastewater.

A7 - Minimize the surface of an impervious surface (eg parking) and provide surface drainage system that conducts water to areas on site.

A8-Grading the site to appropriate slopes and planting vegetation that holds the soil in place to prevent erosion.

A9 - Distinct location characteristics such as rock formations, forests, pastures, streams, swamps, trails and recreational facilities never be replaced .

A10 - Shadow provision, surface or reflective surface surfaces, reflective paving materials. Identifying a building for the best exposure to sunlight and wind increases solar heat gain in winter and reduces it in summer to provide heating fuel and air conditioning.

A11- Protection of trees and areas sensitive to the site from damage during construction.

Soil A12 - Soil should be carefully stored during construction and reused on site.

A13 - Construction waste is recycled.

A14 - When the steel frame is demolished, its materials are recycled.

B1 - Guard against soil erosion by water and wind during construction.

B2 - Construction machinery should be selected and maintained so that air pollution is minimized.

B3-Clay and shale, raw materials for bricks, plentiful.

B4 These wastes usually go to landfills or buried at the site.

B5 -When a brick building is demolished, the proper brick can be cleaned from the mortar and reused.

B6- Waste bricks can be crushed and used in landscaping. Brick and mortar debris can also be used as fill in situ.

B7-Steel is galvanized, or given long-lasting polymer coating, or made of more expensive stainless steel.

C1-Surplus extracted soil should be reused either on site or in another nearby location.

C2 - Clay brick can include recycled brick dust, Post-industrial waste such as fly ash.
C3- Sellers apply to brick construction

C4 - Are some spraying materials used on fire-resistant materials?

C5-Steel exposed to weather needs to be repainted periodically

C6- Steel framing members should be built in walls and the walls are thermally broken or insulated in such a way that they do not run heat between the inside and outside.

C7-Surface oil and protective coating, sometimes outgas and cause inhabitant discomfort, are not used.

2-Waste, recycling and green uses.

A1-Use of waste materials from other industries such as fly ash from power plants and slag from iron kilns, copper slag, masonry sand, mill scale, sand gravel and other components of cement and concrete.

A2- Reduce energy consumption, waste, pollutants emissions from each step of the concrete construction process, from the quarries of raw materials through the eventual demolition of concrete construction.

A3- Templates can be reused many times.

A4 - When a concrete building is demolished, the reinforcing steel is recycled.

B1 - Use of concrete made from locally extracted materials and local processing plants to reduce the transport of building materials over long distances.

B2- Minimize the use of materials for molds and fixation.

B3 concrete forms are reused.

B4 - Fragments of crushed concrete can be crushed, sorted and used as new concrete complexes.

B5-parking garages replacement shop surface parking.

B6-Concrete thermal blocks are used to reduce heating and cooling costs.

B7-photo-catalysts are added to the concrete used for road construction and construction.

C1 - Waste materials such as powdered glass, recycled, used foundry sand, recycled concrete replace part of conventional aggregates in concrete.

C2 - Concrete that uses less water using super plastic materials, air entrainment, fly ash.

C3 - Excess concrete is often thrown on the site, where it is cut and removed later and transferred to the landfill for disposal.

C4 - The empty jumper mixing truck must be washed after each batch transfer, these wastes can be recovered and recycled as aggregates and mixing water

C5- Release compounds and processing compounds are used.

C6 - Destroyed concrete is buried on site, used to fill other sites, or dumped in a landfill.

C7-Previous concrete, made of coarse aggregate only, is used

C8- In the field of brown field development, concrete packing materials can be used to stabilize the soil.

C9-Concrete paving is used in black instead of asphalt pavers.

C10 - Internal concrete slabs made of white concrete are used.

3-Roofs

A1-A Roof Rainwater can be made into a tank, or pond for use as domestic water, industrial water, or irrigation.

A2-A surface can support solar heat collectors to save electricity

B1-A roof is used properly to shade the windows from the high summer sun but recognizing the light warming from the sun in the winter is low.

B2- The light-colored ceiling cover is used.

B3-Reflective surfaces are used.

B4-bitumen is used to rely heavily on asphalt compounds derived from coal and petroleum

B5 - Materials resulting from the demolition of built roof membranes are usually burned or transported to waste dumps.

C1. In hot climates, the shading layer is used above the ceiling, with a free ventilation space in between.

C2-cellulose insulation material is used in surfaces.

C3 - Glass wool and mineral wool thermal insulation materials are used in surfaces.

C4-Polystyrene foam thermal insulation material is used in surfaces.

C5- Roofing panels made of cellulose or glass fiber surfaces.

C6-adhesive bonding, solvent welding, and thermal welding of the layers may give off volatile organic compounds (FOC), are not used.

C7-thermal membranes are used as single chips.

4-Exterior wall system

A1 - The outer wall system is used in the entire glass.

B1- glass is used where it can provide daylight lighting and provide views

The south facing surfaces are used from the outer wall to generate electricity.

C1-Windows is opened and closed by occupants.

C2-Thermal bridges are removed from the outer wall.

C3-Fresh air must be provided by the ventilation system in the building, not by air leaking through the outer wall.

C4 glass is used to provide the solar heat of the building in the winter, but be careful to avoid glare, high local temperature, ultra violet degradation of internal surfaces and furnishings exposed to sunlight.

5-Interior wall system

A1-Gypsum Waste generated during construction is minimized by scaling walls and ceilings to make effective use of entire boards or by ordering custom size plates for non-standard sized surfaces.

B1-gypsum board scrap can be permanently stored in hollow cavities of finished walls, eliminate disposal of transportation costs and reduce the amount of material destined for landfill waste.

C1 - additives used in the manufacture of gypsum boards that are moisture resistant and fire resistant are not potential sources of volatile organic emissions (FOCs)?

C2-paints, adhesives that cover the wall used to finish gypsum surfaces can be significant emitters of VOCs, are not used.

6-Finishing materials

A1- The finished material has high recycled content.

A2-Floor plans that are flexible and easily adaptable are used with new uses and partitioning systems that are easy to modify and encourage building reconstruction.

B1-Finished materials eventually finish in landfills.

B2- Finished materials are processed, and manufactured locally.

B3-Indoor Finishing materials and coatings including emitters do not use? For example glue and folders used in wood panels and other manufactured wood products, the leveling compounds applied to supporting, fabrics, carpets, dressings, carpet cushions, carpet adhesives, antimicrobial treatments, carpet mothproofing, wall adhesives covering flexible flooring adhesives and vinyl in all its forms, gypsum board Common vehicles, curtains and upholstery fabrics, paints, varnishes, stains, and more.

B4-formaldehyde gas is not used? It is irritating to build passengers, causing nausea and headaches, and can aggravate asthma.

B5-Organic compounds folate are not used? They're air pollutants.

B6-Use of high ceilings, low partitions, transparency, reflective surfaces, and light colors can maximize day lighting potential and views to the exterior.

B7- Areas designed with exposed structure and without suspended ceilings.

B8- concrete, stone, construction, ceramic tile, cement mortar and plaster used. It is chemically inert and emission-free.

C1 - Internal finishes derived from rapidly renewable sources, such as bamboo flooring or certified timber, reduce the depletion of limited raw materials and the protection of forest ecosystems.

C2-chemical 4-phenyl cyclohexane is not used. Emitted rubber folders are used in some carpets and pads. A carcinogen.

C3-acoustic ceiling tile are not used? It can be a source of volatile organic emissions (FOC) as well as a repository of emissions from other sources.

C4-light-emitting acoustic tiles used.

C5 - Organic adhesives used in tiles and resins are not used? Could it be sources of emissions.

C6 - Sealants applied to hardwood flooring materials to provide water repellent and protection against staining potential sources of emissions, are not used?

C7-self-leveling used in the preparation of Subfloors for flexible floor coatings are potential sources of emissions, are not used?

C8-vinyl (polyvinyl chloride) is a component of many flexible floor coverings and other interior finishing products, is used.

C9- Carpets and pillows are made with at least some recycled material.

C10- The applied adhesives in the factory are used. They tend to have lower VOC emissions than adhesives applied to the construction site.

C11- Carpet tiles not full carpets are used. Tile allows easy spot replacement, reduces the need to replace the full carpet when the area becomes small worn or damaged, thus prolonging the life of carpet installation and reduce waste.

4. CONCLUSIONS AND RECOMMENDATIONS

This work calls for the raise of awareness of the relevant issues through the media and the holding of seminars, as well as the enactment of laws binding the implementation of sustainability standards in all phases of projects initiated in the region. However, this study represented an attempt to indicate the strengths and weaknesses in the extent to which sustainability criteria were applied in selected projects. They may not live up to high levels of accuracy, but they remain important in determining the indicators that are useful in determining the path of treatments towards this strategic objective.

The current study is an attempt to create a vision of the overall engineering performance of the construction projects and the extent of convergence of the criteria of sustainability and the need to conduct research and studies to cover all aspects of this important subject The questionnaire form should cover more work items and it is better if it is extent to the design. Also the assessments will be more strength if it is support by field observation.

State institutions and ministries must take responsibility for formulating policies and setting standards and controls for all companies and sectors to adopt sustainability standards starting from design, implementation and operation.

REFERENCES

[1] American Society of Civil Engineers, (2006), Code of Ethics.

[2] Andrew Abraham, (2017), Fundamentals of Sustainability in Civil Engineering.

[3] Charles J. Kibert, 2016, Sustainable Construction: Green Building Design and Delivery

[4] Al-Nu'man, Bayan S., Ahmed, Thamir M., Tahir, D. and Agar, B.,"Assessment of sus performant of construction projects in Kurdistan" proc. of the first international conference on development in civil and computer engineering applications, IEC 2014, Ishik University, Erbil, Iraq, Nov. 2014, pp.19-27.

[5] Al-Nu'man, Bayan S., and Ahmed, Thamir M.,"Sustainabiliy in construction projects: part 1 elements" proc. of the second international conference on development in civil and computer engineering applications, IEC 2016, Ishik University, Erbil, Iraq, Feb. 2016, pp.61-68.

[6] Al-Nu'man, Bayan S., and Ahmed, Thamir M.,"Sustainabiliy in construction projects: part 2 case studies" proc. of the second international conference on development in civil and computer engineering applications, IEC 2016, Ishik University, Erbil, Iraq, Feb. 2016, pp.69-77.

APPLICATION OF A PROPOSED SUSTAINABILITY CHECKLIST FOR CONSTRUCTION PROJECTS

Thamir M. Ahmed[1] ,Bayan S. Al-Nu'man[2]

[1&2]Ishik University
[1]thamir.ahmed@ishik.edu.iq,[2]bayan.salim@ishik.edu.iq

doi:10.23918/iec2018.25

ABSTRACT

In the current work, 22 construction projects were evaluated in the province of Erbil / Kurdistan region of Iraq through the inclusion of a set of sustainability criteria in the form of questions addressed to the engineers and project managers. The results were analyzed to determine the implementation approaches of the sustainability criteria. Economic, social and environmental factors were included and construction steps were weighed in the questions of the checklist, developed in a companion paper, according to these factors. The results confirms the effectiveness of the proposed checklist for estimating a sustainability score for construction projects. In average, the score of approximately 54% of applying the sustainability measures was obtained. The results show high variations in applying sustainability measures in the various construction steps in all of the construction projects. The reasons are due to the absence or weakness of binding laws, absence of sustainability requirements as a topic in civil engineering curricula, and the lack of adoption of comprehensive designs based on the pillars of sustainability.

Keywords: Engineering Sustainability, Checklist, Construction Projects.

1. INTRODUCTION

In all areas of civil engineering, engineers are encouraged to ensure that projects have the maximum lifespan for their intended use and employ the least amount of natural resources (e.g., raw materials and energy required for their production) while still meeting client, economic, social demands and code requirements. this subject is of vital importance in Erbil province; with the existence of many construction projects all over the city and the lack of proper knowledge on evaluation and measurement of sustainability of construction projects. The authors tried in previous works to develop a framework of sustainability performance checklist for construction projects. (Al-Nu'man et al,) in 2014, investigated 11 of the largest construction projects in Kurdistan of Iraq to find out to what degree the sustainability measures were implemented. They obtained 40.48% in average as a score of sustainability in construction projects. They found that "building and material reuse", "recycling" and "waste prevention" requires great attention. (Al-Nu'man and Ahmed) 2016, put a detailed checklist useful for construction officials to measure the sustainability condition of construction projects. The same authors (Al-Nu'man and Ahmed) 2016, applied the developed guidelines on 16 large projects in Kurdistan. Approximately 50% was the score for the application of sustainability measures.

2. OBJECTIVES AND METHODOLOGY

The objectives are to examine sustainability assessment for different construction stages, and to evaluate the sustainability of the collected responses on construction process of projects in Erbil province, more thoroughly, through interviews with project engineers.

A project sustainability performance checklist was developed in a companion paper (Al-Nu'man and Ahmed 2018), that can be used by all construction project participants to understand, assess and improve sustainability performance of construction projects. The data used for analysis are mainly from a comprehensive literature review. Interviews were invited and arranged with different project parties, including engineers and managers. These interview discussions provide valuable comments on the sustainability measures that were taken into consideration through the construction process.

3. RESULTS OF AWIDE SURVEY AND DISCUSSION

The checklist described in (Al-Nu'man and Ahmed) 2018 is used in a wide survey on 22 large projects in Kurdistan. Table 1 shows the list of these projects, the corresponding sustainability average scores and weighted average scores. The average score considers all the questions are of the same weight. The weighted average score considers a weighted average based on 3 points for class A questions, 2 points for class B questions and 1 point for class C questions. Figures 1 to 6 show the results of answers on the checklist on the specific main construction steps namely; site, wastes and recycling, roofs, exterior wall systems, interior wall systems, and finishing materials.Figure 7 summarizes the results according to construction category and questions class.

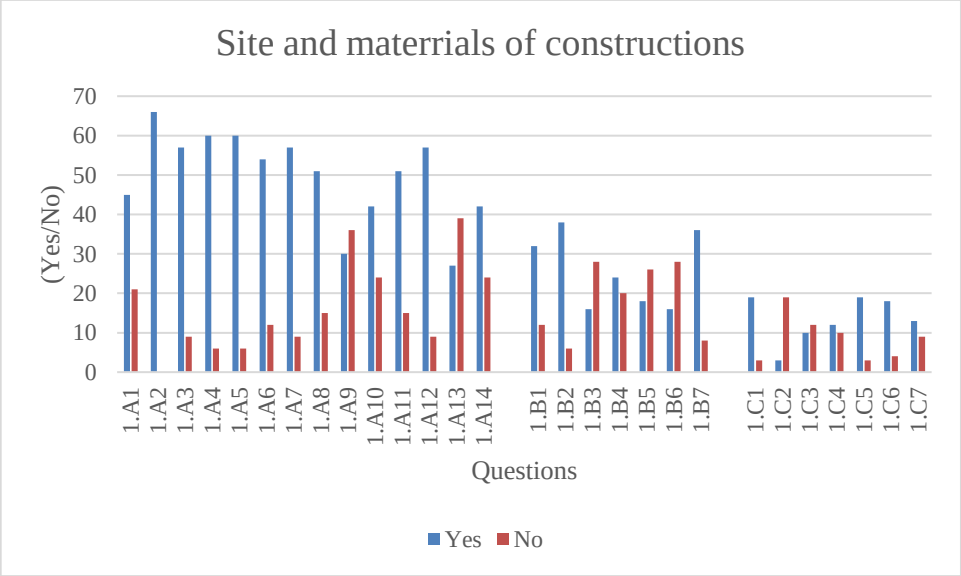

FIGURE 1. Answers for site and materials of constructions

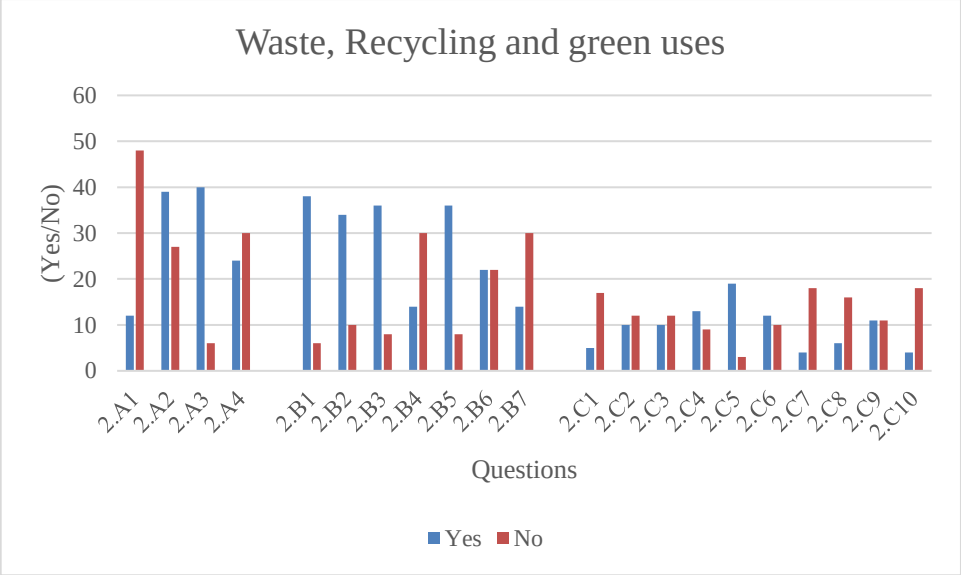

FIGURE 2. Answers for waste, recycling and green uses

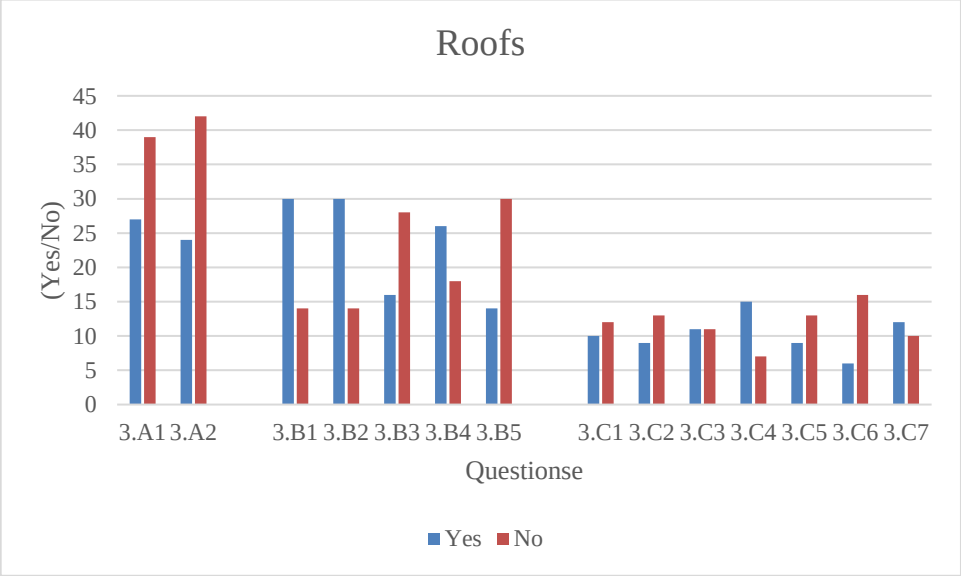

FIGURE 3. Answers for roofs

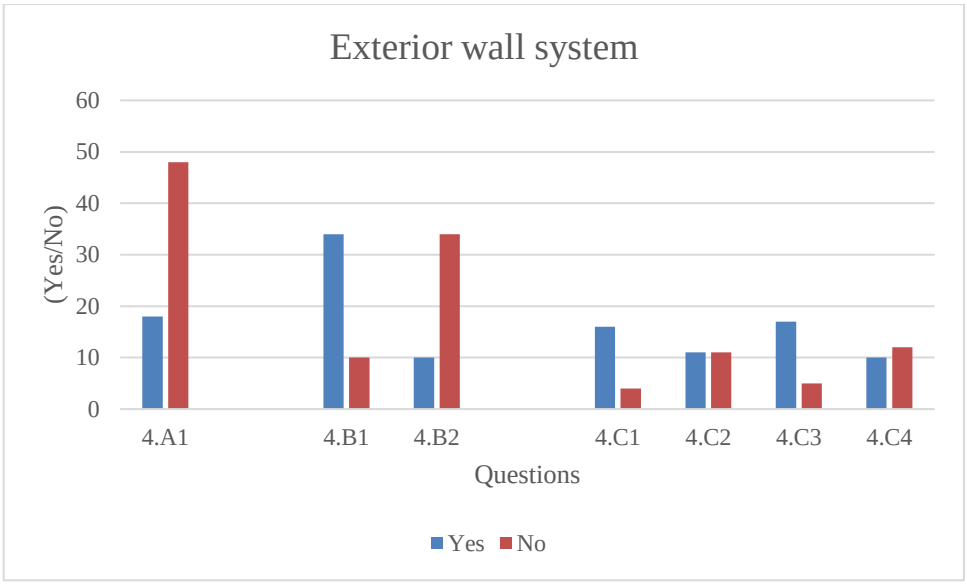

FIGURE 4. Answers exterior wall systems

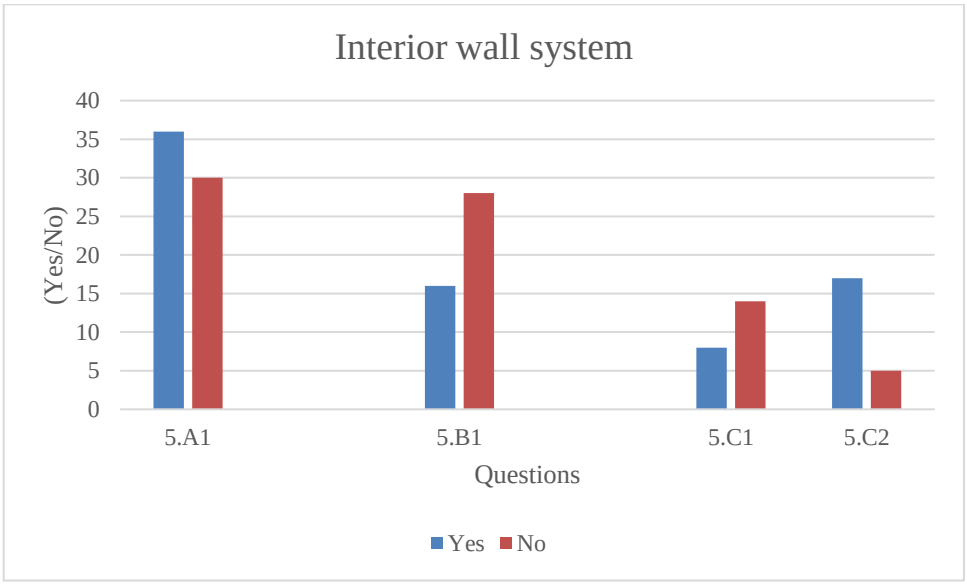

FIGURE 5.Answers interior wall systems

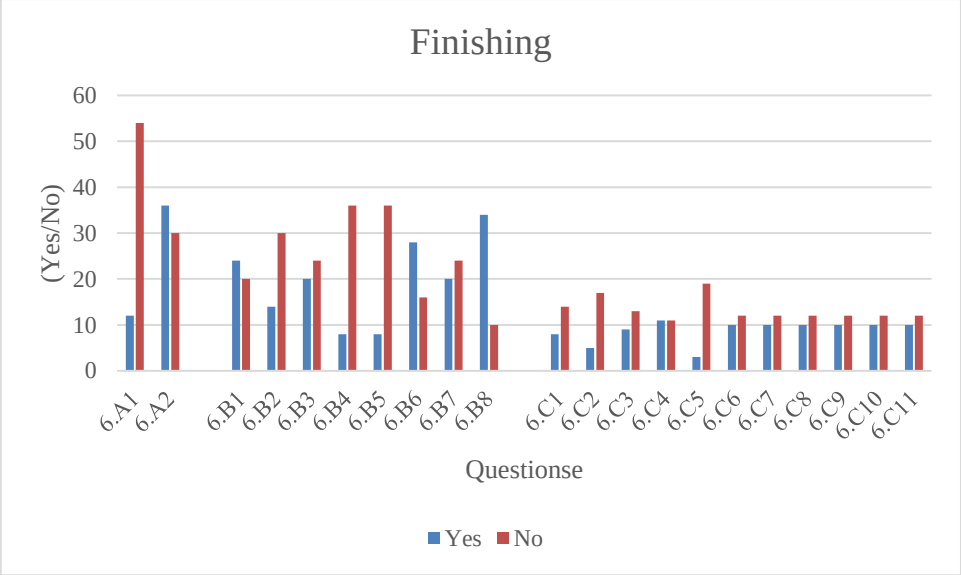

FIGURE 6. Answers for finishing

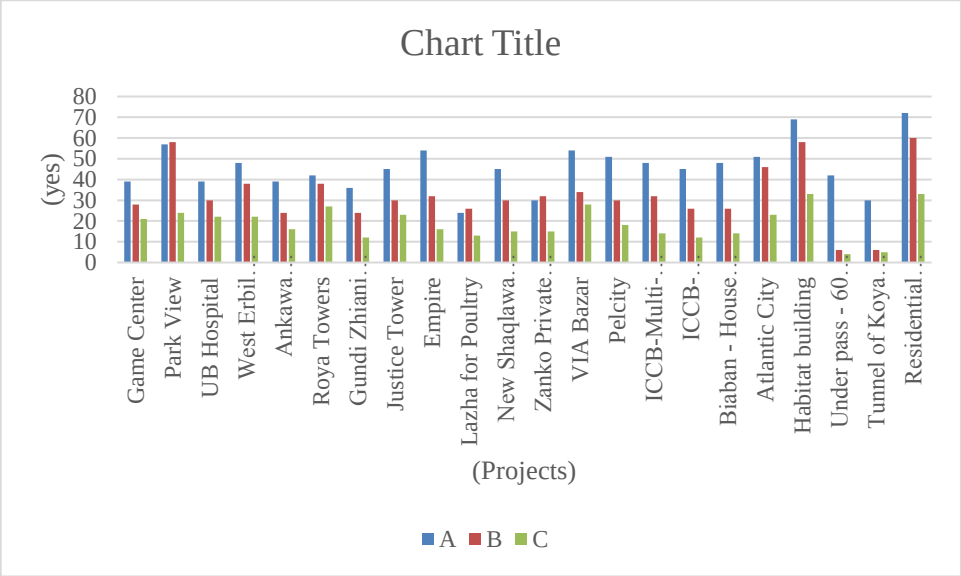

FIGURE 7. Answers for scores of considered projects

From the results it can be concluded as follows:

Most of the projects took into consideration the site selection for various reasons; main reason being the transportation system and how far the project is from main streets. However most of the projects were not making use of recycled materials. from the results it was found that most of the firms or companies did not have specific policies for minimizing wastes and recycling them. The survey results indicated that the five most significant sources of construction waste were design changes, leftover material

scraps, wastes from packaging, design/detailing errors, and poor weather. The result indicated that most of the projects used the traditional design and materials for the roof systems. However, some projects employed insulation layers for minimizing daily heat flow and therefore minimizing daily energy demand. As for water management, it is confirmed that green roofs significantly mitigate storm water runoff generation, most of the projects below did not include this aspect into their roof construction phase. Some aspects of sustainability were not witnessed in designing the exterior walls of most of the buildings. Companies stated that the cost of applying sustainable measures like green walls, for example, outweigh or compensate the benefits of such techniques. It is important to state that most of the projects did not consider the problems associated with using volatile organic compounds while furnishing the interior or during painting. Some stated that sustainability measures were not even discussed during the project feasibility studies. Most of the projects were not compatible with the sustainability requirements for finishing materials. Materials with VOCs has been used in furnishing also no materials of recycled content has been used or what is specified as green materials. The cost of sustainable material use is a factor, as stated before the sustainability standards were not included during the feasibility study nor implemented during the construction stage. Lack of policy within the companies also acts as a major factor.

4. SUMMARY OF QUESTIONAIRE OUTPUT

Overall, the case studies show that the sustainability assessment checklist succeeds in assessing sustainability in civil engineering projects if the data is available and reliable. Sustainability data is therefore the key requirement to successfully apply the sustainability assessment checklist. Without specific indicator data, the framework can still be applied, but it is expected that the indicator is given insignificant points since the assessor cannot substantiate a certain indicator score. Table 1 shows the sustainability scores of the projects.

TABLE 1.

Sustainability Scores of the projects

Project's name	A score %	B score %	C score %	Av.Score	Av.Wt.Score
Game Center	162.50	93.33	51.22	50.68	51.18
Park View	237.50	193.33	58.54	78.12	81.56
UB Hospital	162.50	100.00	53.66	52.61	52.69
West Erbil Emerg. Hosptial	200.00	126.67	53.66	61.22	63.39
Ankawa Private hopital	162.50	80.00	39.02	44.40	46.92
Roya Towers	175.00	126.67	65.85	62.51	61.25
Gundi Zhiani Hawcharekh	150.00	80.00	29.27	39.76	43.21
Justice Tower	187.50	100.00	56.10	56.20	57.27
Empire	225.00	106.67	39.02	55.79	61.78
Lazha for Poultry	100.00	86.67	31.71	36.12	36.40
New Shaqlawa City	187.50	100.00	36.59	49.70	54.01
Zanko Private Hospital	125.00	106.67	36.59	43.86	44.71
VIA Bazar	225.00	113.33	68.29	66.65	67.77
Pelcity	212.50	100.00	43.90	54.91	59.40
ICCB-Multi-Story -building	200.00	106.67	34.15	51.38	56.80
ICCB-Company- Worehouse	187.50	86.67	29.27	45.03	50.57
Biaban - House buildings	200.00	86.67	34.15	48.05	53.47
Atlantic City	212.50	153.33	56.10	67.87	70.32
Habitat building	287.50	193.33	80.49	91.00	93.55
Under pass - 60 m, Erbil	175.00	20.00	9.76	26.03	34.13
Tunnel of Koya Road	125.00	20.00	12.20	21.29	26.20
Residential building , Basra	300.00	200.00	80.49	93.50	96.75
Average %	190.91	108.18	45.45	57.42	54.39

The average of sustainability score was (57.42 %) and the weighted average score was (54.39 %). The classification into ‘strong’, ‘normal and ‘weak’ sustainability questions in the checklist do influence the results and therefore it may be recommended to follow.

8 .CONCLUSIONS AND RECOMMENDATIONS

In this regard, the present study concluded some of the results as follows:

1. Most of the projects took into consideration the site selection for various reasons; main reason being the transportation system and how far the project is from main streets.
2. Most of the projects were not making use of recycled materials.
3. Most of the firms or companies did not have specific policies for minimizing wastes and recycling them.
4. Most of the projects used the traditional design and materials for the roof systems.
5. Materials with VOCs, which are not sustainable materials, have been used in furnishing.
6. The average sustainability score (57.42%) and the weighted one (54.39) are approximately similar to what was scored in previous works (4,5,6) which confirms that this checklist questionnaire is effective in estimating .

REFERENCES

[1] American Society of Civil Engineers, (2006), Code of Ethics.

[2] Andrew Abraham, (2017), Fundamentals of Sustainability in Civil Engineering.

[3] Charles J. Kibert, 2016, Sustainable Construction: Green Building Design and Delivery

[4] Al-Nu'man, Bayan S., Ahmed, Thamir M., Tahir, D. and Agar, B., "Assessment of sustainability performance of construction projects in Kurdistan" proc. of the first international conference on development in civil and computer engineering applications, IEC 2014, Ishik University, Erbil, Iraq, Nov. 2014, pp.19-27.

[5] Al-Nu'man, Bayan S., and Ahmed, Thamir M., "Sustainabiliy in construction projects: part 1 elements" proc. of the second international conference on development in civil and computer engineering applications, IEC 2016, Ishik University, Erbil, Iraq, Feb. 2016, pp.61-68.

[6] Al-Nu'man, Bayan S., and Ahmed, Thamir M., "Sustainability in construction projects: part 2 case studies" proc. of the second international conference on development in civil and computer engineering applications, IEC 2016, Ishik University, Erbil, Iraq, Feb. 2016, pp.69-77.

[7] Al-Nu'man, Bayan S., and Ahmed, Thamir M., "Proposed sustainability checklist for construction projects" to be published in the proc. of the fourth international conference on development in civil and computer engineering applications, IEC, Feb. 2018, Ishik University, Erbil, Iraq.

MODELLING ENERGY DEMAND FORECASTING USING NEURAL NETWORKS WITH UNIVARIATE TIME SERIES

S. Cankurt[1], M. Yasin[2]

[1&2]Ishik University Erbil, Iraq
[1]s.cankurt@ishik.edu.iq ,[2]m.yasin@ishik.edu.iq

doi:10.23918/iec2018.26

ABSTRACT

The new era of consumption and change in the behavior of people in developing countries that we facing in recent decades has made not only the energy sector but also all resource suppliers in different sectors not to fulfill the demand in the field. The electricity, which is one of the main power resources, has become one of the major issues to be overcome for the governments. Predicting the future energy demand is always the most valuable information to achieve any success in many sectors. In this paper, a daily forecasting of the maximum energy demand in Kurdistan region of Iraq is investigated based on an artificial natural network and sliding window techniques. The standard mean absolute percentage error method is used to evaluate the accuracy of forecasting models.

Keywords: Neural networks, Sliding window technique, Energy demand forecasting.

1. INTRODUCTION

One of the most important factors to improve the quality of life is energy, it also ensures the economic and social development. However, rising energy prices, climate change, and global warming has led to an increase in energy demand throughout the world. On the other side the rapid consumption of fossil fuel and being dependent on it, as well as the insufficiency investment for developing new technologies, to meet the growing demand for commercial energy, makes countries worry about the security of energy supply. the Electricity Control Center located in Erbil is the highest authority for distributing the generated electricity to the cities of the region. The city distribution center directorate manages for the equivalent distribution of the supplied energy according to the hourly schedule for each district in the city. The main energy generation in the region comes from dams and fossil fuel. However, since the late of 2014 due to the economic crises, the gas power plants is not used as one of the main energy sources.

1.1. LITERATURE REVIEW

Using ANN for load forecasting is one of the most popular approaches for predicting the energy demand. In 2006, seasonal autoregressive integrated moving average (SARIMA) has been used for monthly peak-load demand forecasting in Sulaimany in KRG governorate [1]. A similar approach in Bagdad has been handled for short-term load prediction based on hourly consumption adding to weather data combining with electricity consumption in 2010 [2]. since 2008 for predicting the electricity price in a liberal electricity market in Turkey, load forecasting has gain importance for the supporting financial market, many researchers focused on using the different approaches for more accurate results. In 2015, a multivariable approach has been used by supporting the time series data combining with weather historical data for just big cities to predict more accurate electricity consumption in Turkey [3]. In the literature, integration of the neural network approach and sliding window time series technique is employed for the forecasting in several different applications. For example, it has been used by Vornberger and Thiesing for sales forecasting [4], and

by Vafaeipour et al. for prediction of wind velocity [5]. In this study, we have used the neural network approach with sliding window time series technique to forecast the maximum energy demand in the Kurdistan region of Iraq.

2. DEVELOPMENT OF THE ENERGY DEMAND MODELS

2.1. DATASET PREPARATION

In this paper, the data used in the development of the forecasting models is the single time series (univariate) of historical electricity demand data obtained from the Electricity Control Center (ECC) of Kurdistan region in Iraq. The data is accumulated daily and involves the maximum electrical demand load in Mega Watt (MW) from 1st January 2014 to 31st October 2017. by using sliding window technique with the lag size of 14, step size of 1 and horizon size of 1, 3, 7 and 14 we have generated 4 datasets in a tabular format from single time series data. normalization of the dataset could help improve the performance of the network by reducing effects of noisy data and flatting the distribution of the attributes [6]. We have used a transformation technique, which scales the data between the upper and lower limits of -1 and 1. This transformation can be archived by using the following expression:

$$x_{normilized} = \frac{2 \times x - (x_{max} + x_{min})}{x_{max} - x_{min}}$$

being x is original value, $x_{normilized}$ is scaled value between -1 and 1, and x_{max} is the maximum value, x_{min} is the minimum value in the data.

2.2 ARTIFICIAL NEURAL NETWORKS

In this paper, we have used the multilayer ANN models to forecast the maximum energy demand. The multilayer perceptron is one of the widely used Multilayer ANN models, which is an advancement of single layer perceptron. A single perceptron [7] and a typical multilayer perceptron network are depicted in Figure 1 and 2 respectively. Multilayer network design of perceptron makes able the ANN models to solve the non-convex classification and non-linear regression problems. MLP models are boosted after the introduction of the backpropagation (BP) algorithm, which is one

of the widely employed training algorithms in ANN models and initially formulated in 1986 by Rumelhart, Hinton, and Williams and it is developed more later [7].

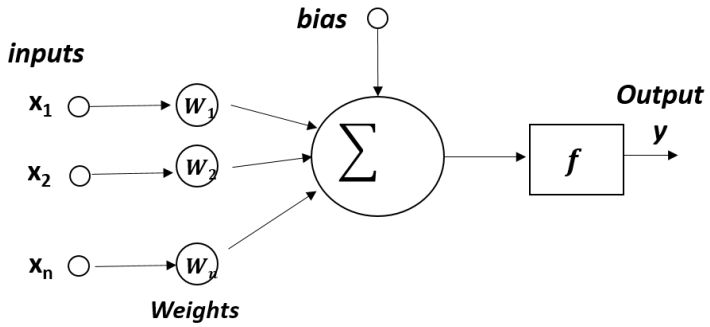

FIGURE 1. A single neuron

Backpropagation method overcomes the adjustment shortcoming of the intermediate weights to justify the strength of the connections in the hidden layers that is the training process of the neural network. BP uses the gradient descent training algorithm, which aims to minimize the total squared error (E), defined as follows [7]:

$$E = \frac{1}{2}\sum_{s}^{S} E_s = \frac{1}{2}\sum_{s}^{S}\sum_{i}^{N}(t_{si} - p_{si})^2$$

where E_s is the error presented after input s, t is the real output and p is the predicted output. This calculation iterated thorough the nested loop for each input set indexed as *s* and each processing unit indexed as *i* [7].

2.3 DEVELOPMENT OF THE ANN FORECASTING MODEL

In this study, we have used the Time Series Analysis and Forecasting package [8] and WEKA workbench [9] to develop time series models based on the multilayer ANN models to forecast the maximum electrical energy demand. Various network models based on multi-layer feedforward architecture are tested with different designs and different configurations of hyper-parameters. After several trials, the near-optimal values for the parameters of the multilayer neural network are observed as the learning rate of 0.05, momentum value of 0.1, and one hidden layer with neurons of 14. The architecture of the network is illustrated in Figure 2. It has 14 sigmoid type of neurons

in the hidden layer and one linear type of output neuron and trained by using the backpropagation algorithm. Also, it has 14 inputs labeled by P_{t-1} to P_{t-14}, which denote the maximum power demands of the day before, two days before and so forth.

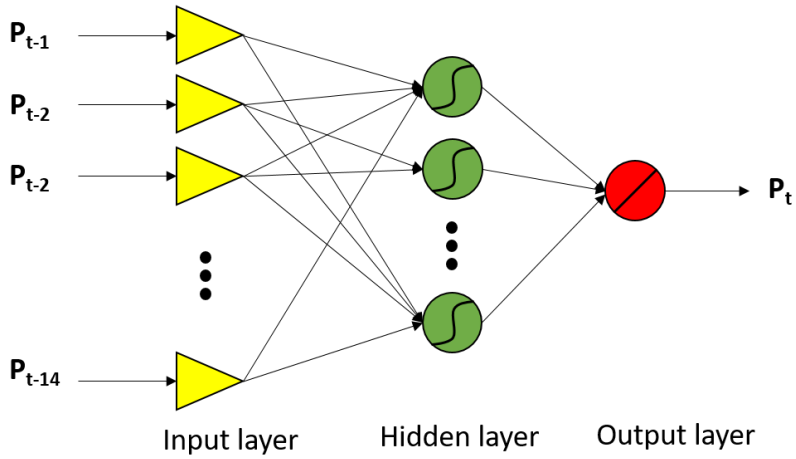

FIGURE 2. ANN model with 14-lag and one-day-ahead horizon

3. RESULTS AND DISCUSSION

Neural network models are evaluated on the out-of-sample dataset, which is obtained by holding out of 20-percent of the whole dataset linearly. We have used the performance metrics of mean absolute percentage error (MAPE) and R^2 to report the results presented by the neural network on the test datasets. with the implementation of the sliding window technique on the time series and neural network, we have developed a forecasting model using the energy demand time series. The addition scaling data transformation is done to adjust the demand time series for the better forecast accuracy. neural network demonstrated R^2 0.9741 and MAPE of 2.98% accuracy results for one-day-ahead forecasting and demonstrated R^2 of 0.72 and MAPE of 9.4557 % accuracy results for 14-day-ahead forecasting for the test dataset as seen in Table 1. from the simulation results shown in tables 1 and 2, and in figures 2 and 3, the proposed model has achieved a reasonable accuracy in one-day-ahead maximum demand load forecasting. However, the model performance by means of accuracy is not as good as one-day-ahead forecasting when the forecasting horizon increases as demonstrated in table 1.

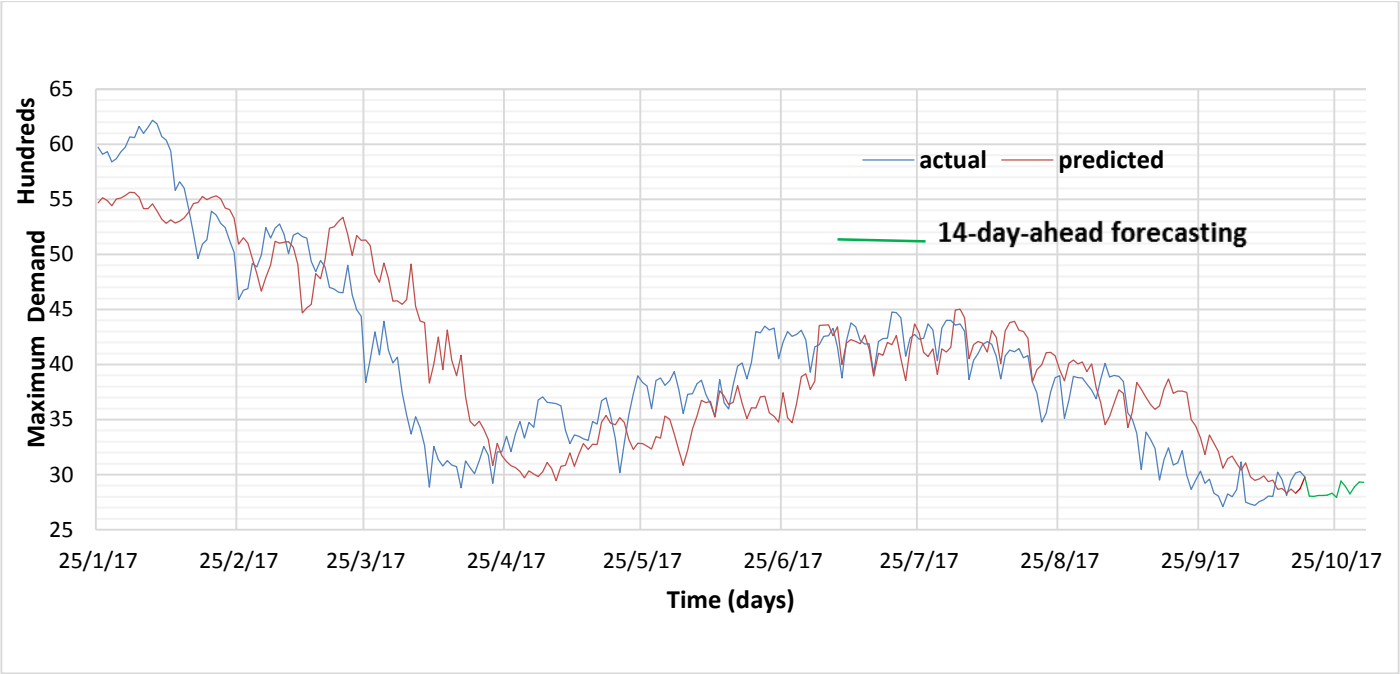

FIGURE 3. Forecasted versus actual maximum demand load for the test dataset and 14 days ahead forecasting

TABLE 1.

Forecasting errors 1 to 14 days ahead for the test dataset

Target	1 day ahead	3 days ahead	7 days ahead	9 days ahead	14 days ahead
Mean absolute percentage error (%)	2.9797	4.7363	6.2725	7.5372	9.4557
R^2	0.9741	0.9326	0.8695	0.8263	0.719

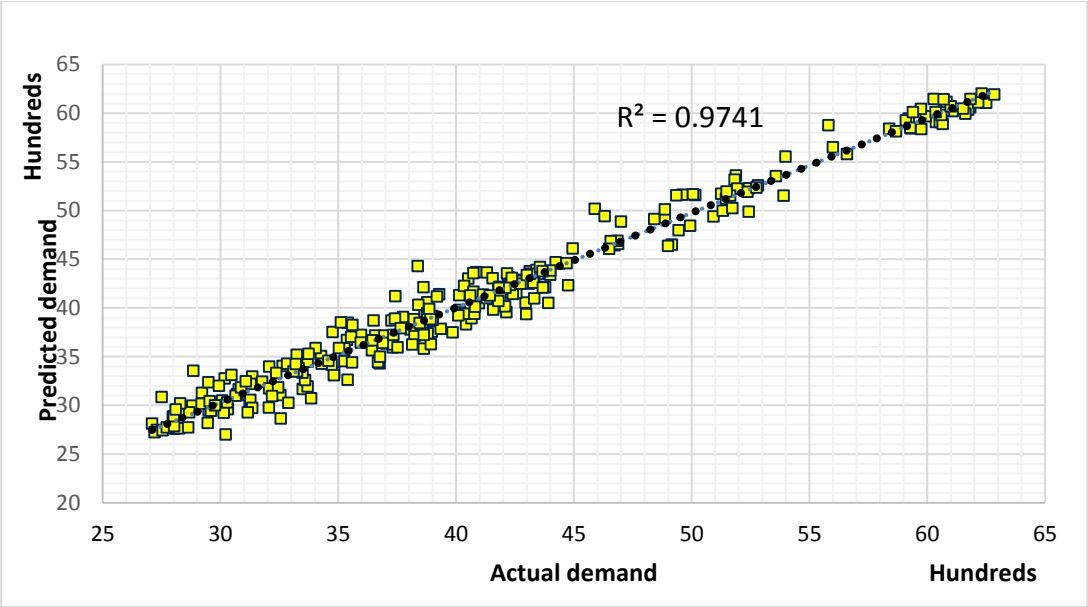

FIGURE 4. Correlation of actual and predicted maximum demand load in MW (1-step ahead)

TABLE 2.

Forecasted versus actual maximum demand load for the last 10 data points in the test dataset using 1-step ahead forecasting model

instance #	actual (MW)	predicted (MW)
1391	2772	2771.29
1392	2804	2783.36
1393	2803	2887.68
1394	3023	2700.35
1395	2954	3041.65
1396	2811	2956.41
1397	2947	2818.57
1398	3014	2922.05
1399	3029	3029.05
1400	2978	2999.72

4. CONCLUSION

In this paper, we have developed a neural network model based on a multilayer feedforward neural network to forecast the maximum electrical energy demand by employing the single time series data (univariate) for the case of Kurdistan region in Iraq. This study treats the single time series data as multivariable by employing the moving window data pre-processing method which is a way to apply the machine learning and data mining forecasting techniques in the case of having the single time series. Like many other previous successful attempts for the demand forecasting and function approximation in the literature, in this case, multilayer neural network is also demonstrated satisfactory estimation with an accuracy of MAPE 2.98%. Neural networks are able to successfully approximate the continuous functions including the non-linear functions and can also efficiently deals with noisy data. These properties make the neural network a strong forecasting tool [6]. Yet another side, it requires a systematic development methodology starting from data pre-processing, designing of the network architecture, configuration of the parameters to the evaluation of the network. Especially implementation and configuration stages of the neural networks are more of an art than science, which requires many trials and fails.

REFERENCES

[1] Y. H. Kareem and A. R. Majeed, "Monthly Peak-load Demand Forecasting for Sulaimany Governorate Using SARIMA.," 2007.

[2] M. R. G. Al-Shakarchi and M. M. Ghulaim, "Short-Term Load Forecasting for Baghdad Electricity Region," Electric Machines & Power Systems, p. 16, 2010.

[3] M. Yasin, T. Göze, İ. Özcan, V. Ç. Güngör and Z. Aydın, "Short term electricity load forecasting: A case study of electric utility market in Turkey," in Smart Grid Congress and Fair (ICSG), 2015 3rd International Istanbul, Istanbul, 2015.

[4] O. Vornberger and F. M. Thiesing, "Sales Forecasting Using Neural Networks," in ICNN97, Texas, 1997.

[5] M. Vafaeipour, O. Rahbari, M. A. Rosen, F. Fazelpour and P. Ansarirad, "Application of sliding window technique for prediction of wind velocity time series," International Journal of Energy and Environmental Engineering, 2014.

[6] I. Kaastra and M. Boyd, "Designing a neural network for forecasting financial and economic time series," Neurocomputing, pp. 215-236, 1996.

[7] D. Graupe, Principles of Artificial Neural Networks, 3rd ed., 2013.

[8] M. Hall, "Time Series Analysis and Forecasting with WEKA," 2014.

[9] I. Witten, E. Frank, M. A. Hall and C. J. Pal, "Data Mining: Practical Machine Learning Tools and Techniques," 2016.

EXPERIMENTAL STUDY AND PREDICTION MAXIMUM SCOUR DEPTH EQUATION OF LOCAL SCOUR AROUND BRIDGE PIER

Mohammed Tareq Shukri[1], M. Günal[2], Junaid Kameran Ahmed[3]

[1&3]Ishik University, Erbil, Iraq,
[2]Gaziantep University, Gaziantep, Turkey
[1]mohammed.tareq@ishik.edu.iq,[2]gunal@gantep.edu.tr,[3]junaid.kameran@ishik.edu.iq

doi:10.23918/iec2018.27

ABSTRACT

Scour is a problem which happen in the flowing stream, rivers and it's a natural phenomenon made due to the erosive action of which removes the sediment particles around the structures placed in water. It means the lowering of the riverbed level by water erosions such that there is a direction to reveal structural foundations. The flowing water cause erosive action, excavating and relocate material from the bed and banks of streams and from around the piers of bridges. In this paper an attempt is made to evaluation the temporal variation of scour depth at non-uniform cylindrical bridge pier, in this paper 3 samples of circular bridge piers tested with different size which conducted in a 8.3 m length and 0.8 m width cannel by analyzing the data from experimental work analyzing the data to estimate equation which predict maximum scour depth.

Keywords*:* scour, local scour, bridge piers.

1. INTRODUCTION

Scour is defined as the erosion of streambed sediment around an obstruction in a flow field (Chang 1988) [1]. It is movement and removal of the sediment around bridge pier. Bridge scour isusually divided into general scour, contraction scour and local scour. The local scour may happen in any time especially in flood time caused collapse for bridges and loss many lives. Figure 1, shows the complex vortex system occure when down flow waves rolls up as it continues to create a hole through interaction with the oncoming flow. The vortex then extends downstream along the sides of the pier. This vortex is often referred to as horseshoe vortex because of its great similarity to a horseshoe. Even though a lot of work, the predicted of equilibrium depth of maximum scour analyzed depending on both the numerical and experimental studies, many researchers still are interested in the basic understanding of the scour mechanism. Local scour was classified into live-bed scour and clear-water scour depend on the variance of the approach flow sediment transportation pattern, (Chabert and Engeldinger, 1956) [2].

.Therefore, the scour study has become a topic of continued interest to the investigators. Review of the important experiments and field studies was given by Breusers et al. (1977) [3]; Dargahi (1982) [4]; Dey (1997) [5]; Hoffmans and Verheij (1997) [6]; Melville and Coleman (2000) [7]; and Richardson and Davis (2001) [8].

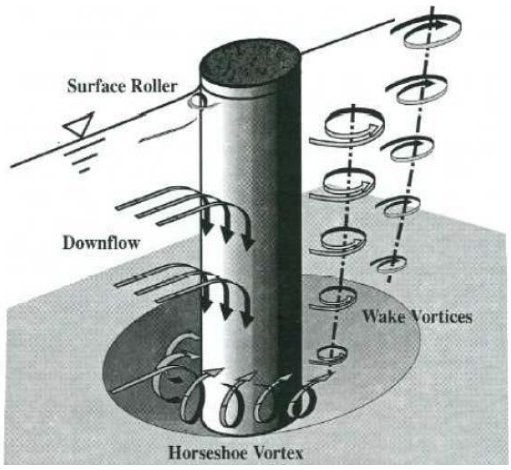

FIGURE 1. Vortex motion around a pier Melville & Coleman (2000) [7]

1.1 . SCOUR PROCESS

The sediment particles close to the pier started to move when flow reaches a certain velocity in the channel; scour is initiated. The eroded particles will carried from the front of the pier to the direction of downstream by following the stream pattern. By flow velocity increase, more particles will get displaced, then creating a scour hole increasing in size and depth. Eventually a maximum scour depth, $(d_s)_{max}$, is reached which corresponds to a flow velocity being near to the critical velocity $U=U_{cr}$. For nonuniform particles, the large size of the particles will be sediment in the scour hole, and an armoring layer forms itself in the scour hole. Then by increasing flow velocity, $U>U_{cr}$, is caused for a transport of sediments *in* and *out* of the scour hole, but the scour depth remains essentially constant. Thus an average equilibrium scour depth, d_s, establishes itself, being slightly smaller than the maximum scour depth, $(d_s)_{max}$ (Figure 2) .

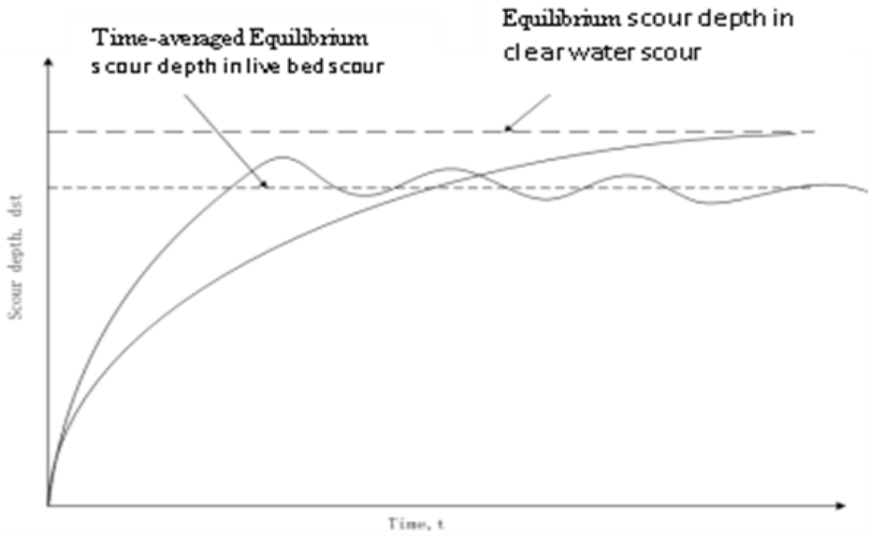

FIGURE 2. Time-dependent development of scour depth (Raudlivi and Ettema 1983) [9].

2. EXPERIMENTAL SETUP

A circulating flume used in this study for the experiment work as shown in figure 3 and figure 4. The size of the flume are (8.3 0.8, 0.9) m. The study section was setup about 2.8 m from inlet of the flume which is filled with sand according to the literature study the medium size of the particles d_{50}= 4mm and gradation coefficient σ_g=1.15 the depth of the section is 20 cm and with a length of 1.5m. The

shape of the models is circular with a diameter of 5cm and 7.5 cm 11.1cm respectively. The pump ability 25 l/sec located at the left of the channel served the system and by a valve the flow in the channel controlled. A rectangular weir located at the end of the channel to measure the discharge and there is a point gage to measure the depth of the scour hole. To keep the flow uniform before and after the bridge pier, a ramp was constructed and fastened to the upstream and downstream of the test section of the channel. The detail of experimental data given in Table 1. The variation of local scour depth with time is measured at various time by stopping the experiments and run it again.

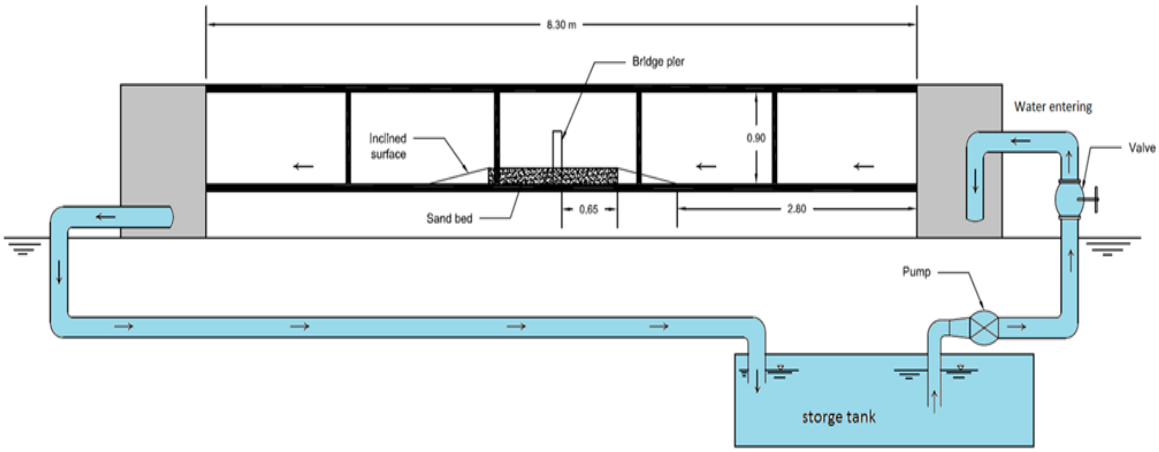

FIGURE 3. Schematic illustration of the experimental flume system

FIGURE 4. View of experimental work

TABLE 1.

Experimental conditions

Run	diameter (cm)	h (cm)	time (min)	discharge (m3/s)	observed ds (cm)	computed ds (cm)
A1	5	2.5	15	0.00629	6	5.482703675
A2	5	4.4	30	0.016	7.7	6.496038265
A3	5	5.4	30	0.02326	8.2	6.907659147
A4	5	5.7	30	0.02519	8.5	7.057342092
B1	7.5	2.5	50	0.00629	6.1	7.28213382
B2	7.5	4.4	30	0.016	9.1	8.628046079
B3	7.5	5.4	30	0.02326	9.7	9.174761444
B4	7.5	5.8	50	0.02519	10.5	9.373570517
C1	11.1	2.5	30	0.00629	6.4	9.805482815
C2	11.1	4.4	40	0.016	11.2	11.35260838
C3	11.1	5.4	35	0.02326	11.7	12.07196539
C4	11.1	5.8	30	0.02519	11.9	12.33355434

*A: code for 5 cm circular pier *B: code for 11 cm circular pier *C: code for 7.5 cm circular pier

3. PREDICTED MAXIMUM SCOUR DEPTH

In this study there are parameters effects on maximum scour depth; results of Group 3 tests show us the relation between these parameters and maximum scour depth. Computer software Step-wise Regression© which it was one of the regression analysis methods and fitted data, Step-wise Regression used in this study to analyses the results of the maximum scour depth to get formula which give us maximum scour depth (d_s). The parameters like (d) pier width, (t) time of equilibrium, (Q) discharge, (h) flow depth, used to analyses a formula for maximum scour depth. In the program, there are many types of regression method as shown in Figure 4, it will necessary to try all methods to know the best one. In this study, linear method, linear+ interaction method, and full quadratic method are used to predict maximum scour depth, it is seen that the last method is the best method in this study to predict maximum scour depth.

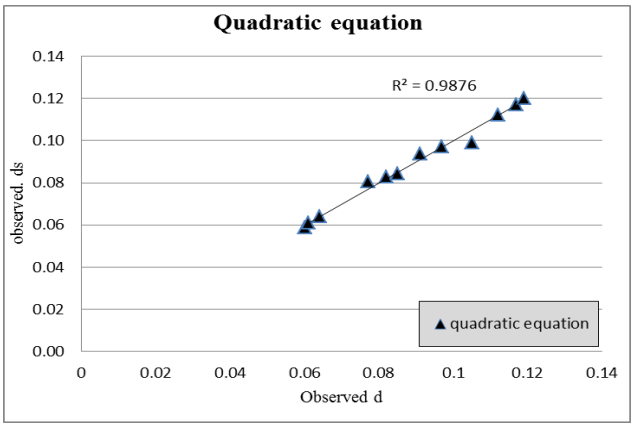

FIGURE 5. Step-wise regression input window

3.1. QUADRATIC REGRESSION METHOD

The formule rusults acoording to this method depending on, (h) depth flow, (d) pier diameter, (Q) discharge, with R- square value R^2= 0.988 and Standard Error of 0.00260. According to this results the quadratic method was an best suited method to predict eqilibrium scour depth by Equation (1) for this study. Figure 5, shows the comparison between determined and observed maximum scour depths using quadratic equation.

$$dse = 0.0548 - 0.0427\ d * 1/h - 0.351\ d * lnQ \quad (1)$$

Where d_{se}: Equilibrium scour depth (m), d: Pier diameter (m), Q: Flow discharge (m^3/s)

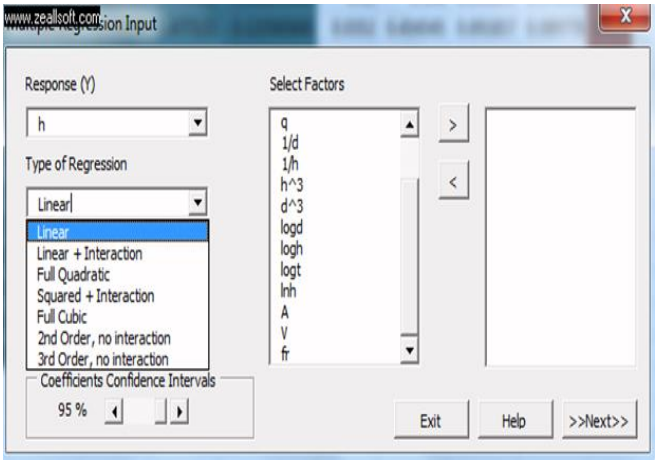

FIGURE 6. Comparing between determined and observed scour depth for quadratic equation

3.2. COMPARISON BETWEEN PREDICTED EQUATION AND EQUATIONS FROM LITERATURE

In this study, the experiments were carried with (5, 7.5 and 11) cm circular piers with four discharges. Shen II [10] developed an equation to predicted maximum scour depth by depending on Froude number (Fr), Flow depth and pier size

$$d_{sp} = 3.4\ {b_p}^{0.67} F^{0.67} Y^{0.33} \qquad (2)$$

Laursen and Toch (1956) [11] developed equations by depend on experimental work in Iowa institute of hydraulic research, laursen and Toch equations assumes that flow depth is the most important factor in determining scour depth

$$d_{sp} = 1.5\ {b_p}^{0.7} Y^{0.3} \qquad (3)$$

(Figure 6a,6b,6c) shows the comparison between Shen II [10], Laursen and Toch (1956) [11], with experimental data and the predicted maximum scour depth, it's clear from the figure that maximum scour depth in experimental work close to the results of predicted equations from this study and the results of Laursen and Toch (1956) [11] for the three sections, the results of Shen II equations shows some variance with other results and this due to "Laursen and Toch (1956) [11] equation assumes that the flow depth is most important factor in determining the scour depth, whereas the Shen II [10] equation assumes that velocity is important by including the Freud number" (Les Hamill, 1999) [12].

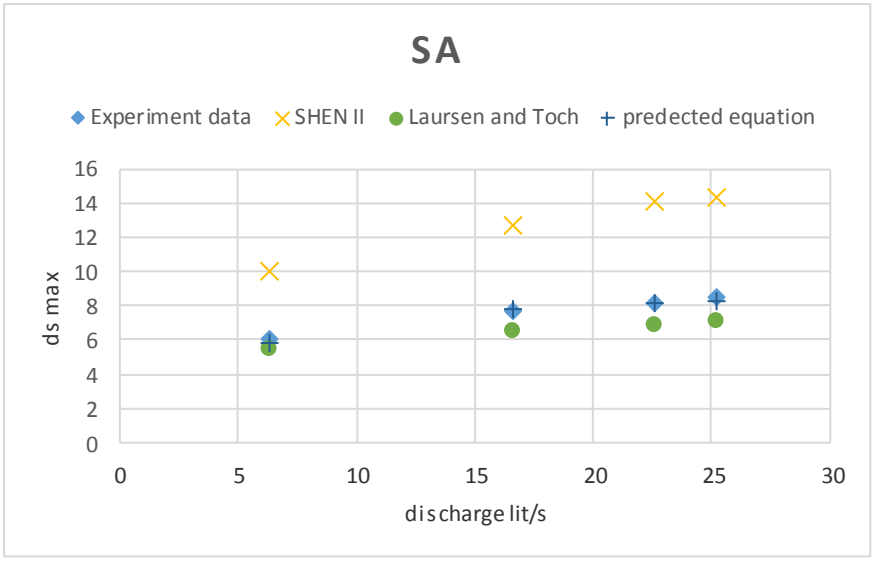

FIGURE 7. (a) Comparison between m.s.d results for sample A

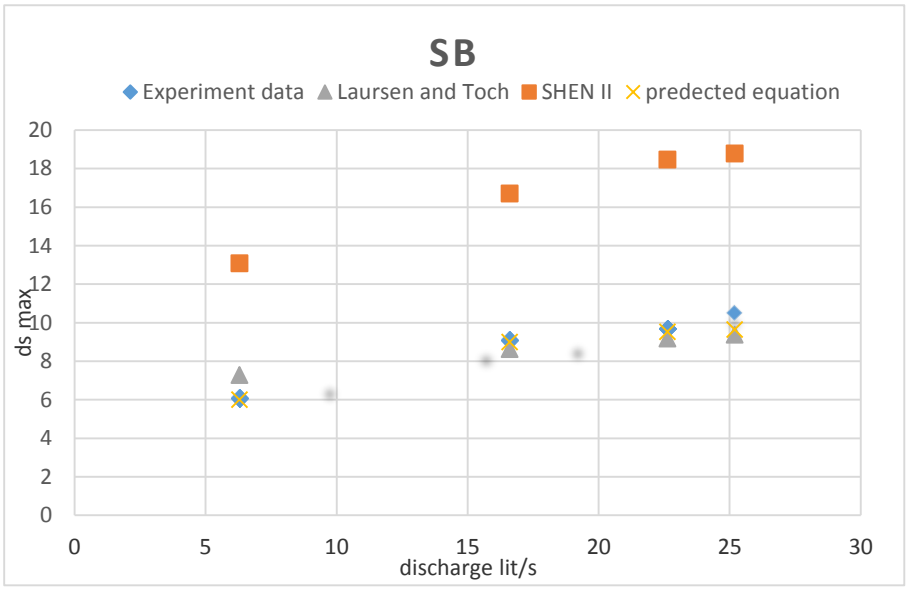

FIGURE 7. (b) Comparison between m.s.d results for sample B

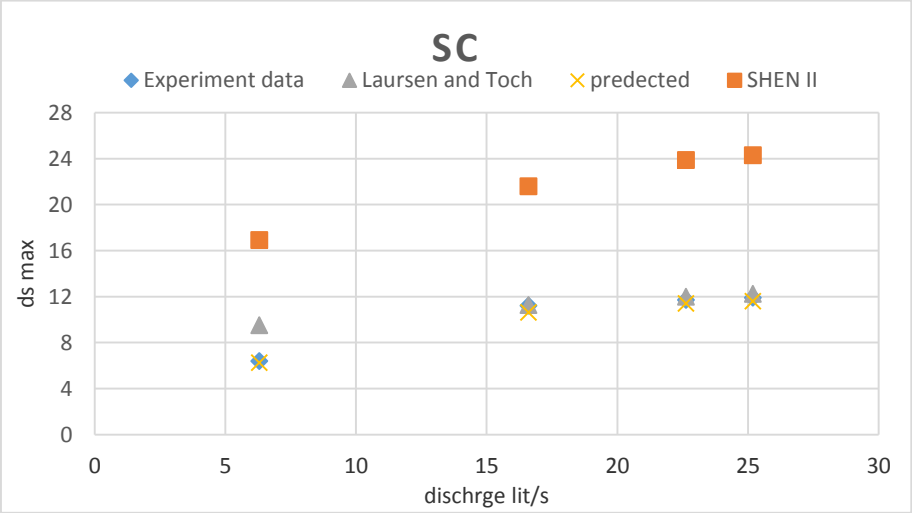

FIGURE 7. (c) Comparison between m.s.d results for sample C

4. CONCLUSIONS

1. The present experimental results showed that for the same sediments size and discharge the depth of scour is directly proportional with pier diameter
2. The results of the predicted equation of this work regarding the flow depth factor indicated a good agreement with Laursen and Toch (1956) [11].

REFERENCES

[1] Chang, H.H. 1988. Fluvial processes in river engineering. John Wiley & Sons, 432 p.

[2] Chabert, J. and Engeldinger, P. (1956). "Etude des affouillements autor des piles depoints (Study of scour at bridge piers)." Bureau central d'Etudes les Equipment d' OutreMer, Laboratory National d' Hydraulique, France.

[3] Breusers, H.N.C., Nicollet, G. and Shen, H.W.*"Local scour Around cylindrical piers"*.(1977) Journal of Hydraulic Research, 15(3): 211-252

[4] Dargahi, B. (1982): Local scour at bridge piers- A review of theory & practice. TRITA-AMI 114, RIT, Hyr. Eng. Stockholm.

[5] Dey, S, 1997, Local scour at piers, A review of development of research Int. J. Sediment .Res IJSH, 12 .23-46.Fluvial hydraulics, Walter H. Graf, 2003, "local scour" CH 9, 611-662.

[6] Hoffmans, G.J.C.M. and Verheij, H.J. 1997. Scour manual. A.A. Balkema, Rotterdam, Netherlands, 205 p.

[7] Melville, B.W. and Coleman, S.E. 2000. Bridge scour. Water Resources Publications, LLC, Colorado, U.S.A., 550 p.

[8] Richardson, E.V., and Davis (2001). Evaluating Scour at Bridged, Hydraulic Engineering Circular No. 18 Fourth Edition. US Federal Highway Administration, Publication FHWA NHI 01-001.

[9] Raudkivi, A. J. and Ettema, R. (1983). "Clear-water scour at cylindrical piers." J. Hydraul. Engrg., 109(3), 339 350.

[10] Shen, H.W., Schneider, V.R. and Karaki, S.S., (1966), "Mechanics of Local Scour", *Colorado State University, Civil Engineering Dept., Fort Collins, Colorado*, Pub. No. CER66-HWS22.

[11] Laursen, E.M. and Toch, A. 1956. Scour around bridge piers and abutments. Iowa Highway Research Board, Bulletin # 4, Bureau of Public Roads, Iowa.

[12] Less Hamil, Bridge Hydraulics, 1st, London: E &FN spon, 1999

USE OF DIFFERENT GRADED BRASS DEBRIS IN EPOXY-RESIN COMPOSITES FOR IMPROVING MECHANICAL PROPERTIES

Younis Khalid Khdir[1], Gailan Ismail Hassan[2]

[1&2]Erbil Polytechnic University (EPU), Erbil, Technical Engineering College, Erbil
[1&2]Ishk university, Erbil, Iraq
[1]younis.khdir@epu.edu.krd, [2]gailan_hareri@epu.edu.krd

doi:10.23918/iec2018.28

ABSTRACT

This study deals with the brass debris which is obtained through matte smelting and refining of brass or different machining process like grinding operation, to use as filler in epoxy-resin composites. The common uses options for brass debris are recycling, and production of value-added waste products. In this study random mixing processes to prepare (Epoxy / brass) composites done by using brass debris of three different grades with different grain size (600, 800 and 1180) µm as reinforcement in epoxy resin with different weight percentages (2%, 4%, 6% and 8%) respectively. Using tensile and impact test to evaluate the mechanical properties of the prepared composites. Results show that with coarse grain size of brass debris added to epoxy resin, it is very important to decrease the amount of weight percentage added to it, so as to improve the tensile or impact properties of (Epoxy / Brass debris) composites. On the other hand a very low weight percentage (2%, 4%, 6%, 8%) of metal brass debris which there is no significant improvement in toughness, noticed that can significantly reduce the impact absorbed energy (impact toughness) of the composite samples. The best value of the toughness can be obtained with the epoxy-BD600 and weight percent of 8%. This research includes processing procedure, and study of the mechanical behavior of grades of such brass debris filled epoxy-resin composites. This paper concluded that the possibility of utilize of brass debris as secondary filler element for the preparation of composite materials and producing the bras debris such as added-value products.

Keywords: Waste Utilization, Debris, Composites, Epoxy Resin, Reinforcement.

1. INTRODUCTION

Using debris of waste materials obtained during matte smelting and refining of different machining process like grinding operation, to use as filler in epoxy-resin composites. In our study we focused on brass debris, because of there is limited studies using this type of filling. The best options for brass debris are recovery of waste metal, recycling, and production of composite products. The advantage of these type of composites is that they are strong and light. By choosing a suitable combination of matrix and filler material, a new composite can be made that exactly has a property which is suitable for the requirements of a particular application.

Yun Liu et al., (2016) used Cu-doped graphene (graphenit-Cu) as a filler to prepare epoxy composite, in his research to study the effect of Cu-doped graphene on the thermal properties of epoxy composites, they concluded that adding graphenit-Cu had slight effect on the thermo-mechanical properties of epoxy composite materials [1]. Keong et al., (2017) used municipal solid waste (MSW) is incineration ash, which is rich in a mixture of oxide and carbonate ceramics, as fillers for composite materials. [2]. Li and Cui (2016) focused on improving the mechanical properties of epoxy base material by adding of an amino-terminated hyper branched polymer (ATHBP) grown on glass fiber [3]. Chang et al., (2015) investigated the characterization of tungsten-epoxy composites for ɤ-rays radiation shielding by blending epoxy resin through adding different weight percent of tungsten powder [4]. Lee et al., (2016) studied using of polyethersulfone as filler material to increase the thermal and mechanical properties of triglycidyl-p-aminophenol epoxy resin [5]. Yang et al., (2016) used simple hot-press with vacuum treatment to prepare silk fabric reinforced epoxy composites so as to achieve a maximum volume fraction of reinforcement, 70% silk. They investigated mechanical properties so that the flexural strength increased linearly by increasing silk volume fraction from 30 to 60 volume % but diminished slightly at volume 70%. [6]. He et al., (2011) showed impact strength of ceria-epoxy resin composites adding the ceria nanoparticles with different shapes and sizes added to epoxy resin. [7]. Goud and RAO (2011) investigated the fibre content effect on the mechanical properties of

unidirectional Roystonea regia natural-fibre-reinforced epoxy composites. [8]. Couillard and Peter (1997) studied the behavior of bending fatigue on one-dimensional, continuous-carbon-fiber/epoxy composite strands by producing a maximum strain. They determined that this type of composite did undergo fatigue and at high strains, damage occurred through matrix cracking, fiber breakage, and interfacial shear failure [9].

Papargyris et al., (2008) studied composite manufacturing techniques using conventional and microwave heating methods to prepare carbon fibre/epoxy composites to compare their mechanical and physical properties. Based on the mechanical testing similar values of the flexural strength for the two types of carbon fibre/epoxy composites were obtained [10]. Biswas and Satapathy (2010a, 2010b) fabricate hybrid composites from bamboo fiber epoxy matrix composites with various weight proportions of red mud to study erosion characteristics in comparing with glass-epoxy composites under same test conditions. They concluded that even the bamboo based composites behave relatively inferior mechanical properties, their performance of erosion wear is better than the glass fiber reinforced composites. [11, 12]. Kim et al., (2013) prepared fiber reinforced epoxy/hybrid silica composite to study their mechanical properties by adding super fibers such as aramid fiber. They confirmed that the effect of the epoxy/hybrid silica on the mechanical properties affecting in a demand for a resin system with very good mechanical properties [13]. In this work, brass debris was combined with epoxy resin by handily cold process technic to prepare different composites with various weight percent of brass debris and different size of reinforcement. The aim of this research is development of a composite with higher tensile strength as compared with pure epoxy and in the other hand we can use the wasted materials such as brass debris. The reinforcement particles distributed over the epoxy resin randomly and homogenous, to prepare these specimen for tensile and impact tests. In the experimental procedure we explained the fabricating all of these composites. And in results explained well in next section, and the conclusions of this job were written in the last paragraph.

2. EXPERIMENTAL DESIGN

2.1. MATERIALS

Transparent epoxy (Sikadur -52) is used as matrix which is a liquid of low viscosity as compared with other thermosets and its converted to solid state by adding hardener (Sikadur -52 hardener) at ratio of 2:1 the technical properties of Sikadur -52 according to the data sheet of Sika company are listed in Table 1.

TABLE 1.
Technical properties of Sikadur -52, according to data sheet of the company.

Compressive Strength	Flexural Strength	Tensile Strength	Pot life	Density	Viscosity
53 MPa for 10 days at 20˚C	50 MPa at 20˚C	25 MPa	~ 120 min at 5˚C ~ 10 min at 30˚C	1.1 kg/l at 20˚C	~ 1200 MPa at 10˚C ~ 430 MPa at 20˚C

While the reinforcement are brass debris with different grain size (600, 800 and 1180 µm) with different weight percentages (2%, 4%, 6% and 8%) respectively. These different grain size prepared by using sieve analysis (or gradation test) is a practice or procedure used to assess the particular size distribution of a granular material. It is a simple technique of particle sizing.

2.2. PREPARATION OF BRASS DEBRIS-EPOXY COMPOSITES

A series of brass debris reinforced epoxy composites has been manufactured using simple cold techniques. The composite was made using a steel mold according to standard specifications ASTM D638, the specimen size is shown in figure 1a for tensile test. The Universal Tensile Machine LY-1066A was used to test the specimen for tensile tests. And for impact test according to standard specification ISO 179, the specimen dimension explained in the figure 1b. The LY-XBD-5 Electric Charpy Impact test machine was used for impact tests, at room temperature

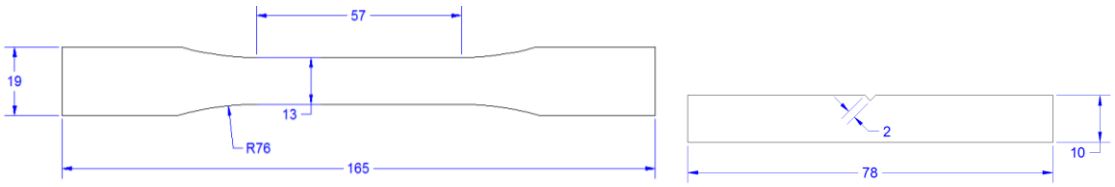

(a) (b)

FIGURE 1. Specimen of (a) tensile test, (b) of Charpy Impact test, all dim. in mm.

Tensile and Impact composite samples were prepared by pure epoxy matrix (rate of 2:1 base to hardness) into both impact and tensile molds then distribute the different grades of brass debris (600 µm, 800 µm and 1180 µm) with weight percentages (2, 4, 6, and 8%) manually into both kinds of mold. The prepared tensile and impact samples (Epoxy-BD600), (Epoxy-BD800) and (Epoxy-BD1180) properties shown in Table 2.

TABLE 2.
Specifications of the prepared specimen for tensile and impact tests

No.	Symbol	Refinement	Weight fraction of Refinement WtR %
1	Epoxy	-	-
2	BD 600	brass debris of grain size 600 µm	2%, 4%, 6%, 8%
3	BD 800	brass debris of grain size 800 µm	2%, 4%, 6%, 8%
4	BD 1180	brass debris of grain size 1180 µm	2%, 4%, 6%, 8%

Both tensile and impact samples were left for one week at room temperature to be cared as shown in figure 2.

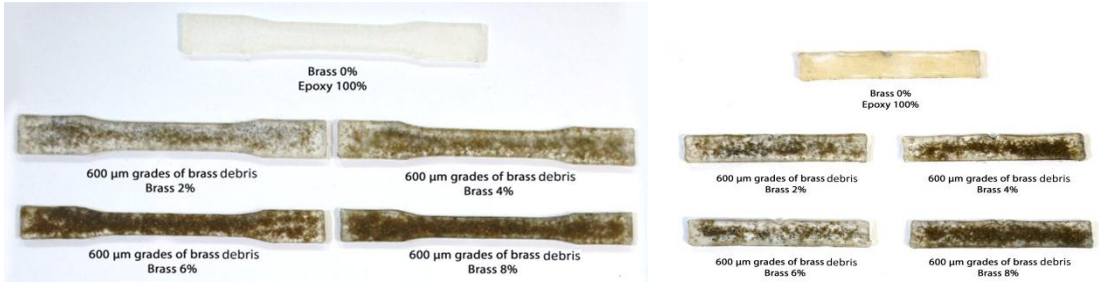

(a) (b)

FIGURE 2. Samples of prepared specimen of (a) tensile and (b) impact tests for 600 µm

3. RESULTS AND DISCUSSION

3.1. TENSILE TEST

We noticed that the fracture occurred in different areas, this phenomenon can be interpreted physically, because of the random distribution of brass debris particles and the agglomeration of some particles in some location while the density of these particles change from a location to another microscopically. The results as in figure 3a, 3b, 3c and 3d indicated that the tensile strength of the brass debris-epoxy composite increased as compared with the pure epoxy, and the elongation also increased for different sizes of reinforcement (600, 800 and 1180 μm) and different weight percent (2, 4, 6 and 8%) because of the increasing bonding area between the brass particle and epoxy resin. The existence of brass particles leads to more elongation and more strength also. Noticed that the enhance of tensile properties reaches the maximum value at Epoxy-BD600 with 8% of brass debris weight percent and the tensile strength become 48.9 MPa, as compared for pure epoxy which is 33,65 MPa. Where for the composite Epoxy-BD800 with 6% of brass debris weight percent the tensile strength reaches the maximum value of 49.16 MPa which is little greater than the tensile strength of Epoxy-BD600. Also we found that the maximum tensile strength can be obtained by the Epoxy-BD1180 with brass debris weight percent of 2% and become 45.95 MPa. And for other composite such as Epoxy-BD800 with brass debris weight percent of 6% can reach the maximum tensile strength.

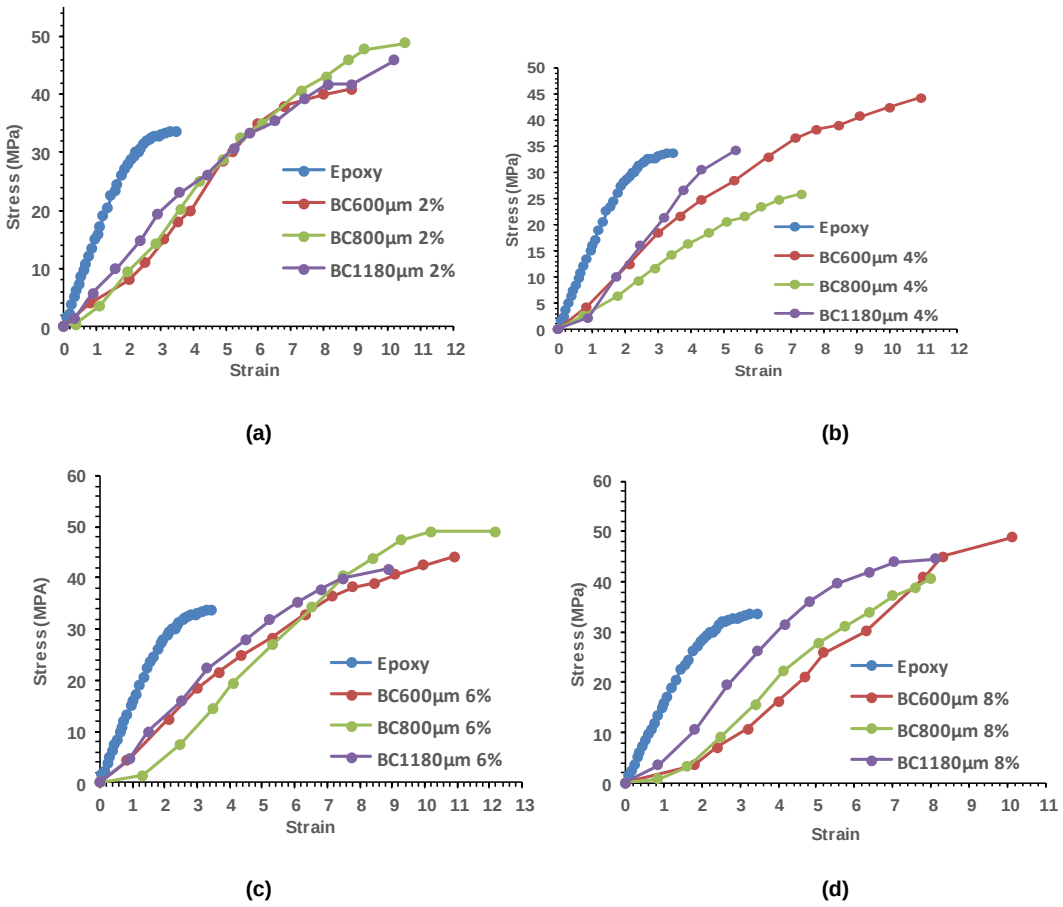

FIGURE 3. Stress-Strain curves of Epoxy and BD (600,800 and 1180 µm) for weight percentage (a) 2%, (b) 4%, (c) 6%, and (d) 8%

Comparing all the combined results explained in figure 4. According to the practical data obtained, we found that the overall maximum tensile strength can be reached by the composite Epoxy-BD800 with 6% of brass debris weight percent, as noted in the figure and reaches 49.16 MPa which is very important to be selected to produce a composite with higher tensile strength properties. Understanding of the mechanical properties of composite materials is very important for scientific professions and technical. This knowledge leads to select the suitable composite material. The materials test provides the essential data in a quantified manner. We can conclude that with increasing the grain size of the brass debris added to pure epoxy matrix, it is suitable to decrease the amount of weight percentage added. And the best of all specimen is 6 wt% (Epoxy-BD800) because it's has the highest value of maximum stress (49.16 MPa) with the highest value of strain (12.17 mm/mm). According to the result of this research, it is

able to use the waste materials such as brass debris to fabricate new developed composite with higher tensile strength which can be used for different purpose.

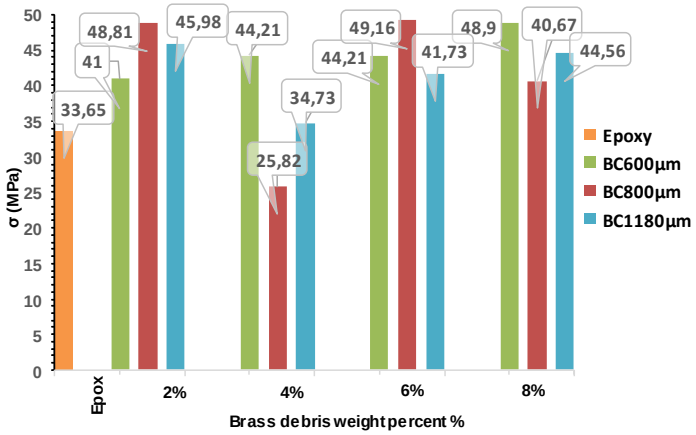

FIGURE 4. Maximum stress value of [(Epoxy-BD600), (Epoxy-BD800) and (Epoxy-BD1180)] for all weight percentage (2, 4, 6 and 8%)

3.2. IMPACT TEST

The second group of the tests is impact test. We noted that the entire specimen is broken in the notch location, for different size of reinforcement composites and different weight percent of brass debris. The results as indicated in figures 5a, 5b, 5c and 5d showed that the toughness of the composites increase with increasing the size of the reinforcement, till 800 µm, and after that any increasing in the reinforcement size leads to slight decrease in the toughness values because of the randomly distributed of the brass debris particles in the epoxy resin.

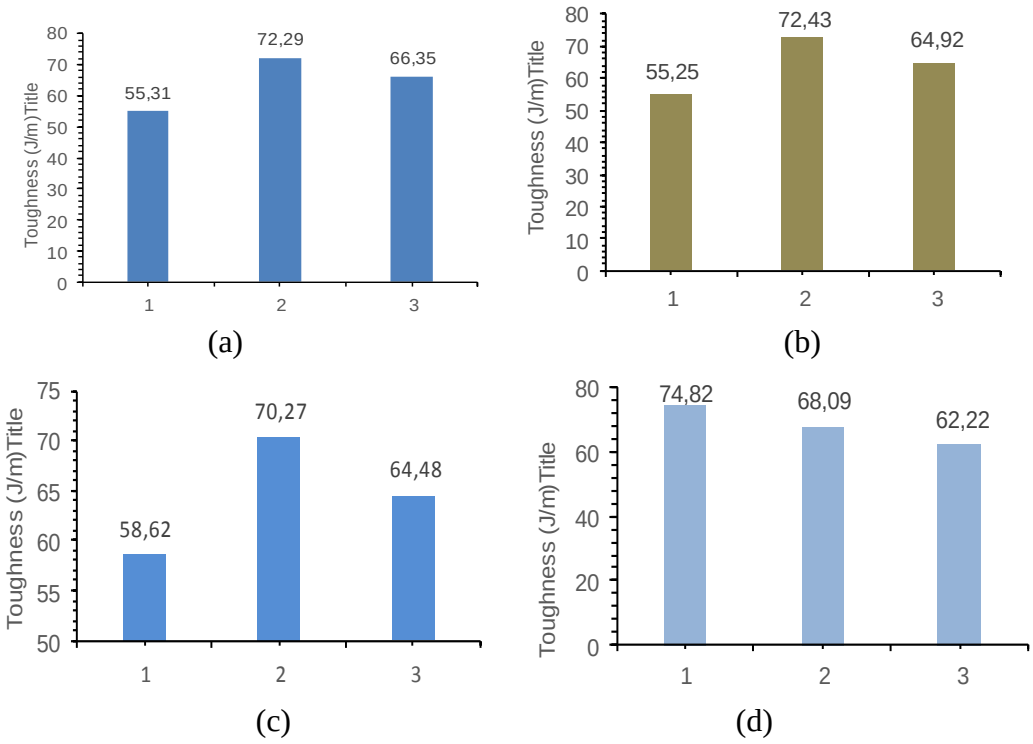

FIGURE 5. Impact Toughness of (a) 2%, (b) 4%, (c) 6% and (d) 8% for [(Epoxy-BD600), (Epoxy-BD800) and (Epoxy-BD1180)]

With increasing the weight percentage of the reinforcement particles to 8%, there is a slight decrease with increasing the particle size from 600 µm to 1180 µm as showed in figure 5d. Then if we compare all the results of toughness together with the toughness of pure epoxy see figure 6, we found that with different grades of brass debris (600 µm, 800 µm and 1180 µm) with weight percentages (2, 4, 6, and 8%), the best value of the toughness can be obtain with the epoxy-BD600 and weight percent of 8%. It is important to note that although change weight percentage addition of brass debris with different grain size, there are no significant improvement in toughness. Overall, Epoxy sample without any reinforcement has a higher toughness than the other samples. In general, there is no a significant effect for the toughness purpose for this type of composite.

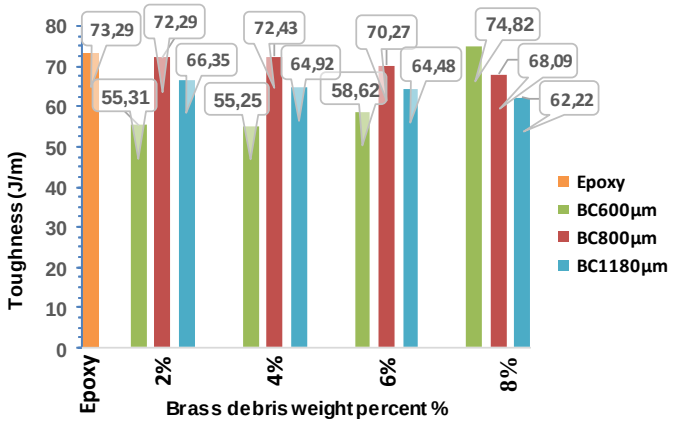

FIGURE 6. Impact Toughness of Epoxy reinforced by (Epoxy-BD 600, Epoxy-BD 800 and Epoxy-BD 1180 µm) for weight percentage (2%, 4%, 6% and 8%)

4. CONCLUSION

1. It is possible to fabricate a new epoxy composite using waste materials such as brass debris, with higher tensile strength.
2. With increasing grain size of added reinforcement to the epoxy resin, it is very important to decrease the amount of weight percentage added to it so as to improve the tensile properties of (Epoxy-Brass debris) composites.
3. It is important to note that there is no significant improvement in toughness, pure epoxy has a slight difference toughness than the other epoxy brass composites.
4. The best value of the toughness can be obtain only with the epoxy-BD600 and weight percent of 8%.

ACKNOWLEDGMENTS

Thanks to engineer Mustafa Sabah, Goran Ghafur and Rawand Younis for their efforts helping us in the practical part.

REFERENCES

[1] Y. Liu, H. V., Babu, J., Zhao, A., Goñi-Urtiaga, R., Sainz, R., Ferritto, M., Pita, De-Yi. Wang, "Effect of Cu-doped graphene on the flammability and thermal properties of epoxy composites", Composites Part B: Engineering, vol. 89, pp. 108-116. 2016.

[2] G. C. Keong, M. H. B. M. Walad, O. W. Xiong, M. N. Haikel, C. H. Ling, R. K.S/O Ravichadran, L. T. Kiang, T. L. Hing, "A Study on Mechanical Properties and Leaching Behaviour of Municipal Solid Waste (MSW) Incineration Ash/Epoxy Composites", Energy Procedia, vol. 143, pp. 448-453. 2017.

[3] S. Li and C. Cui, "Enhancing the mechanical properties of epoxy resin by addition of an amino-terminated hyperbranched polymer grown on glass fiber", Journal of materials science, vol. 51, (4), pp. 1829-1837. 2016.

[4] L. Chang, Y. Zhang, Y. Liu, J. Fang, W. Luan, X. Yang, W. Zhang, "Preparation and characterization of tungsten/epoxy composites for γ-rays radiation shielding", Nuclear Instruments and Methods in Physics Research Section B: Beam Interactions with Materials and Atoms, vol. 356, pp. 88-93. 2015.

[5] S.-E. Lee, E. Jeong, M. Y. Lee, M.-K. Lee, Y.-S. Lee, "Improvement of the mechanical and thermal properties of polyethersulfone-modified epoxy composites", Journal of Industrial and Engineering Chemistry, vol. 33, pp. 73-79. 2016.

[6] K. Yang, R. O. Ritchie, Y. Gu, S. J. Wu, J. Guan, "High volume-fraction silk fabric reinforcements can improve the key mechanical properties of epoxy resin composites", Materials & Design, vol. 108, pp. 470-478. 2016.

[7] X. He, D. Zhang, H. Li, J. Fang, L. Shi, "Shape and size effects of ceria nanoparticles on the impact strength of ceria/epoxy resin composites", Particuology, vol. 9, (1), pp. 80-85. 2011.

[8] G. Goud, and R. Rao, "Effect of fibre content and alkali treatment on mechanical properties of Roystonea regia-reinforced epoxy partially biodegradable composites", Bulletin of Materials Science, vol. 34, (7), pp. 1575-1581. 2011.

[9] R.A.A. Couillard, and P. Schwartz, "Bending fatigue of carbon-fiber-reinforced epoxy composite strands", Composites science and technology, vol. 57, (2), pp. 229-235. 1997.

[10] D. Papargyris, R. Day, A. Nesbitt, D. Bakavos, "Comparison of the mechanical and physical properties of a carbon fibre epoxy composite manufactured by resin transfer moulding using conventional and microwave heating", Composites science and technology, vol. 68, (7), pp. 1854-1861. 2008.

[11] S. Biswas, and A. Satapathy, "A comparative study on erosion characteristics of red mud filled bamboo–epoxy and glass–epoxy composites", Materials & Design, vol. 31, (4), pp. 1752-1767. 2010.

[12] S. Biswas, and A. Satapathy, "Use of copper slag in glass-epoxy composites for improved wear resistance", Waste Management & Research, vol. 28, (7), pp. 615-625. 2010.

[13] D. Kim, I. Chung, and G. Kim, "Study on mechanical and thermal properties of fiber-reinforced Epoxy/Hybrid-silica composite", Fibers and Polymers, vol. 14, (12), pp. 2141-2147. 2013.

A NEW TAXONOMY OF MOBILE BANKING THREATS, ATTACKS AND USER VULNERABILITIES

Saman Mirza Abdullah[1], Bilal Ahmed[2], Musa M.Ameen[3]

[1]Koya University, Koya, Iraq
[1,2&3]Ishik University,Erbil, Iraq
[1]saman.mirza@koyauniversity.org, saman.mirza@ishik.edu.iq
[2]bilal.ahmed@ishik.edu.iq ,[3]musa.ameen@ishik.edu.iq

doi:10.23918/iec2018.29

ABSTRACT

Mobile banking becomes an interested technique within the modern bank establishments. It facilitates the transactions and day lifestyle of customers. It minimizes the impact of location and time for doing bank activities and communicate with bank servers. However, the process is not less risks from attackers and hackers, especially, user behaviors that opens and creates many vulnerabilities in this system. This work presents a new taxonomy for mobile banking attackers and threats. Through this taxonomy, this work will identify the important user vulnerabilities that attackers may misuse them for penetrating systems and steal privacy and sensitive date. The main contribution of this work is providing important suggestions for mobile banking users so that they can take them as precaution for protecting their privacy and financial aspects. The work concluded that there are many user behaviors of mobile banking leading to bring threats inside to systems. The work presents many suggestions for users so that their systems be protected from malicious activities and malwares. Many future aspects have been presented.

Keywords: Mobile Banking, Threats and Attacks, User Vulnerabilities.

1. INTRODUCTION

Mobile malwares (MM) are considered as a new and unlike threats for the mobile users. It is a growing security concern and expected to be continue as users perform sensitive actions on their smartphones. Most mobile users have no idea about different ways that thoroughly MMs (attackers and intruders) are penetrating their mobile systems without their privileges and prior knowledge. The worst case is the users consider themselves immune from such threats and they don't have enough knowledge about the rapid growth in the number and the type of mobile malwares[1] . According to a report from the McAfee Labs, 1.5 million of new incidents have been detected in the first quarter of the year 2017. With such increase, the landscape of the mobile threats and attacks are evolving in such a way that makes financial institutions (such as banks) and their customers always worry about the risks that expected from the process of online and mobile banking [2]. Therefore, it is necessary to study the feature(s) of every new mobile malware soon they have been propagated and defected systems. It is also necessary to conduct researches to find precautions for future possible threats and increase users' awareness towards such MMs.

New malwares, which are also known as the zero-day threats and attacks, are coming with different features and they follow varieties of policies and techniques. Malware analyzers need to perform reverse engineering processes on each new malware as they appear, so that they can reveal their secrets, such as the group that they belonged to. However, each malware has different policy in the design. The common point between malwares is that they misuse wide range of vulnerabilities to penetrate targeted systems. To simplify the revealing process, researchers are always grouping malwares based on the similarity among some defined features [3]. The most common grouping, is classifying malwares based on the technique(s) they are using while they penetrate mobile systems. In the other hand, researchers are grouping malwares based on the device type and the software platform. Other groupings are done based on the goals and purposes that MMs has been designed for. As an example, some malwares aimed to disclose privacy on the victim mobile, by steeling sensitive information or money, and in some cases attackers are penetrating mobile systems just for fun. At the end, breaking the defense systems of the mobile devices or the banks by bypassing the

security solutions is the main target for all MMs in each group. Understanding the MM features through grouping them under different categories may help the task of mobile defense systems much easier, better analyze and evaluate malwares, and mobile users can understand their behaviors more, which will consequently, minimize the impact of malicious codes on the mobile systems[4]. this work describes the environment of the MMs in a form of some interrelated assets. Each asset covers some parts or elements that are essential in performing the mobile banking or transaction communication. This paper consist of six sections. The first section is introduction to the field of the mobile banking in the view of security. Section two is describing the fundamental framework of mobile banking and briefly states some differences between online banking and mobile banking. Section (3) is proposing a new taxonomy for the mobile vulnerabilities that misused by the MMs. Section (4) gives some examples of threats and attacks that are related to user vulnerability asset with a brief description on the policies of each MM family. Finally, some recommendations, suggestions, and advices have been explained on how to be on the safe side while enjoying using mobile banking facilities.

2. LITERATURE REVIEW

Based on the best knowledge of the author, the activities of the mobile banking have been started with SMS services, and the history of initiating such services is going back to 1999 [5]. Many countries at that time tried to employ the mobile devices in the financial and banking issues and they suggested better processor and communication facilities to cover more services. Soon developed countries encouraged the banks to provide customers with mobile services [6]. Even more, developed countries tried to include some multimedia services of the mobile in the banking issues [7]. Services, such as paying bills, payment transferring, online shopping and checking accounts were the expected and required services for the future of the mobile banking [8]. However, the security concerns became an important problem within the infrastructure of the mobile banking. Therefore, many works developed some security frameworks and others argued some security assessment processes [9, 10]. Within these frameworks and assessments, the mobile users and their behaviors were the most important security questions. User vulnerabilities still important in many recent works as they become the main vulnerabilities for the mobile attackers' penetration, beside system vulnerabilities. one of the recent works

addressed an assessment of the mobile vulnerabilities within Android and iPhone OS[11]. The work argued some vulnerabilities of the mobile banking applications that released and certified by the banks. The work showed that some banks are using simple HTTP protocol without concerning to the security issues that related to the man in the middle attack. The work just focused on the vulnerabilities of those applications and forgot to analyze user vulnerabilities that also misused by attackers work in the middle way. Many works focused on securing the communication channels between customers and bank servers. In those works, stronger encryption methods are proposed [12]. However, the weak point of the mobile banking systems are the users themselves. Within any downloading of games or unknown applications, a Trojan malware could insert itself to the system and make itself active for opening a back door for attackers. The possibility of downloading Trojan is in increase as the work [13] reported that number of Trojan infected apps in the mobile application sources, such as Google Play Store and iOS app store, are increased unpredictably.

Another part that more concerned the security of the mobile banking systems are the security of the physical storage of data in bank sides. One of the most important attacks that related to the server security is SQL injection. Such attacks inject a malicious code inside the database of the bank and do activities they need. Many authors worked on that problem and they designed SQL Injection detection systems [14]. Although mobile users may not have impact on those database security, employers in the bank whom working on such dataset may be misused by attackers.

It seemed that all framework of the mobile banking needed to be securable. Moreover, a great part of the security breaching is the responsibility of the user vulnerability. Therefore, this work presents a new taxonomy of the mobile banking threats and attacks and discusses the impact of user vulnerabilities on each part.

3. SECURTIY PERSPECTIVES OF MOBILE BANKING

Today, banks in most developed countries offer mobile banking services for their customers. It is putting essential banking services as a mobile applications and let users (bank customers) to use them remotely either from their smartphones or tablets. The most common services that provided through mobile banking applications are bill payments, fund transferring, checking transactions and balance, and sending some security alerts or reminders [15]. The most important part of the mobile bank services

is to ensure users that their communication with the bank is been transferred via a secure and protected channel. This will increase the trust of mobile bank users and their acceptance to the system, which is not really an easy matter as shown in some statistical figures. Researches been conducted for specific countries and bank. A paper found that 69% of German banks are providing m-banking services, and it showed that 79% of the people are using m-banking. Among all users and nonusers of mobile banking, only 77% of them are still worrying about the security of m-banking [16]. Therefore, securing the systems of the m-banking is becoming a very essential issue, however, it is not easy. the typical infrastructure of any m-banking is shown in Figure-1 [17] . The core idea is establishing a communication channel with the core bank systems using mobile communication system, Internet networks, and mobile banking servers. In the figure, the part of the mobile communication systems, implicitly, comes within the Internet network. Another implicit part of the m-banking systems is the users, or the bank customers that are performing banking transactions through their mobile devices.

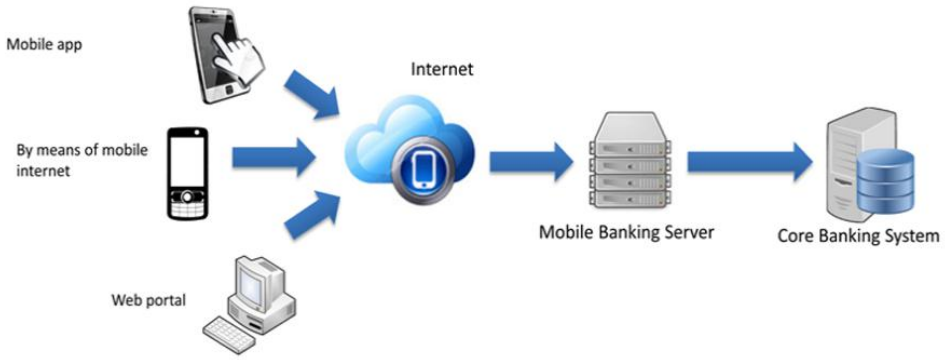

FIGURE 1. Typical Mobile Banking Systems

At each stage or part of the m-banking infrastructure, a special level of security defense systems are required and many security challenges will be there. According to this scenario, this work has divided the different parts of the m-banking systems, specifically from a security perspective, into four groups or assets; mobile user behaviors, mobile applications, hardware, and the mobile or the Internet network systems. Classifying the whole m-banking systems into four assets from a security perspective have been done according to the type and the policy of the attacks penetrating the m-banking systems. At each part (asset), special types of threats are misusing the vulnerabilities that could be found only in the corresponding part. To

provide a full immune m-banking service, special defense systems should be designed. The proposed defense systems firstly need to know and analyze all threats and attacks at each part. Secondly, the defense system should be aware about the policies and vulnerabilities that might be misused by attackers and various threats to penetrate the corresponding part. Then, designing a fully protective system for securing m-banking system can be achieved [4]. next section explains in detail about the taxonomy of the MMs in the viewpoint of the above mentioned assets.

4. NEW TAXONOMY OF MM

The new MM taxonomy proposed in this work is considering each part of the mobile banking system as an asset, as shown in Figure 2.

FIGURE 2. The main assets of the mobile banking systems

As shown in Figure 2, no part of mobile banking system is free from threats and attacks. Every single piece of the mobile banking system, from the device to the server, either physical or software are all entitled to different attacks through the vulnerabilities and flaws found in each asset. Table 1 lists the names of most known attack types under four different categories or assets. The mentioned attacks at each level can be considered as serious threats on mobile bank systems and customers.

TABLE 1.

The New Taxonomy of Mobile Banking Threats and Attacks [1, 16, 18]

Assets-1 Devices	Assests-2 Network	Assets-3 Physical Storage	Assets-4 User Vulnerabilities
Phishing	Wi-Fi (No Encryption or Weak Encryption)	Platform Vulnerabilities	No Passcode/Weak Passcode
Framing	Rogue Access Point	Server Misconfiguration	iOS Jailbreak
Click Jacking	Packet Sniffing	Cross-Site Scripting (XSS)	Android Rooting
Man-in-the-Middle (MITM)	Man-in-the-Middle (MITM)	Cross-Site Request Forgery (CSRF)	Password and Data Accessibility
Buffer Overflow	Session Hacking	Weak Input Validation	User-Initiated Code
Data Caching	DNS (Domain Name Systems) poisoning	Brute Force Attacks SQL Injection	Sensitive Data Storage
No Encryption/Weak Encryption	SSL (Secure Sockets Layers)	Privilege Escalation	User skills and experience about security
Baseband Attack	Fake SSL certificate	Data Dumping	Phishing
SMIshing		OS Command Execution	
Improper SSL Validation			
Dynamic Runtime Injection			
Escalated privileges			

One of the best ideas of classifying mobile banking threats and vulnerabilities is to provide solutions that come fit with each asset. Therefore, this work will provide security solution(s) for each threats and attacks that more related to the user vulnerabilities.

5. USER RELATED ATTACKS IN MOBILE BANKING

Categorizing mobile banking threats makes the process of finding security solutions easier for security specialists and researchers. It divides the task of a fully immune mobile banking system on individual defense and protective systems. As shown in Table-1, assets of mobile banking are divided into four parts. Each part covers a group of attacks and threats, and of course, each individual attack has its own policy and technique to penetrate systems. In Table-2, most attacks that related to the user vulnerabilities have been described shortly. Next section, important suggestions for mobile banking users will be given.

TABLE 2.

Attacks, their policies and some solutions [1-4, 19]

Attacks and Threats	Definition and Policies
Phishing	It uses legitimate personation for stealing privacy or login credential information. It dose that through urgent emails to target victims.
Framing	It inserts some fake frames in a legitimate website for a bank or company for collecting privacy or login credential information.
Click Jacking	It is exactly like framing, but the attacker will put an invisible button on some interested button. The malicious activities will be done when a user clicked the interested bottom and it doesn't has idea that there is a hidden bottom
Man-in-the-Middle (MITM)	This type of hacking is done through a lot of malicious ways. The most popular ways are the email hijacking and WiFi eavesdropping
Buffer Overflow	Attackers try to write into some temporary memory locations more than they can hold.
Data Caching	This attack has some similarity with buffer overflow. They try to over follow the cache memory, breaking AES keys based on some timing or power consumptions, or sometime through provoking the eviction of recently accessed data
Baseband Attack	This attack can penetrate both Android and iOS based devices. It is usually attacking a device over the air. It starts through operating an adversary on a rough based station that somehow close enough to communicate with target device. It has ability to locate the position of the user and can break the privacy that stored on the device.
SMiShing	SMiShing is shorten of SMS Phishing. It sends an interested SMS thoroughly a user will be motivated to download Trojan Horse, virus, or other type of malwares.
Improper SSL Validation	It is very important to secure the communication between the bank and the client. This process done using a valid Secure Sockets Layer (SSL), which is standard security technology, and it depends on encryption. Using improper SSL makes the job of attacker easy to listen to these communications and steal privacies.
Dynamic Runtime Injection	It is the process of calling and controlling a library that permit a malicious code to be injected or replaced in a mobile device. It starts with clicking an unknown email then it controls the SSL communication process at run time.
Unintended permission	Many permission requests will be accepted set by applications and mobile users are accepting them. These permissions, after they allowed, they change the status of many private objects to public among applications.
Improper Certificate Validation	It comes with using or installing invalid, cracked, illegal software and applications. The attacker will try to overcome the SSL protocol and conduct an illegal communication with client.
Escalated Privileges	Is gaining the access to many parts of the mobile through different way, which one of them is rooting the devices
No Passcode/Weak Passcode	Passcode used to lock mobile devices and protect it from an authorized person.
OS Jailbreak and Rooting	These to apps used by mobile users (iPhone and Android) to get apps free.
Password and Data Accessibility	The most common way for protecting data is avoiding accessibility through using passwords.
User's Initiated Code	Quick Response (QR) Code becomes very come among mobile users.
Sensitive Data Storage	Sensitive data should be kept in a very secure storage (Strong password and Encryption algorithm). Attackers typically don't break crypto directly.
User skills and experience about security	Most attackers are penetrating systems because of unawareness of the users to the mobile devices and apps.

6. SUGGESTIONS FOR MOBILE BANKING USERS

The pillars' responsibility of security framework for any mobile banking system should be includes Bank Strategic IT Policy, IT technician beside the behaviors of the bank customers themselves. All involved parties in the system need to cooperate to have a safeguard zone and to minimize the risk of threats and attacks penetrations. In this section, this work provides the role of users in keeping the vulnerabilities as close as possible and increase their awareness about the possible open gates that thoroughly attackers may penetrating their systems. Although this work classified the attacks in the process of mobile banking into four assets (Figure 1), attacks due to user behaviors and vulnerabilities are more focused. In general, user vulnerabilities come in the first and fourth assets. While asset number two and three are more about the mobile communication and bank establishments. To avoid vulnerabilities in any mobile banking system, users should strongly consider the following recommendations and suggestions:

1. Users should not open any urgent notes or emails that originated by their banks, especially, if the email or note asks private information. Banks never send or ask privacies through mobiles or in urgent ways. Such messages or emails have high probability of containing phishing.
2. Many emails or note senders will ask customers some privacy information through filling sort of forms sent through a link. Once the link opened customers will see some frames added to the opened website. Or, the link will direct customers to a fake page where looks almost like the correspondence bank website. Any information given to such frames and websites will put users in the risk of stealing their privacy and financial information through a type of attack known as the man in the middle. Through such links the attacker can control the communication of customers and the corresponding banks.
3. Many mobile users are interested in downloading free apps and software through the process of rooting or jailbreaking their device. Such rooting processes will bypass the security and the permission controls that protecting the Kernel root of the mobile devices, thus the device becomes open for attackers to access any private and sensitive data that kept inside the mobile. Of course, stealing the credit card numbers and QR codes will be one of the

revealed data. Moreover, buffer over follow and data catching attacks will get advantages from jailbreaking mobiles for making devices working slowly and have bad respond.

4. Many attackers are working within the asset three, which is related to network part. However, users of mobile banking are also involving in this process of penetration. It is the role of the mobile users to give permissions to an app to escalate their privileges. Dynamic runtime injection attack is the most effective attacks that gets the advantages form the user permission. Users should be aware about the type of the access that an app is asking for controlling Kernel or other applications. For example, a game asking you to access your contact number list or read your SMS lists. Users should ask themselves about the relation between this app and contact list. If users couldn't find any relation the requested access should be blocked.
5. SMS is the main gate of attackers toward the mobile devices in mobile banking apps.
    a. A type of phishing called SMIshing is the most popular attack that thoroughly many Trojans and worms are penetrating systems. Users should not open SMS messages from unknown or suspicious senders or should not click on any link that comes through an SMS from strangers.
    b. Another type of attack is called DDoS attack. This attack may come inside the mobile devices through opening and clicking a link inside an SMS came from stranger destination. The attack will control the communication or the SSL validation between the mobile and the bank server.
6. The fist access control type of any mobile devises is the passcode. All type of passcode should be strong and undetectable. When a mobile become physically with an attacker the first trial that the attacker will do is hacking the passcode. Mobiles that supporting bioinformatics access are much safer than others. There are many attackers use the track of keystrokes as type of breaking the access defense process. If the user depend on QR access, it should be aware that his/her QR could be extracted somewhere
7. Storage places of sensitive data should be strongly protected through a very powerful password. There are many recommendations about the formulation

of the passwords. Users should have knowledge about distinguishing weak passwords from strong one.

7. CONCLUSION

This work concluded that responsibility for building a strong security framework of any mobile banking is not on the bank or just on the customer, it a pair responsibility. It is very important for users to understand their vulnerabilities and avoid them. To be more understandable, this work classified the attacks in the process of mobile banking into four categories. The work focuses more on the user vulnerabilities, as it is relevant to all categories. This work found that user behavior couldn't be separated from the main framework of mobile banking security. Moreover, the only way for educating mobile users is through publishing some suggestions, which are not easy to be well understood as they required security skills and experiences. For the future work, this work preferred and designing a security framework for mobile banking that put all assets together in one frame. It will be great if some intelligent techniques as detection systems for each asset will be designed, and it will be better if an intelligent mobile banking systems could be presented in the viewpoint of smart cities, such as using the concept of Internet of Thing (IoT).

REFERENCES

[1] P. Y an and Z. Yan, "A survey on dynamic mobile malware detection," Software Quality Journal, pp. 1-29, 2017.

[2] MaCafee, "McAfeeLabsThreatsReport, "https://www.mcafee.com/us/resources/reports/rp-quarterly-threats-jun-2017.pdf2017 2017.

[3] F. Martinelli, F. Marulli, and F. Mercaldo, "Evaluating Convolutional NeuralNetwork for Effective Mobile Malware Detection," Procedia Computer Science, vol. 112, pp. 2372-2381, 2017.

[4] R. Unuchek and V. Chebyshev, "Mobile malware evolution: 2013," AO Kapersky Lab, 2014.

[5] D. irch, "Banking on the Move The internet isn't the only new digital channel," 1999.

[6] B. Must and K. Ludewig, "Mobile money: cell phone banking in developing countries," Policy Matters Journal, vol. 7, pp. 27-33, 2010.

[7] M. H. Hasan and A. Khalid, "Development of Multimedia Messaging Service (MMS)-based receipt system for mobile banking," in Information Technology (ITSim), 2010 International Symposium in, 2010, pp. 1-6.

[8] N. Mallat, M. Rossi, and V. K. Tuunainen, "Mobile banking services," Communications of the ACM, vol. 47, pp. 42-46, 2004.

[9] D. Weerasinghe, V. Rakocevic, and M. Rajarajan, "Security framework for mobile banking," in Trustworthy Ubiquitous Computing, ed: Springer, 2012, pp. 207-225.

[10] L. Nosrati and A. M. Bidgoli, "Security assessment of mobile-banking," in Computing and Communication (IEMCON), 2015 International Conference and Workshop on, 2015, pp. 1-5.

[11] S. Bojjagani and V. Sastry, "VAPTAi: A Threat Model for Vulnerability Assessment and Penetration Testing of Android and iOS Mobile Banking Apps," in Collaboration and Internet Computing (CIC), 2017 IEEE 3rd International Conference on, 2017, pp. 77-86.

[12] H. N. Huxham, "Mobile banking system with cryptographic expansion device," ed: Google Patents, 2017.

[13] S. K. Shukla, "Trust and Security Must Become a Primary Design Concern in Embedded Computing," ACM Transactions on Embedded Computing Systems (TECS), vol. 17, p. 1, 2018.

[14] N. Shah, "Securing Database Users from the Threat of SQL Injection Attacks," 2017.

[15] K. Kavitha, "Mobile Banking Supervising System-Issues, Challenges and Suggestions to improve Mobile Banking Services," Advances in Computer Science: an International Journal, vol. 4, pp. 65-67, 2015.

[16] C.-. Insights, "Mobile Banking Security: Challenges, Solutions," USA, Report2015.

[17] mpss. (2018). Myanmar Paymnet Solution Services.

[18] A. Feizollah, N. B. Anuar, R. Salleh, and A. W. A. Wahab, "A review on feature selection in mobile malware detection," Digital Investigation, vol. 13, pp. 22-37, 2015.

[19] S. M. A. Ghani, M. F. Abdollah, R. Yusof, and M. Z. Mas'ud, "Recognizing API Features for Malware Detection Using Static Analysis," Journal of Wireless Networking and Communications, vol. 5, pp. 6-12, 2015.

CASE STUDY: INVESTIGATING THE 2013 ASIACELL WAREHOUSE STEEL PORTAL FRAME FAILURE

Razaq Ferhadi

American University of Kurdistan, Duhok, Kurdistan Region-Iraq
razaq.ferhadi@auk.edu.krd

doi:10.23918/iec2018.30

ABSTRACT

In a windy morning of March 17, 2013, a warehouse belonged to Asiacell Telecom collapsed during construction. The structure was a relatively large 108m by 48m double-span steel portal frame designed by an Iranian engineering firm and constructed by a local construction company. This catastrophic structure collapse that killed three workers and injured few, was a sudden failure that triggered an intense investigation to determine the cause to avoid the occurrence of the same mistake in the future.

This research paper is the product and outcome of the forensic structural analysis performed by the author for Asiacell that indicates the exact reasons behind the catastrophic failure. It provides the evidence to be a lesson-learned document for the future steel structure construction in Iraqi Kurdistan.

Keywords*:* Case Study, Steel Portal Frame, Structural Failure.

1. INTRODUCTION AND PROBLEM STATEMENT

This paper is a further investigation of the original analysis prepared to fulfill the request of Asiacell, who owns the warehouse complex. The case was originally investigated and reported to Asiacell in 2013 [1]. As such, an evaluation of the design and construction process started few days after the incident to determine the cause. The evaluation includes construction as well as the structural design. The structure (Figure 1) was located in Sulaimany in Kurdistan Region and was a part of a warehouse complex that consisted of a total of four portal frame structures besides few other buildings for the office. This frame, which was the largest one of the group, catastrophically collapsed during the construction process and triggered an investigation by Asiacell to enhance the construction safety and insure that this kind of tragedies will not happen again.This paper depicts the structural analysis and design, and evaluates the construction management in order to highlight the cause of the catastrophic failure of the structure. As this type of failure is dangerous being a source of safety concerns and cause of losing money besides time consumption, Asiacell demanded that work to be halted immediately and strong measures to be taken seriously through a thorough forensic analysis to prevent this type of failures in the future. The author of this paper was a part of the team of investigators hired by Asiacell for this purpose and this paper is the result of the calculation and evaluation of the frame.

As in any construction failure in the world, fingers were pointed to the design and construction process. As such, it was necessary to review the design documents first and determine whether there are any flaws in it that might caused the failure.

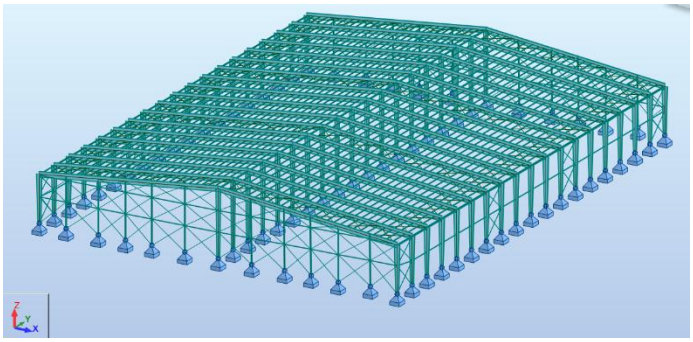

FIGURE 1. Asiacell Warehouse Portal Frame Model

2. WHAT WENT WRONG?

The 108m x 84m steel portal frame collapsed during construction as a result of a dynamic lateral load caused by the collapse of the 50 ton rough terrain crane and hitting one of the rafters. The rafter that was connected to the outer columns and fixed on the concrete via four anchor rods, collapsed under the impact as one piece frame and hit the adjacent frame section and caused a catastrophic abrupt-action collapse of the whole structure as a domino effect (Figure 2).

The collapse was catastrophic as it killed three steel workers and injured few others. The crane failed under the strong wind while its telescopic boom was extended all the way. Despite that the load that the crane carried during the failure was well within its capacity, a question was raised as to why the construction was not halted during the high wind weather that was above 50 km per hour? Obviously, this was a flaw in the construction management of the project but then another question popped up: why the frame collapsed under the relatively-low impact load? This question is answered in the following paragraphs.

3. INVESTIGATION METHODOLOGY

The frame design was evaluated using Autodesk Robot Structural Analysis Professional 2013 software. The pitched roof steel portal frame was modeled to have the same member sections as the original design and was analyzed using the conventional LRFD method for steel structure. As the structure is a moment resisting and braced frame, special care has been taken to have members of tapered sections whereby the bigger sections are located at the location of bigger bending moment.Stiffeners have been provided to tackle torsion and lateral torsional buckling. The analysis is in accordance with ANSI/AISC 360-2013 [2].

The base plates were analyzed in accordance with AISC Steel Construction Manual, 9th Edition using Allowable Stress Design (ASD) [3] and following the procedures specified in the book Design of Welded Structures [4] and AISC Steel Design Guide 1 [5]. The anchor rods were analyzed in accordance with Appendix D of ACI 318-08 using LRFD Method [6].

The construction aspect was evaluated using a site visit investigation by checking the damages caused in the frame members, connections, and foundation. The observations were

photographed and illustrated in this paper. First, the design details are clarified and analyzed. Then, the construction process is investigated and the causes of the failure are concluded.

4. FRAME DESIGN DETAIL

The steel portal frame, which had a span of 84.0m and a length of 108m, was designed to have two spans and 18 bays (Figure 3). It was designed to be supported by side and intermediate columns on the direction of 84.0m span, which makes it to have two successive spans of 42.0m long (Figure 4). The frame possessed bays of 6.0m span on the traverse direction with column height of 10m on the sides and 15m in the middle. The structural steel was of Grade S275 according to Eurocode 3.

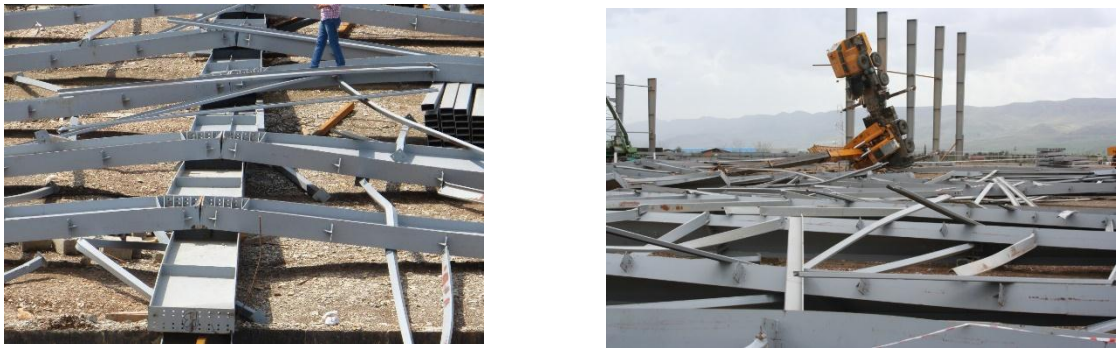

FIGURE 1. Collapsed Frame as Domino Action

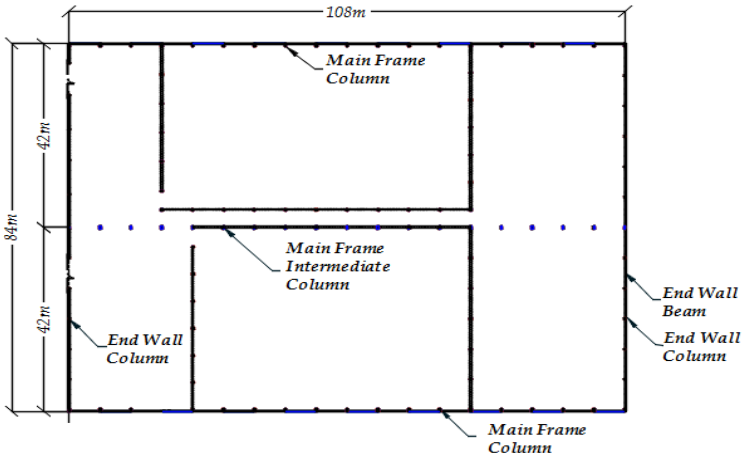

FIGURE 3. Asiacell Warehouse Frame Plan

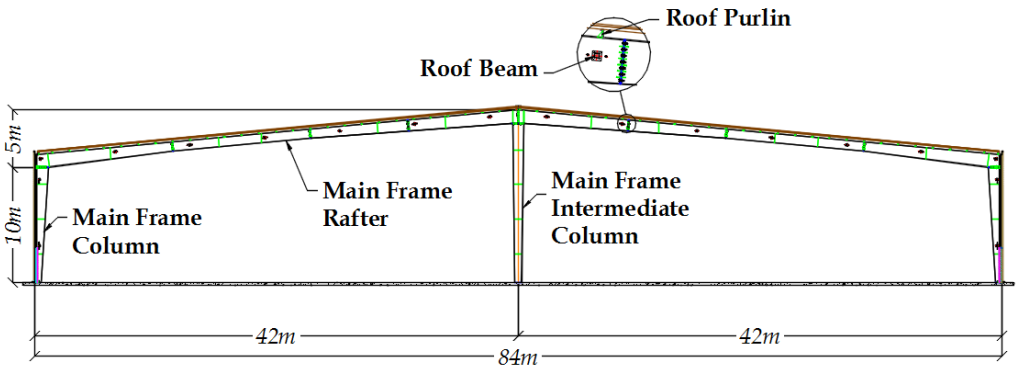

FIGURE 4. Typical Portal Frame Elevation

The frame consisted of the following main elements that were analyzed in detail:

1. Main Frame Columns: The main frame columns were designed to have tapered section on one side that were 600mm at the base and 1200mm at the top. The flanges had a width of 300mm and thickness of 16mm while the web had 10mm thickness.
2. Main Frame Rafters: The main frame rafter beams were designed to have four sections that were 1200mm at the column connections and at the pitch point and tapered for 12m to a constant section of 800mm. The flanges had a width of 300mm and thickness of 16mm while the web was 10mm thick.

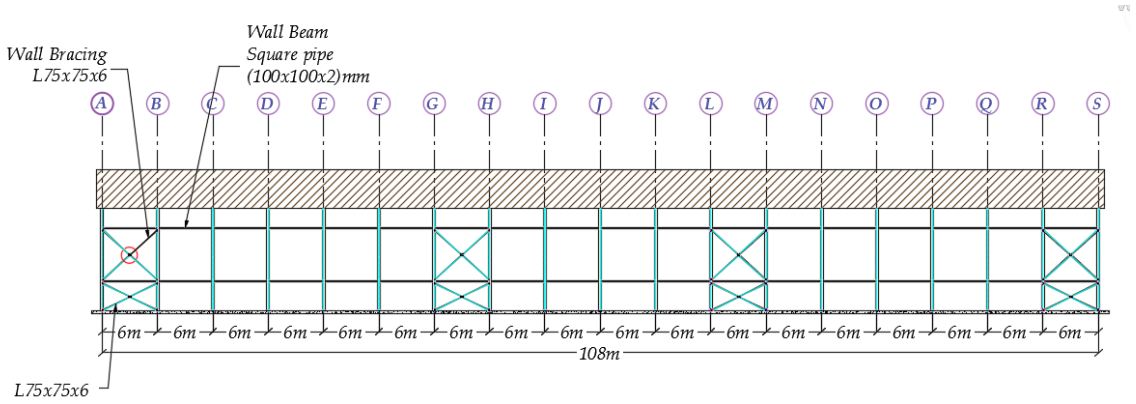

FIGURE 5. Portal Frame Side Wall Detail

3. Main Frame Intermediate Columns: The main frame intermediate columns were tapered sections on both sides that were 600mm at the base and 1200mm at the top and had the same plate thicknesses as the main frame columns.

4. End Wall Columns: The end wall columns were the standard sections of IPE 240.
5. End Wall Beams: The end wall beams were the standard sections of UAP 100.
6. Wall Bracings: The walls were braced in four bays with CAE 70x6 sections as shown in
7. Wall Beams: The wall beams were 100x100x2 box section beams.
8. Roof Beams: The main frames were tight together through 12 roof beams of steel tubes of 100x100x2 equally spaced.
9. Roof Purlins: The roof purlins were designed to be 175mm Z sections.
10. Wall and Roof Covers: The walls were designed to be covered with 50mm thick sandwich panels while the roofs to be covered with 80mm thick sandwich panels (Figure 6)
11. Roof Bracing: The roof was designed to have the bracing plan showing in Figure 7 with ϕ16 smooth steel bars.
12. Foundations: The columns were supported on isolated footings connected together with tie beams through the footing pedestals as shown in Figure 8.
13. Foundation Connections: The main columns were designed to be connected to the foundation through four ϕ29, 600mm long anchor rods that were embedded 470mm in concrete. The base plates were 620mm x 320mm x 20mm (Figure 9).

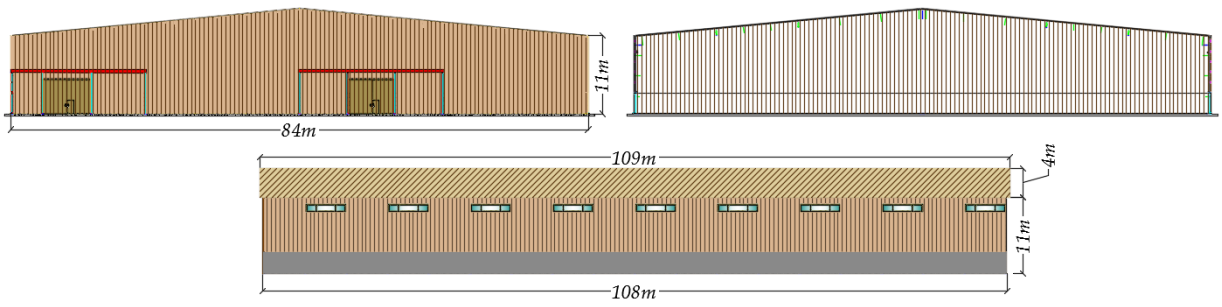

FIGURE 6. Front, Rear, and Side Elevations

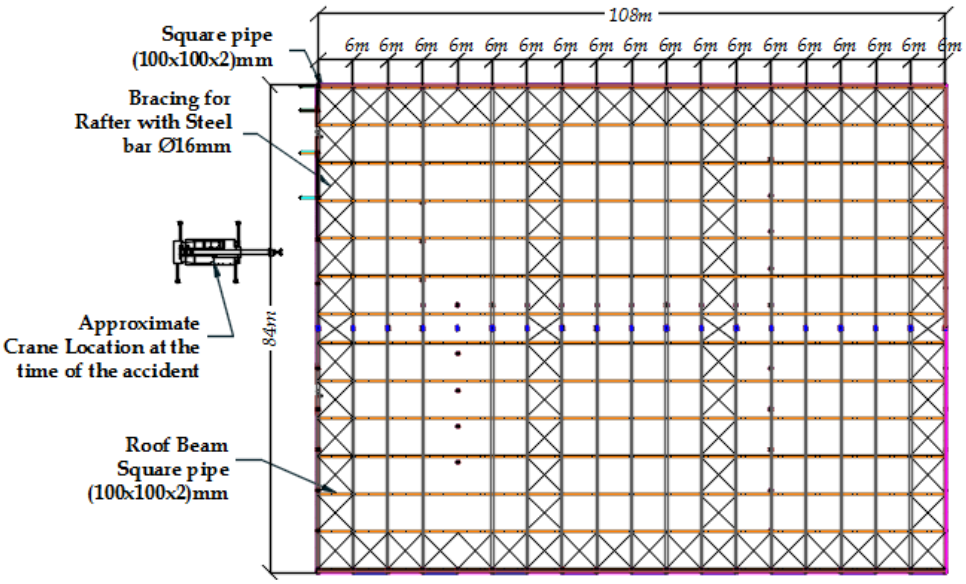

FIGURE 7. Portal Frame Structural Roof Plan

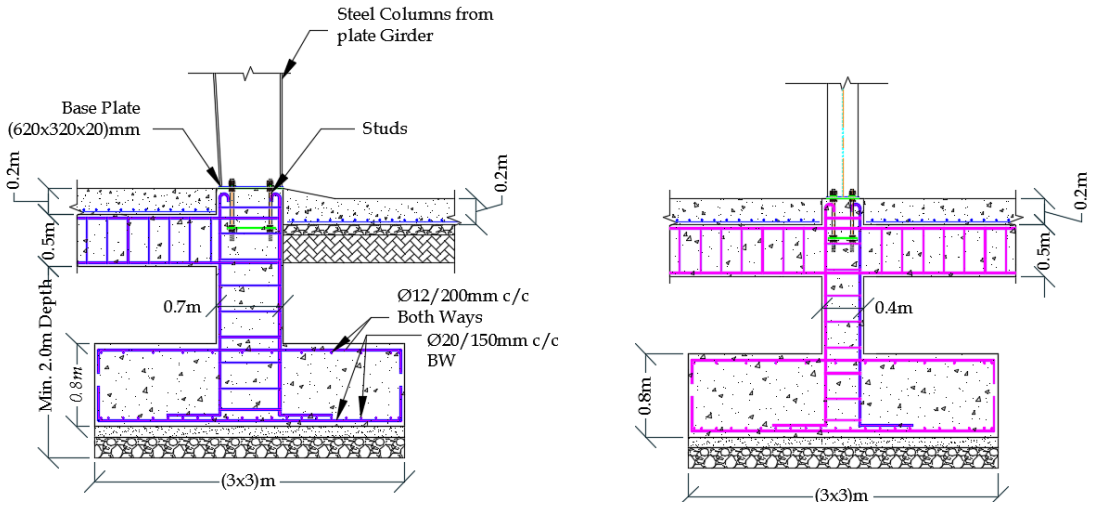

FIGURE 8. Footing Details

5. DESIGN LOAD

The frame has been designed for the following loads (Table 1):

a) Self-Weight : Steel frame own weight

b) Cladding and Purlin Load : 25 Kg/m²

c) Service Load : 10 Kg/m²

d) Snow Load : 30 Kg/m²

e) Wind Loading of 120km/h as per ASCE7-10.

Seismic load is ignored since it seldom controls with this type of structure and in that region. A total of 34 Load combinations are created using LRFD method in accordance with ASCE7-10 (Table 2).

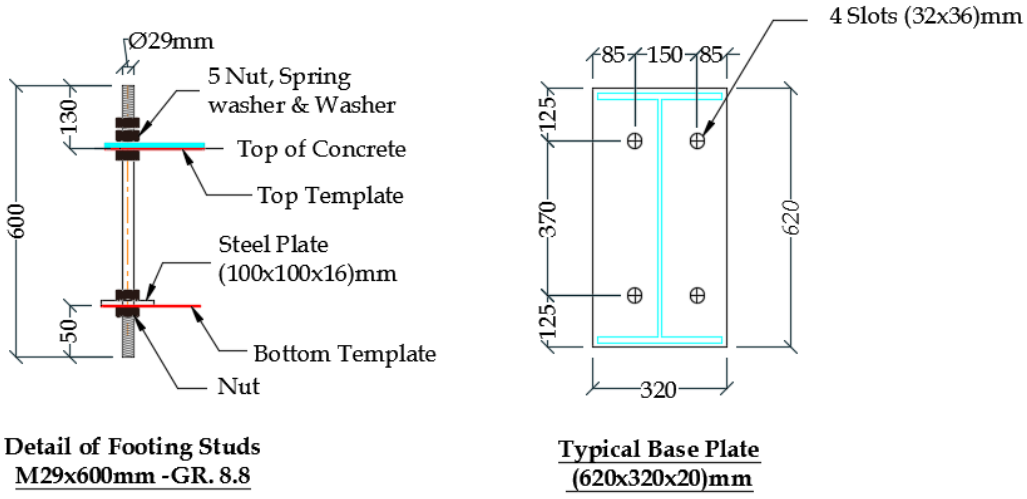

Detail of Footing Studs M29x600mm -GR. 8.8

Typical Base Plate (620x320x20)mm

FIGURE 9. Anchor Rod and Base Plate Details

TABLE 1.
Design Loads

	Label	Case name	Nature	Analysis type
1	Self-weight	Self-weight	dead	Static - Linear
2	W_lr(+)	Wind L/R pres.(+)	wind	Static - Linear
3	W_lr(+)_C(+)_	Wind L/R pres.(+) Cp 1	wind	Static - Linear
4	W_lr(-)	Wind L/R pres.(-)	wind	Static - Linear
5	W_lr(-)_C(+)_	Wind L/R pres.(-) Cp 1	wind	Static - Linear
6	W_rl(+)	Wind R/L pres.(+)	wind	Static - Linear
7	W_rl(+)_C(+)_	Wind R/L pres.(+) Cp 1	wind	Static - Linear
8	W_rl(-)	Wind R/L pres.(-)	wind	Static - Linear
	Label	Case name	Nature	Analysis type
9	W_rl(-)_C(+)_	Wind R/L pres.(-) Cp 1	wind	Static - Linear
10	W_fr(+)	Wind Fr./Rear pres.(+)	wind	Static - Linear
11	W_fr(+)_C(+)_	Wind Fr./Rear pres.(+) Cp 1	wind	Static - Linear
12	W_fr(-)	Wind Fr./Rear pres.(-)	wind	Static - Linear
13	W_fr(-)_C(+)_	Wind Fr./Rear pres.(-) Cp 1	wind	Static - Linear
14	Wrf(+)	Wind Rear/Fr. pres.(+)	wind	Static - Linear
15	Wrf(+)_C(+)_	Wind Rear/Fr. pres.(+) Cp 1	wind	Static - Linear
16	Wrf(-)	Wind Rear/Fr. pres.(-)	wind	Static - Linear
17	Wrf(-)_C(+)_	Wind Rear/Fr. pres.(-) Cp 1	wind	Static - Linear
306	SNOW1	Snow case I	snow	Static - Linear
307	SNOW1	Snow case I edge	snow	Static - Linear
308	SNOW2_lr	Snow case II l/r	snow	Static - Linear
309	SNOW2_lr	Snow case II l/r edge	snow	Static - Linear
310	SNOW2_rl	Snow case II r/l	snow	Static - Linear
311	SNOW2_rl	Snow case II r/l edge	snow	Static - Linear

TABLE 2.

Design Load Combinations

Combs	Definition	Combs	Definition	Combs	Definition	Combs	Definition
ULS/ 1	1(1.4)	ULS/ 10	1(1.2) + 10(1.6)	ULS/ 19	1(0.9) + 2(1.6)	ULS/ 28	1(0.9) + 11(1.6)
ULS/ 2	1(1.2) + 2(1.6)	ULS/ 11	1(1.2) + 11(1.6)	ULS/ 20	1(0.9) + 3(1.6)	ULS/ 29	1(0.9) + 12(1.6)
ULS/ 3	1(1.2) + 3(1.6)	ULS/ 12	1(1.2) + 12(1.6)	ULS/ 21	1(0.9) + 4(1.6)	ULS/ 30	1(0.9) + 13(1.6)
ULS/ 4	1(1.2) + 4(1.6)	ULS/ 13	1(1.2) + 13(1.6)	ULS/ 22	1(0.9) + 5(1.6)	ULS/ 31	1(0.9) + 14(1.6)
ULS/ 5	1(1.2) + 5(1.6)	ULS/ 14	1(1.2) + 14(1.6)	ULS/ 23	1(0.9) + 6(1.6)	ULS/ 32	1(0.9) + 15(1.6)
ULS/ 6	1(1.2) + 6(1.6)	ULS/ 15	1(1.2) + 15(1.6)	ULS/ 24	1(0.9) + 7(1.6)	ULS/ 33	1(0.9) + 16(1.6)
ULS/ 7	1(1.2) + 7(1.6)	ULS/ 16	1(1.2) + 16(1.6)	ULS/ 25	1(0.9) + 8(1.6)	ULS/ 34	1(0.9) + 17(1.6)
ULS/ 8	1(1.2) + 8(1.6)	ULS/ 17	1(1.2) + 17(1.6)	ULS/ 26	1(0.9) + 9(1.6)		
ULS/ 9	1(1.2) + 9(1.6)	ULS/ 18	1(0.9)	ULS/ 27	1(0.9) + 10(1.6)		

The other side of this investigation includes the construction management to determine whether all the members of the structure are assembled per the design drawings and the specifications, if any, are followed. A field trip investigation was performed on March 18th 2013 for this purpose.

6. THE STRUCTURAL ANALYSIS RESULTS

As mentioned above, the 108m x 84m steel structure was modeled and analyzed in Autodesk Robot Structural Analysis Professional. The loads are applied as shown in the previous section. The structural analysis resulted in the following:

Outer Columns: The outer columns are tapered I sections. They all maintain their structural integrity for the loads with an interaction ratio of 0.26.

Center Columns: Center columns fail to resist the loads. Despite that it has an interaction ratio of 0.26, it fails the stability requirement with kL/r to exceed the maximum required of 200 by16.64. These columns must be tied and braced to each other to reduce the unbraced length. The controlling column fails under the load combination number 16, which is dead load plus wind load.

Rafters: Rafters fail to resist the loads. The controlling member has an interaction ratio of 3.24. The controlling load combination is combination number 8.

Purlins: The purlins fail under the wind and snow load combinations. The controlling member got an interaction ratio of 3.24. This member also fails the stability requirement as mentioned above by a large amount. Side Wall Bracing: The controlling member, which did not have a sufficient section modulus, failed the stability requirement by approximately 200. The enveloping load combination is number 4. Roof Bracing: These members failed in both of the strength requirements. The controlling member has an interaction ratio of 57.26.

Base Plate Analysis: Base plates are analyzed using AISC ASD9 methodology. For that, the load combinations in the Autodesk Robot Structural Analysis Professional are changed to ASD. The results of the reaction forces are calculated and the envelop values are taken as conservative approach to evaluate the base plates. These envelop values are shown in Table 3 and Figure 10.

TABLE 3.

Envelop Reactions Per ASD Combinations

	FX (kN)	FY (kN)	FZ (kN)	MX (kNm)	MY (kNm)	MZ (kNm)
MAX	31.24	0.99	102.45	0.32	81.61	0.01
Node	96	3	1254	96	96	101
Case	6	1	1	1	6	14
MIN	-31.18	-0.88	-110.88	-0.28	-81.61	-0.01
Node	94	101	1255	1176	94	99
Case	2	1	10	1	2	14

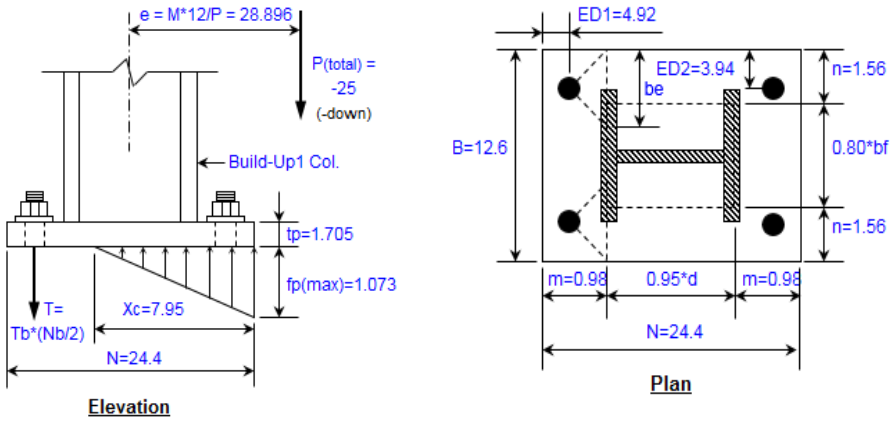

FIGURE 10. Base Plate Analysis

These values are inserted in an Excel sheet created specifically to analyze the base plates. The results show that the base plates are capable to resist the loads and maintain their structural integrity as follows. Note that the bearing pressure is exceeded the allowable by approximately 2%, which is acceptable in this case.

Front and Back Wall Bracing: The 4mm thick plate that was designed and used as bracing member, is not sufficient to handle the loads. The interaction ratio is huge.

Anchor Rod Analysis: The controlling footing was chosen for the analysis of the anchor rods since these bolts pulled out from the concrete. The base plate dimensions are 620mm x 320mm x 20mm and the anchor rods are φ29mm M8.8 bolts of 600mm long. The base plates were supported by a concrete pedestal of 700mm x 400mm. As such, the base plate is flush oriented with the pedestal on the outer edge as shown in Section C-C of sheet number 32 of the design drawings. The anchor rods are embedded in concrete for a distance of approximately 470mm.

The representative core tests taken from the foundation on April 7, 2013 shows that the concrete passed the required compressive strength of 32 MPa. The results of the anchor rod analysis indicate that if they were installed as per the design drawings they were maintaining their structural integrity (Table 4). However, it is quite clear that the anchor rods failed to fulfill the requirements of the ASTM A307-97 since the elongation did not reach the lower limit [7]. According to ASTM A307-97, the minimum elongation percent in 50mm bar shall be 23% but the bars tested have elongations of 2.6%, 1.7%, and 1.4% as shown in Table 5. These values are too low. Based on the test results, although the tensile strength of the anchor rods has reached the required value, its elongation ratio did not meet the requirements. This has caused an abrupt pull out and/or premature ductile failure of the anchor rods which led the structure to collapse (Figure 11).

TABLE 4.
Summary Anchor Rod Analysis

Failure Type	Utilization Ratio
Steel Failure (T)	0.063
Concrete Breakout (T)	0.49
Pullout (T)	0.111
Side-face Blowout (T)	0.416
Steel Failure (V)	0.028
Concrete Breakout (V)	0.351
Concrete Pryout (V)	0.102
Stress Ratio	0.841

A trial and error was conducted to determine the lowest compressive strength of concrete that provides the sufficient capacity. The minimum f_c' that maintains the structural integrity and ensures that the anchor rods will not pull out from the concrete and the concrete will not crush under the interaction of shear and tension is 17.0MPa. The core tests show that the actual compressive strength exceeds the required value of 32MPa, which is almost twice as this value that ensures that concrete will not crush during stress. The high value of concrete compressive strength would have been an advantage if the anchor rods acted as ductile material but that never happened.

Therefore, the concrete crush is not from any glitches or quality from the foundation concrete but rather from the large impact pulling load that transferred almost wholly to concrete because the anchor rods failed to elongate as a ductile material.

TABLE 5.

Anchor Rod Lab Test Result

حدود المواصفات /الصنف Requirment(Grade)			Tensile Requirement
Grade A	Grade B	Grade C	
ـــــ	ـــــ	905 908 927	(Mpa)N/mm2 مقاومة الشد حد ادنى Tensile Strength Min.
ـــــ	ـــــ	X2.6 X1.7 X1.4	الاستطالة لطول قياس 50 ملم حد الادنى ٪ Elongation in (50) mm Min.٪ (27.0 mm) قطر القضبان

FIGURE 11. Anchor Rod Pull-Out Fail

7.ANALYSIS OF THE CONSTRUCTION ASPECT

It was noticed during the field trip that the rafter-column connection bolts were not snug tight and lacked the appropriate torque. This was noticed in several connections (Figure 12). This loose connection caused bolt thread failure in shear in some of these connection and bolt threads totally or partially sheared away as the result of the large dynamic impact from the collapsed members (Figure 13).

FIGURE 12. Snug Tight Connection During Construction

FIGURE 13. Shear Failure of Bolt Threa

As mentioned above in The Structural Analysis section, few anchor rods at the frame sections close to the assembly crane failed and caused the collapse of the frame sections. Few of these anchor rod failures were ductile as shown in Figure 14 (left) while several others pulled out from the concrete as shown in Figure 14 (right). This can be caused by a glitch in the design of the anchor rods that caused the concrete to crush under the pull-out force (Figure 14 and Figure 15) or by construction negligence. However, as discussed in the design section, the laboratory tests showed that the bolt materials lacked elongation; as such, did not act as a ductile material and caused this pullout failure. Few base plates failed besides the anchor rods. Some of them bent, while some others went one step further by failing under tear through by the anchor rods (Figure 16).

The base plate design evaluation shows that they have been designed to maintain their structural integrity for the applied loads. This indicates that the anchor rods were not tightened as required that permitted a dynamic impact on the anchor rod holes (Figure 16). On the other hand, the construction process of casing the pedestals that contained the anchor rods lacked quality work and common practice.

FIGURE 14. Anchor Rod Failure, Ductile Failure (left) and Non-Ductile Failure (right)

The pedestals that contained the anchor bolts were fairly short and was much better to cast them monolithically with the tie beams. The ideal method to cast the pedestals monolithically with the other parts of the foundation and install the anchor rods is by leaving a hole through

the top leveling plate to allow the pedestals to be casted concrete monolithically with the other parts of the foundation (Figure 17).

Anchor bolts must be designed to be ductile. To do this, the designing pullout strength of the concrete failure cone (U_p) must be equal to the minimum specified tensile strength ($F_u A_t$) (Shipp & Haninger, 1963). Unfortunately, this was not the case in this structure.

FIGURE 15. Anchoor Rod Pull-Out and Concrete Crush Failure

FIGURE 16. Base Plate Tear Through Failure

Despite having small height, it was noticed that the foundation pedestals were not casted monolithically with the rest of the foundation but rather after casting the footing. This can be noticed from Figure 18 that a gap was left underneath the top plate that was filled with concrete after casting a portion of the pedestal. This created a construction joint not so far from the top plate and the contractor was not able to vibrate that portion of concrete and made it prone to having voids in the pedestals.

FIGURE 17. Typical Common Practice Pedestal Construction

FIGURE 18. Actual Pedestal Casting

In few column bases, it was noticed as shown in Figure 19 that the gap underneath the column base plate was filled when the floor slab was cast and therefore, created a weak joint between the old concrete of the pedestal that connects to the tie beams and that portion of it that is above it. This is also an indication that normal common practice was not followed and the construction process lacked quality. In addition, the construction management was poor. The bolts should have been tested in a certified laboratory and the designers' approval should have been taken prior to using them. Also, the manufacturer's certification is missing for the rest of materials used such as the nuts, washers, etc. As such, this flaw is a glitch in the construction management of the project that should become lesson-learned for future similar projects.

FIGURE 19. Gap Under Base Plates Casted with Floor

7. CONCLUSION

a. CONSTRUCTION MANAGEMENT AND MATERIALS

The following results are concluded based on the investigation:

I. The 108m x 84m portal frame structure was not erected in a safe way. Safety rules are not followed and wise engineering judgment was altered. The rigging process was not conducted in an appropriate way by continuing construction during an extreme wind that caused the crane to collapse.

II. Connection bolts were not snug tightened to ease the construction process. This method is very risky and is normally used when the connection holes are not in accurate spots so the installer does not tight the bolts until all the frame parts are installed. This is was a part of the collapse cause. The dynamic force associated with the collapse of the crane and the wind transferred the impact into the bolts. Since the bolts were not tightened enough, it caused a severe damage to the connection bolts that the threads of some of them sheared away by the impact. Also, few base plates failed under the impact load since the anchor rods were not snug tightened that caused a punch through the bolt holes in addition to severe buckling.

III. The catastrophic collapse of the structure occurred because of failure in the anchor rods and the base plates in addition to concrete failure that caused the anchor pull-out in few places.

IV. The abrupt-action collapse occurred as a result of bad anchoring the structure and bad connecting the rafters to the columns. Construction sequence of the member installation was managed poorly.

V. The concrete of the footing pedestals where the columns are anchored to the footing crushed during the collapse. This must not happen under any circumstances because the anchor rods are designed correctly. The analysis of these anchor rods shows that they are designed to be ductile. This means if any failure has to happen, the anchor rods to fail prior to failure in concrete and prevent crushing concrete to avoid an abrupt collapse. As the concrete of the pedestals crushed in few places and the anchor rods pulled out from concrete, and the core tests show that the compressive strength of concrete meets the requirement of 32MPa, fingers are pointed to the material of the anchor rods. The anchor rods failed the elongation requirement test per ASTM A307-97 as per Seko Engineering House's report number 2468 on March 27, 2013. This means that the anchor rods did not act as ductile material and allowed concrete to crush.

VI. The gap underneath the column base plate was filled when the floor slab was cast and therefore, created a weak joint between the old concrete of the pedestal that connects to the tie beams and that portion of it that is above it. As such, the weak spot in the anchor embedment was participated in the concrete breakout mechanism as per part iii of Figure RD.4.1 of ACI Code 318 [6].

b. DESIGN

As mentioned above in this paper, the warehouse structure was evaluated for structural integrity. The following are the conclusion of this analysis:

I. The outer columns maintain their structural integrity per the design.
II. The interior columns fail to maintain their structural integrity and lack lateral bracing.
III. The rafters fail to maintain their structural integrity and are not qualified for the load.
IV. None of the lateral bracings of the wall and the roof are capable to maintain their structural integrity for the load.
V. The base plates are capable to maintain their structural integrity and are qualified for the load per the design.
VI. The design anchor rods are capable to maintain their structural integrity and are qualified for the load per the design.

c. V3. CAUSE OF THE CATASTROPHIC COLLAPSE

Based on the evaluation shown above and calculations, fingers are pointed to both of the design and construction management. Since the design lacks integrity, constructing it is not safe either. However, it is believed that the catastrophic collapse is caused by construction mistakes, safety negligence, and not following the standards by not tightening the bolts and poorly managing the sequence of the construction process. Despite that the design lacks integrity; if it was constructed the right way then it would not be going to collapse under the circumstances of the time of failure because the wind that blew at that time did not have the sufficient pressure on the structure to push it down. This is because the structure was open in all directions and the siding was not installed yet. In this case, the structure can withstand its own weight plus a minor pressure from the wind. As such, the cause of the collapse is from the negligence in construction management and materials not meeting the design requirements. Details of the mistakes are outlined in Construction Management and Materials section clarified above.

REFERENCES

[1] R. Ferhadi and H. Khoshavi, "Evaluation of the Structural Design of the Steel Portal Frames, Part A: 108m X 84m Storage Warehouse," Seko Engineering House, Sulaymani, 2013.

[2] American Institute of Steel Construction, Inc., Steel Construction Manual, ANSI/AISC 360, 13 ed., AISC, 2013.

[3] American Institute of Steel Construction, Inc., Steel Construction Manual, ANSI/AISC 360, Allowable Stress Design, 9 ed., AISC, 1989.

[4] W. Blodgett, Design of Welded Structures, James F. Lincoln Arc Welding Foundation, 1966.

[5] J. M. Fisher and L. A. Kloiber, Steel Design Guide 1, Base Plate and Anchor Rod Design, 2nd, Ed., AISC, 2006.

[6] American Concrete Institute, Building Code R quirements for Structural Concrete (ACI 318-08) and Commentary, ACI, 2008.

[7] American Society for Testing and Materials (ASTM International), ASTM A307-97, Standard Specification for Carbon Steel Bolts and Studs, 60 000 PSI Tensile Strangth, vol. A307, ASTM International, 1997.

[8] G. J. Shipp and R. E. Haninger, "Design of Headed Anchor Bolts," Engineering Journal, vol. 20, pp. 5-69, 1963.

This Page Intentionally Left Blank

Sponsors of IEC2018

This Page Intentionally Left Blank